CRANFIELD UNIVERSITY

SCHOOL OF MECHANICAL ENGINEERING

PhD THESIS

Academic Year 1994-95

P W GRIFFITHS

An examination of the thermophysical nature of solar-control films using an illuminated hot box and computer based simulation modelling techniques

Supervisor: W J BATTY

November 1994

Abstract

Solar-control films are increasingly being retrofitted to the windows of buildings as a means of reducing solar gain. At present, there is a dearth of information concerning how these films effect the thermal comfort of occupants within buildings where these films have been applied. An illuminated hot box, utilising a xenon lamp to simulate sunlight, has been designed as a testing facility. The illuminated hot box has been used to obtain information on how much thermal radiation enters the internal space from a window fitted with a solar-control film. The data from the experimental apparatus was verified using a finite-difference model written on a personal computer, with the aim of the computer program being used to compare different films, and thereby avoiding expensive experiments. The experimental rig produced usable data for the tested films only when the lamp was orthogonal to the plane of the glass, with errors occurring, and increasing, as the angle of incidence between the lamp and the glass increased. This conclusion was verified by the computer based model. It was seen that the illuminated hot box was too small to give accurate measurements for angles of incidence other than 0°. It is suggested that a larger illuminated hot box which is able to eliminate the problems encountered when measuring for angles of incidence above 10° would be desirable. Furthermore, a more complex transient finite-difference computer based simulation model is needed, taking into account the conclusions that were made during this study.

Contents

List of Figures

List of Tables

Nomenclature

A	Avagadro's number
A	Area (m^2)
Bi	Biot number
°C	Temperature, degrees centigrade
c	specific heat capacity ($Jkg^{-1}K^{-1}$)
c_o	phase velocity of radiation (m^{-1})
d	thickness of medium (m)
E	Energy of a quantum (J)
e	electron charge (As - ampere second)
F	Shape Factor
Fo	Fourier number
Gr	Grashof number
g	gravity (ms^{-1})
h	Plank's constant (Js)
h_c	Convective heat transfer coefficient ($Wm^{-2}K^{-1}$)
h_r	Radiative heat transfer coefficient ($Wm^{-2}K^{-1}$)
I	Solar Radiation (W)
I_λ	monochromatic solar irradiation (W)
K	Kelvin
k	absorption index also the imaginary part of the complex index
k	thermal conductivity ($Wm^{-1}K^{-1}$)
l	length (m)
M	molecular weight
m	metres
m^*	effective mass of a free electron in a plasma
N	complex index of refraction
N	volumetric electron number density
Nu	Nusselt number
n	real part of refractive index
n_x	real part of refractive index - the subscript refers the layer number
n_x	energy shell of an atom
Pr	Prandtl number
Q	heat transfer rate (W)
q	heat transfer rate per unit volume (Wm^{-2})
R	thermal resistance (Km^2W^{-1})
Ra	Rayleigh number
r_n	reflectance at surface n
rc_i	fraction of solar insolation that is absorbed by the glass and convected to the internal environment
rc_o	fraction of solar insolation that is absorbed by the glass and convected to the external environment
S	Shadow factor
t	time constant
T	Temperature (°C)
TE	subscript representing the electric field of electromagnetic radiation
TM	subscript representing the magnetic field of electromagnetic radiation
U	U-value, thermal transmittance ($Wm^{-2}K^{-1}$)
x	path length through medium (m)
Δx	distance between nodal points (m)
α	absorptivity

α_e average electronic polarisability of the dielectric molecule

β volumetric thermal expansion coefficient ($K^{-1)}$

ε emissivity

ε_o dielectric permittivity for a vacuum (Fm^{-1} $AV^{-1}m^{-1}$ ampere per volt per metre)

ε_s dielectric constant of free space (Fm^{-1} as ε_o)

ε_∞ relative permittivity for a vacuum for $\nu \rightarrow \infty$ (Fm^{-1} as ε_o)

κ absorption coefficient (m^{-1})

λ wavelength (m)

λ_o wavelength in a vacuum (m)

σ Stephan-Boltzmann's constant (5.67×10^{-8}, $Wm^{-2}K^{-4}$)

σ_e electrical conductivity ($ohm^{-1}m^{-1}$)

ϕ phase change of electromagnetic wave (degrees)

θ angle of incidence (degrees)

θ_i angle of incidence of incident radiation (degrees)

θ_r angle of incidence of refracted radiation (degrees)

ρ density, (kgm^{-3})

ρ reflectivity

τ transmissivity

μ magnetic permittivity (Fm^{-1})

ν frequency of radiation (s^{-1})

ν kinematic viscosity (m^2s^{-1})

ω_e frequency of electron vibrations (s^{-1})

ω_p critical frequency (Hz)

ψ thermal diffusivity, (m^2s^{-1}) this is defined as the ratio of thermal conductivity to the density and specific heat capacity of a fluid, ($k/\rho c$)

Chapter 1 The Background to this Investigation

1.1 Introduction

Solar control films and glasses treated with thin metal surface coatings have been used extensively by designers and engineers for a variety of reasons. For some architects the colour and reflectivity of coated glazings have alluring visual effects, while engineers may be more interested in the influence which these films may exert on the thermal and visual environments within the building. However, the effects of these construction materials on the physiological and psychological well-being of the building occupants are not well understood. A large number of different surface finishes exist which exhibit a variety of physical behaviours. The designer needs to be aware of how the choice of a particular film or glazing will affect later choices about heating, cooling or lighting systems to provide comfortable environments for the occupants.

Humans can survive in a wide range of climates, because they have modified the ambient environment through the agency of buildings. The building enclosure acts to moderate temperature extremes and provide a barrier to wind and rain. Over time the construction of these enclosures has changed as new building materials and technologies have become available. However they still perform the same functions. These include strong walls, externally and internally, to support upper storeys and the roof. These walls are generally opaque and so the use of openings such as windows and doors are included to provide natural lighting for illumination, access, ventilation and the psychologically important contact with the outside world.

However windows can cause problems by, (a) allowing heat loss to the ambient environment, (b) allowing excess solar energy to enter a room and causing overheating and (c) causing problems of visual discomfort because of glare. For example, Lynes (1968) states that complaints of glare will occur when the sun is seen through a vertical window at an angle of incidence less than 45°. In temperate latitudes (50°-60°), this occurs at some point in the day all year round depending upon the orientation of the window. For example, for a building on a latitude of 52° in the northern hemisphere, glare occurs on the south-facing window at some time during the day for the nine months from September to May. However, it is only during spring and autumn that the solar intensity is great enough to cause discomfort. Therefore there is a need to control the amount and type of sunlight entering an internal environment through the windows. This is particularly true of the working environment, where the changes in building

design are more frequent, and often occur for purposes which take little account of the occupants comfort.

1.2 Window Design as a Climatic Response

The climatic regions of the earth vary enormously. A design suitable for temperate Europe, may not be suitable in Northern Africa. Investigations of traditional buildings with regard to climate, such as that by Reid (1984), highlight how, through experience, traditional local design practice has overcome the problems which windows pose. In lower latitudes there are two types of climate, namely hot and arid and hot and humid. Traditional buildings in arid climates are invariably in compact form with a high thermal mass, few windows and substantial shading, which is either provided by the structure or by hanging cloths. The windows which are present usually have large recesses which reduce or eliminate direct solar radiation gain, but allow reflected light to enter the room. In traditional architecture the windows are unglazed, with security provided by wooden or metal lattices across the window opening. Although there is a high solar intensity there are also high sun angles for a large part of the day and there is less of a difference in expected solar gains between the northern and southern façades. In humid climates traditional buildings provide shade from the sun and shelter in the rainy season, while being expansive and open-walled for ventilation purposes. In towns, the buildings may be of a stone construction with verandas providing shade for large windows or shutters, while in the country the traditional material is wood. High intensity light produces discomfort for the eyes, so shading is used for visual comfort, while still maintaining adequate light levels for work.

The lower to middle latitudes, for example the Mediterranean, have adapted the architecture of the lower latitudes to suit the climate. These buildings are usually expansive with verandas to protect the rooms from excessive solar gain and glare, and also to induce ventilation. The buildings are constructed with thick walls of high density materials and are therefore of high thermal mass. The thermal behaviour of massive constructions is such that the temperature pulse entering the wall is delayed so that the inside can be kept cool in the summer, while in the winter the mass acts as a heat store helping to keep it warm. This mass element of the building relies upon moderate to large diurnal and seasonal temperature swings. The windows in these climates are usually glazed and can be opened for ventilation.

The middle latitudes, that is, those of northern Europe and southern Canada have relatively large seasonal swings of temperature and sun angles. Traditional buildings in these climates have smaller windows which are shaded using internal blinds. Because of the wide inter-seasonal variations of climates experienced, the building design solutions adopted have been the result of a series of "trade-offs". Also because of cheap fuels and their relative wealth, the people of these latitudes have recently developed life styles and building designs which take little heed of climate.

A simplistic solution in the middle latitudes of the Northern Hemisphere is demonstrated by the orientation of the building, Figure 1.1. In winter, the long south wall is heated by the low-angle noon sun, (Figure 1.1 Diagram A), while in summer the oblique sun angle keeps the heat gain down during the middle of the day and the smaller areas of the east and west walls reduce the impact of low sun-angle in the early morning and evening sun, (Figure 1.1 Diagram B). With appropriate building features, the seasonally changing angle of the sun can be utilised to offset the problem of solar gain in the summer and heat loss in the winter. If the building is orientated with a long south wall and short east and west walls, solar gains can be maximised during the winter. However, planning procedures and site constraints may not allow such an approach, so different measures of solar protection/capture must often be considered.

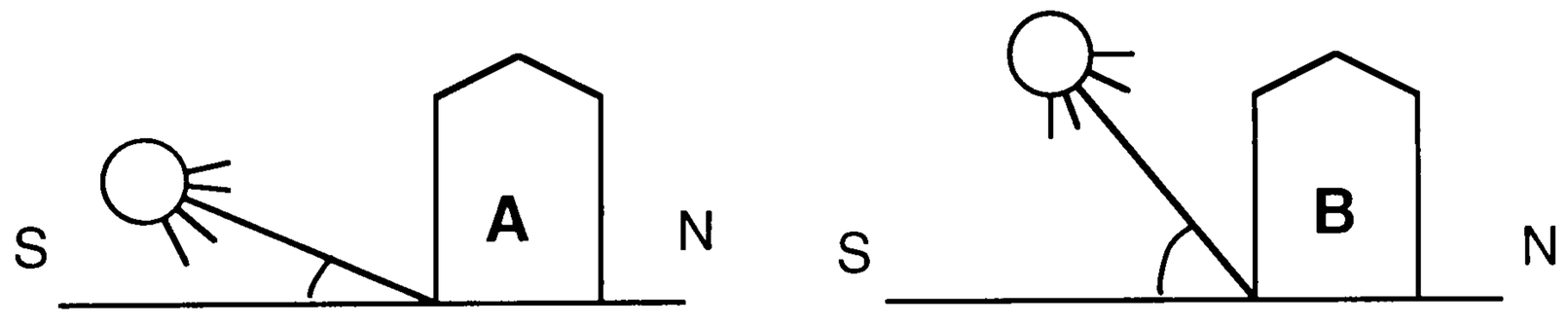

Fig 1.1 Sun Angle with a south facing wall at mid-north latitudes: A - winter, B - summer (Reid 1984)

In the high latitudes, small houses, with small windows which are strategically placed to catch the sun, are adopted. For the people who live in such latitudes, excessive solar gain is not a problem, instead there exists a problem of gaining as much daylight as possible without losing too much energy through the window. Hence they chose a low wall to window ratio in order to reduce heat loss from their buildings while the windows which are present, face the sun in order to gain maximum daylight as a result of the low azimuth angle of the sun. In this context, any glazing strategy which can maintain good daylight levels whilst reducing thermal losses would offer advantages.

1.3 The Need for Solar-Control

Today, with the age of instant world-wide communication and the often unintended aesthetic imperialism of the Euro-American culture, there is a desire to erect buildings of particular designs in climates which do not suit them. This is especially demonstrated in the architecture of Mies van der Rohe, (Harkness and Metha, 1978). They may lead to high heating costs, or more extensively, excessive demands for air-conditioning. Although there is a move to learn lessons from vernacular designs in the West, the desire to be seen as "developed" by Third World countries, fuels the demand to have buildings of the same style as those in the West proving that they have "joined the club". These buildings are often imposed by 'western' companies, who are often more concerned with promoting a corporate image than providing comfortable environments for occupants within the realms of the traditional, regional architecture.

The need to be able to the control the intensity of solar radiation entering buildings is evident in all the world's climatic regions. Differences in climatic conditions and sun angles experienced at different latitudes, demand particular building design responses. This is particularly true where windows or apertures in the building structure are concerned.

Solar-control films have been developed largely as a response to the large areas of glazing which have become prevalent in commercial buildings since the 1950's. Their intended function is to modify the solar thermal behaviour of windows as shown by Theissen (1968), Hassall (1971), Yellot (1971) and Minne (1990). An energy-effective window should be capable of providing sufficient natural lighting during the day, without causing thermal discomfort due to heat loss, excessive solar gains or visual discomfort from glare. Unfortunately tall office-blocks are often uncomfortable, because glazing which constitutes a high percentage of the wall area, permits strong glare from the sun. Because of excessive rates of solar energy gains, such offices become uncomfortably hot in which to work. For a modern office building in the United Kingdom, with a large proportion of its outer wall glazed, the ideal specification would be to achieve an optimal glazing which provides good daylighting without the consequent risk of excessive solar gain, or the inhibition of heat transfers, to or from the building according to the needs of the season. The means for satisfying these criteria should ideally be considered at the design stage of the proposed building, through the use of devices such as blinds, external shading or by employing low-emissivity glass surfaces in the windows.

Glare is a world-wide problem and it is most troublesome at low sun angles. Pulker (1984), suggested that sky glare from diffuse solar radiation and reflected glare from highly reflecting surfaces can only be controlled by glass with polarising properties. Direct glare, however, can only be overcome with the use of shading devices.

To solve solar-induced thermal-comfort problems, air-conditioning plant is often installed. This requires major capital investments, as well as incurring significant maintenance costs and high rates of fuel consumption. Poor zoning of the control of air-conditioning plant may lead to a number of areas or rooms with different orientations being controlled by a single temperature sensor. During winter the Sun-exposed areas of the building may become overheated, while simultaneously the system fails to supply sufficient heat to other areas. During the summer, the opposite may occur and some areas then become too cold!

In order to attempt to overcome such problems relatively-cheap commercially viable coatings and films have been developed which may be applied to window glazing. Such layers, for example, metals of thickness ~30nm, can inhibit the transmittance of solar radiation into the room, while in some cases, simultaneously preventing the reverse transmittance of long-wave radiation emitted by internal surfaces of the room, to the ambient environment. The presence of such films on windows generally leads to a reduction of the mean radiant temperature within the rooms exposed to high rates of insolation in the summer, and so contribute to the achievement of greater thermal comfort. For example, the cooling capability of the a-c plant at the London Borough of Croydon's municipal offices was designed so that at peak load the internal temperature of the building should not exceed 24°C. However the mean radiant temperature in the building, with its air-conditioning plant operating at maximum rate was 26°C during the summer of 1990. The presence of a solar film (Courtaulds AG35) applied to the windows of one solar-exposed office, reduced the mean radiant temperature by approximately 2°C and consequently reduced the resultant temperature, (Rose 1990).

This suggests that improved thermal comfort can be achieved by the use of such solar films. Jennings (1973), stated that in a typical air-conditioned room, with an average internal air-temperature of 20°C, the external ambient environment being at 15°C, it is possible for an occupant sitting 1m away from a $2m^2$ south-facing window to experience a maximum mean radiant temperature of 38°C, during a period when direct insolation is received through a double-glazed window. However, when a film was applied which reduced the insolation transmitted by 33%, the mean radiant temperature

experienced by the occupant fell to 28°C. This represented a reduction in the resultant temperature from 29°C to 24°C. Also, because of the reduced solar-gain, smaller capacity air-conditioning plant could be considered. Thus the application of solar-control films is often recommended as a beneficial remedial measure.

1.4 Previous Analysis of Solar-Control

The physical principles describing the behaviours of these films have been well documented by Granqvist (1989). They use a metallic or metal oxide layer to reflect or absorb short wave solar radiation typically within the wavelength range 0.1 to 1μm, or to reflect thermal radiation without reducing the transmittance of visible light. However, these references detail the performance of the films in terms of transmittance, reflectance and absorptance only.

A number of detailed studies have been undertaken to evaluate the thermal performance of windows with solar-control films, in terms of heat losses through the window and using this information to determine their realistic thermal transmittances or U-values. This work has concentrated on the need to reduce heat loss through windows for domestic applications. Klems' (1979) constructed a calibrated hot box within a laboratory. This facility was then used to study improvements to the thermal performance of windows. However, this work did not take into account the effect of solar radiation upon the temperature of the glass, which would effect it's thermal performance. MaCabe and Hill (1987) developed a 'field measurement box' to determine the solar and optical properties of insulating glass windows. This produced data for the thermal performance of a window, but with solar radiation present. However, due to shading from surrounding buildings, direct solar gain could not be measured. Littler (1979) developed a working model to compute heat loss from single or double glazed windows with various coatings and gases in the cavity between glass panels. Rubin et. al. (1980) investigated the energy savings when using low-emissivity on glass. They concluded that a low-emissivity film was more cost effective in terms of energy saving than the addition of another pane of glass. They also investigated the energy savings achieved when a film was applied to different surfaces of a window. They concluded that a film placed on a cavity surface of a double-glazed system gave the lowest U-value. If the film was attached to the cavity surface of the inner pane, then a relatively larger proportion of the absorbed solar radiation subsequently flowed inwards by conduction through the glass and so contributed to heating the room. Also,

overall energy transmittance was reduced because a relatively large portion of the absorbed radiation was conducted through the outer pane of the glass to the ambient environment. Working at the Building Research Establishment, Watford, UK, Rayment (1989), analysed the comparative energy consumption of houses with single and double glazing and systems with low-emissivity coatings. The double glazing gave a 9% (±2) saving, and the reflective coating on a single glazing layer gave a 10% (±2) saving in energy consumption, when compared with the uncoated single glazing.

Until now there has been a dearth of scientifically reliable data relating to the various effects which commercially available solar-control films have upon the thermal and visual environments of the spaces which they enclose, in terms of reducing solar heat gain especially the radiant energy which is transmitted and emitted by the glazing system. Thus it is difficult for designers to predict accurately the thermal and daylighting performances of rooms over various periods of the year.

An initial study by Griffiths et. al. (1992), of the energy transmittance of these films, demonstrated unexpected behaviours. The increase in the resultant temperature, over time within the illuminated hot box for the absorbing films, rose for angles of incidence between 0° - 30°, see Figure 1.2. This behaviour could only be explained by an increased absorption within the film, due to an increase in the path length along which the radiation had to travel through the film.

An analysis of the steady-state resultant temperature rise attained by a space enclosed behind treated glass, which was irradiated by energy from a lamp simulating the solar spectrum, suggested that behaviours of the films could be grouped depending on whether they were of the types designated by the manufacturers as absorbing, reflecting or insulating, see Figures 1.3 to 1.5. The reflective and insulating films show similar behaviours because both are essentially reflecting films; the reflective film is designed to reflect solar radiation away from the building and the insulating film is designed to reflect the long wave thermal radiation back into the internal environment. The lower resultant temperatures for the insulating films may be due to their dark appearance. Insulating films such as those produced by Pilkingtons Glass allow a greater light transmittance and produce higher resultant temperatures. Also, by analysing the three graphs (Figures 1.3 to 1.5) it can be seen that the behaviour of the insulating films is somewhat independent of the angle of incidence at the angles measured.

In order to gain a better understanding of the mechanisms by which these special coatings act, a further and thorough investigation of the film constructions and present theory has been undertaken. The aim of this work has been to derive an experimental process to obtain the resultant-temperatures experienced within an enclosed space behind the glazed aperture. A theoretical model to describe the behaviour of these systems has been developed in order to determine the validity of this experimental results. It was decided that the earlier experimental work by Griffiths et.al (1992) would be repeated using an improved illuminated hot box. Again, this box would be in the laboratory where a controlled environment and solar illumination could be maintained. The improvements were expected to achieve more accurate measurements of air, globe and surface temperature. Further experimentation would allow for the separation of the thermal and visual components of the transmittances of the film types. The computer modelling would be used to assess the efficacy of the illuminated hot box.

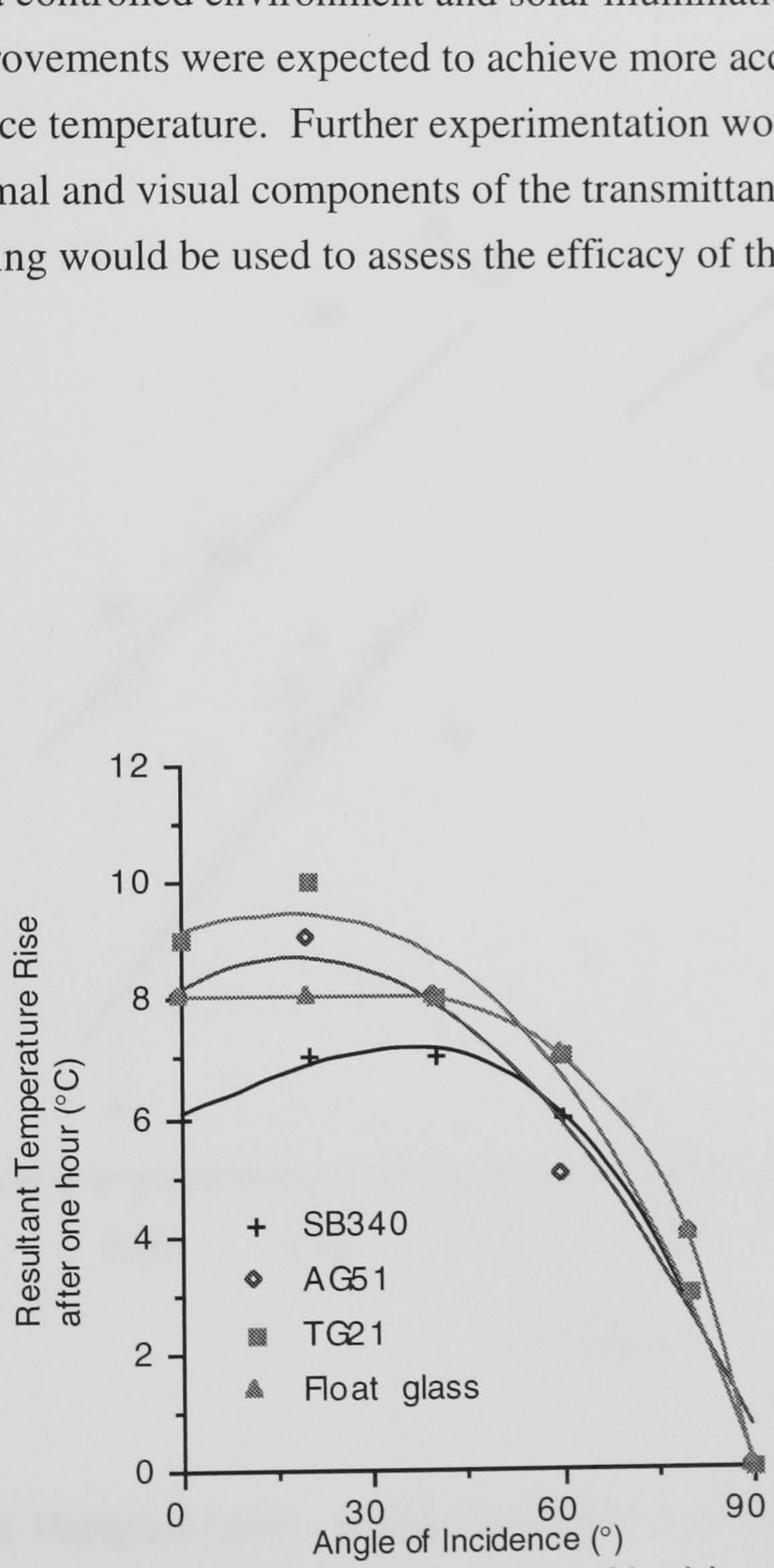

Fig 1.2 Resultant temperature rise vs. angle of incidence for Absorbing films(Griffiths 1992)

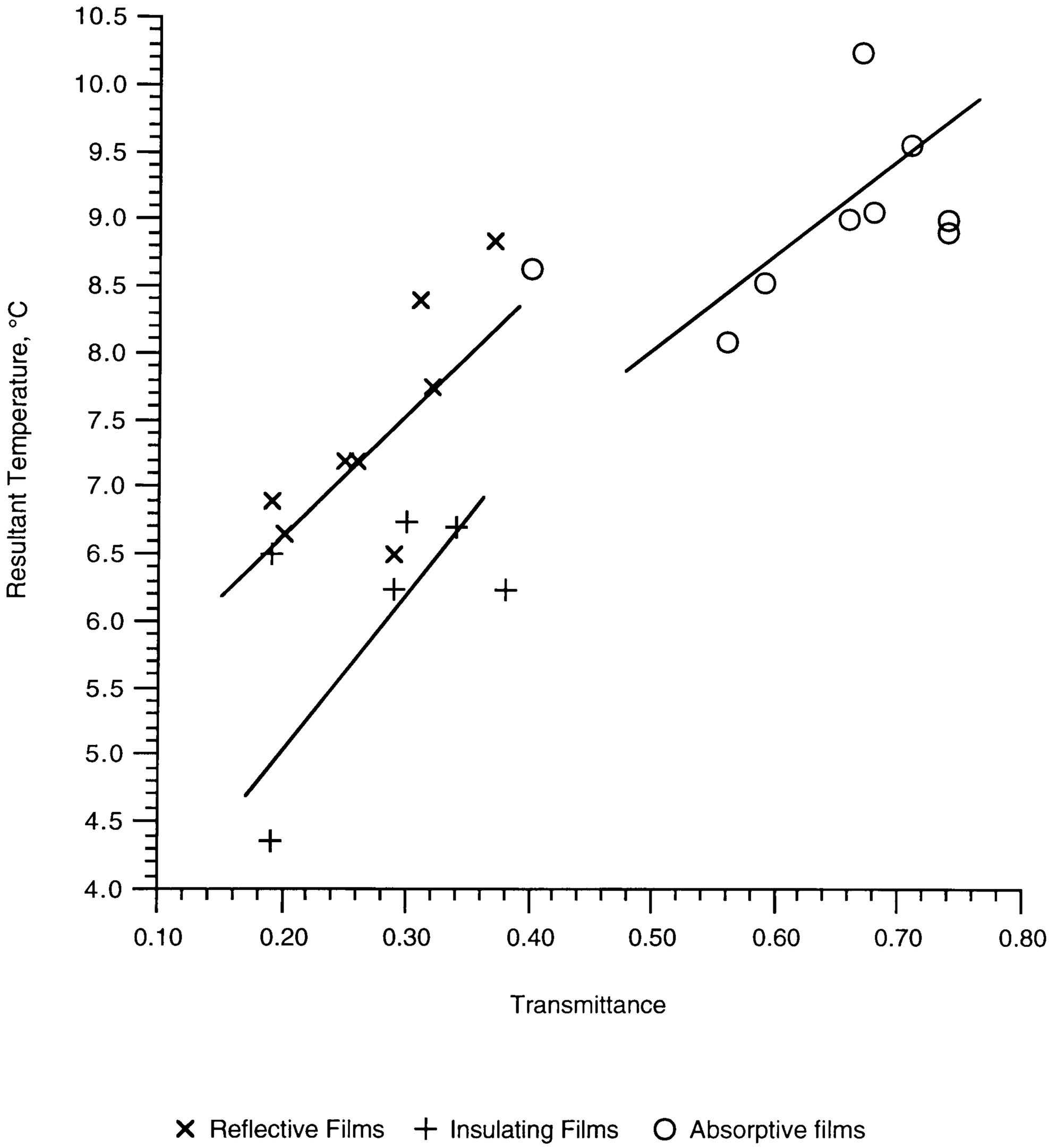

Fig 1.3 Steady-state resultant temperature rise of the enclosure vs transmittance at 0° angle of incidence

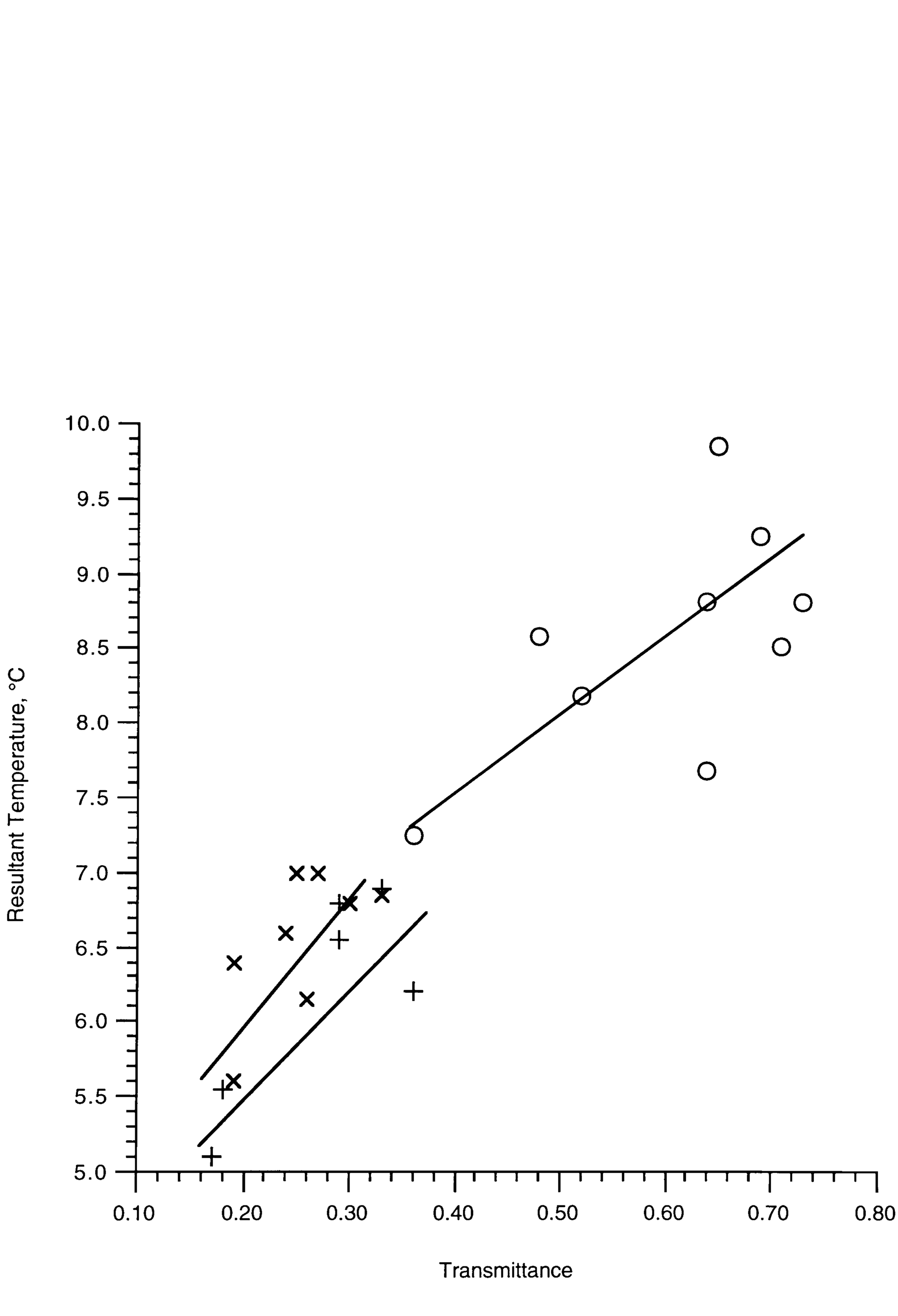

Fig 1.4 Steady-state resultant temperature rise of the enclosure vs transmittance at 20° angle of incidence

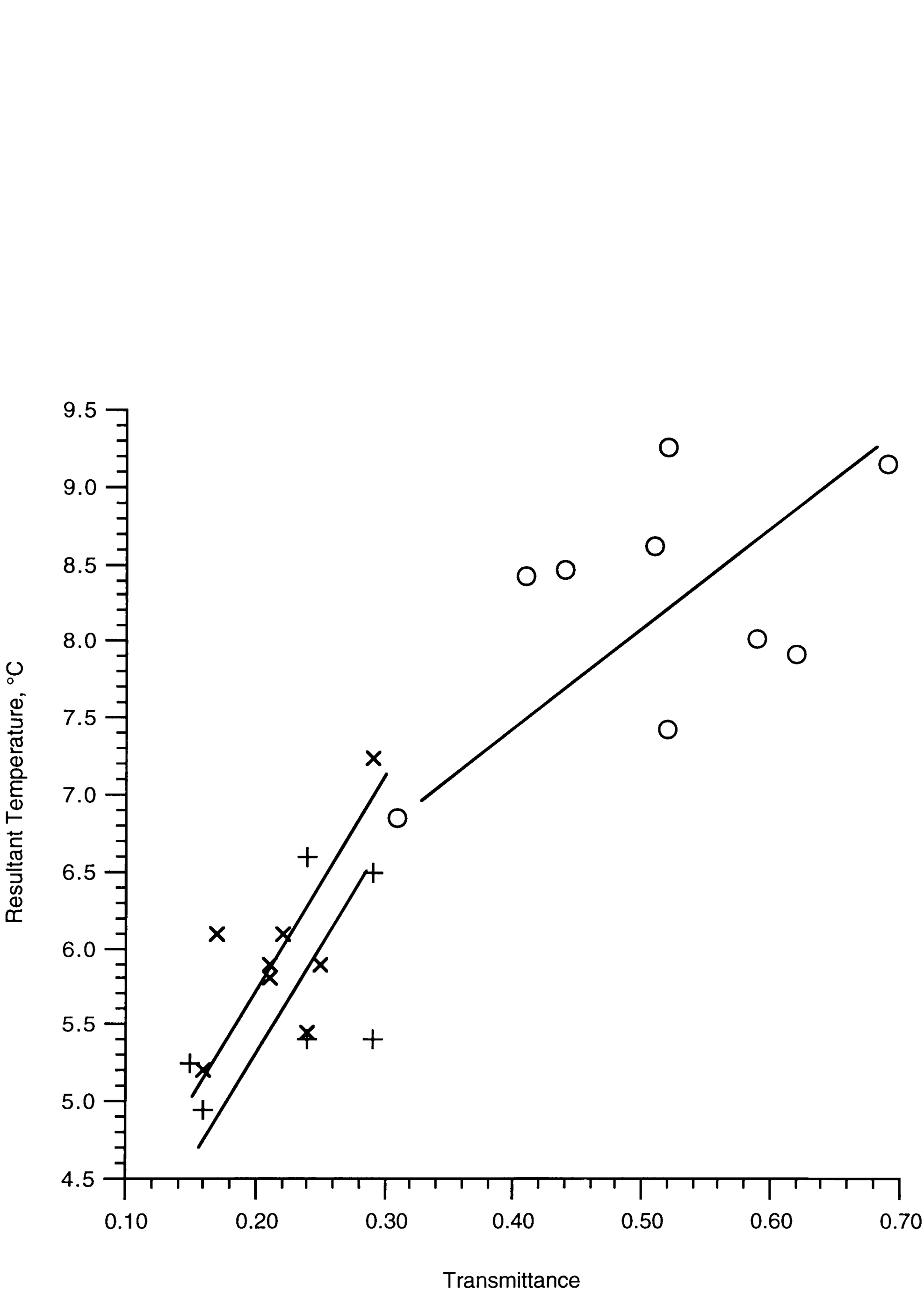

Fig 1.5 Steady-state resultant temperature rise of the enclosure vs transmittance at 40° angle of incidence

1.5 History of Solar Control films

In domestic buildings, across all cultures and climates, it has generally been easier to make a compromise between visual acuity and thermal comfort in favour of the latter. However, in the workplace the requirement for good task lighting makes such a compromise less desirable. The designer can maximise the use of daylight or chose to provide artificial lighting. Unfortunately, if windows are made large enough to provide good daylighting throughout the year, there is often a consequent risk of glare in spring and autumn, along with excessive solar gain on façades from the East through south and to the West in all seasons. One way to reduce the thermal effects of excessive solar gain at certain times of the year is to reduce glazing area. This incurs the penalty of the loss of potential incidental heat gains during the winter when they are most useful.

Various solutions have been developed to deal with this need to vary the behaviour of window areas in response to ambient conditions. The use of venetian and vertical blinds allow occupants to restrict the amount of daylight and glare entering a room. However blinds and opaque shades can result in a large reduction, if not the elimination, of visibility and daylight. Furthermore, if blinds are placed inside the room they do not restrict short wave solar energy gain significantly, as a large proportion of the incident energy is absorbed by the blinds and then re-radiated into the room, see Figure 1.6 and Table 1.1.

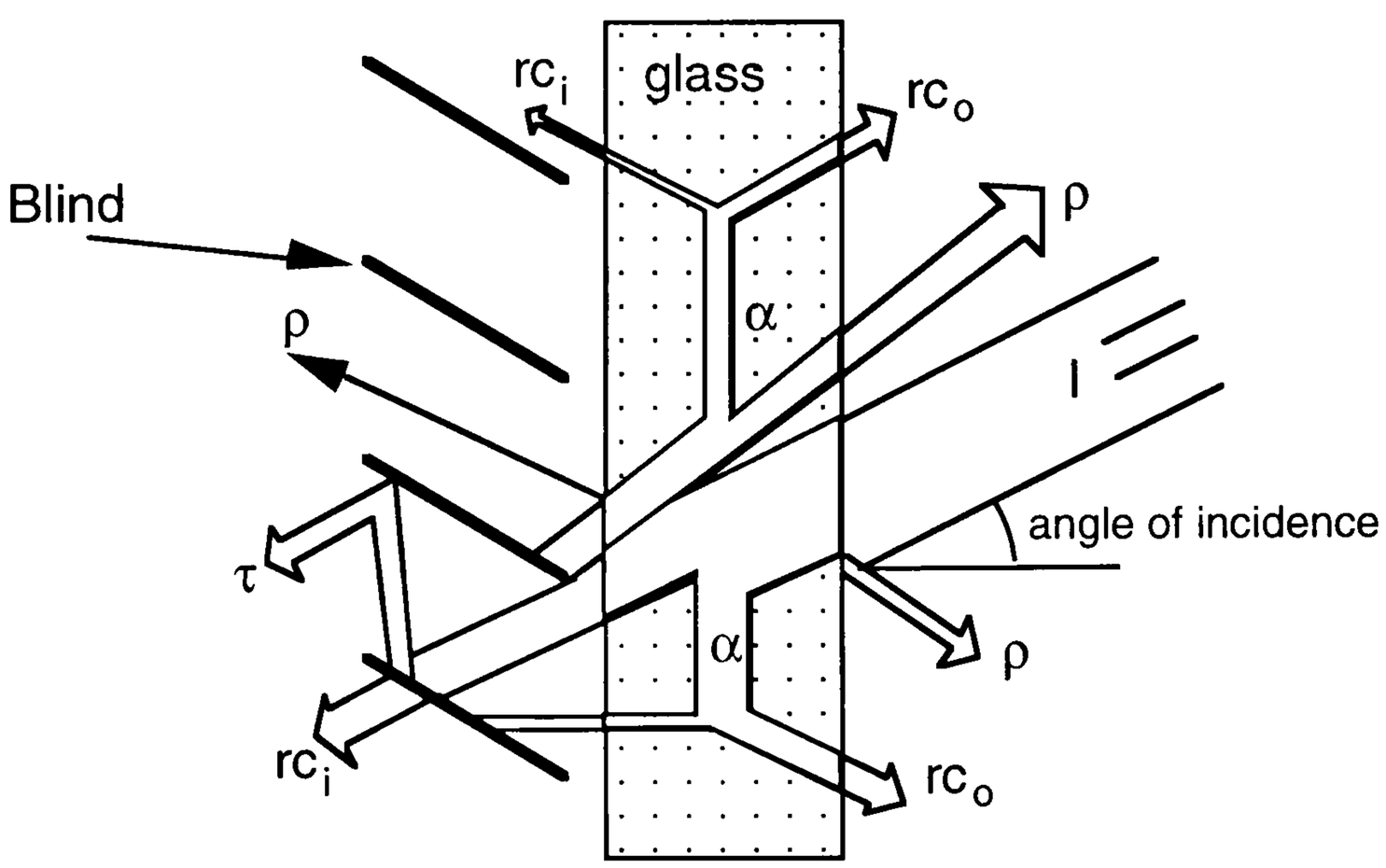

Fig 1.6 Schematic illustration of solar transmittance through a window with venetian blinds (van Straatem 1967)

If building designers were asked to specify the perfect glazing material then it would be a membrane with varying properties which could filter out or reduce the transmittance of particular wavelengths at different times of the year, and which could differentiate their behaviours with respect to energy transmitted from the ambient and internal environments with regard to variations in seasonal needs. The search for such materials is almost comparable with the alchemists search for the secret of turning base metal into gold.

Label	Description	Totals
α	absorption	0.21
ρ	reflectance	0.39
τ	transmittance	0.09
rc_i	absorbed fraction convected to the internal environment, including radiation absorbed by the blind and then convected into the room	0.38
rc_o	absorbed fraction convected to the external environment	0.14

Table 1.1 The proportions of solar radiation (1) incident upon floatglass which is absorbed, reflected and transmitted and their different paths as designated in Figure 1.6

This requirement has led to the development of tinted glasses and coloured transparent coatings. These reduce the transmittance of heat both to and from the internal environment. However, the need to reduce transmittance further, and to improve the wavelength selectivity of the glazing, led to the development of metallic films for solar control. These coatings have enhanced the degree of wavelength specific filtering of the transmittance of electromagnetic radiation naturally found in glass.

Until World War I only the absorbing properties of clear glass could be altered by doping the glass during manufacture with, for example, small amounts of iron oxide. This gave significant reductions in transmittance for infra-red solar radiation and a reduction in heat admission.

Scientific investigation of thin films started in the nineteenth century. Reflective coatings for glass were developed around 1835, by depositing silver films onto glass using wet chemical processes. Deposition by evaporation of, and the subsequent condensation of a metal coating upon glass, was successfully attempted in 1912. This allowed a greater uniformity of the film thickness. The development of surface

treatments during the 1930's widened the scope for solar-control using glazing. The initial work involved the investigation of coatings applied directly to glass, for reflectance and anti-reflectance purposes (Pulker 1984). During this period aluminium replaced silver as it showed several advantages; i) reflectivity for aluminium, while the same as silver in the visible spectrum, is much higher in the ultra-violet waveband and ii) the aluminium does not tarnish as badly as silver and so maintains a high proportion of its initial properties. These single layer anti-reflectance coatings were produced by the evaporation and subsequent condensation of metal fluorides onto glass under a vacuum. Anti-reflection layers are not discussed in this work.

During the next decade various materials were assessed. However, while these displayed the required optical properties, their mechanical and environmental performances were poor, with the films being easily eroded. By the 1950's these problems of film erosion were overcome by pre-heating the glass to temperatures of 300°C before deposition. Low emissivity coatings were formed by spraying a doped solution of stannic chloride onto the hot glass. The solution oxidised immediately to form tin oxide, and was know as the pyrolytic process. This process was expensive so the initial use of low-emissivity glass was as transparent heat shields in industry. (Johnson 1991)

The costs of producing thin films on glass remained high until the 1970's when Pilkingtons patented the float glass process. This process allowed glass to be sprayed immediately after production while it was still hot.

The progress in the understanding of plastics which has occurred this century, and especially since World War II, has allowed experimentation with and the development of the deposition of thin films onto thin plastic sheets. Because plastics have a lower melting point than glass, a whole new range of deposition techniques had to be developed. 3M in the United States first used a sputtering process in 1961 to lay down aluminium on a polyester film. This process was aided by the timely development of adhesive technology. By the late 1970's 3M had established a world-wide market for retrofitted metalised films, however mechanical and chemical breakdown meant that they had a short life-span. In 1981, 3M patented a means of preventing corrosion of a silver coating by overcoating the film with ultraviolet stabilised polypropylene. Johnson (1991) has shown that these films have made a marked difference to the thermal performance of single glazing. Figure 1.7. shows a typical thin film stack produced by 3M.

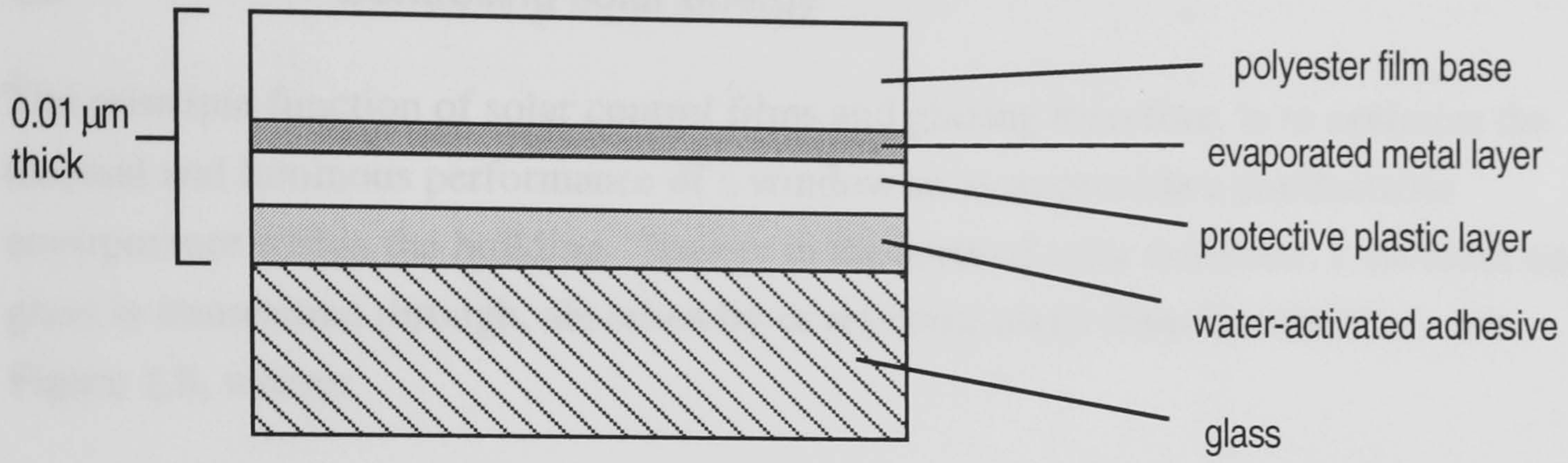

Fig.1.7 Schematic cross-section through early 3M film (Alderson 1969)

Further research led to the development of films based primarily on highly electrically conductive metals, e.g.. gold: (Au), silver: (Ag), and copper: (Cu). With the development of different deposition techniques, oxides, dielectrics - non-conducting solids - and other molecules could be considered as alternative control layers. Today many solar-control films have multiple layers which include anti-reflectance coatings, to avoid colour aberration. The desire to develop the perfect glazing material has led scientists and engineers to investigate different films and materials. Thin film research today is concentrated in the field of developing thermochromatic, electrochromatic and photochromatic films whose transmittance and reflectance properties change with respect to either the amount of sunlight incident upon them, as in the case of the photochromatic film or by the use of electronic sensors and electrical current controls for the electrochromatic films. These are the films of the future and will not be ready for some years in commercial form. Eventually the electrochromatic film could be extensively utilised in the skin of the 'intelligent buildings' of the future.

1.6 Controlling solar energy

The principle function of solar control films and glazing therefore, is to optimise the thermal and luminous performance of a window so as to provide a comfortable environment within the building. Energy in the form of solar radiation, I, incident upon glass is transmitted through, absorbed by or reflected away from the material, see Figure 1.8, where:

$$I_\lambda = I_{\lambda,\alpha} + I_{\lambda,\rho} + I_{\lambda,\tau} \qquad (1.1)$$

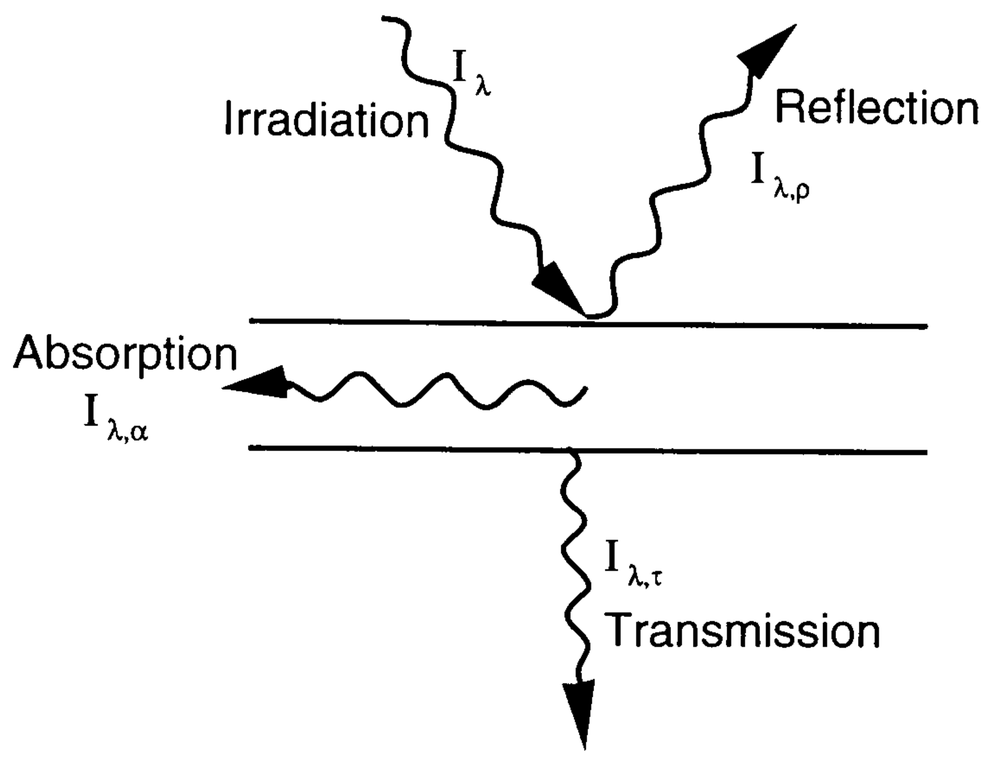

Fig 1.8 Interaction of Incident Radiation glass

These fractions of absorbed - $I_{\lambda,\alpha}$, reflected - $I_{\lambda,\rho}$ and transmitted -$I_{\lambda,\tau}$, radiation are a result of the optical characteristics of the glass and may change with respect to wavelength. This is illustrated in Figure 1.9, where for clear window glass the transmittance of visible light - 0.3-0.7μm - is allowed while ultra-violet - radiation below 0.3μm - and infra-red radiation - 2μm and above - are attenuated. At a specific wavelength - λ, the measured transmittance is designated τ_λ, and is known as the monochromatic or spectral transmittance. When the response of the material to the full spectrum of the incident radiation is considered, the transmittance, τ, is the fraction of the total irradiation, I, which falls upon the glass surface and is transmitted through the material. The transmittance is calculated as thus:

$$\tau = \frac{I_\tau}{I} = \frac{\int_0^\infty \tau_\lambda(\lambda) I_\lambda(\lambda) d\lambda}{\int_0^\infty I_\lambda(\lambda) d\lambda} \qquad (1.2)$$

Similar equations can be used to derive absorptance - α, and reflectance - ρ, from the integration of the monochromatic properties across the full electro-magnetic spectrum.

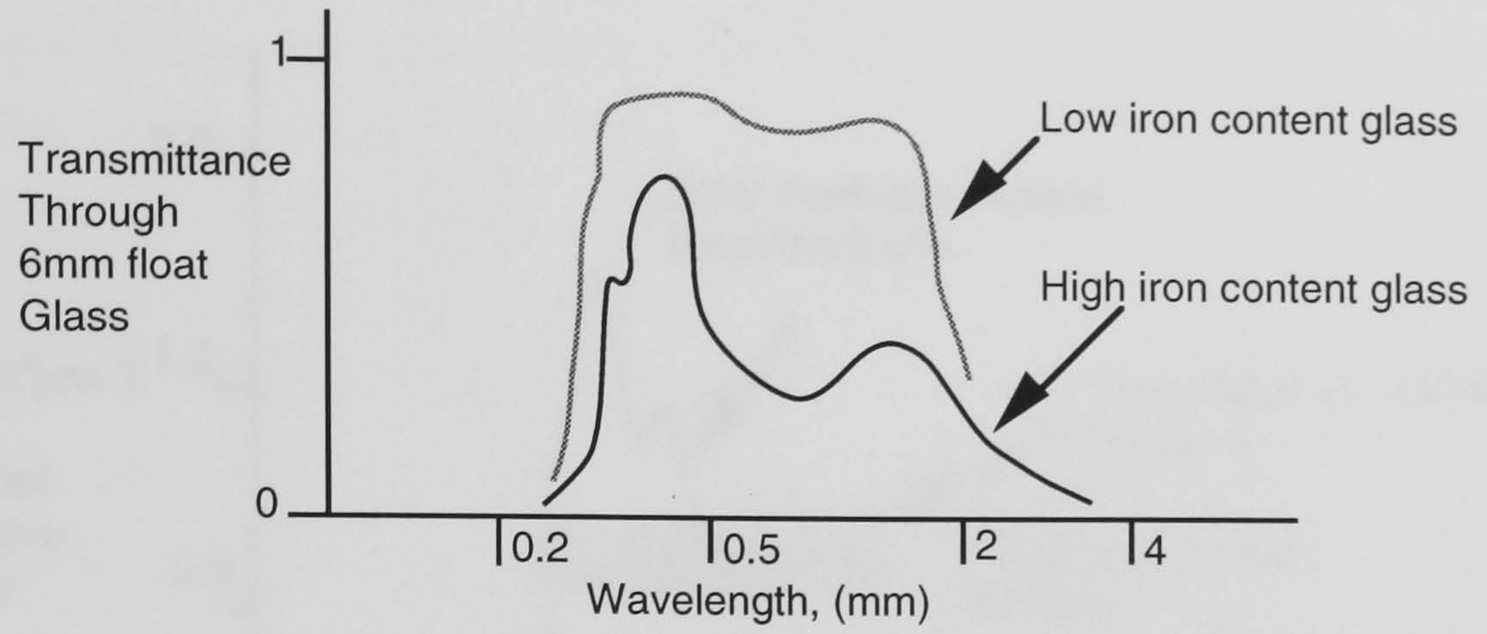

Fig 1.9 The variation of transmittance through glass with respect to wavelength

Figure 1.10 shows the variation of the spectral emissive power of the solar radiation incident upon the earth's surface and the radiation emitted by an object at a temperature of 300K. The transmittance 'window' for glass is between the wavelengths of 0.3-2μm, (see Figure 1.9). Therefore ordinary float glass will, because of its selective behaviour, allow the transmittance of visible light and near infra-red, while it is effectively opaque to thermal radiation above 2μm which includes nearly all the energy emitted at the characteristic temperatures of the earth's surface. Thus the majority of incident solar energy will be transmitted by the glass whilst it is opaque to terrestrial radiation. This process is responsible for the 'greenhouse effect' and is successfully utilised in agriculture to produce seasonally early crops. However this opaqueness means black, that is highly absorptive (Johnson 1991). The glass acts as a sponge in the presence of re-radiated far infra-red radiation. Most of this radiation is absorbed and conducted through the glass and is then radiated and convected to the external environment. Only polished metal surfaces and low-emissivity films reflect the far infra-red radiation.

One objective of solar-control films and coatings is to enhance this natural selectivity to improve the 'greenhouse' performance by trapping solar energy which has been absorbed within the building, and subsequently re-radiated, so providing passive heating. Alternatively they can be used to reduce the transmittance of incident solar radiation so that excessive over-heating can be avoided. These films - of a few molecules thick - are deposited onto the surface of the glass either directly or as part of a multi-layer film. The optical characteristics of these films are determined by their

molecular structure, surface and interface morphology and their chemical composition and homogeneity. These properties are all strongly influenced by the film preparation method.

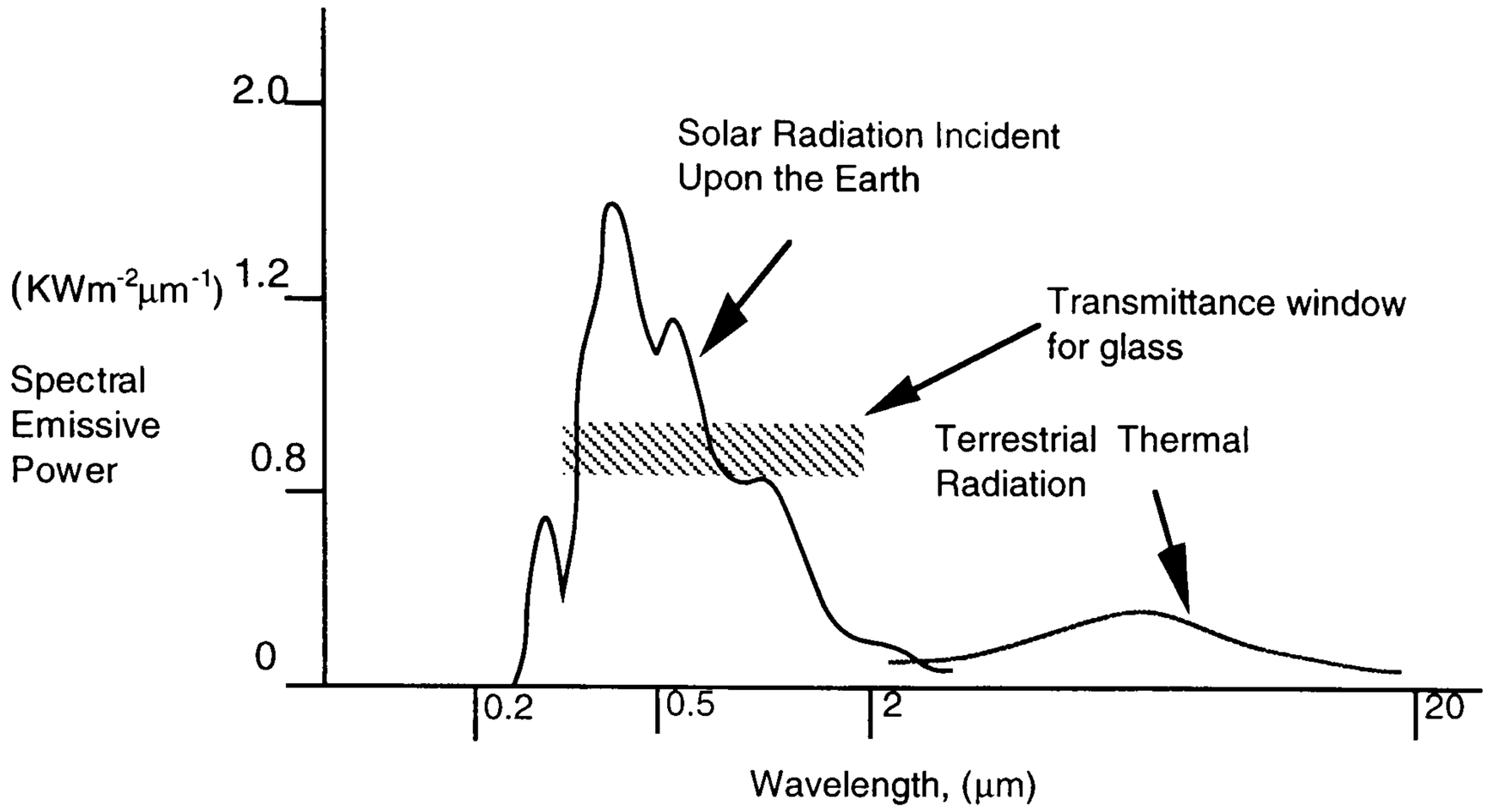

Fig 1.10 A comparison of the spectral emissive power the solar radiation incident upon the earth's surface and the radiation emitted by an object at a temperature of 300K

In order to understand how films can change the wavelength selectivity of glass, an understanding of electromagnetic radiation and how it interacts with materials is desirable.

1.7 The Theory of Light

The wave theory of light was first championed by Robert Hooke in the seventeenth century. He proposed that light consisted of rapid vibrations propagated instantaneously, or with very great speed, over any distance. His work was taken further by Christian Huygens, who suggested the principles which were subsequently named after him. Primarily he stated that every point of an "aether" upon which the luminous disturbance falls, may be regarded as the centre of a new disturbance propagated in the form of spherical waves. These secondary waves combine in such a manner that their envelope determines the wave front at any later time. This hypothesis allowed Huygens to derive the laws of reflectance, refraction and led to further study which established the principle of polarisation.

However, it was not until the nineteenth century that the wave theory was generally accepted through the work of Thomas Young, Etienne Louis Malus and Augustin Jean Fresnel. By the middle of the nineteenth century James Clarke Maxwell had taken previous work within the field of electricity and magnetism, and presented it in the form of mathematical equations which established the possibility of electromagnetic waves, having a velocity which could be calculated by utilising the electrical properties of a material. Rudolph Konlrausch and Wilhelm Weber measured these properties and by substituting their values into Maxwell's equations, calculated the velocity of the electro-magnetic radiation. This value was shown to be very similar to the measured values of the velocity of light. This led Maxwell to propose that light waves were electromagnetic waves, as was verified by Heinrich Hertz in 1888.

In parallel with the investigations into the propagation of light, work was being undertaken to explain the processes of its emission and absorption by surfaces. In 1816, Josef Frauhofer observed dark lines in the solar spectrum. These were later named after him. In 1861, Robert Bunsen and Gustav Kirchoff interpreted these lines to be the absorption of particular wavelengths in the solar spectrum. These are now known to be caused by absorption, by the hydrogen in the sun's atmosphere. The work by men like Bunsen and Kirchoff led to the acceptance that every gaseous chemical element when excited to fluorescence, possesses a characteristic line spectrum. This knowledge helped in the understanding of how electromagnetic radiation interacted with materials. However, wave theory could not explain all the phenomena observed, regarding electro-magnetic radiation.

In 1900, Planck proposed the quantum theory of radiation energy. He suggested that radiant energy could be absorbed or given off only in definite quantities called quanta. He proposed that the energy of a quantum, E, was proportional to the frequency of its radiation, ν, i.e.

$$E = h\nu \qquad \text{where h is Planck's constant, } 6.626\times10^{-34}\ \text{Js.} \qquad (1.3)$$

In 1905 Einstein proposed that Planck's quanta were discontinuous waves of energy, which were later named photons. (The basic theory of electromagnetic radiation is explained by Heavens and Ditchburn (1991) in great detail and clarity.)

The application of Planck's theory to the atomic structure led Niels Bohr to explain the simple laws of line spectra in 1913. When gases or vapours of a chemical substance are excited, light is emitted. If this light is passed through a prism a line spectrum is

produced which consists of a number of coloured lines, each representing a different wavelength of light. The line spectrum for each element is unique. The reason for these lines in hydrogen is explained by Bohr's theory. According to Bohr, the energy of the electron can exist only in certain energy shells. These shells are concentric zones at particular distances which surround the nucleus. Energy is radiated when an electron of an atom 'falls' from one shell at a particular energy level to another of lower energy. The photon emitted (which is responsible for the line spectrum) has a particular wavelength as a consequence of the energy difference between the two shells. Bohr derived an equation for the energy which an electron would have in each shell, that is, E_{shell}; where n = 1, 2, 3,... and relates to the shell number.

$$E_{shell} = -\frac{(2.179\times10^{-18}\,J)}{n^2} \qquad (1.4)$$

By using the above equation and Planck's equation, the frequency of the line spectrum could be predicted. If an electron in shell, n_o has energy E_o and the energy of the electron in an inner shell, n_i is E_i, then when it falls from the outer to the inner shell then the energy it will emit will be E_o-E_i and this gives off a photon of electromagnetic radiation with a wave motion of a specific frequency.

$$h\nu = E_o - E_i \qquad (1.5)$$

$$h\nu = \frac{(2.179\times10^{-18}\,J)}{n_i^2} - \frac{(2.179\times10^{-18}\,J)}{n_o^2} \qquad (1.6)$$

$$h\nu = (2.179\times10^{-18}\,J)\left(\frac{1}{n_i^2} - \frac{1}{n_o^2}\right) \qquad (1.7)$$

since h = 6.626x10^{-34} Js

$$\nu = \left(\frac{2.179\times10^{-18}\,J}{6.626\times10^{-34}\,Js}\right)\left(\frac{1}{n_i^2} - \frac{1}{n_o^2}\right) \qquad (1.8)$$

therefore

$$\nu = (3.289\times10^{15}\,s^{-1})\left(\frac{1}{n_i^2} - \frac{1}{n_o^2}\right) \qquad (1.9)$$

In the hydrogen atom the lines produced from the electron transitions have been grouped into series. Transitions to the innermost shell, n=1, are part of the Lyman series and produce energy of wavelengths within the ultra-violet. The transitions to the second shell, n=2 are grouped into the Balmer series. These transitions are of lower energy than the Lyman series and occur within the visible spectrum. Transitions to the

shell, n=3 are grouped into the Paschen series and are of lower energy than the Balmer series and produce energy within the infra-red spectrum, Figure 1.11. Bohr's theory accurately predicted these observed behaviours. However, this theory was soon discovered to be limited in its application and could not be applied to the other elements. Work by de Broglie and Heisenburg expanded this field. Further work by Pauli concluded that electron levels must be broadened into energy bands as atoms are brought together into solids. He also proposed an exclusion principle which states that only two electrons can exist within a given orbit. This led Schrodinger to adopt a theory of electron orbitals for atoms where electronic sub-shells existed within the orbitals. This theory allowed improved predictions of the observed nature of multiple electron elements.

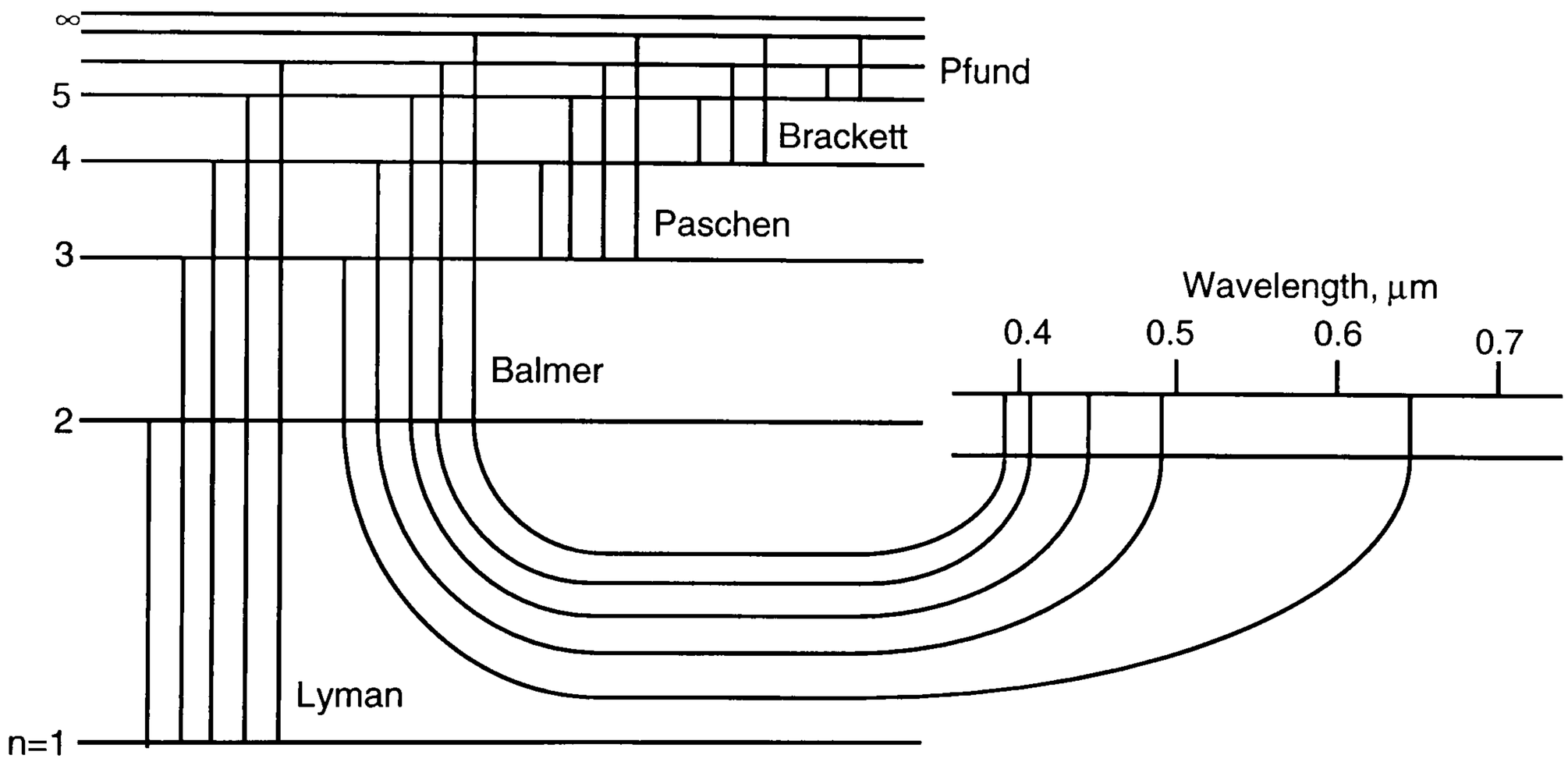

Fig 1.11 The relation between some electron transitions of the hydrogen atom and the named groups of spectral lines of the ultra-violet through to the infra-red spectral region (Mortimer 1986)

When atoms are brought together in solids with amorphous or crystalline structures the inter-atomic interactions result in energy bands rather than energy shells within which the electrons exist. These bands are a result of the bonding of the atoms with one-another to form the solid matrix. This bonding of the molecular structures occurs in terms of molecular orbitals which extend over an entire crystal. These orbitals, taken together make up what is called an energy band, with each electron orbital constituting an energy level within the band, see Figure 1.12. These levels are very closely spaced in terms of energy potential, and for all practical purposes form a continuous energy

band, allowing electrons to occupy energy levels between those of the band's boundary potentials. Even at low temperatures, electrons have enough energy to move from level to level within a band.

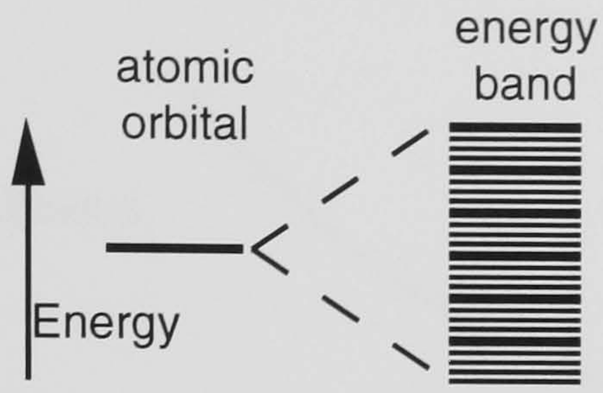

Fig 1.12 Formation of an energy band by the interaction of atomic orbitals in an atom (Mortimer 1986)

However, the orbitals of an atom can only hold a certain number of electrons. When an electron is in an orbital and cannot move to a lower orbital because it is full, that electron is said to be at ground state. The electrons at ground state in the outermost occupied orbital are known as valance electrons. This orbital is called the valance band. Beyond the valence band is an empty band which is known as the conduction band. If a material has a band gap, which is also referred to as a forbidden energy zone, between a completely filled valance band and the empty conduction band, then the material is a non-conductor, that is, an insulator or a semiconductor. The insulators are characterised by a large band gap while the semiconductors have a narrow band gap. If the valence band is partially filled or overlaps the conduction band, then this material is known as a conductor. This is explained in Figure 1.13. All metals are conductors.

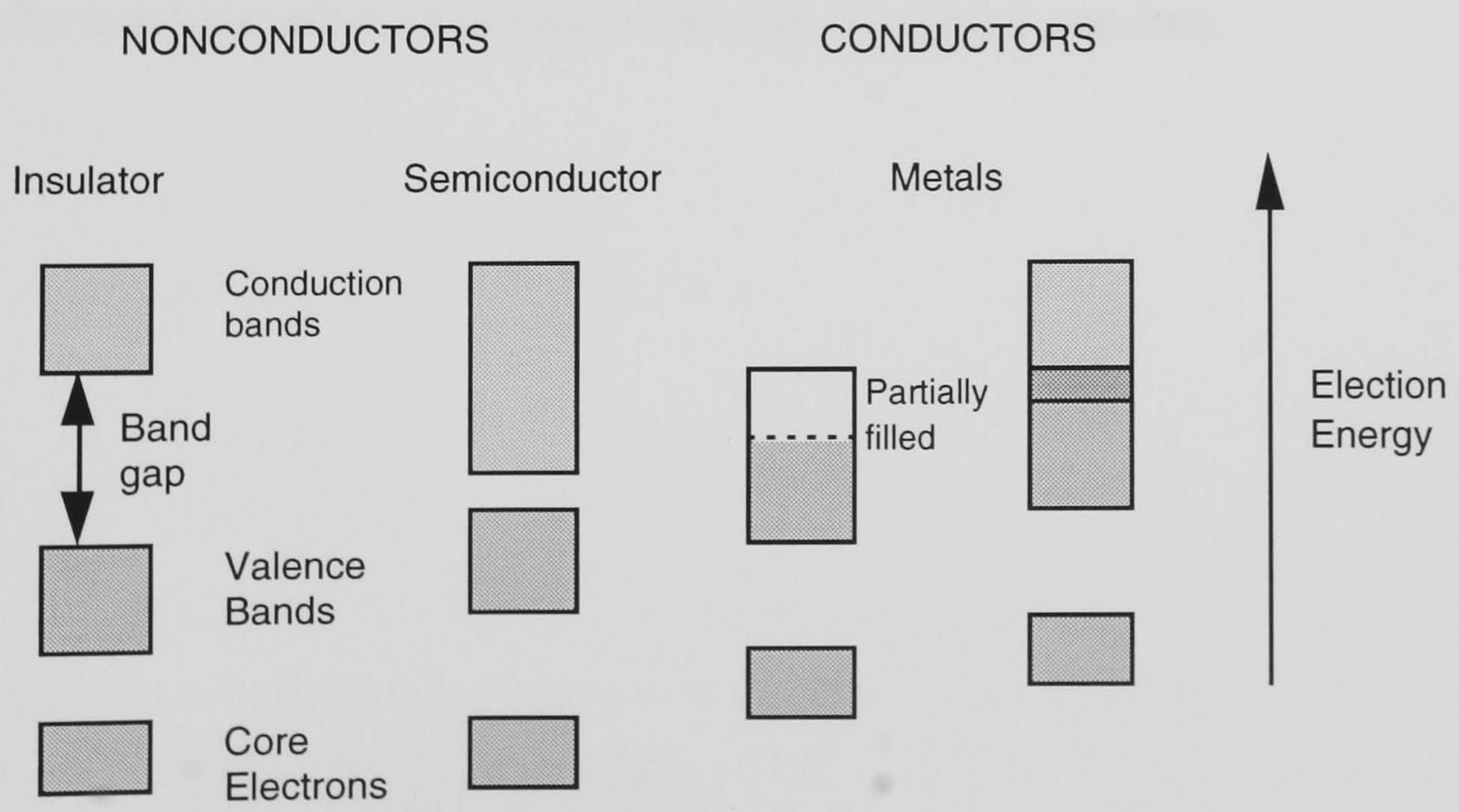

Fig 1.13 Electron energy bands and band gaps in a solid (Modest 1993)

The relative widths of the allowed bands and forbidden bands depend upon the elements involved and the distance between the adjacent atoms in the lattice. From Figure 1.14 it can be seen that as the interatomic distance is increased so the valence and conduction bands cease to overlap.

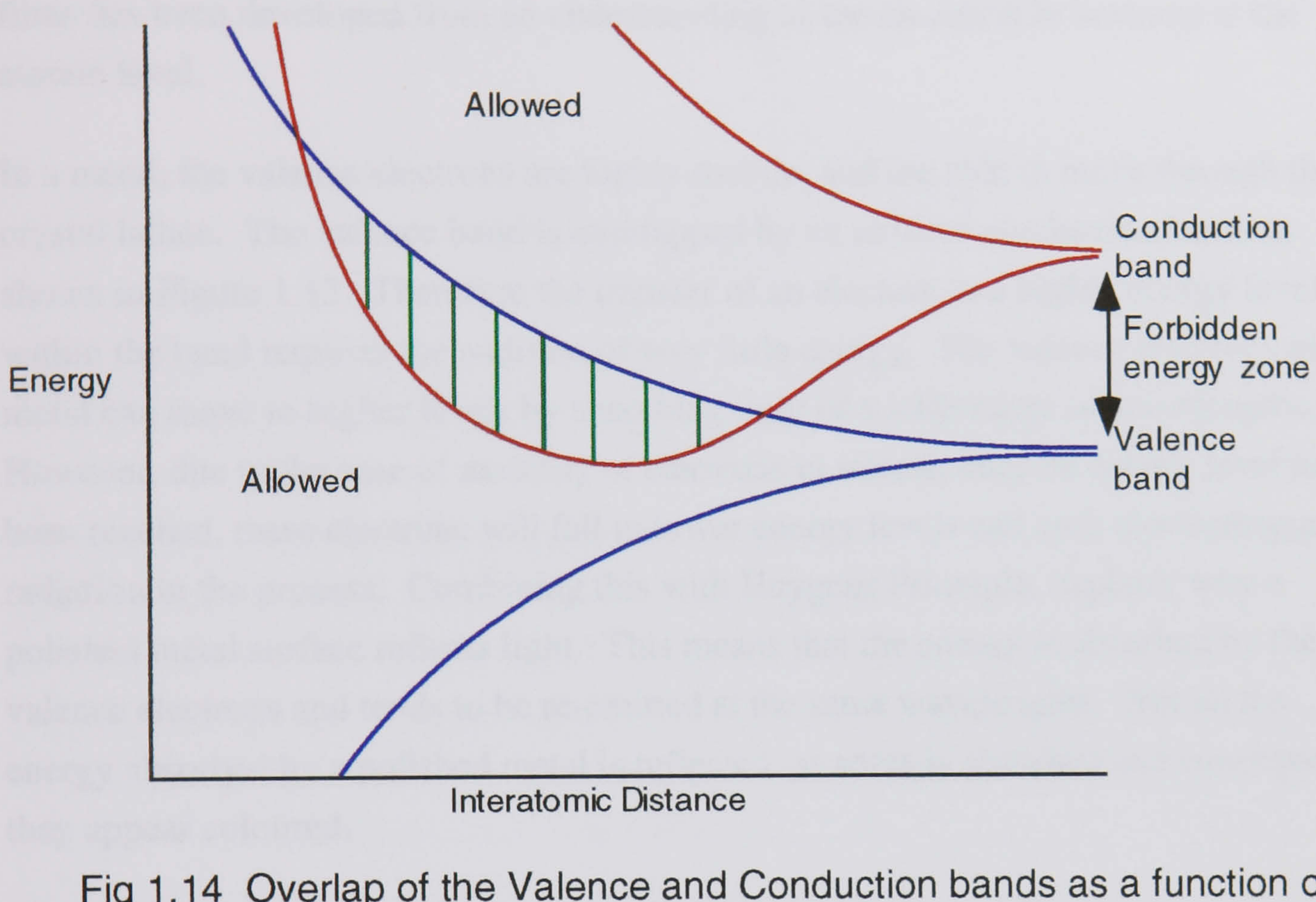

Fig 1.14 Overlap of the Valence and Conduction bands as a function of interatomic distance (de Waard & Lazarus 1966)

Materials where these bands cease to overlap tend to be non-metallic in nature and are poor electrical conductors due to the large energies needed to promote an electron into the conduction band where it can move through the crystal structure.

1.8 Metallic, Dielectric and Semiconductor Substances

With regard to their electrical conductivity, materials can be classified in two types -metals and non-conductors - the latter being further split into semiconductors and electrical insulators, sometimes referred to as dielectrics. The physics of solar-control films has been developed from an understanding of the electrical behaviours at the atomic level.

In a metal, the valence electrons are highly mobile, and are able to move through the crystal lattice. The valence band is overlapped by an unfilled conduction band, as shown in Figure 1.13. Therefore the transfer of an electron to a higher energy level within the band requires the addition of very little energy. The valence electrons of a metal can move to higher levels by absorbing light of a wide range of wavelengths. However, due to the ease of mobility of electrons in metals, once an energy level has been reached, these electrons will fall to lower energy levels and emit electromagnetic radiation in the process. Combining this with Huygens Principle, explains why a polished metal surface reflects light. This means that the energy is absorbed by the valence electrons and tends to be re-emitted at the same wavelengths. Not all the energy absorbed by a polished metal is reflected, as some is absorbed and consequently they appear coloured.

The mobile electrons in the valance band of the metal are known as free electrons. These free electrons are collectively known as the electron plasma. When the metal absorbs radiation, this plasma will vibrate, and depending upon the frequency of the absorbed radiation, it will either be reflected or transmitted. The frequency at which this transition occurs is known as the critical frequency, ω_p. If the frequency, ν, of the absorbed radiation is less than ω_p, then reflectance will occur, while if ν is greater than ω_p, then transmittance will occur (Main 1978). The value of ω_p can be calculated from the known atomic characteristics of the metal:

$$\omega_p = \frac{Ne^2}{\varepsilon_\infty \varepsilon_o m^*} \tag{1.10}$$

where e is the charge of an electron, N is the volumetric electron number density, m^* is the effective mass of a free electron in the plasma, ε_0 is the dielectric permittivity for vacuum and ε_∞ is the relative permittivity of the vacuum for $\nu \rightarrow \infty$. The relationship between the wavelength and the reflectivity of a metal, with respect to the critical frequency ω_p, can be seen schematically in Figure 1.15.

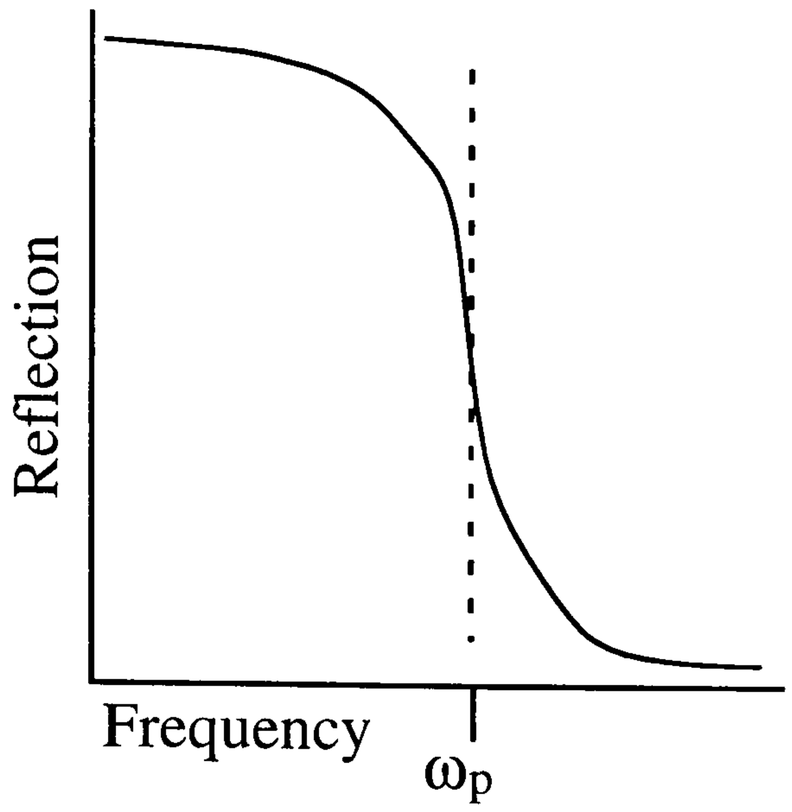

Fig 1.15 The relationship of the critical frequency ω_p to the reflectivity of a metal with respect to frequency of electromagnetic radiation

Therefore the transition from transparency to opacity of a thin metal film is a cut-off phenomenon, with most metals having a critical frequency in the ultra-violet. At wavelengths above the critical frequency, the thin metal film becomes opaque. The transmittance of visible light through thin metal films is a consequence of it being only of the order of a few molecules thick, and allowing the light to pass through the lattice structure. Once the critical frequency and the frequency of the electron vibrations - ω_e - are known, then the refractive index of the metal can be determined:

$$N = \sqrt{1 - \frac{\omega_p^2}{\omega_e^2}} = n - ik \qquad (1.11)$$

in which N is known as the complex index of refraction, n is the real part of the refractive index while k is the imaginary part and is also known as the absorption index. From the absorption index, the absorption coefficient, κ, can be determined. The absorption coefficient is a measure of how deeply the energy can penetrate into a substance and its units are m^{-1}.

Modest, (1993) showed that n and k could be determined by applying Maxwell's equations to the equation N = n - ik. This produces the following definitions for n and k;

$$n^2 - k^2 = \varepsilon\mu c_o^2 \qquad (1.12)$$

and,

$$nk = \frac{\sigma_e \mu \lambda_o c_o}{4\pi} \tag{1.13}$$

where ε is the electrical permittivity, μ is the magnetic permittivity, c_o is the phase velocity, σ_e is the electrical conductivity and λ_o is the wavelength for the wave in the vacuum, which is equal to ν/c_o where ν is the frequency of the wave. Equations (1.12) and (1.13) may be solved for the refractive index, n, and the absorptive index, k, as shown by Modest (1993);

$$n^2 = \frac{1}{2}\left[\frac{\varepsilon}{\varepsilon_o} + \sqrt{\left(\frac{\varepsilon}{\varepsilon_o}\right)^2 + \left(\frac{\lambda_o \sigma_e}{2\pi c_o \varepsilon_o}\right)^2}\right] \tag{1.14}$$

$$k^2 = \frac{1}{2}\left[-\frac{\varepsilon}{\varepsilon_o} + \sqrt{\left(\frac{\varepsilon}{\varepsilon_o}\right)^2 + \left(\frac{\lambda_o \sigma_e}{2\pi c_o \varepsilon_o}\right)^2}\right] \tag{1.15}$$

From Equation (1.15) it can be seen that a large absorptive index corresponds to a large electrical conductivity, σ_e. This shows how good conductors, for example metals, tend to attenuate the transmittance of electromagnetic waves such as light better than a material with poor electrical conductivity such as an insulator. Howson et. al. (1981) showed how possible changes in the relaxation time and the plasma frequency can determine the relationship between the electrical and the visible optical properties.

Insulators are sometimes called dielectrics. A dictionary, definition of dielectrics is that they are materials which can withstand electrical stress, but which can also transmit electrical effects without conducting. In a dielectric, the valence band is completely filled and there is a wide band gap. This is sometimes called the forbidden energy zone, between the valence and the adjacent conduction band. The filled valence band and the large band gap inhibit the electron motion which is needed for conduction. Hence they are good insulators. Movement of electrons into the conduction band is possible only if a large energy (~4-9eV) is provided to promote electrons across the large band gap to the conduction band. Therefore considering Equation 1.15, dielectrics tend to be transparent and reflect weakly, photons of energy, with energies less than the band gap. Energy in the infra-red section of the electromagnetic spectrum tends to be absorbed with the photons causing an increase in internal energy through an increase of the lattice vibration. Dielectrics have a high transmittance and are used in stacks to produce anti-reflectance or high reflecting surfaces, depending on their thickness and the number of layers used. This effect will be looked at more closely in Chapter 2.

The refractive index for a dielectric can be determined from the Lorentz-Lorenz correlation. This correlation shows the relationship between a material's refractive index, its density - ρ, and the molecular weight -M:

$$\left(\frac{n^2-1}{n^2+1}\right)\frac{M}{\rho}=\frac{4\pi}{3}\frac{A\alpha_e}{\varepsilon_s} \tag{1.16}$$

where A is Avagadro's number, α_e is the average electronic polarisability of the dielectric molecule and ε_s is the dielectric constant of free space. From the above, it can be seen that the refractive index increases with density.

Semiconductors are materials with a low electrical conductivity. For a semiconductor, the forbidden zone is sufficiently narrow so that electrons can be promoted from the valence to the conduction band by, for example, heat. The vacancies left by the removal of electrons from the valence band, allow the electrons remaining to move under the influence of an electric field, therefore conduction takes place through the motion of electrons in both the valence and conduction bands. The addition, or doping, of small traces of certain impurities to semiconductors enhances the conductivity of these materials. The impurity is an element similar in nature to the semiconductor material but having either one less or one extra electron in the valence band. Where an element is used with one less electron, this creates an electron vacancy within the valence band. This results in the addition of a thin, empty energy band just above the filled valence band, and promotion of electrons to this band requires comparatively little energy. Where an element containing one extra electron is added to the semiconductor, the extra electron acts like a conduction electron. Its energy band is just below the empty conduction band, and the electrons in this band are easily excited into the conduction band. A consequence of the energy bandgap in semiconductors is that the material allows good transmittance of electromagnetic radiation throughout the visible spectrum. Doping increases the metallic nature of the semiconductor and its electrical conductivity, giving good reflectance at the infra-red frequencies.

1.9 Interaction of Radiation with Glass

The previous two sections consist of an explanation of the theory of how electromagnetic radiation interacts electrically with materials at the molecular level. By using this information, an understanding of how different films can change the optical characteristics of glass can follow.

Glass is naturally a selective material, and an understanding of how it interacts with electromagnetic radiation helps in deciding which films are needed to enhance this inherent property. Its characteristics can be modified by adding various substances during its production. Figure 1.16 shows schematically the curve of transmittance verses wavelength for glass. Three main regions can be considered. Region I occurs in the ultra-violet part of the spectrum. Most ultra-violet radiation is absorbed by electronic transitions from one energy band to another. The point at which the energy quantum of a photon becomes too large for the electrons to be absorbed is called the 'Fundamental Absorption Edge', see Figure 1.16. For glass, the limit of transmittance in the ultra-violet is determined by the ferrous oxide (Fe_2O_3) content, which causes maximum absorption in the near ultra-violet. The inclusion of alkaline or alkaline-earth cations in the glass, shifts the fundamental absorption edge to longer wavelengths, as the valance electrons are more easily excited due to weaker oxygen bonds within the atomic structure.

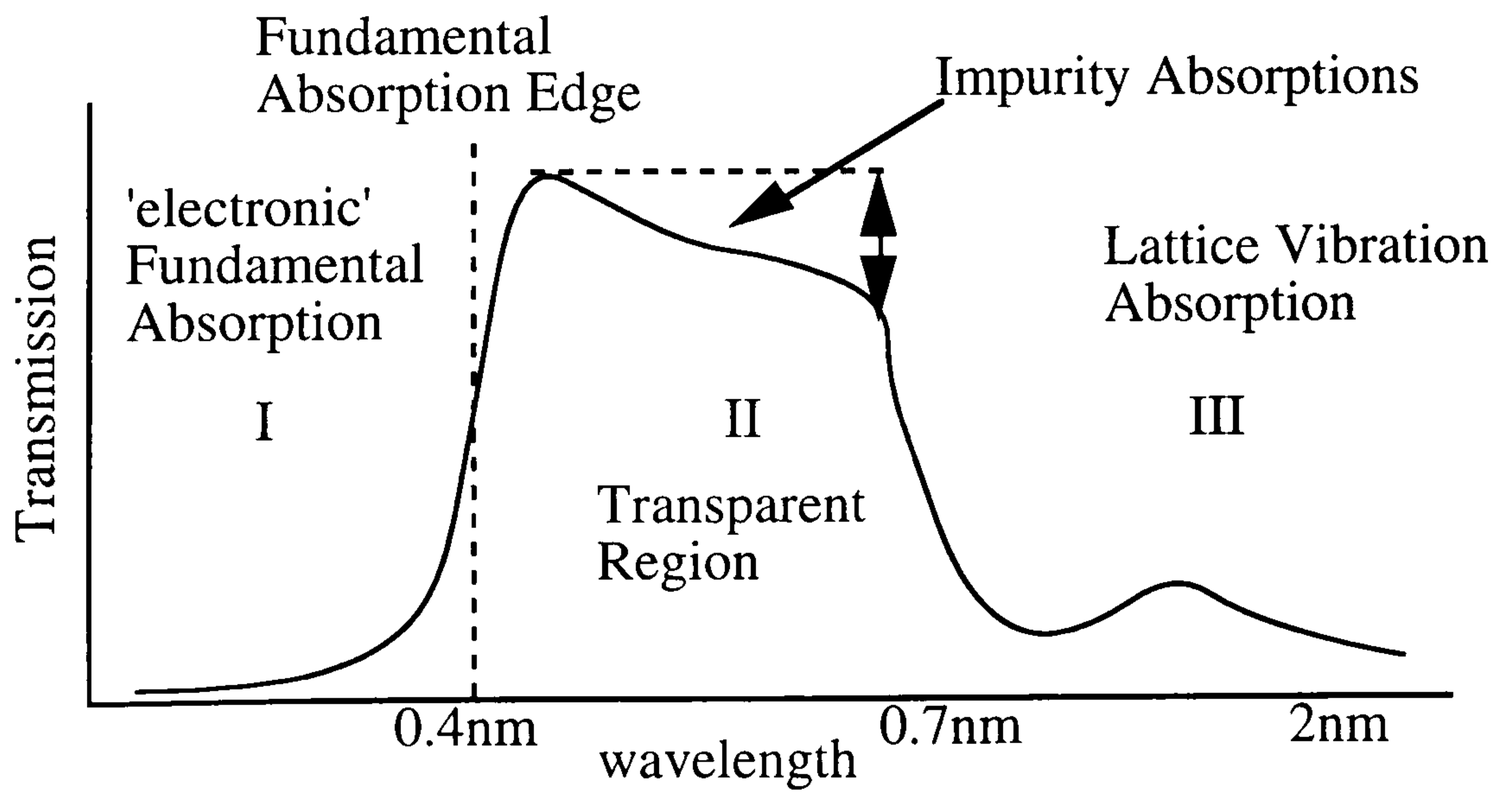

Fig 1.16 Schematic curve of transmittance verse wavelength of glass (Pulker 1984)

The second region, II, is where high transmittance occurs and corresponds to the visible section of the solar spectrum. Within this region, the energies of the electromagnetic quanta are too high to be absorbed by the electrons, but they are also too low to cause lattice vibrations and so they are transmitted through the solid. There may be some loss of transmittance here due to particular impurities, with the extent of the loss depending strongly upon the proportion of additional compounds such as iron oxides. The third region, III, corresponds with the long wave infra-red radiation. Within this region the energy is absorbed as the wavelengths are greater than the interatomic distances. The absorbed energy then causes lattice vibrations within the molecular structure of material. These vibrations occur at high frequencies and are determined by the relative molecular weight, bond strengths and lattice geometry of the material. In glass the cut-off point where the energy is no longer transmitted, but rather absorbed or reflected, is determined by its ferrite (FeO) content which has strong absorption at the wavelengths of 1μm and upwards. A higher absorption can be obtained in this region by the use of dielectric materials with high molecular masses and greater interatomic distance, so that absorption occurs at longer wavelengths and the lattices vibrate at lower frequencies.

1.10 Thin Films on Glass

There are many different types of materials and compounds used to construct solar-control films. Copper, gold, aluminium and silver have critical frequencies in the near ultra-violet and so have a high reflectance in the visible region of the electromagnetic radiation. This is demonstrated in Equation (1.10) and Figure (1.15). Such a metallic layer needs to be very thin (~30nm) in order to permit transmittance in the visual spectrum. Discontinuities in this layer sometimes occur during manufacture, thereby leading to reductions in the films' selective properties. The use of the sputtering process in production has diminished these problems, producing thin continuous films with a smooth surface. These metal films are very soft and can be easily damaged, causing difficulty with handling. The transition waveband from low to high reflectance for metal films generally occurs in the visible or ultra-violet part of the spectrum. If a dielectric such as tin oxide is used on either side of the thin metal layer, the transition waveband can be moved into the infra-red while the oxide helps reduce ultra-violet transmittance, see Figures 1.17 and 1.18.

This dielectric/metal/dielectric assembly is known as an 'optical interference stack'. The dielectric is known as a "high-index optical-matching layer". It can act as an anti-reflectance layer, if the thickness is controlled, to promote destructive interference in radiation reflected at its surfaces. The properties of the dielectric depend upon the absorption characteristics of the oxide layers, its thickness and its refractive index when a stack is constructed to increase visible transmittance, and reflectance in the infra-red. Compounds used include Bi_2O_3, In_2O_3, SnO_2, TiO_2 , ZnO and ZnS. Where single layer metal films are required, aluminium is preferred to silver, as the silver degrades significantly when exposed to sulphur containing atmospheres, thereby reducing its usefulness. Aluminium films, after an initial oxidation, maintain a high reflectivity with the oxidised layer (Al_2O_3) forming a glass-like protective film.

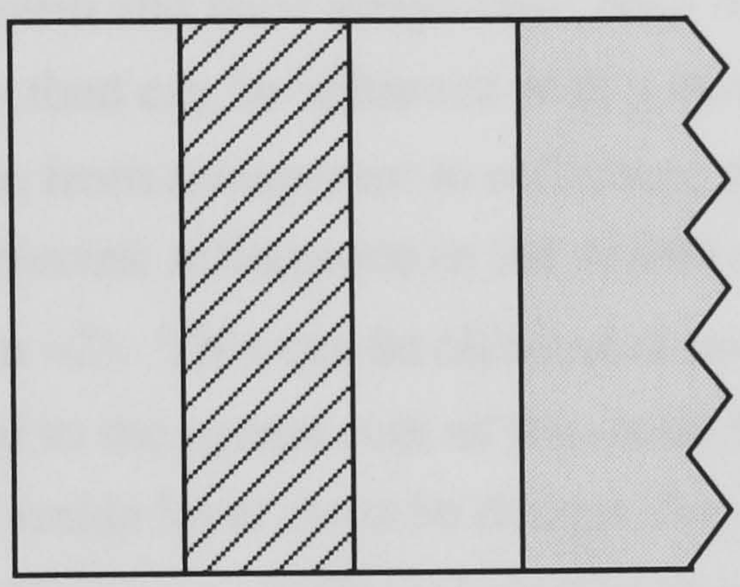

Fig 1.17 The construction of a three layer, dielectric/metal/dielectric mirror.(Howson 1988)

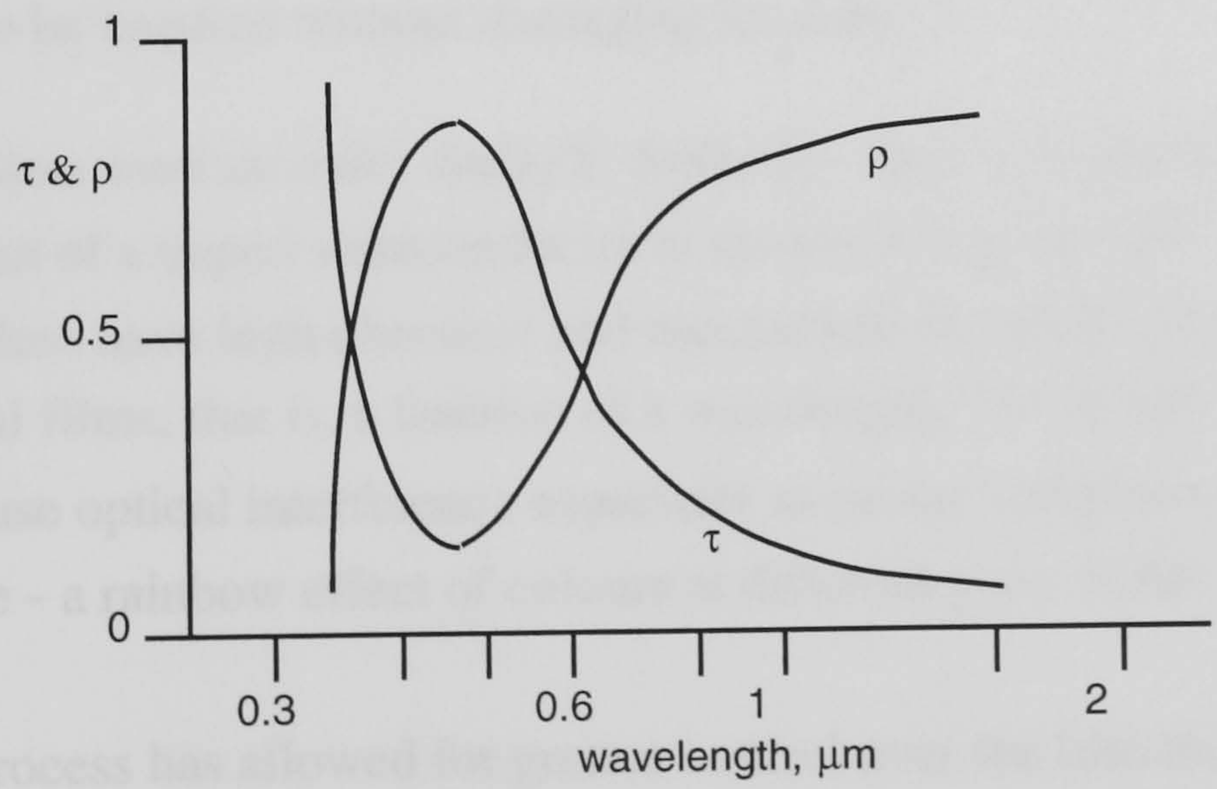

Fig 1.18 The performance of a three layer, dielectric/metal/dielectric mirror.(Howson 1988)

Nitrides of Group IV transition metals such as titanium and zircon have also been used to produce solar control films. They have better mechanical stability and chemical durability characteristics when compared with metal films, and have similar optical properties. However, they are less effective in inhibiting the transmittance of infra-red radiation. Georgson, Roos and Ribbing (1991) have improved the solar-optical properties of nitride films by placing them in a multi-layer stack, between layers of titanium oxide. However, if the deposition temperature was allowed to go above 300°C, a reduction in the optical performance occurred due to oxidation growth on the outer TiN-TiO_2 interface. They suggested that this could be remedied by the inclusion of an aluminium layer 2-4nm thick, between these two layers in order to hinder oxidation.

Oxides of indium, tin, cadmium and their alloys have been employed successfully and result in greater reflectances than can be achieved with a mono-molecular metal layer or a nitride film, with transition from transparent to reflecting behaviour occurring around 2μm. They show strong dielectric reflectance in the visible spectrum associated with their high refractive index (n ~2). This can be eliminated using anti-reflectance layers with a refractive index equal to the square root of the oxide layer and a thickness equal to λ/4. However, the metal-oxide layer must be thicker than that for metals in order to achieve similar infra-red reflectances. Such an increase in thickness leads to the occurrence of colour patterns in the visible waveband, due to spectral interference which changes with the viewing angle. To avoid this, thicker layers with multiple wavelength reflecting peaks can be used which are seen as 'white'. The oxide films exhibit high mechanical and chemical stability because they maintain their polycrystalline - bulk properties - when deposited. This allows the composite system of glass plus film, to be handled without damaging the film.

Semiconductor films used include: SnO_2:F, SnO_2:Sb, In_2O_3:Sn and ZnO:Al. A schematic diagram of a doped semiconductor is shown in Figure 1.19. These semiconductor films have high chemical and mechanical durability and need to be thicker than metal films, that is, a fraction of a wavelength, λ/4 or λ/8. However, this thickness can cause optical interference especially as minor variations in thickness may cause iridescence - a rainbow effect of colours at different parts of the film.

The sputtering process has allowed for greater control over the film thickness. Hartig et al.(1987), demonstrated that a greater amount of visible light could be transmitted without ultra-violet and infra-red radiation, by replacing the dielectric in the silver "sandwich" - see Figure 1.17 - by two layers of indium tin oxide (ITO). Further work

by Karlsson et.al. (1988) showed that semiconductor coatings gave the best contribution to the net energy gain of a window when under insolation. The ITO has been shown to be stable under typical environmental conditions; it is resistant to chemical attack and has good mechanical properties. It has a high transmittance in the visible region of the spectrum, and exhibits a drop in transmittance to around 8-10% below that of uncoated glass, whereas reflectance of room temperature thermal radiation has been quantified at 92% compared with approximately 80% for uncoated glass (Pulker 1984).

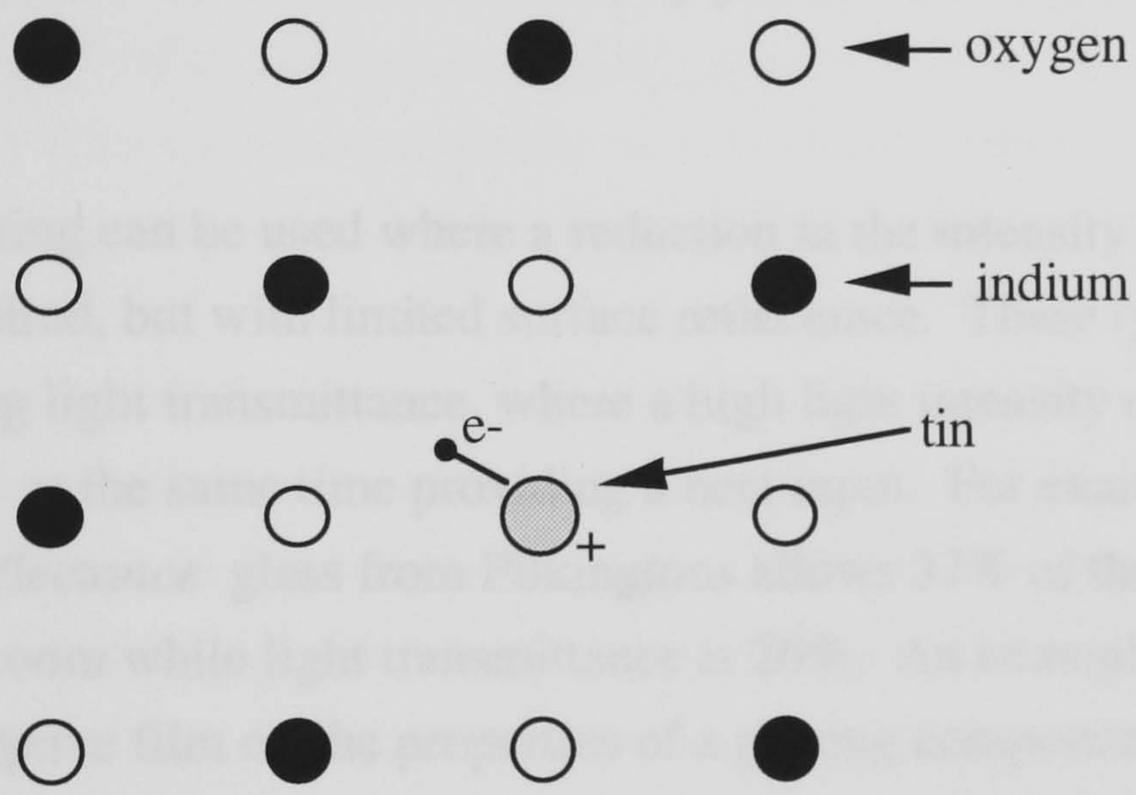

Fig 1.19 Oversimplified crystals structure model for Indium-Tin Oxide (In_2O_3:Sn) (Granqvist 1991)

Therefore the choice of material depends upon the intended application for which the film is needed. The manufacturing process can also influence the types of material which may be used.

1.11 Absorptive, Reflective and Insulation Films

The choice of material used for a thin film is dependent upon its required function. As can be seen from the previous section, glass itself displays selective behaviour. However, in certain cases there is a need to enhance its selectivity. Fig 1.20 shows the solar radiant heat gain through a sheet of 4mm clear float glass. A high transmittance of 0.86 for the total solar radiation is exhibited, while the figure for the visible part of the spectrum is slightly higher at 0.89. These high values for solar radiant heat and light transmittance for window glass can cause discomfort from glare and overheating as previously discussed. Solar-control films may provide the wherewithal to overcome these problems.

An absorptive coating can be used where a reduction in the intensity of radiation being transmitted is required, but with limited surface reflectance. These types of films can also aid in reducing light transmittance, where a high light intensity can cause visual discomfort, whilst at the same time providing a heat input. For example, a 6mm sheet of Suncool *low-reflectance* glass from Pilkingtons allows 37% of the incident solar radiation into the room while light transmittance is 26%. An example showing the effects of an absorptive film on the properties of a glazing component can be seen in Figure 1.21. Absorptive films are made of metals, alloys and oxides, and depend upon the density of the material and its thickness for limiting transmittance. As the electrical conductivity increases so the absorptive index increases, see Equation 1.15, and with increasing thickness, this limits transmittance and increases absorptance as will be discussed in Chapter 2.

Reflective films describe their purpose exactly, see Figure 1.22. They are primarily constructed using a metal film. As shown in Equation 1.10 and Figure 1.15, most metals such as gold, copper and silver have a critical frequency in the ultra-violet and so are highly reflective to the longer wavelengths of visible light. The transmittance of light which does occur, is a result of the thinness of the film, and the consequent gaps allowing the incident radiation to pass through the film.

Insulating films are used to reduce thermal loss from the room through the window, while retaining a good visible transmittance, and therefore they cannot be classed as solar-control films. It does this by almost eliminating outward heat transmittance by long wave radiation as shown in Figure 1.23. Insulating films are also called low-emissivity films. Low-emissivity is defined in the 1990 edition of the Building

Regulations - Part 2 Conservation of Fuel and Power (Note (a) Para 1.8), as: "glass with a coating or film which has an emissivity of less than 0.2 and relates to longwave, that is, infra-red emission". The insulating properties can also be incorporated within solar-control films such as the Courtaulds film E1235, which has a low transmittance. Figure 1.24 shows the solar-control performance of a film similar in nature to E1235.

In most cases a low-emissivity film is used to minimise condensation, reduce heat loss and to improve the thermal comfort of the internal environment in close proximity to the window. This is achieved while maintaining a high visual transmittance, see Figure 1.23. This diagram shows that heat loss is reduced by decreasing the amount of thermal radiation which is emitted by the internal glazing into the cavity. The characteristics of an indium-tin oxide film are most frequently used to achieve this purpose. Examples of low-emissivity coatings are Pilkington K Glass and Kappafloat.

It is clear from Figure 1.21 that there is only a slight reduction in the transmittance and reflectance of visible light when Pilkington K glass is used. However, the U-value from the double glazed unit is reduced from 2.8 to 1.9 W/m^2K. The reduction in light transmittance in the glazing system containing the Pilkington K glass, is compensated by an increase in the amount of solar energy which is retained in the inner pane. This is radiated to the room as thermal radiation, giving a total solar thermal transmittance near to that for an ordinary double glazed system. Coatings such as Pilkingtons K, which are used for insulating purposes only, are usually neutral in colour in order to provide maximum light transmittance.

The energy absorbed heats up the glazing system. At steady-state, the glass wil radiate to the internal and external enviornments the same amount of energy that it absorbs. Yellot (1983) stated that the proportion of the absorbed energy that is radiated to the indoor and outdoor environments are approximately 275 and 73% respectively.

Films can also be used to colour glass for architectural uses, or materials can be added to the glass and its surface during manufacture, to achieve the same purpose. Nickel, chromium, palladium, platinum and rhodium give a neutral colour, silver and aluminium give a blue colour, gold and copper give green or a blue-green whereas antimony and titanium give brown and grey brown respectively. Oxide films tend to create a brown colour.

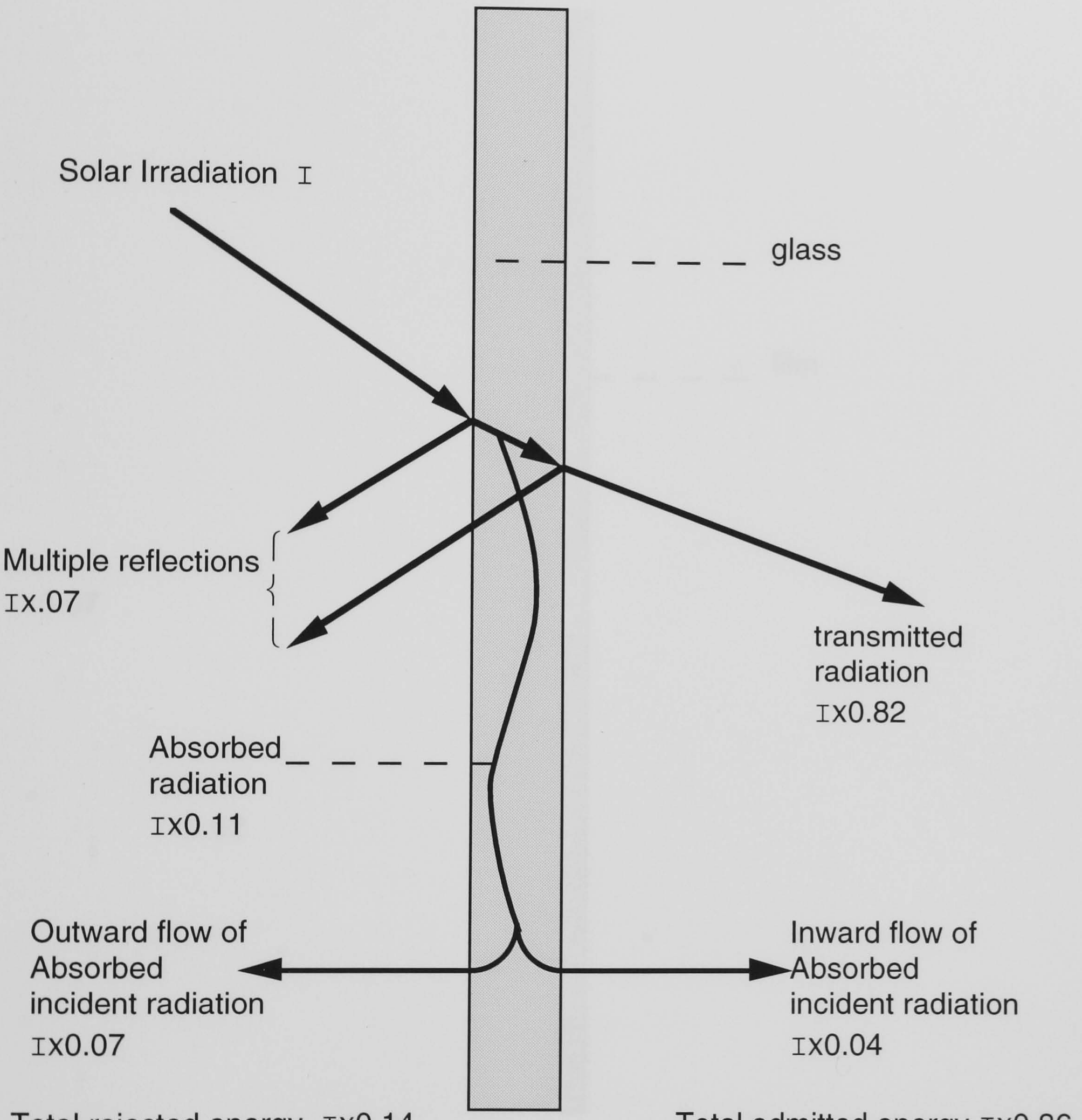

Fig 1.20 Schematic diagram of energy transmittance through 4mm float glass.

In practice, multiple reflections will occur within the glass, though only the overall effect is shown in this, and the following four diagrams.

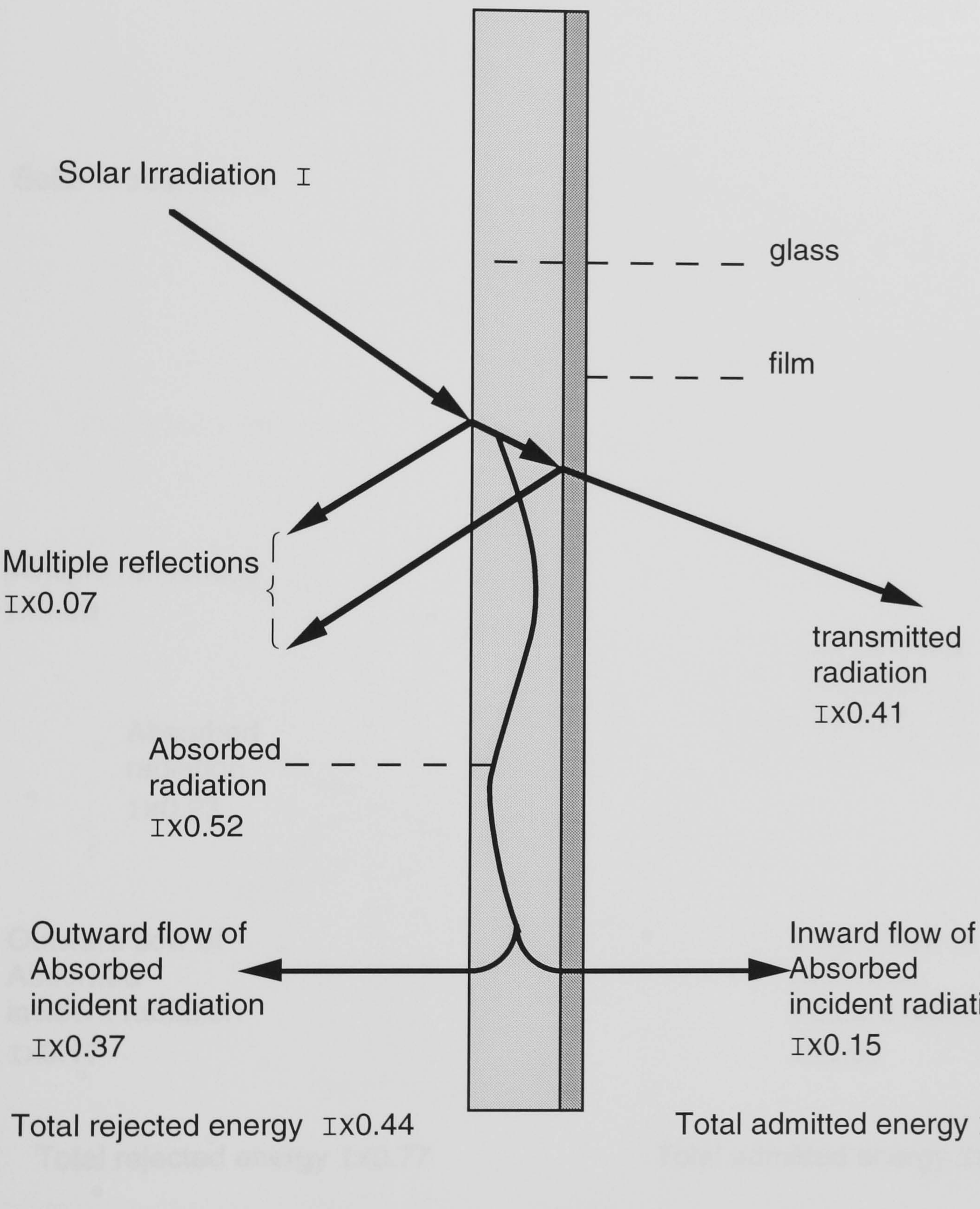

Fig 1.21 Schematic diagram of energy transmittance through glass with a typical absorptive film.

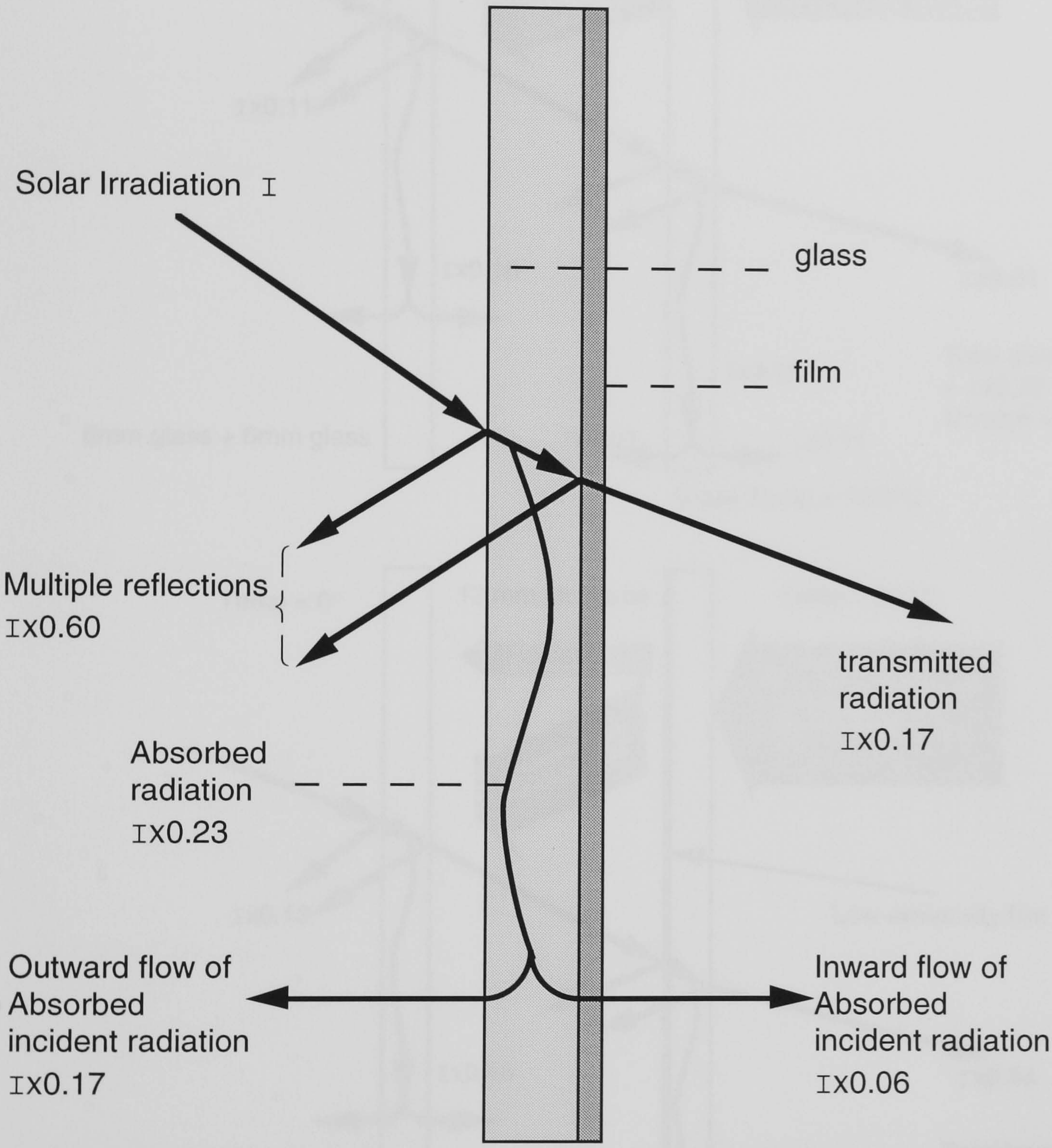

Fig 1.22 Schematic diagram of energy transmittance through glass with a typical reflective film.

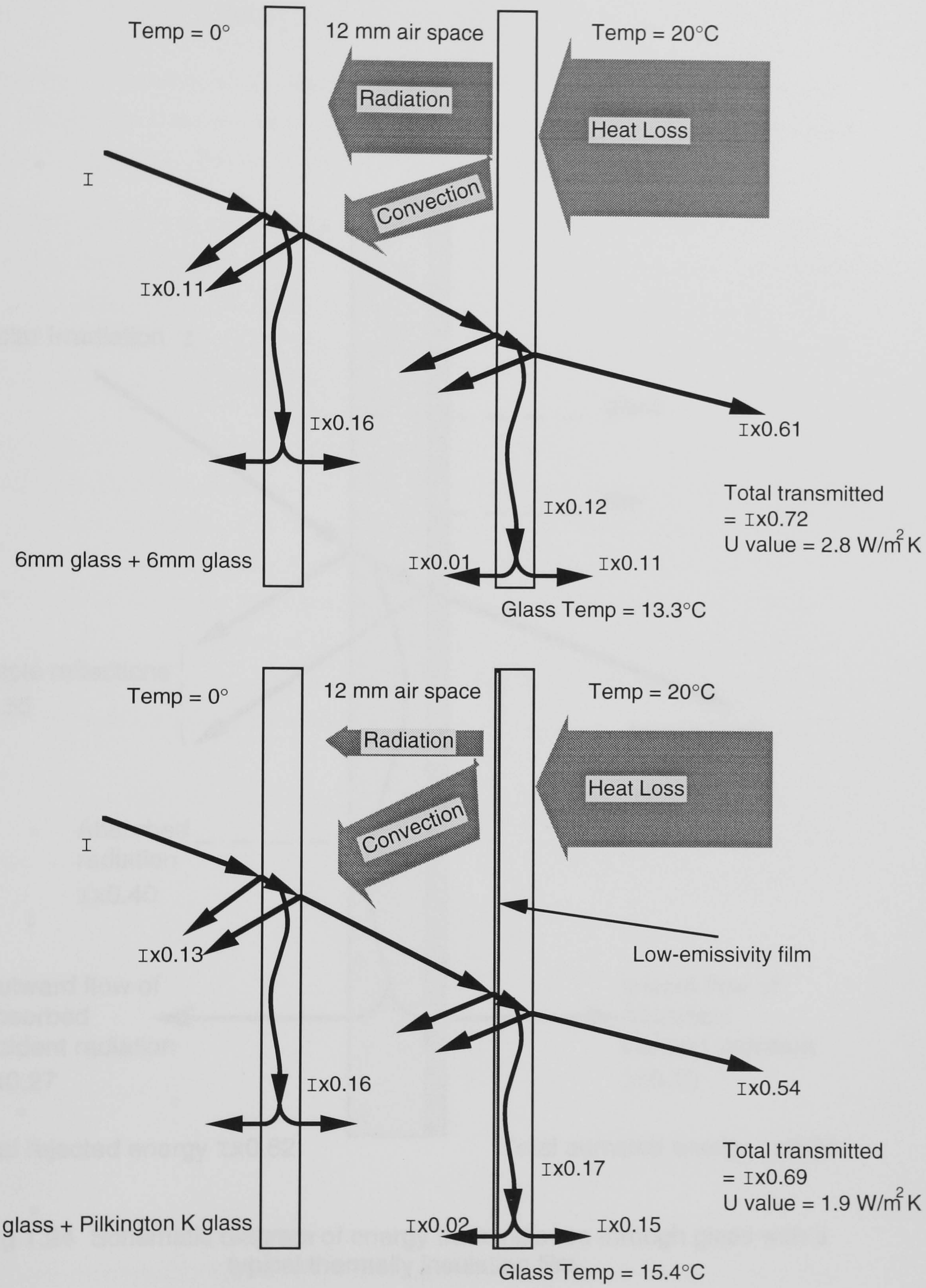

Fig 1.23 Schematic diagram of heat loss and solar transmittance across a double glazed cavity, with and without a low-emissivity coating. (The total transmittance is a combination of the directly transmitted light and the energy radiated off the inner pane into the room).

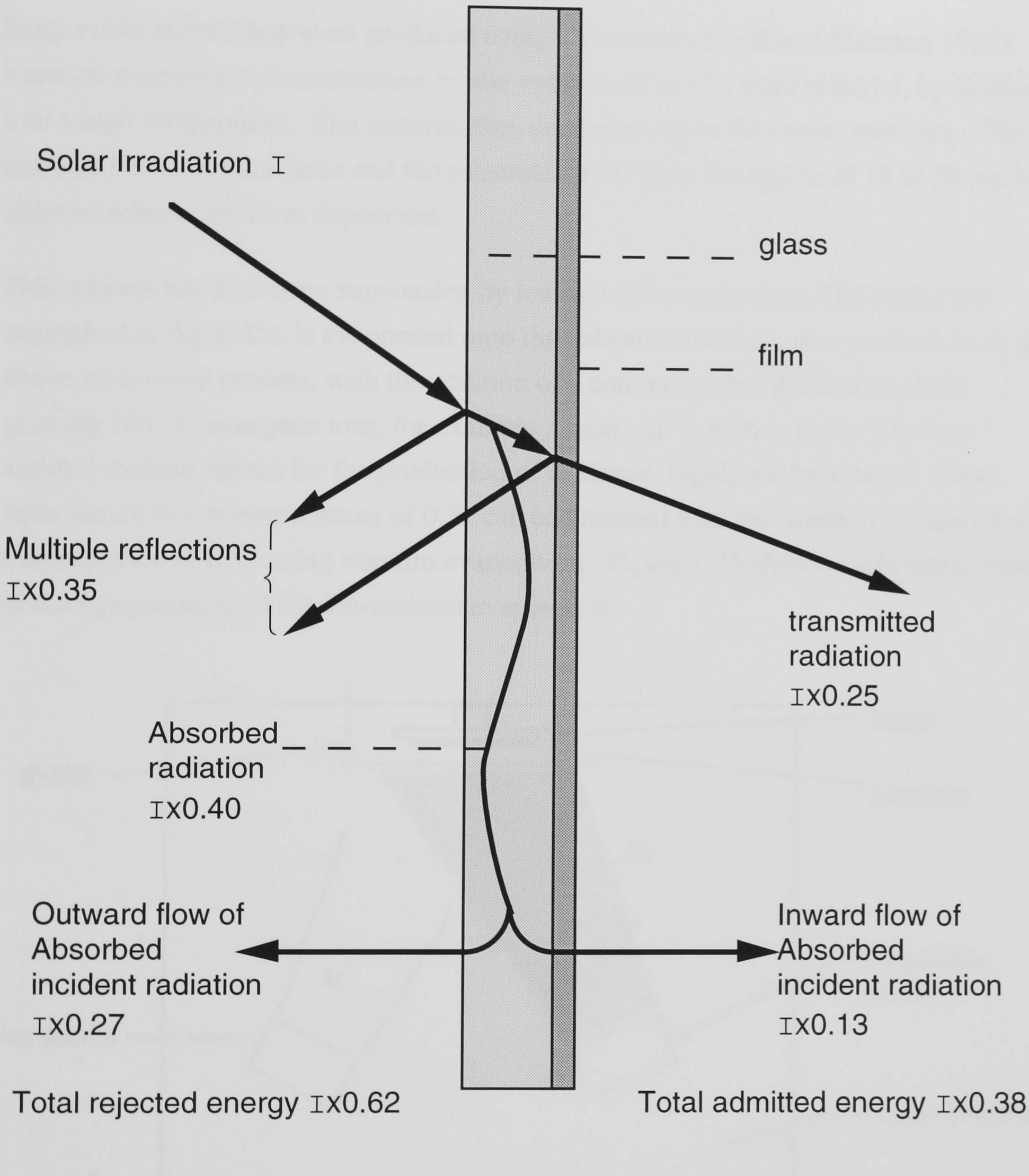

Fig 1.24 Schematic diagram of energy transmittance through glass with a typical thermally insulating film.

1.12 Film Production

There are various methods of producing solar films or putting the metallic layers onto glass. The nature of the substrate or the size of the product needed, usually governs the method of deposition. Below, a number of methods are discussed.

Early noble metal films were produced using vacuum evaporation, (Alderson 1969). Vacuum evaporation is undertaken by the vapourisation of a solid material, by heating it to a high temperature. The material then condenses upon the cooler substrate. The distance between the source and the substrate has to be in the region of 10 to 50 cm in order to achieve uniform deposition.

This process has now been superseded by ion-assisted evaporation. The metal, for example Au, Ag or Cu, is evaporated onto the unheated substrate in a vacuum, as in the above mentioned process, with the addition of a continuous bombardment of the growing film by energetic ions, for example Argon, Ar^+ which is inert. The ion-assisted method allows for the production of a thinner, highly uniform layer. Tests have shown that transmittances of 0.51 can be obtained with this method compared a transmittance of 0.37 using vacuum evaporation. Figure 1.25 shows a schematic view of the equipment used for ion-assisted evaporation.

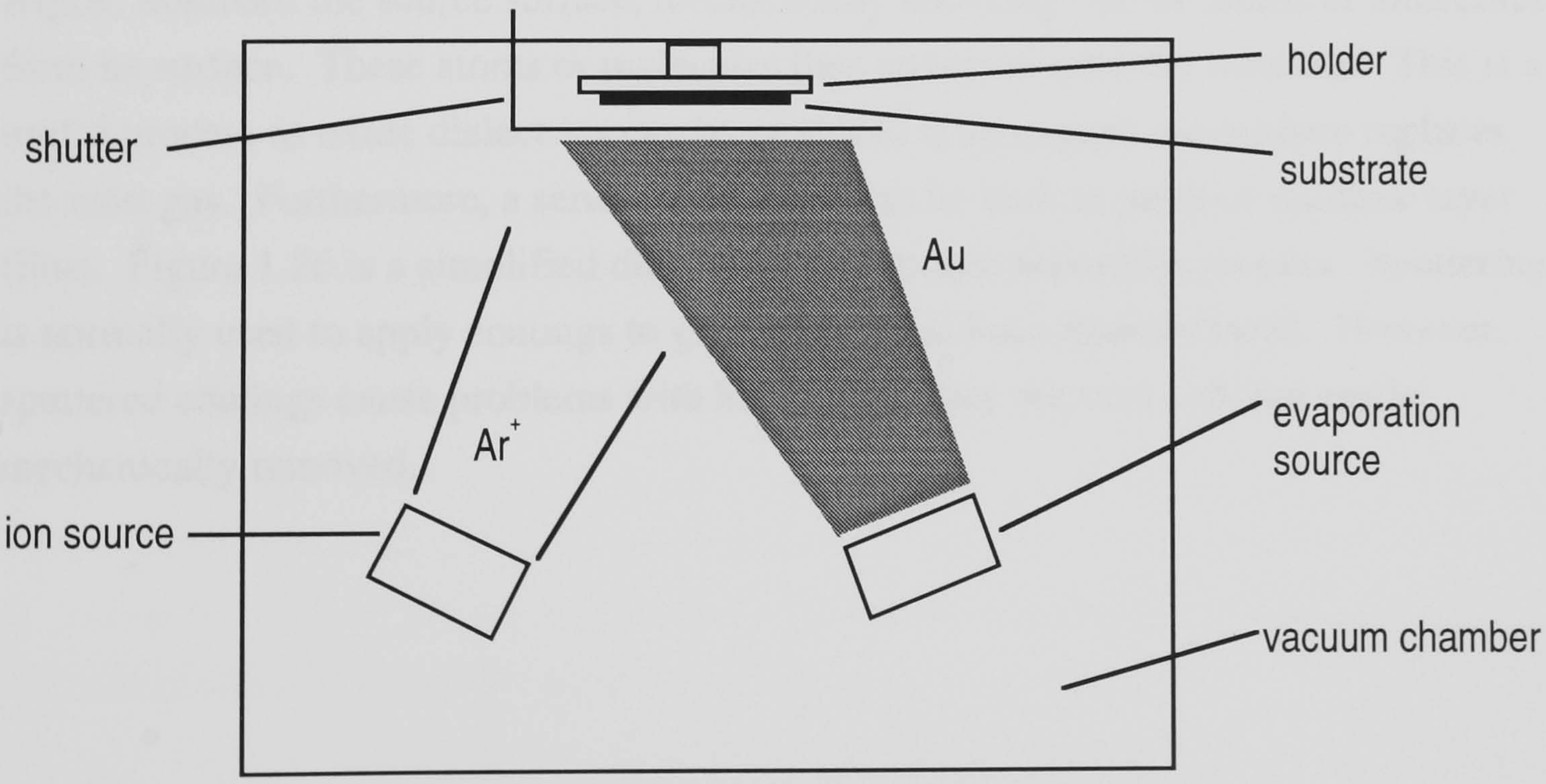

Fig.1.25 Schematic view of the equipment used for ion-assisted evaporation

The production of dielectric layers and semi-conductors, such as tin oxide (SnO_2) and indium tin oxide (ITO, In_2O_3:Sn), have been carried out using electron beam

evaporation. Instead of heating the source material via its electrical resistance or by inductance, the vapourisation of the source can be accomplished by electron bombardment. The electron beam is focused onto the source; on hitting the source, the kinetic energy of the electrons is converted into heat. This method directs the energy to where it is required, that is, at the surface of the source material. This encourages the material to condense and deposit itself upon the substrate, while keeping the rest of the source at a lower temperature. Hence interactions between the source and its support material are greatly reduced, increasing the purity of the resultant film. This method can only be used for glass, and the substrate needs to be heated to high temperatures (~300°C) in order to produce films with highly controlled optical properties and greater uniformity of the coating. (Granqvist 1991) The above three methods only allow small areas to be coated. These have been adapted to allow continuous/semi-continuous deposition processes which are outlined in the following text.

A common process used industrially is sputter deposition (Pulker 1984). Spencer et .al (1988) demonstrated a sputtering device for the manufacture of thin films of titanium nitride between layers of titanium oxide. Sputtering involves the coating of the substrate surface within a low pressure, inert gas environment with a pressure of ~1Pa, or in a vacuum chamber. The unheated substrate is transported through the chamber a few centimetres below the cathode targets. Energised ions of the inert gas, for example, Argon, bombard the source surface, mechanically knocking out the atoms or molecules from its surface. These atoms or molecules then condense onto the substrate. This is a useful process as oxide dielectrics can be produced if an oxygen atmosphere replaces the inert gas. Furthermore, a series of cathodes can be built to produce multiple layer films. Figure 1.26 is a simplified diagram of the sputter deposition process. Sputtering is normally used to apply coatings to glass after it has been manufactured. However, sputtered coatings cause problems with handling as they are very soft and easily mechanically removed.

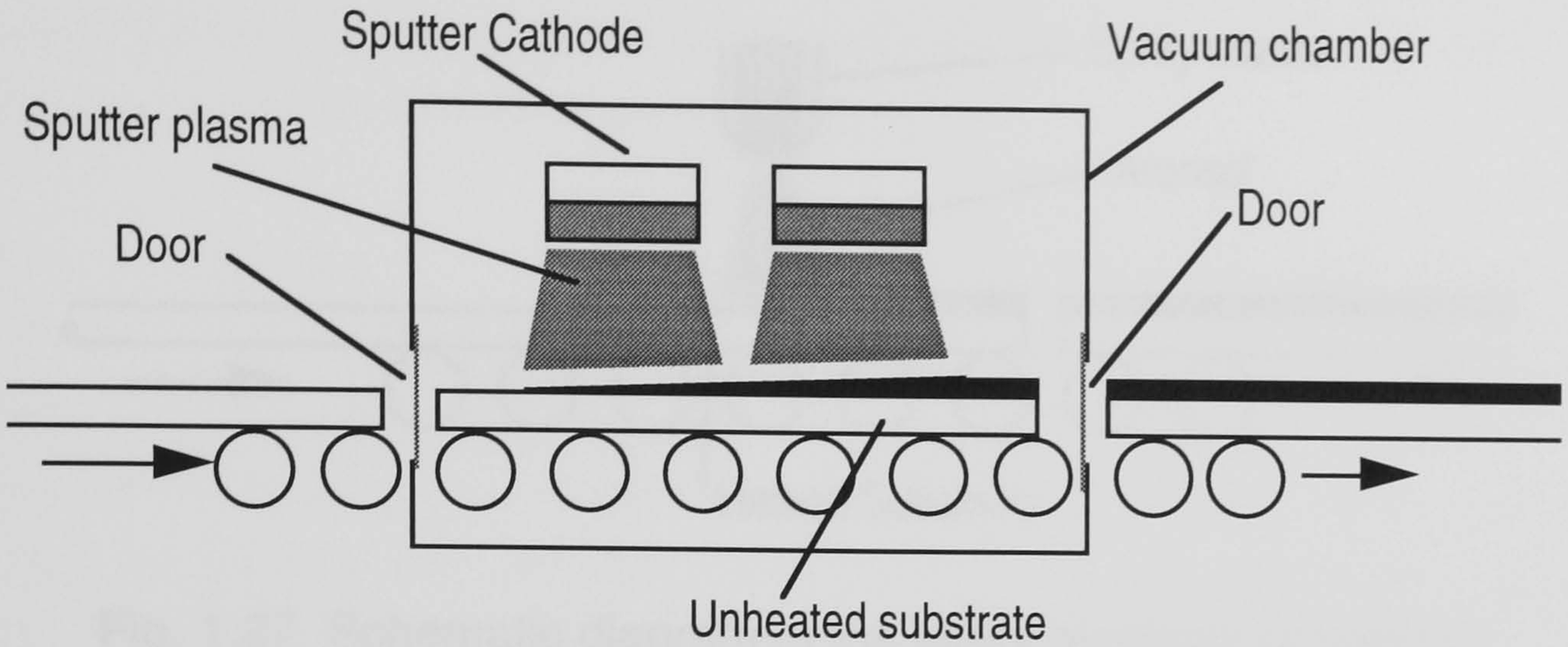

Fig 1.26 Schematic view of a sputter deposition process for producing a metallic layer upon an unheated substrate

Chemical vapour deposition is a material synthesis in which constituents of the vapour phase react chemically to form thin solid films as a solid phase reaction product which condenses on the substrate. The procedure needs to be controlled so that the reaction takes place near to, or on, the substrate surface, and not in the gaseous phase, in order to avoid powdery deposits being formed. The reaction can be activated by various means including heat, electric arc, electron bombardment or the catalytic action of the substrate surface to name a few. This process lends itself well to the production of nitrate films, high deposition rates and the controlled doping of films with impurities. The reactions which are used in chemical vapour deposition can be placed into one of five categories - decomposition reactions, reduction & oxidation reactions, hydrolysis reactions, polymerisation reactions or transport reactions. These methods and variations within the area of chemical vapour deposition are discussed by Pulker (1984).

Spray coating is traditionally not considered as a chemical vapour deposition process. Spray coating involves highly dispersed liquids or vapours, which are allowed to react on mixing in a humid atmosphere immediately before or during deposition, or are allowed to undergo pyrolysis upon the substrate.

Spray pyrolysis involves the spraying of a metallic salt solution which is suspended in a carrier gas, through a nozzle, to form an aerosol which is directed towards a heated substrate, see Figure 1.27.

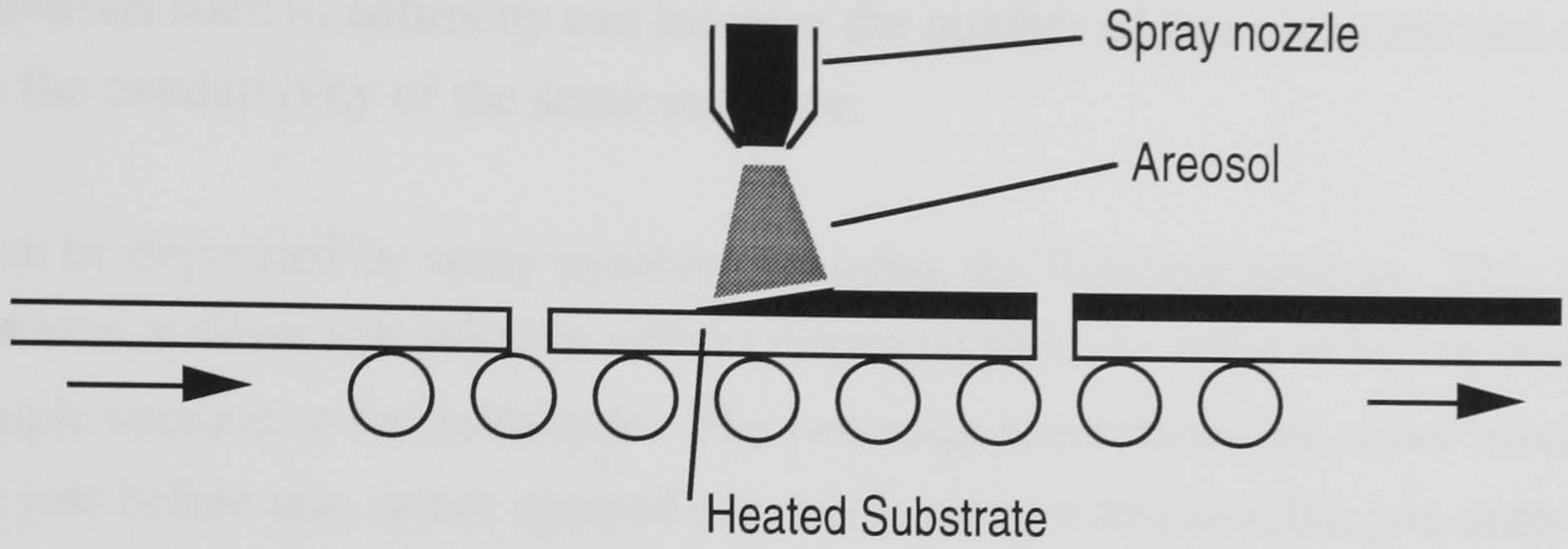

Fig. 1.27 Schematic diagram of the spray pyrolysis procedure

The carrier gas is usually nitrogen, argon or air, or if required, a reactive gas such as water vapour. After the film has been deposited, the substrate enters a furnace which produces a mechanically and chemically durable film. This is easier to handle than a sputtered coating. Substrate temperature is a very important parameter, because if it is high, then it follows that the deposition rate is increased and a more uniform film is achieved, compared with lower temperatures at which impurities can react and form in the film. The maximum temperature for spray coating is usually 500°C. Spray pyrolysis is used extensively to coat glass as it emerges from the float glass process. Spray coating is useful for the deposition of oxide, metallic and semiconductor films.

Gracin and Desnica, (1984) showed how the deposition of tin-oxide is undertaken using tin chloride, ($SnCl_2$) and water vapour as the carrier gas. In an endothermic reaction the formation of an oxide layer takes place, accompanied by evaporation of the volatile products of the chemical reaction. The formation of the film occurs on the heated substrate through the chemical reactions below;

$$SnCl_2 + H_2O \rightarrow SnO + 2HCl \qquad (1.17)$$

$$2SnO + O_2 \rightarrow 2SnO_2 \qquad (1.18)$$

If the temperature of the substrate is higher than 380°C, the tin-oxide dissociates to:

$$2SnO \rightarrow Sn + SnO_2 \qquad (1.19)$$

This last reaction results in a defect SnO_x (where $x<2$). As vacancies of oxygen act as donors, the SnO_x becomes a highly conductive n-type semiconductor. The addition of

other materials such as antimony can increase the number of free electrons and so enhance the conductivity of the semiconductor.

Silver can be deposited by spray pyrolysis by using the Brashear process. This involves two solutions, a silver salt solution - silver nitrate ($AgNO_3$) - and a reducing compound for example sucrose or formaldehyde. The two reagent solutions are either mixed together just before use, or are sprayed separately using a two nozzled gun onto the substrate. On the substrate a reduction reaction occurs, depositing the pure metal on the surface. Copper and gold can both be deposited in similar fashion.

Dip coating and spray coating share similar reactions and materials, but differ in the method of application of the film to the substrate. It involves the immersion of the substrate into a reaction mixture which can be an aqueous solution with the deposition source in ionic form, for example, a silver salt or an organo-metallic solution. These processes involve chemical and or electrochemical reactions for the formation of the film. The process does not require a vacuum and can be carried out at temperatures less than 100°C. The thickness is governed by the rate at which the substrate is withdrawn from the solution and the temperature and the viscosity of the solution. The substrate is then heat treated to remove excess liquid and to harden the film. The lower temperature requirements allow this method to be used to coat plastic films. The formation of oxide films from solution by immersion or dipping, are old methods which benefit from not requiring a vacuum or inert atmosphere.

Howson et. al. (1984) demonstrated a technique of vacuum deposition for producing heat reflecting films onto a plastic sheet. Thin metal films of copper, silver, gold and titanium nitride were sandwiched between dielectric films and electrically conducting oxide coatings of indium, indium doped with tin and cadmium tin were produced and shown to have the properties required for heat reflecting coatings for windows. Figure 1.28 shows a schematic diagram of the equipment used to coat the plastic sheet. It involved a roll-to-roll coating apparatus within a vacuum chamber which slowly exposed the plastic sheet to a magnetron evaporation source.

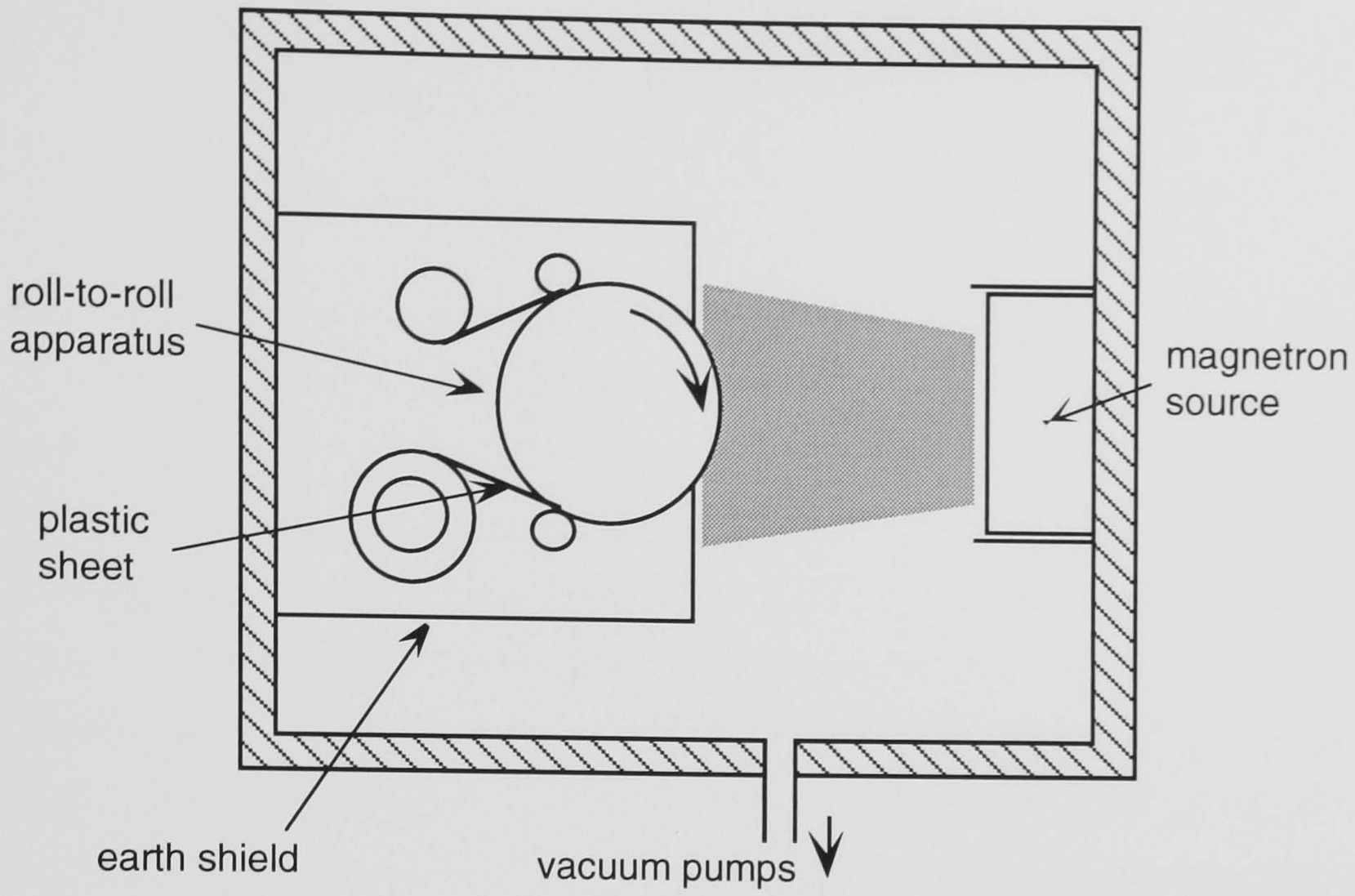

Fig. 1.28 Schematic diagram of the roll-to-roll coating apparatus and vacuum system with magnetron source as used by Howson et.al 1984

Sputtering, spray pyrolysis, chemical vapour deposition, and dip coating are automatic and can be carried out on a large scale. The drawbacks of chemical vapour deposition, are that it requires higher temperatures than sputtering and that the reactive gases used, can produce volatile reactive products which can be corrosive, toxic or even explosive! It is also difficult to control the uniformity of the film. Sputtering is noted for its versatility, multi-layer facility and low substrate heating; hence it can be used to coat plastics. However it is highly energy inefficient, as most of the energy used is converted to heat. Spray pyrolysis is very good for depositing metal oxide films onto hot glass as it comes out of the tin bath as part of the float glass process. Furthermore, due to the manufacturing process, these films can withstand high temperatures, in excess of 300°C - and so are good for use on solar collectors and windows in high temperature manufacturing areas. Spray pyrolysis is, theoretically, the most economical process for the manufacture of low-e and solar-control films. However there are problems with the collection and disposal of the dangerous reactant products which are produced by the process. Furthermore, the hard coatings usually have a higher emissivity, ~0.2, as compared with some sputtered coatings whose emissivity has been measured at 0.03 (Johnson, 1991).

Pulker (1984) and George (1992) have produced a comprehensive study of the various advantages and disadvantages in the production techniques of thin-films. In this brief study it is not necessary to detail their work further.

BLANK IN ORIGINAL

Chapter 2 Determination of Absorptance, Reflectance and Transmittance

2.1 Introduction

Solar energy absorption and consequently the mean temperature of the glass depends upon the insolation intensity, I, the angle of incidence, θ, of the insolation upon the surface and the variations of the solar-optical properties of the glass with respect to the wavelength of the incident insolation. The intensity, I, is a function of the solar geometry which is dictated by the latitude, date, time of day and orientation of the window, to the solar radiation on the glass as shown by Yellot (1971). Harkness & and Mehta (1978), give an in-depth study of solar geometry. In Chapter 1, it was shown that the optical behaviour of glass can be altered by changing its electrical conductivity, surface and inter-surface characteristics, by either altering the optical properties of the glass itself or by adding a thin film to one of its surfaces. These optical properties concerning the transmittance, reflectance and absorption of electromagnetic radiation can be summarised by the absorption coefficient, κ and the refractive index, n.

The absorption coefficient of a material may be determined mathematically from a knowledge of its absorptive index k, or experimentally from its refractive index, n, as will be shown later. This simplifies the task in determining the transmittance, τ, absorption, α, and reflectance, ρ of the glass. Once the absorption coefficient and the refractive index of the glass are known, then the optical properties can be determined. Table 2.1 shows typical values of the refractive and absorptive indices of metals for normally incident light in air.

Metal	n	k
Silver	0.05	30
Copper	12	60
Aluminium	23	86
Nickel	2.8	5
Gold	7.6	72
Dielectrics	Any	0

Table 2.1 Typical values of refractive and absorptive indices for metals with normally incident light in air (Rancourt 1987)

These indices can be determined from the electromagnetic wave theory as set out in Chapter 1. For the determination of n and κ from first principles, then the work of Born

and Wolf (1970), Heavens and Ditchburn (1991), or Modest (1993) is highly recommended.

2.2 Single Layer Systems

Electromagnetic waves are influenced by thin films and glass. These influences include the attenuation, reflectance and changes in polarity of the incident radiation. The refractive indices of materials, either side of a surface, influence the proportion of the incident radiation which is reflected at that surface. The normal reflectance at an interface between two semi-infinite non-absorbing materials of different indices of refraction, refers to the ratio of the reflected intensity to the incident intensity, see Figure 2.1. This relationship is expressed by the Fresnal formula;

$$r = \frac{(n_o - n_1)^2}{(n_o + n_1)^2} \qquad (2.1)$$

where n_o is the refractive index of the incident medium, n_1 is the refractive index of the second medium.

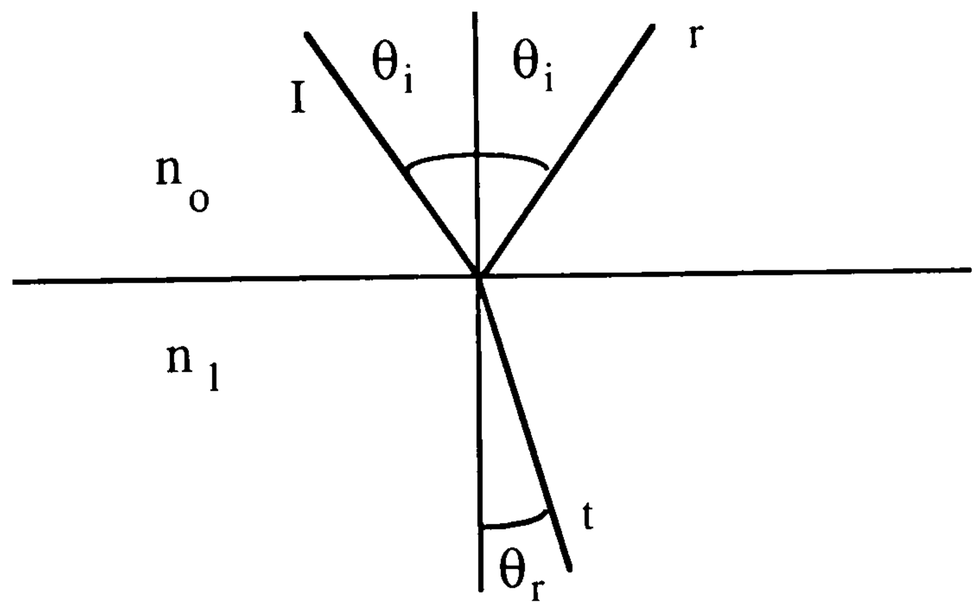

Fig 2.1 Relationship of the angles of incidence, reflectance and refraction at a surface

Where the second medium is absorbing, the refractive index is considered to be complex, therefore the reflected intensity at the surface becomes;

$$r = \frac{\left[(n_o - n_1)^2 + k_1^{\,2}\right]}{\left[(n_o + n_1)^2 + k_1^{\,2}\right]} \qquad (2.2)$$

where the complex component of refraction of the substrate is encapsulated in the absorptive index, k, and was described by Equation (1.11).

However, calculating the proportion of incident electromagnetic radiation which is transmitted, reflected or absorbed, is complicated by the wave possessing both an electric field (TE) and a magnetic field (TM), each operating in planes, perpendicular to the other, see Figure 2.2. These vectors behave identically at a surface where the angle of incidence is 0°, but at all other angles the different fields behave separately.

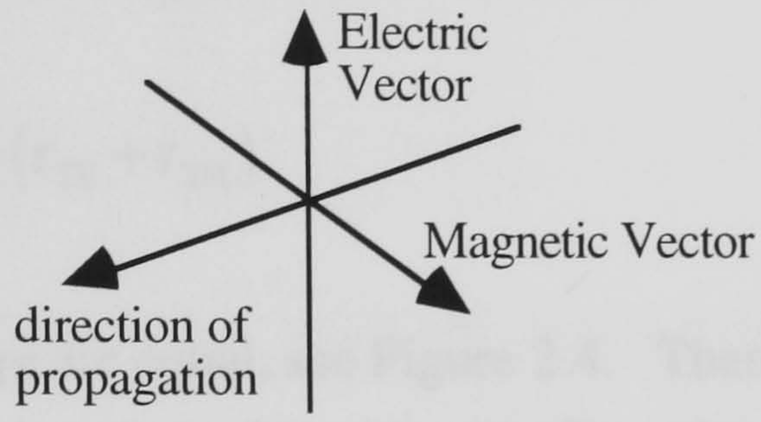

Fig 2.2 The different components of an electromagnetic wave

This has lead to Fresnal's Equation (2.1) being adapted for these different components. The resulting Equations, (2.3) & (2.4), allow the component reflectance intensities to be calculated. Figure 2.3 is a plot of the magnetic, r_{TM}, and electric, r_{TE}, fields of the reflected electromagnetic radiation and against the angle of incidence.

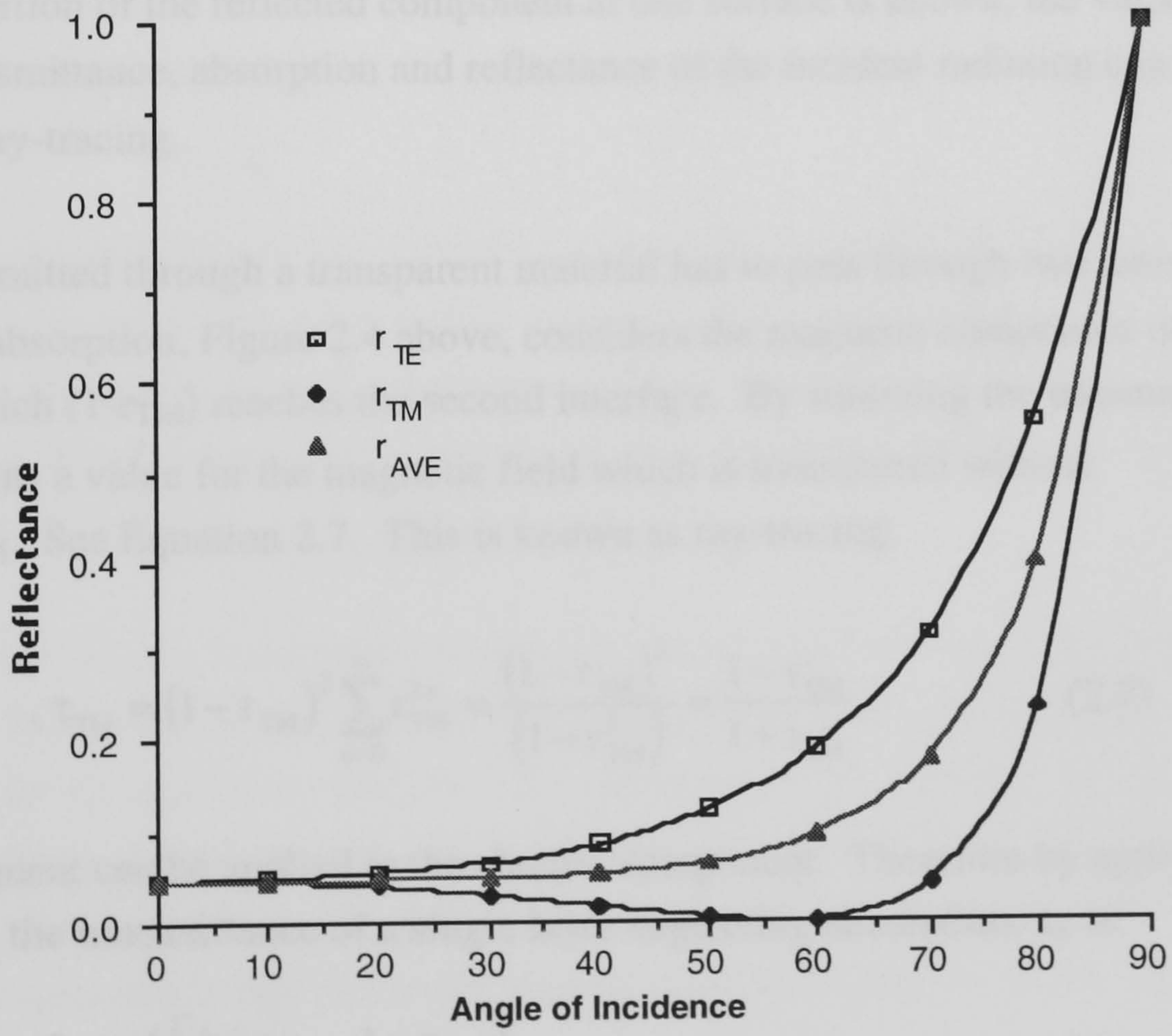

Fig 2.3 Polarised Reflectance vs angle of incidence for glass, n=1.54

$$r_{TE} = \frac{\sin^2(\theta_r - \theta_i)}{\sin^2(\theta_r + \theta_i)} \tag{2.3}$$

$$r_{TM} = \frac{\tan^2(\theta_r - \theta_i)}{\tan^2(\theta_r + \theta_i)} \tag{2.4}$$

By taking the mean of r_{TE} and r_{TM} the overall reflectance can be determined.

$$r_{AVE} = \frac{1}{2}(r_{TE} + r_{TM}) \tag{2.5}$$

When θ_i is zero r_{TM} and r_{TE} are equal, see Figure 2.4. Therefore reflectance of an air-medium interface when θ_i is zero is determined by Equation (2.6).

$$r_{(0)} = \left(\frac{(n_1 - 1)}{(n_1 + 1)}\right)^2 \tag{2.6}$$

where n_1 is the refractive index for the medium, and 1 is the refractive index of air.

Once the proportion of the reflected component at one surface is known, the values for the overall transmittance, absorption and reflectance of the incident radiation can be calculated by ray-tracing.

Radiation transmitted through a transparent material has to pass through two interfaces. By neglecting absorption, Figure 2.4 above, considers the magnetic component of the radiation of which ($1-r_{TM}$) reaches the second interface. By summing the transmitted terms one obtains a value for the magnetic field which is transmitted without absorption, τ_{TM}. See Equation 2.7. This is known as ray-tracing.

$$\tau_{TM} = (1 - r_{TM})^2 \sum_{n=0}^{\infty} r_{TM}^{2n} = \frac{(1 - r_{TM})^2}{(1 - r_{TM}^2)} = \frac{1 - r_{TM}}{1 + r_{TM}} \tag{2.7}$$

The same treatment can be applied to the electric component. Therefore by applying Equation (2.5), the transmittance of a single layer neglecting absorption, τ_r, is:

$$\tau_r = \frac{1}{2}\left[\frac{1 - r_{TE}}{1 + r_{TE}} + \frac{1 - r_{TM}}{1 + r_{TM}}\right] \tag{2.8}$$

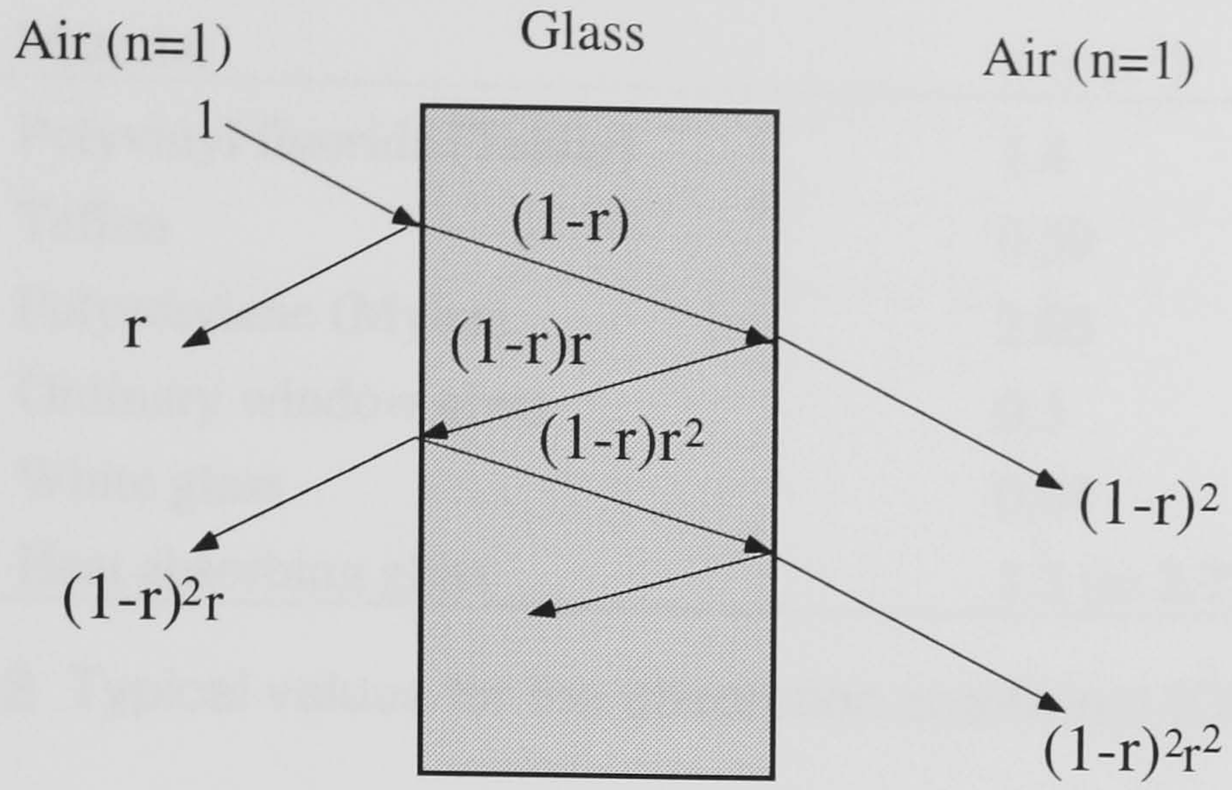

Fig 2.4 Multiple reflections in a slab of non-absorbing glazing material

However some absorption occurs in all materials and this needs to be taken into account. As was seen in Equation (1.15) in Section 1.8, the absorptive index k, which is a dimensionless number like the refractive index, is a measure of the absorptive properties of a material. To calculate absorption, the absorption coefficient, κ, is required. The absorptive index can be converted into the form of the absorption coefficient, κ, as shown in Equation (2.9).

$$\kappa = \frac{4\pi k}{\lambda_o} \qquad (2.9)$$

where λ_o is the electromagnetic wavelength in a vacuum. κ varies with material, it is very low for opaque materials and high for transparent materials, see Table 2.2. It can also vary across the electromagnetic spectrum as shown for float glass in Figure 2.5. The value of κ is integrated across the electromagnetic spectrum to obtain a broad band value where that is desirable.

The attenuation of the electromagnetic energy by means of absorption is explained by Bougers Law. This law is based upon the absorbed radiation being proportional to the solar intensity, the absorption coefficient, κ, of the medium and the distance travelled through the medium, x, see Equation (2.10) (Duffie and Beckman 1991). Equation (2.10) is for monochromatic wavelengths, but as κ does not vary much throughout the visible section it can also be applied to the broad band wavelengths related to solar energy.

Material	κ (cm^{-1})
Polyvinyl fluoride (Teldar)	1.4
Teflon	0.59
Polyethylene (Mylar)	2.05
Ordinary window glass	0.3
White glass	0.04
Heat absorbing glass	1.3 (to 2.7)

Table 2.2 Typical values for the absorption coefficient (Clarke 1985)

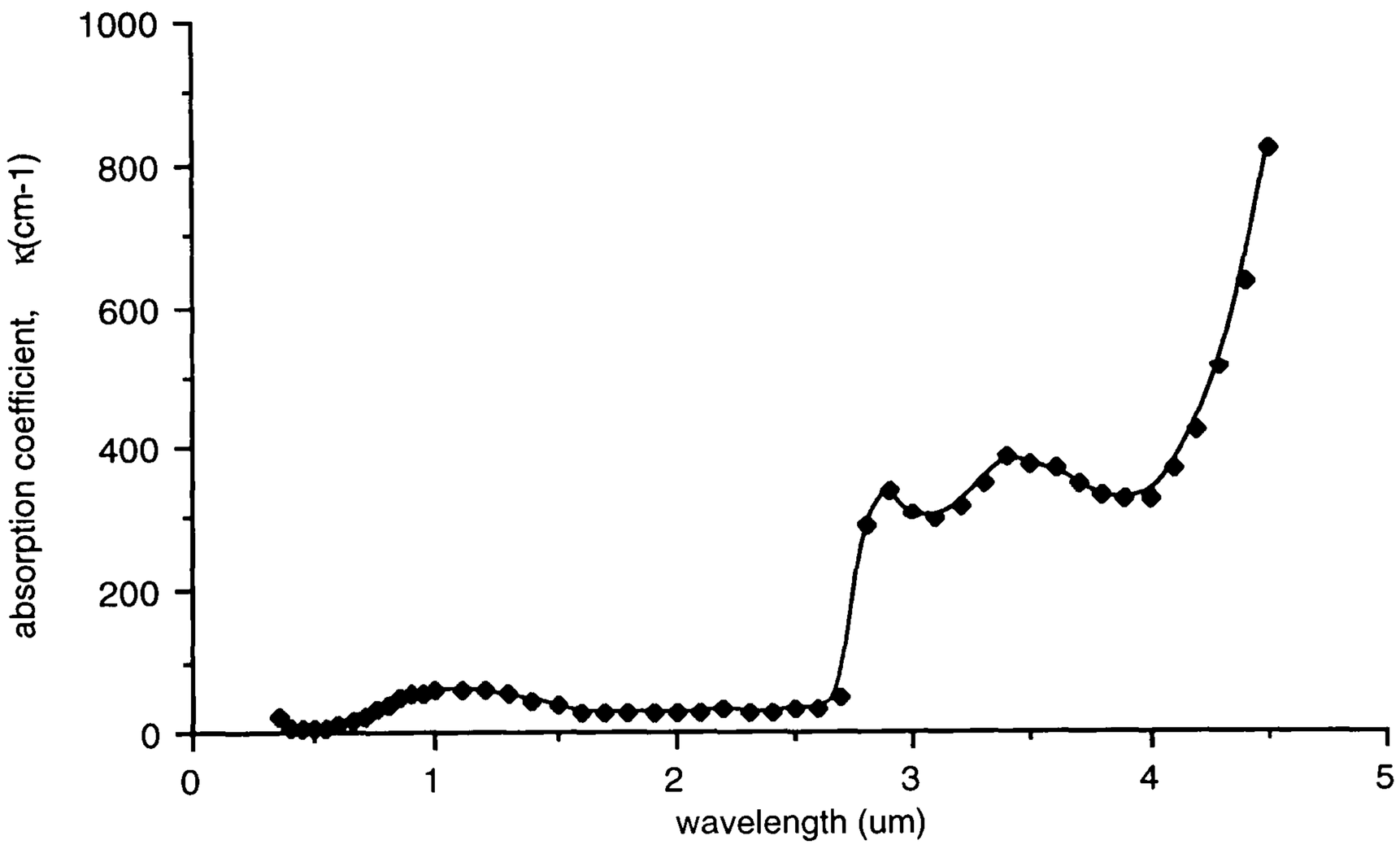

Fig 2.5 Absorption coefficient vs wavelength for clear float glass (Rubin 1985)

$$dI = -I\kappa dx \tag{2.10}$$

By integrating Bougers equation the attenuation of a beam of light in an absorbing material, neglecting reflectance losses at the surfaces can be obtained:

$$1 - \alpha = \frac{I_\tau}{I_o} = \mathbf{exp}^{(-\kappa x)} \tag{2.11}$$

where I_τ is the emergent intensity, I_o is the incident intensity, α is the absorptance of the radiation neglecting reflectance losses, and x is the path length of the of the light in the medium.

Rubin (1982a), took Bougers Equation, (2.10), and obtained Equation (2.12) by integrating the absorption over the actual path length which the light travels in the medium, (from 0 to $d/\cos\theta_r$), see Figure 2.6, where d is the thickness of the material and θ_r is the angle of refraction.

$$\alpha = 1 - \mathbf{exp}^{\left(\frac{-\kappa d}{\cos\theta_r}\right)} \qquad (2.12)$$

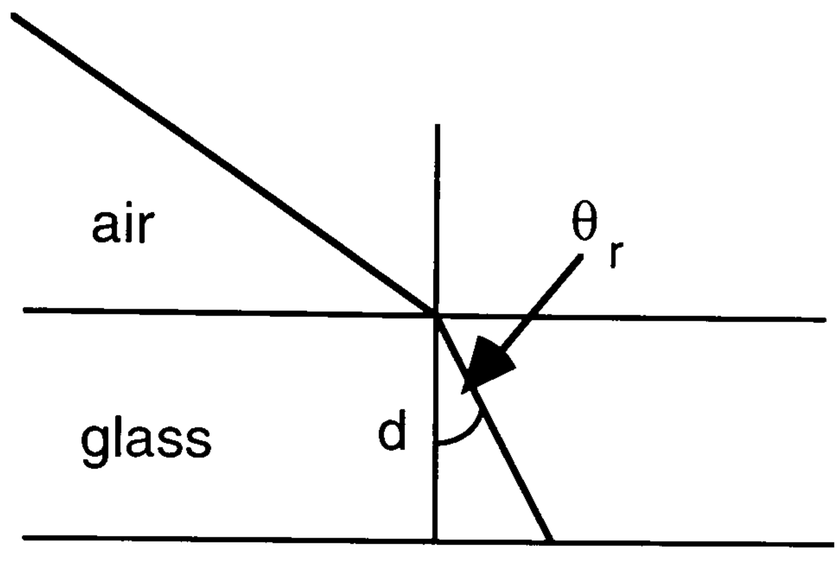

Fig 2.6 Path length of radiation through medium

The angle of refraction can be determined by applying Snell's law,

$$\mathbf{sin}\,\theta_i n_0 = \mathbf{sin}\,\theta_r n_1 \qquad (2.13)$$

Again, using the ray-tracing techniques demonstrated in Figure 2.4, the transmittance can be determined. This time absorption, α, within the medium, is included, thus giving a value of $1-\alpha$, for the transmittance of energy from the one surface to the other, τ_a. Once again the summation of the terms, provides values for the reflectivity, absorptivity and transmissivity of the medium. See Figure 2.7 and Equations (2.14-16). The equations below represent those for the magnetic component of the electromagnetic wave and similar results are found for the electric component.

$$\tau_{TM} = (1-r)^2(1-\alpha) + (1-r)^2(1-\alpha)^3 r^2 + \ldots\ldots \qquad (2.14a)$$

$$\tau_{\mathrm{TM}} = \frac{\tau_a\left(1-r_{\mathrm{TM}}\right)^2}{1-\left(r_{\mathrm{TM}}\tau_a\right)^2} \qquad (2.14b)$$

$$\rho_{TM} = r + (1-r)^2(1-\alpha)^2 r + (1-r)^2(1-\alpha)^4 r^3 + \ldots. \qquad (2.15a)$$

$$\rho_{\mathrm{TM}} = r_{\mathrm{TM}}\left[1 + \frac{\left(1-r_{\mathrm{TM}}\right)^2 \tau_a^2}{1-\left(r_{\mathrm{TM}}\tau_a\right)^2}\right] \qquad (2.15b)$$

$$\alpha_{TM} = (1-r)\alpha + (1-r)(1-\alpha)r\alpha + (1-r)(1-\alpha)^2 r^2\alpha + \ldots \quad (2.16a)$$

$$\alpha_{TM} = (1-\tau_a)\left(\frac{1-r_{TM}}{1-r_{TM}\tau_a}\right) \quad (2.16b)$$

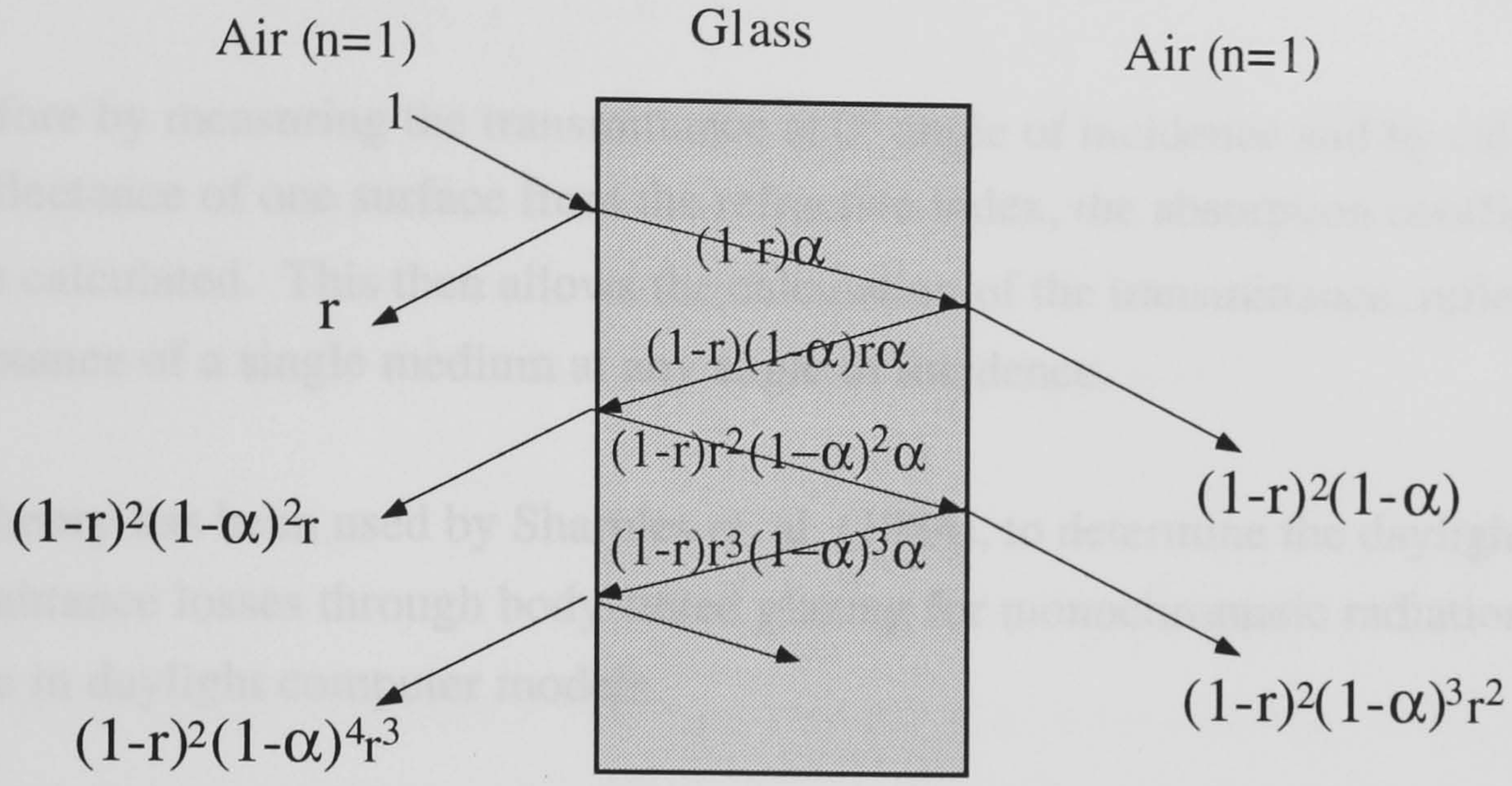

Fig 2.7 Multiple reflections in a transparent absorbing material

By using Bougers theory and ray-tracing techniques as shown in Figure 2.8, Rubin (1982a) proposed a framework from which κ can be determined. The only inputs required for this process are the refractive index and the transmittance which can be measured experimentally.

First, a value of absorption at normal incidence, $\alpha_{(0)}$, is determined by re-arranging Equation (2.14b) to give Equation (2.17), replacing the term τ_a with $(1-\alpha_{(0)})$. The reflectance of a surface at normal incidence, $r_{(0)}$, is calculated using Equation (2.6) while the transmittance, $\tau_{(0)}$, is measured experimentally.

$$\alpha_{(0)} = 1 + \frac{(1-r_{(0)})^2 - \sqrt{(1-r_{(0)})^4 + 4r_{(0)}^2\tau_{(0)}^2}}{2r_{(0)}^2\tau_{(0)}} \quad (2.17)$$

Once the absorption $\alpha_{(0)}$ is known, κ can be calculated by re-arranging Equation (2.12) as seen in Equation (2.18).

$$\kappa = -\frac{1}{h}\ln(1-\alpha_{(0)}) \quad (2.18)$$

The value obtained for the absorption coefficient from Equation (2.18) is constant for any angle of incidence. Finally, the total reflectance of the medium is determined using the energy balance,

$$\rho = 1-\alpha -\tau. \qquad (2.19)$$

Therefore by measuring the transmittance at 0° angle of incidence and by calculating the reflectance of one surface from the refractive index, the absorption coefficient, κ, can be calculated. This then allows the calculation of the transmittance, reflectance and absorptance of a single medium at any angle of incidence.

This theory has been used by Sharples et. al. (1984), to determine the daylight transmittance losses through body-tinted glazing for monochromatic radiation values for use in daylight computer models.

2.3 Multi-layer Systems

The initial studies of single layers and multiple covers have led to investigations into determining the transmittance, reflectance and absorptance of systems with multiple adjoining layers. Equations for multi-layer systems have been developed by Modest (1993) and Siegel (1973).

The work by Modest assumes that no absorption occurs in either the substrate or the film and therefore a transmittance $\tau_a \cong 1$ can be assumed. He developed a formula for analysing the reflectivity of a thick dielectric layer, with refractive index n_2 and absorptive index $k_2 \cong 0$, which is placed on a sheet of glass (n_3 and $k_3 \cong 0$).

With $\tau \approx 1$ and at 0° angle of incidence, the reflectances at the air-coating interface and the coating-glass interface are:

$$r_1 = \left(\frac{n_1 - n_2}{n_1 + n_2}\right)^2, \text{ and } r_2 = \left(\frac{n_2 - n_3}{n_2 + n_3}\right)^2 \qquad (2.20\ a\&b)$$

The coating reflectivity becomes

$$\rho_{coat} = \frac{r_1 + r_2 - 2r_1r_2}{1 - r_1r_2} = 1 - \frac{(1-r_1)(1-r_2)}{1 - r_1r_2} \qquad (2.21)$$

$$\rho_{coat} = 1 - \frac{(4n_1n_2)(4n_2n_3)}{(n_1+n_2)^2(n_2+n_3)^2 - (n_1-n_2)^2(n_2-n_3)^2} \qquad (2.21)$$

which is simplified to

$$\rho_{coat} = 1 - \frac{4n_1n_2n_3}{(n_2^2+n_1n_3)(n_1+n_3)} \qquad (2.23)$$

From Equation (2.23), it can be seen that, to reduce the overall reflectivity of the semi-transparent sheet, then a value for the refractive index of the coating , n_2, must be chosen to make ρ_{coat}, a minimum. To do this Modest explains that:

$$n_{2,min} = \sqrt{n_1n_3}\,. \qquad (2.23a)$$

In his work, Siegel employed a different method. He showed that by adapting the net radiation method for enclosures with opaque surfaces, it could be used for semi-transparent regions. He analysed an absorbing layer adjacent to a non-absorbing layer, and from his work determined the following equations for transmittance and reflectance:

$$\tau = \frac{(1-r_1)(1-r_2)(1-r_3)(1-\alpha)}{(1-r_2r_3)\left[1-r_1r_2(1-\alpha)^2\right] - r_1r_3(1-r_2)^2(1-\alpha)^2} \qquad (2.24)$$

$$\rho = r_1 + (1-r_1)^2(1-\alpha)^2\left(\frac{r_2(1-r_2r_3)+r_3(1-r_2)^2}{(1-r_2r_3)\left(1-r_1r_2(1-\alpha)^2\right) - r_1r_3(1-r_2)^2(1-\alpha)^2}\right) \qquad (2.25)$$

where r_1, r_2 and r_3 are the reflectances at the three surfaces , air-glass, glass -film and film-air, see Figure 2.8. Again, the absorption for the glass can be calculated using Equation (2.12).

By taking Siegel's work further, and specifying that both layers are absorbing, new equations can be derived for transmittance and reflectance. Equations (2.26 a-f) represent the energy leaving each surface in Figure 2.8. The energy incident upon a surface is $q_{i,n}$, while the energy leaving a surface is $q_{o,n}$.

$$q_{o,1} = r_1q_{i,1} + (1-r_1)q_{i,2} \qquad (2.26a)$$

$$q_{o,2} = (1-r_1)q_{i,1} + r_1q_{i,2} \qquad (2.26b)$$

$$q_{o,3} = r_2 q_{i,3} + (1 - r_2) q_{i,4} \tag{2.26c}$$

$$q_{o,4} = (1 - r_2) q_{i,3} + r_2 q_{i,4} \tag{2.26d}$$

$$q_{o,5} = r_3 q_{i,5} + (1 - r_3) q_{i,6} \tag{2.26e}$$

$$q_{o,6} = (1 - r_3) q_{i,5} + r_3 q_{i,6} \tag{2.26f}$$

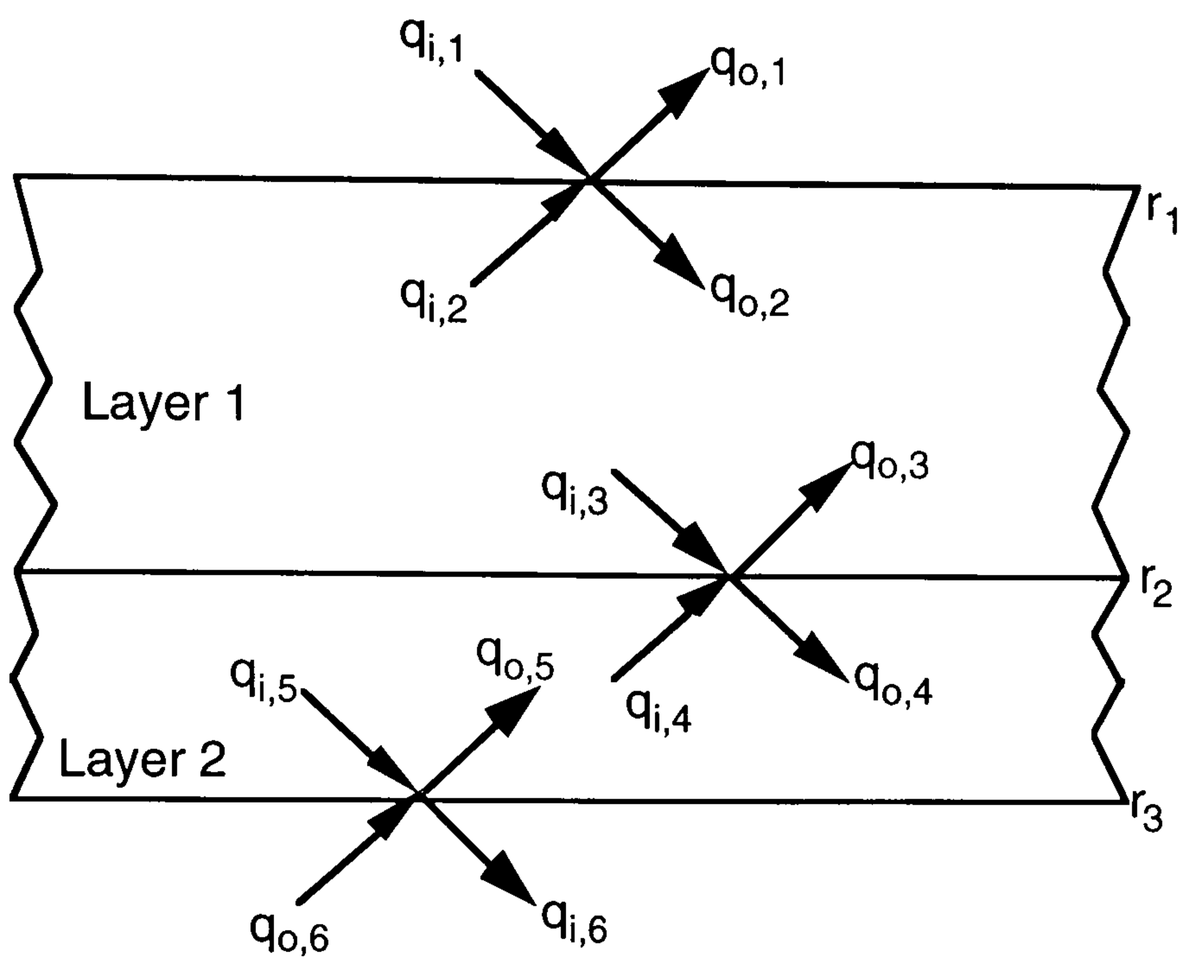

Fig. 2.8 Transmittance for adjacent layers by the net radiation method. (Siegel 1973)

The energy arriving at each surface, q_i, is related to Equations (2.26a-f) by the following Equations (2.27a-f):

$$q_{i,1} = q \tag{2.27a}$$

$$q_{i,2} = (1 - \alpha_1) q_{o,3} \tag{2.27b}$$

$$q_{i,3} = (1 - \alpha_1) q_{o,2} \tag{2.27c}$$

$$q_{i,4} = (1 - \alpha_2) q_{o,5} \tag{2.27d}$$

$$q_{i,5} = (1 - \alpha_2) q_{o,4} \tag{2.27e}$$

$$q_{i,6} = 0 \tag{2.27f}$$

By using Equations (2.27 a-f) the values for q_i can be eliminated in the Equations (2..26 a-f). This provides the following Equations, (2.28a-f):

$$q_{o,1} = r_1 q + (1 - r_1)(1 - \alpha_1) q_{o,3} \tag{2.28a}$$

$$q_{o,2} = (1 - r_1) q + r_1 (1 - \alpha_1) q_{o,3} \tag{2.28b}$$

$$q_{o,3} = r_2 (1 - \alpha_1) q_{o,2} + (1 - r_2)(1 - \alpha_2) q_{o,5} \tag{2.28c}$$

$$q_{o,4} = (1-r_2)(1-\alpha_1)q_{o,2} + r_2(1-\alpha_2)q_{o,5} \quad (2.28d)$$

$$q_{o,5} = r_3(1-\alpha_2)q_{o,4} \quad (2.28e)$$

$$q_{o,6} = (1-r_3)(1-\alpha_2)q_{o,4} \quad (2.28f)$$

Equations can then be determined for the overall transmittance, Equation (2.29), and reflectance, Equation (2.30), for the two layered stack.

$$\frac{q_{o,6}}{q} = \tau = \frac{(1-r_1)(1-r_2)(1-r_3)(1-\alpha_1)(1-\alpha_2)}{\left(\begin{array}{c}\left(1-r_2r_3(1-\alpha_2)^2\right)\left(1-r_1r_2(1-\alpha_1)^2\right)\\ -(1-r_2)^2(1-\alpha_1)^2(1-\alpha_2)^2r_1r_3\end{array}\right)} \quad (2.29)$$

$$\frac{q_{o,1}}{q} = \rho = r_1 + (1-r_1)^2(1-\alpha_1)^2\left(\begin{array}{c}\dfrac{r_2\left(1-r_2r_3(1-\alpha_2)^2\right)+r_3(1-r_2)^2(1-\alpha_2)^2}{\left(1-r_2r_3(1-\alpha_2)^2\right)\left(1-r_1r_2(1-\alpha_1)^2\right)-}\\ r_1r_3(1-r_2)^2(1-\alpha_1)^2(1-\alpha_2)^2\end{array}\right) \quad (2.30)$$

Therefore by using the net radiation method, values for the transmissivity, absorptivity and reflectivity can be obtained for multiple thin films upon glass, where the thickness, the absorptive coefficient, and the refractive index for each layer are known.

2.4 Multi-cover Systems

Multiple cover systems, that is, double glazing, can be treated in a similar manner as multi-layer windows. Shurcliff, (1974), proposed a matrix method for determining the transmittance and reflectance of a multiple plate window. However, this method was only proposed and tabulated for non-absorbing glass. Wijeysundera, (1975), extended the work of Siegel (1973) by using the net radiation method to obtain expressions for the transmittance and absorptance of a series of parallel plates of glass.

A similar approach to that demonstrated in Section 2.2, was applied to multiple glazing systems by Duffie and Beckman (1991) using ray-tracing techniques, and taking into account multiple reflections between the two sheets of glass. From his process they derived appropriate equations for transmittance and reflectance as shown by Equations (2.31-32);

$$\tau = \frac{1}{2}\left[\left(\frac{\tau_1\tau_2}{1-\rho_1\rho_2}\right)_{TM} + \left(\frac{\tau_1\tau_2}{1-\rho_1\rho_2}\right)_{TE}\right] \qquad (2.31)$$

$$\rho = \frac{1}{2}\left[\left(\rho_1 + \frac{\tau\rho_2\tau_1}{\tau_2}\right)_{TM} + \left(\rho_1 + \frac{\tau\rho_2\tau_1}{\tau_2}\right)_{TE}\right] \qquad (2.32)$$

where the subscript 1 refers to the outer cover and subscript 2 to the inner cover and the values of τ and ρ are determined for each cover from Equations (2.14) and (2.15). The values of τ for the electric and the magnetic components of the wave, are determined from the respective parts of Equation (2.31). From the above equations it can be seen that the reflectance from the system, depends upon which cover first intercepts the radiation. The ASHRAE handbook (1985) provides equations to calculate absorption in each sheet of glass in a double-glazed unit:

$$\alpha_o = \alpha_1 + \alpha_2\frac{\tau_o\rho_3}{1-\rho_2\rho_3} \qquad (2.33) \qquad\qquad \alpha_i = \alpha_3\frac{\tau_i}{1-\rho_2\rho_3} \qquad (2.34)$$

where α_o represents the total absorption in the outer cover, α_i represents the total absorption in the inner cover; α_1 represents the absorption in the outer cover from incident solar energy; α_2 represents the absorption in the outer cover from of solar energy which has been reflected off the inner pane; α_3 represents the absorption in the inner cover of incident solar energy, which includes a part that has been reflected from within the air gap; α_4 represents the absorption of the inner cover as a result of solar energy reflected from the room; τ_o represents the solar energy transmitted through the outer sheet, while τ_i represents the solar energy transmitted through the inner sheet. Finally, the reflectance subscripts 2 and 3 represent the glass surfaces counting in, from the exterior surface of the system.

Rubin, (1982b), published a procedure for determining the heat-transfer characteristics of multiple pane windows. By using his earlier work, (Rubin 1982a), he produced a procedure using a net radiation-convective balance of a window, to determine the total solar energy transmittance and the U-value of the window.

Therefore by applying the knowledge in the Sections 2.1, 2.2, 2.3 and 2.4, values for the transmittance, reflectance and absorptance can be achieved, and the total solar heat gain for a glazing system can be calculated.

2.5 Measurement of Solar Optical Properties using Laboratory Methods

In Chapter 1, Sections 1.6,1.8 and 1.9, it was shown how solar-control films utilise the natural selective properties of their materials so that certain wavelengths are transmitted while others are either absorbed or reflected. Values for the transmittance and reflectance of transparent materials at individual wavelengths can be obtained experimentally by a number of methods. The two principle methods are: the integrating sphere and spectrophotometry.

Spectrophotometry experiments are undertaken using laboratory bench equipment with small samples being tested. The basic concept of spectrophotometry is a system which measures the heat flux emitted by a monochromatic lamp, with and without the sample to be tested in situ. The ratio of the two readings gives the monochromatic transmittance, τ_λ. By adjusting the angle of incidence, θ, at which the heat flux hits the sample, values of transmittance can be obtained between 0 and 90°, see Figure 2.9.

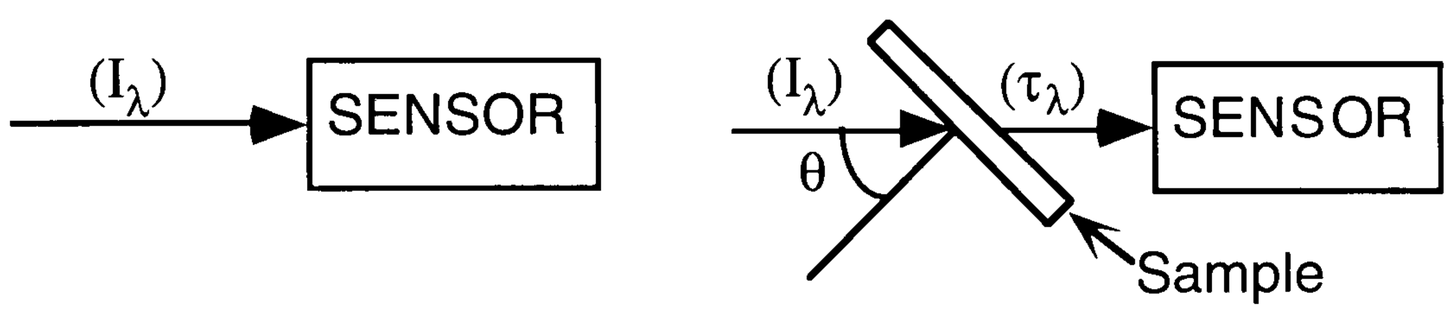

Fig 2.9 A schematic diagram showing the measurement of transmittance using spectrophotometry

Values for reflectance using spectrophotometry can be obtained by using a number of deflecting mirrors, see Figure 2.10. The use of multiple mirrors complicates the calculation and also increases experimental error. The measurement of reflectance from a semi-transparent object is further complicated by multiple reflections originating from the inner surface, see Figure 2.11. This procedure does not allow the evaluation of reflectance for angles of incidence below 6°; furthermore, at high incidence angles, the results become inaccurate because of the spread of the reflected components due to the thickness of the glass sheet, (Prasad 1993).

Hutchins and Ageorges (1992), in a review of techniques used for the measurement of spectral transmittance and reflectance at different angles of incidence, presented a technique for measuring the angular dependent reflectance of glazing material. It involved irradiating a sample with a narrow beam of light at different angles of

incidence, see Figure 2.12. This technique requires a reference reflectance standard with which the measured results are calibrated.

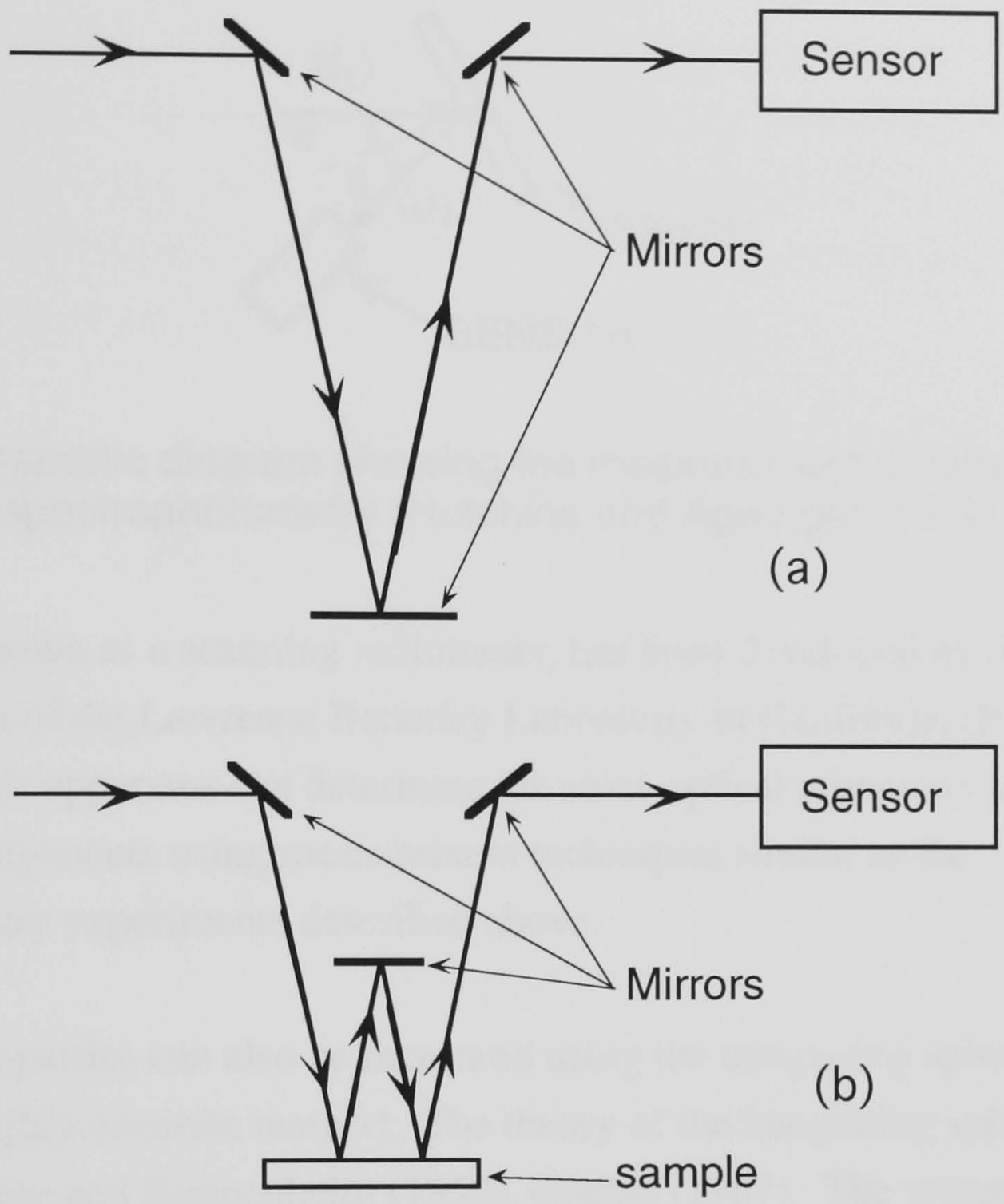

Fig 2.10 Schematic diagram showing the measurement of reflectance using spectrophotometry: a) reference measurement, b) sample under test. (Prasad 1994)

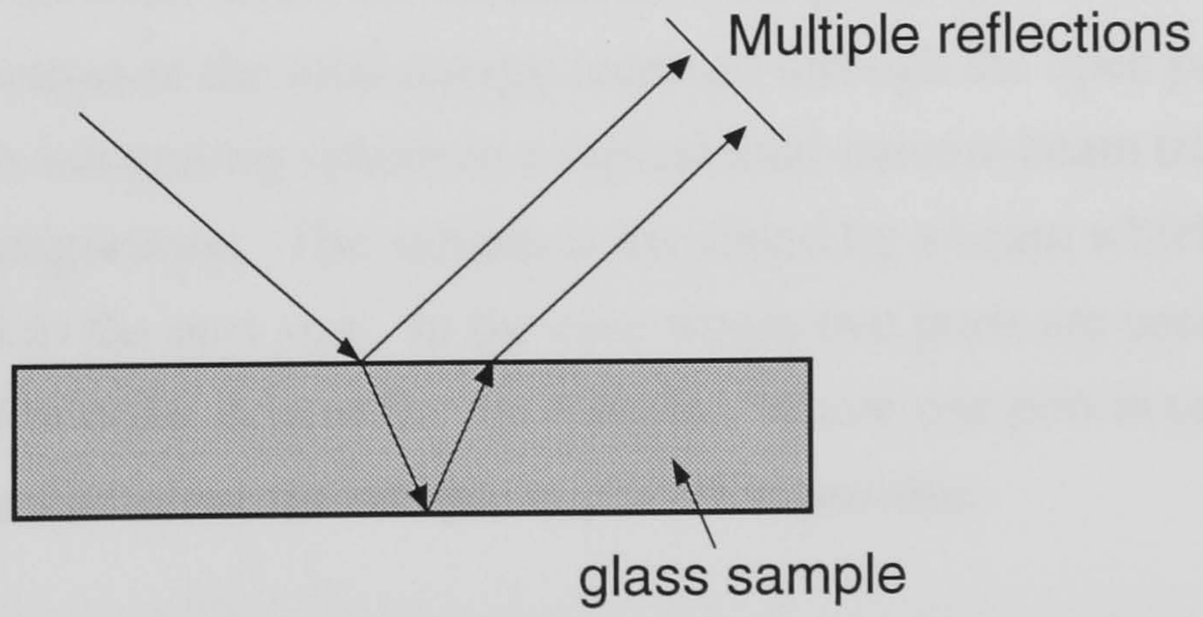

Fig 2.11 Schematic diagram showing the multiple reflections from a sheet of glass (Prasad 1993)

Once the transmittance and the reflectance of glazing unit is established, the absorption can be calculated using Equation (2.19).

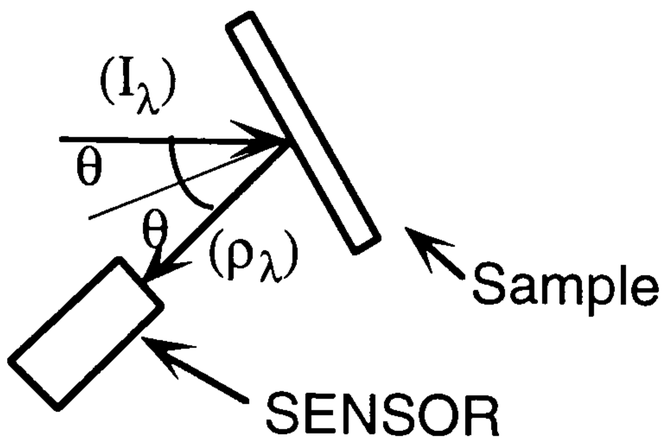

Fig 2.12 Schematic diagram showing the measurement of reflectance using spectrophotometry (Hutchins and Ageorges 1992).

An apparatus known as a scanning radiometer, has been developed by the Applied Science division of the Lawrence Berkeley Laboratory in California, (Papamichael et.al., 1988) This apparatus can determine the solar-optical properties of large fenestration components using measurement techniques similar to the spectrophotometry experiments described above.

Solar optical properties can also be measured using the integrating sphere which is a complex, but highly accurate method. The theory of the integrating sphere is discussed in detail by Jacque and Kuppenheim (1955), Goebel (1967). The integrating sphere is defined as a hollow spherical enclosure, usually 10 cm in diameter, whose interior walls are constructed of a material which diffusely reflects radiation of all wavelengths of interest, with highly reflecting power. Ideally, the wall coating is uniform, spectrally non-selective and an ideal diffuser. At a point on the sphere there is a port to allow the radiation into the interior, while on the interior wall of the sphere there is a detector which is used to measure the total energy received through the open port. Figure 2.13 is a diagram of an integrating sphere in a typical dual-narrow-beam transmittance measurement configuration. The sample is irradiated by a beam which covers an area less than or equal to the port size. In the case where two ports are used, one is used as reference, while the other is used for the sample. Where one port is used, a reference standard is measured before the sample is placed in position.

The integrating sphere has undergone a number of developments over the last few years. Materials such as transparent insulation material are complex in their construction, and as a result, light is scattered as it is transmitted through it. The small spheres are not adequate in capturing all this scattered transmitted energy. Karlsson

(1987), developed a 1 metre diameter sphere to characterise the solar optical properties of transparent insulation material to overcome this problem of scattering. Platzer (1992), developed a traditional size integrating sphere with broad area radiation, to measure larger samples. The narrow-beam spheres can only measure thin homogeneous samples, because out-scattering losses increase as the sample thickness increases. The broad area radiation integrating sphere allows thicker samples to be measured as out-scattering from radiation incident near the sample centre is compensated by in-scattering from rays near the aperture.

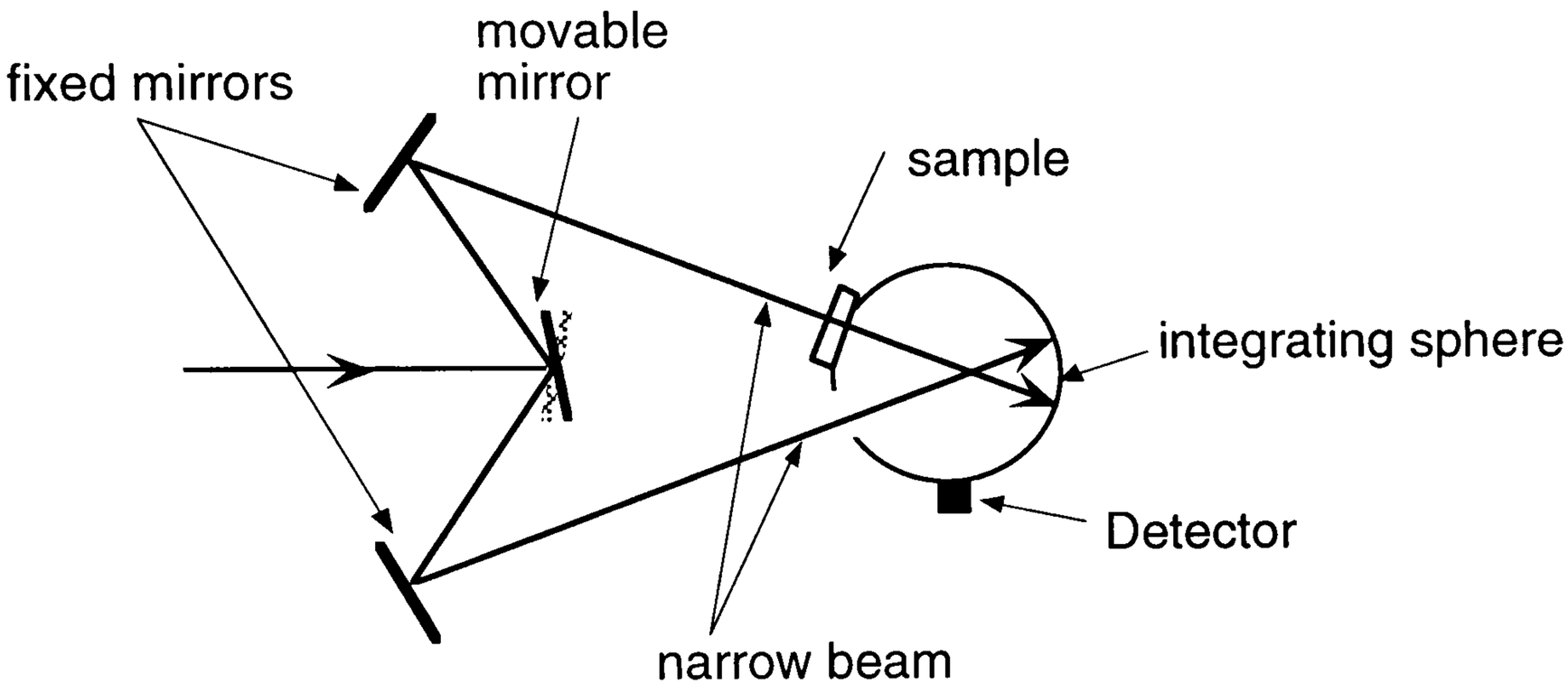

Fig 2.13 Schematic diagram of a dual narrow-beam arrangement integrating sphere (Milburn and Hollands 1994)

Relevant data on the wavelength dependent transmittance, absorption and reflectance of a thin film material is useful in defining the use of that material as shown by Granqvist (1989) and Minne (1990), and highlighted in Chapter 1.

2.6 The Effect of Phase Change

Finally, the phase change of electromagnetic radiation can be utilised to produce interference stacks. These stacks can be either destructive or constructive, and can aid the reflective properties of the glazing system.

The phase change of a reflected wave from a film on a non-absorbing substrate is

$$\phi = \begin{cases} 0 \text{ if } n_o > n_i \\ \pi \text{ if } n_o < n_i \end{cases} \qquad (2.35)$$

For an absorbing substrate, the phase change is more complex and is given by:

$$\phi = \mathbf{tan}^{-1} \frac{2n_o k_1}{\left(n_o^2 - n_1^2 - k_1^2\right)} \qquad (2.36)$$

A wave reflected at an air/glass interface undergoes a phase shift of π or 180°, while the transmitted wave does not undergo a phase change. The incident wave may interfere with one or more of the waves which are reflected from the interfaces formed by the thin film and the substrate. Rancourt, (1987) stated that the phases and the amplitudes of these waves determine whether the resultant sum of the waves leads to constructive or destructive interference. If the wave emerging from the film, is of the same phase as the wave reflected at its surface, then constructive interference occurs giving rise to increased surface reflectance. If the wave emerging from the film is 180° out of phase to the wave reflected at its surface, then destructive interference is said to have occurred and no surface reflectance exists.

By using non-absorbing films of thickness $\lambda/4$, constructive and destructive interference is kept to a minimum for light wavelengths. This thickness only holds for a certain part of the spectrum, and so the typical wavelength used is 550nm which occurs in green light and at which the human eye is most effective. (Rancourt 1987) As the range of the visible spectrum is narrow when compared to the rest of the electromagnetic spectrum, a thickness of $\lambda/4$ is the best compromise. Any iridescence which occurs therefore, happens at the edges of the visible spectrum where the human eye is not so effective. The reflectance of the film can be changed by altering its refractive index, see Equation (2.23).

BLANK IN ORIGINAL

Chapter 3 Experimental Apparatus and Procedure

3.1 Introduction

The purpose of the experimentation was to obtain data on the thermophysical properties of solar-control films. This involved the collection of data concerning the total solar energy transmittance of the glass and film, the daylight transmittance and the temperatures which arise for a certain illuminance at a specific angle. This would allow the calculation of a centre-pane U-value for the glass and film and also a measure of how well the solar-control film reduced the internal air and globe temperatures. With known air and globe temperatures, a measure of thermal comfort could then be established for the solar-control film. With these aims in mind an experimental procedure and a test rig was established.

The experimental work concerning hot boxes up to 1990, concentrated upon thermal performance of windows in terms of heat loss. A hot box to measure the thermal characteristics of building products was developed at the Institute for Research in Construction in Canada, in the early 1960's, (Bowen et.al 1961). This facility was developed in the 1980's to test heat transmittance through window products as discussed by Bowen and Solvason (1984) and Elmahdy and Bowen (1988). The work by the Canadian team became one of the standards for determining heat loss through window systems. Klems' (1979), presented a paper concerning a laboratory hot box. His work produced beneficial results, showing how the thermal performance, the U-value, of windows could be improved by simple measures such as heat mirror coatings. However, this work and that of the Canadians did not take into account the effect of solar radiation upon the temperature of the glass, which would effect its thermal performance. From his initial laboratory work, Klems et.al (1982), developed a mobile field test facility (MoWitt), to measure the thermal transmittance, solar heat gain and overall thermal performance of windows under solar irradiation. The MoWitt facility was able to provide good results for the thermal performance of the windows tested, (Klems 1989), but at an operating cost of $1,300 a week, it use was limited, (Sullivan 1994). McCabe (1987), developed two 'field measurement boxes' to determine the solar and optical properties of windows already installed in buildings. He reported separate results for night-time thermal losses and day-time solar heat gain. He concluded that the portable hot box had the "potential for absolute measurement of night-time U-values for windows, provided the effects of the radiative heat exchange with the night sky and

the outdoor surfaces were properly evaluated." The experimental procedures and apparatus following, were set up, with the conclusions of the previous work in mind.

3.2 Experimental Apparatus

In previous work at Cranfield, Burek et. al. (1989) concluded that the indoor test procedure was more easily controlled, in that, a constant radiation flux could be obtained, independently of the prevailing ambient conditions. Griffiths et. al (1992), used an indoor test-rig during an initial study into the thermal performance of solar-control films. The use of an internal solar simulator, allowed the experiments to be conducted in a controlled environment within a laboratory. However, these experiments were hindered by the fact that they were carried out in a laboratory which was lit by daylight, and was also where other work was going on around the experimental apparatus. So for this study, a laboratory was established within the middle of the School of Mechanical Engineering which did not have these hindering features. By eliminating any windows and natural ventilation, a controlled environment was established. A fan-coil air-conditioning system was used to control the temperature of the room. A schematic diagram can be seen in Figure AII.1 in Appendix II.

In order to simulate the sun's emissions as received at ground level, a Philip's pulsed xenon lamp was used (rated at 20 lm W^{-1} and 3 kW with an effective surface temperature of 5600 K). The spectral composition of the light from the lamp can be seen in Figure AII.4. The lamp was mounted into a luminaire which was air-cooled. This lamp was previously used as an energy source for the modelling of line-axis solar collectors, (Eames 1989). During this previous work, a glass filter was used to reduce the radiant heat transmittance from the lamp itself, to the object under test. When the new apparatus was being designed, the filter caused a problem in that it needed rigid support and it also reduced the amount of simulated solar energy reaching the hot box. It was decided therefore, to remove it, and to include within the computer based simulation, the heat transfer path of this thermal radiant energy. In total, the thermal radiant energy from the lamp which was received by the illuminated hot box amounted to approximately 3 Wm^{-1}, compared with the solar insolation at the glass surface of 100 Wm^{-1}. The lamp, its luminaire, the cooling fan and the lamp's starting system were held on two arms. The arms were made out of box-section metal tube as the luminaire, fan and starting equipment were very heavy. These arms were pivoted, the axis of which corresponded with the top surface of the glass, when placed in the hot box for testing. See Figure 3.1. These pivots allowed the lamp to be positioned, so that the

emergent beam could be set at any angle of incidence, with respect to the horizontal glass, with a range of zero to 90°. As the lamp/luminaire support structure was heavy, and a high degree of accuracy was needed to position the lamp at a specified angle of incidence, a redundant lathe screw was employed, as a support and positioning mechanism. The height of the lamp from the glass surface was chosen to give an illuminance upon the glass plane of approximately 100Wm^{-1}.

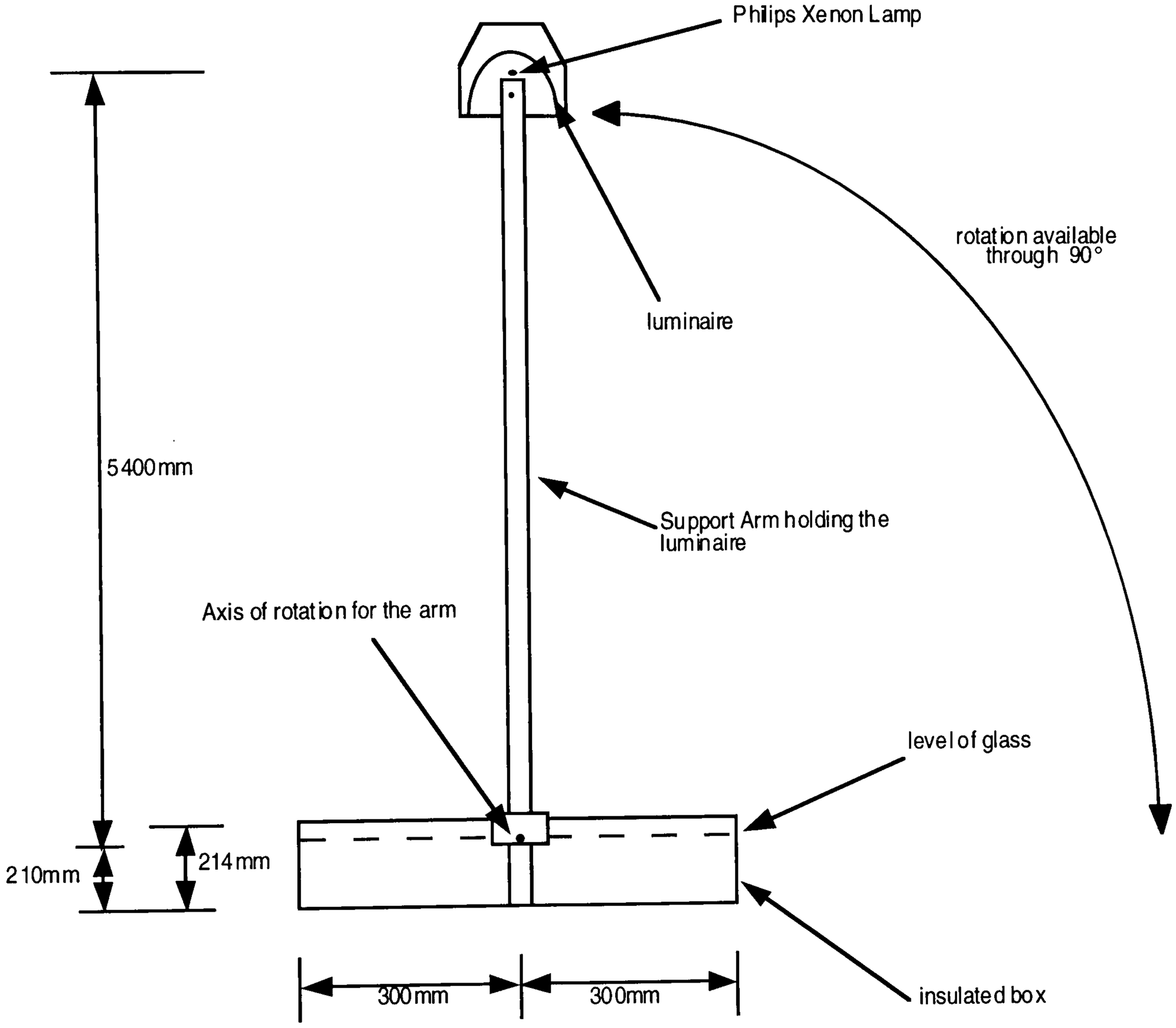

Fig 3.1 The test rig: side view

For the purpose of clarity, the lifting gear which supported the luminaire, the start-up equipment for the lamp and the fan unit, have been omitted from this figure.

The hot box was constructed out of 12mm plywood, with a thermal conductivity of 0.14 Wm^{-1}K^{-1}. The dimensions of the box were 638 by 638 by 210 mm. Two sheets of the plywood were bonded together to make the base and walls. Around the outside of the plywood 20mm of expanded polystyrene, with thermal conductivity of 0.03 Wm^{-1}K^{-1},

was then used as an insulant. The box was painted matt black using a paint with a high absorptance 0.9 and emissivity 0.96. This was done to reduce the reflectance from the internal surfaces so that the box would act as a pseudo thermally-isolated small-scale room. The walls of the box were designed to create a shelf for the glass under test. This was achieved by making the internal plywood sheet 4mm lower than the external plywood sheet. Figure 3.2 is a diagram of the box.

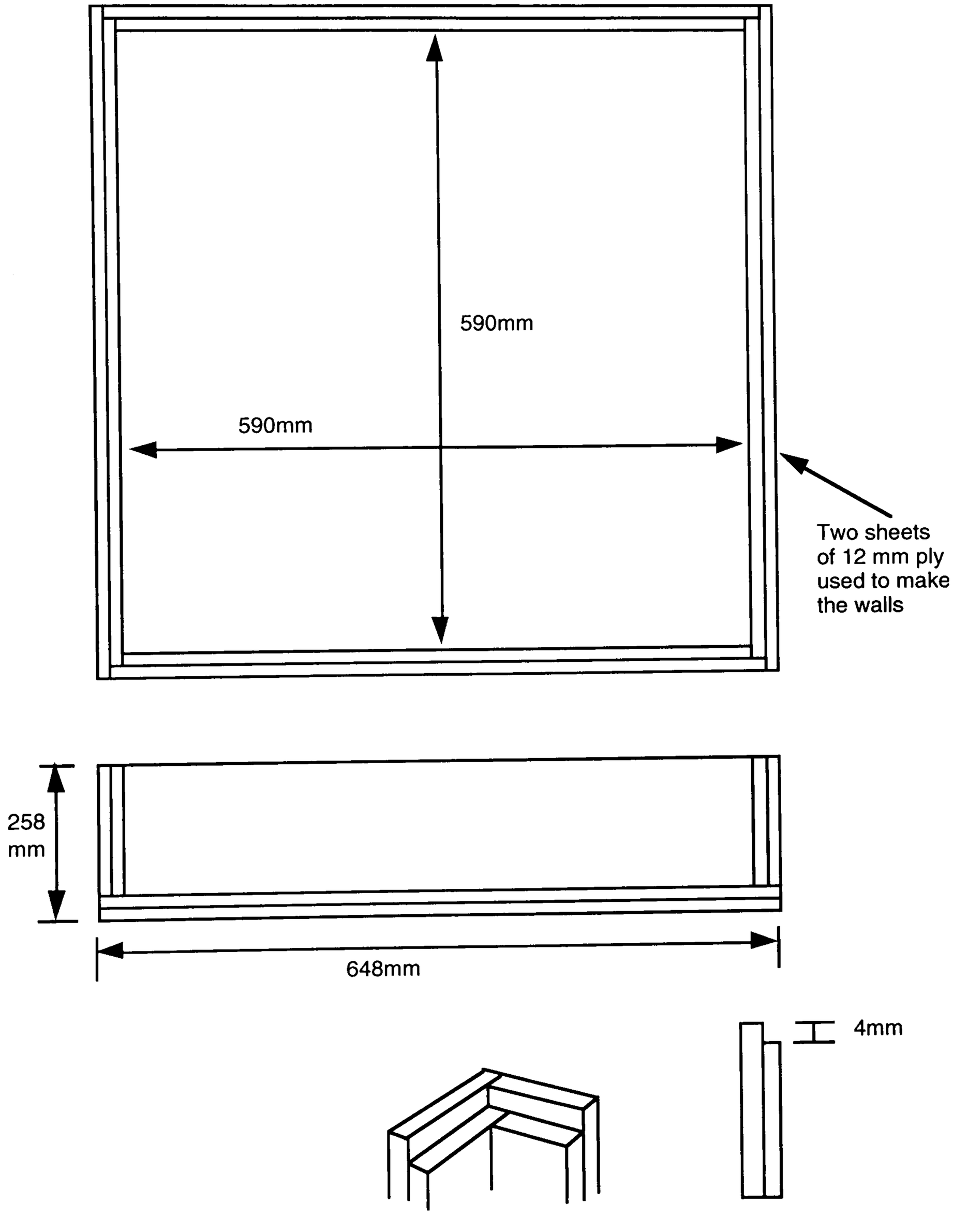

Fig 3.2 Schematic diagram of the plywood walls of the hot box showing the shelf for the glass

The box was placed so that the solarimeters used inside the box were sitting horizontally. This was done because information obtained from Duffie and Beckman (1974), stated that the efficiency of the Kipp and Zonen solarimeters available for this work declined, as they were tilted off the horizontal axis. In their new publication, Duffie and Beckman, (1991), stated that this error was never more than a few percent, however by this time, the design of the experimental rig was complete.

The hot box having been constructed, was instrumented using the type-T thermocouples. These were placed to measure the following; internal and external glass surface temperatures; internal floor and wall temperatures; external wall and base temperatures; internal and ambient air temperatures, and globe temperature within the illuminated hot box. Radiator shields were used for the thermocouples, measuring the internal and ambient air temperatures. Radiation shields were also used on the thermocouples, measuring surface temperature, where these temperatures were required without any radiative component. All the surface measuring thermocouples were located mid-plane so that the edge effects could be limited. The same argument was used for the internal air temperature thermocouples within the hot box.

A delay in the implementation of the experimental work occurred due to fluctuations in the power supply to the laboratory. Figure 3.3 shows the voltage supplied to the laboratory over a 48hr period. This was overcome by the use of a voltage stabiliser.

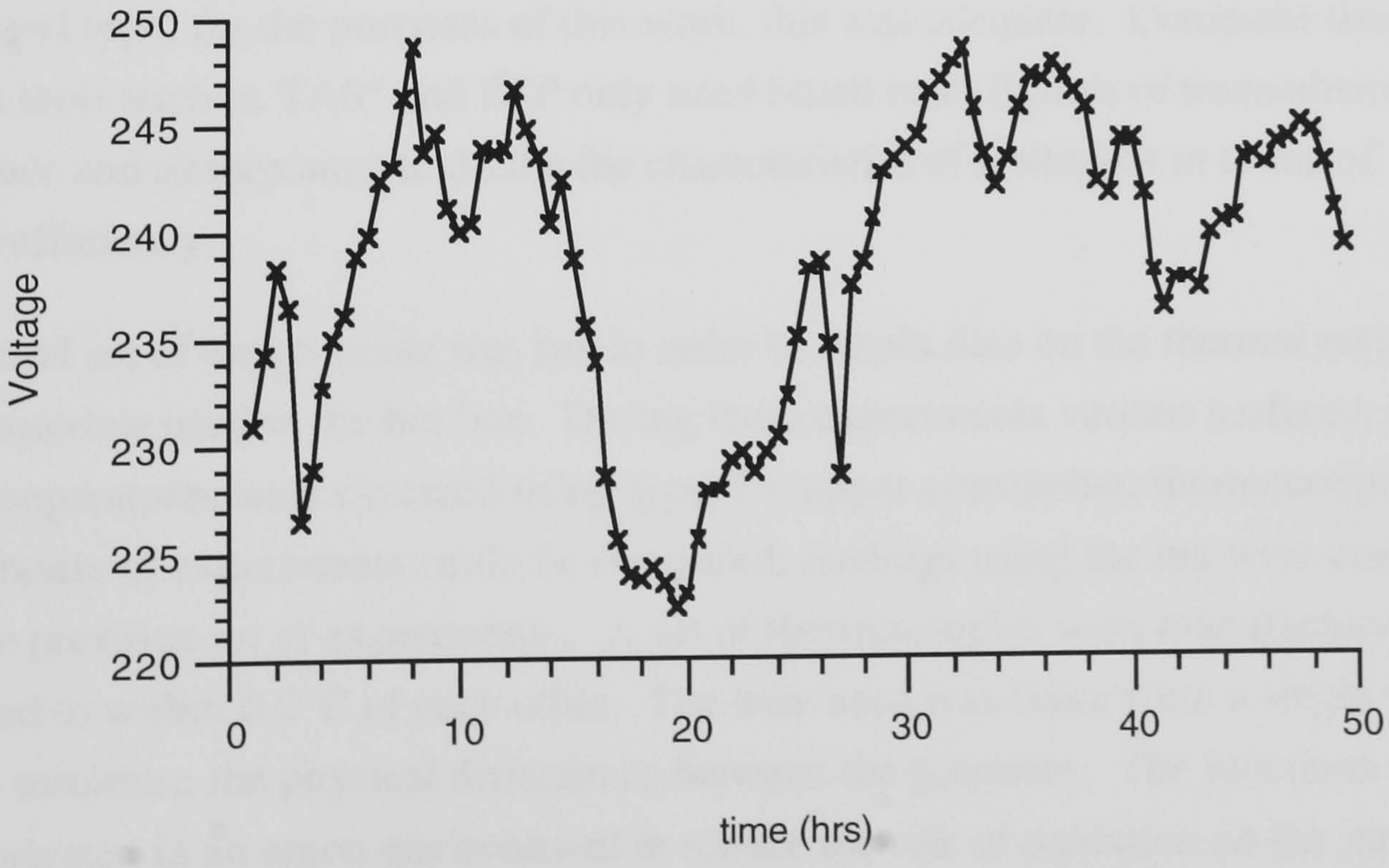

Fig 3.3 Voltage supplied to the laboratory over a 48hr period

3.3 Experimental Procedure

It was decided to run two sets of experiments. The first set of experiments sought to determine the solar energy transmittance and the daylight transmittance for each film. The temperatures of the surfaces, air and globe would then be determined from the second set of experiments. These experiments were run separately, as the solarimeter inside the hot box produced a shadow, covering nearly 90% of the hot box floor, thus reducing the amount of solar energy which reached the floor. To keep the computer model simple, it was decided that the temperature measurements should be taken without the solarimeter present.

The first set of experiments to be undertaken were seeking to determine the solar energy transmittance and the daylight transmittance for each film. The requirements here were to obtain steady-state conditions so that the output from the solarimeters used were stable. Steady-state conditions for the solarimeter were gained after about seven minutes. A series of readings was then taken over five minutes and then averaged. A figure for the solar transmittance of the film was obtained by comparing the solarimeter readings, with and without the glass and film present, at the angle of incidence required. Any readings after fifteen minutes had to be discounted as the rise in the internal air temperature was starting to affect the efficiency of the solarimeter. The solarimeters used were Kipp & Zonen CM5. These were calibrated, by the manufacturers, in August 1991 with a sensitivity of 12.07×10^{-6}V per Wm^{-2} at 20° and $500 Wm^{-2}$. The data for daylight transmittance was obtained, using a lux meter, which registers light between 400 and 700nm. The data gained from the solarimeter and the lux meter were of the broad-band type; for the purposes of this work, this was adequate. Computer thermal analysis tools such as TAS° and ESP only need broad band figures of transmittance, reflectance and absorptance to define the characteristics of a window in terms of thermal efficiency.

The second set of experiments was run in order to obtain data on the thermal response of the materials used in the hot box. During these experiments various surfaces, air and globe temperatures were obtained using type-T (copper-constantan) thermocouples. So that both sets of experiments could be compared, readings using the lux were continued from the previous set of experiments.. A set of thermocouples were manufactured and calibrated to within 0.2°C of each other. The wire used was taken from a single roll in order to minimise the physical differences between the junctions. The junctions were then fabricated in an argon environment to reduce the risk of oxidation on the junction. This action prevented the junction from oxidising which would in turn have reduced the efficiency of the electronic junction and the accuracy of the results. Where possible

three thermocouples were used to obtain a required temperature. This was done so that a failure of a junction could be identified, and its results then ignored. Finally, all the thermocouples measuring surface temperatures were shielded by highly reflective aluminium foil in order to reduce the effect which thermal radiation would have upon the junction.

Unlike the first experiments which determined the solar energy transmittance, the second set were run over a longer period of time, usually four hours, by which time the temperatures of the box were reaching steady-state. Initial runs were undertaken over a twenty-four hour period, and from these it was seen that the temperature rise after four hours was minimal, compared to that over the first four hours.

3.4 Apparatus Calibration

Several calibration procedures were reviewed when deciding how to calibrate the experimental hot-box. The calibration procedure adopted by Bowen and Solvason (1984), used a glazing specimen with known thermal properties. With this specimen, the thermal properties of the rest of their hot-box was tested. A similar procedure had been adopted by Klems (1979). Klems used a sheet of polyurethane foam as his specimen, so that the thermal loss rate through the hot-box skin could be determined. This type of procedure has been shown to give accurate results when calibrating thermal insulation hot-boxes, where the nature of the specimens used is opaque. However, this arrangement does not suit a solar simulator - hot-box arrangement. The portable nature of the hot-boxes designed by McCabe and Hill (1987), meant that their calibration procedure concentrated on heat loss where the hot-box jutted up against the frame of the window under test. They also carried out a calibration test in order to determine the electrical load on the heating apparatus, which was used when testing thermal efficiency of the glass under night-time conditions.

It was decided to carry out a calibration test of the hot-box by performing a heat balance for the box under steady-state conditions in order to provide data which verified the heat losses from the box. An experiment, using a 4mm thick pane of float glass, with known thermal and optical properties was run for 20hrs by which time the box had reached steady-state. The temperatures obtained were then used in an energy balance to determine whether the energy coming in, equalled the energy flowing out. Figure 3.4 shows the temperature rise against time over the 20hr period. The results are plotted in

Table 3.1, along with the solar input from the lamp. Figure AII.2 in Appendix II shows the positions of the thermocouples

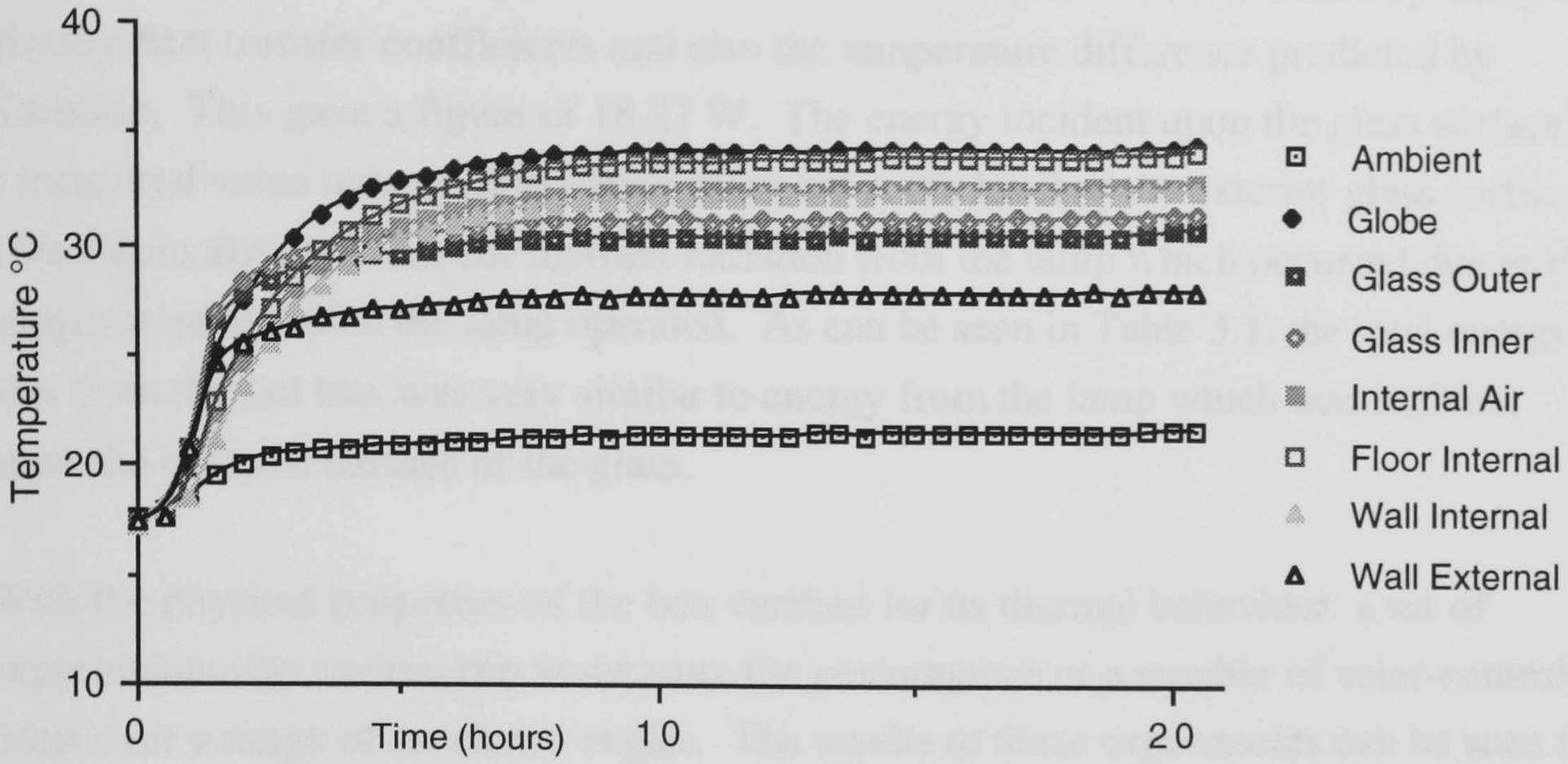

Fig 3.4 Temperatures of the box over a twenty hour period

Calculation	Area	Resistance, 1/R	ΔT	Q, Watts
walls	4AΔT/R	0.59x0.21	1.1932	4.574	2.705
floor	AΔT/R	0.59^2	1.0825	7.14	2.69
glass	AkΔT/L	0.59^2	262.5	0.79	72.19
				Total	77.585
	Correction to glass thermal transmittance			ΔT=0.2	18.27
				Total	22.92
	Power from the lamp incident on the glass				22.96

Table 3.1 The steady-state energy balance of the hot-box

During the calibration it was observed that the thermocouples measuring the glass surface temperatures, were giving different readings to those obtained from contact probes. Karlsson et.al (1988) stated that the typical temperature difference across a sheet of thin glass is approximately 0.2°C, while the computer model gave a figure of 0.12°C. Furthermore, the most resistance to heat loss through glass is in the thin air films on either side of the glass. This led to further investigation of the aluminium foil

covering the thermocouples on the glass, which showed that they were absorbing the electromagnetic radiation in the infra-red region. It should also be observed that the calculation of heat loss through glass is complicated where solar absorption is present. Therefore a figure for the thermal transmittance of the glass was calculated by using the glazing heat transfer coefficients and also the temperature difference predicted by Karlsson. This gave a figure of 18.27 W. The energy incident upon the glass surface is a measured value using a solarimeter mounted at the level of the exterior glass surface. This figure also includes the thermal radiation from the lamp which occurred due to the temperature at which the lamp operated. As can be seen in Table 3.1, the total energy loss from the hot box was very similar to energy from the lamp which was incident upon the external surface of the glass.

With the physical properties of the box verified for its thermal behaviour, a set of experiments was undertaken to measure the performance of a number of solar-control films over a range of incidence angles. The results of these experiments can be seen in Chapter 5.

To further corroborate the experimental work, several computer based simulations were undertaken to determine the thermal performance of the box. An understanding of the nature of the energy flows within and around the hot box needed to be fully understood, so that these computer models could be developed.

BLANK IN ORIGINAL

Chapter 4 Theoretical Modelling

4.1 Introduction

Alongside the experimental work, a theoretical study was carried out to determine algorithms to model the thermal behaviour of window films. Brunello and Zecchin (1982), proposed a system of energy balances based on the resistance method in order to determine the energy transmitted into a building through a window. It was decided to extend this idea to the hot-box, and so a thermal resistance network was developed for the experimental apparatus, as shown in Figure 4.1 and AII.3 in Appendix II.

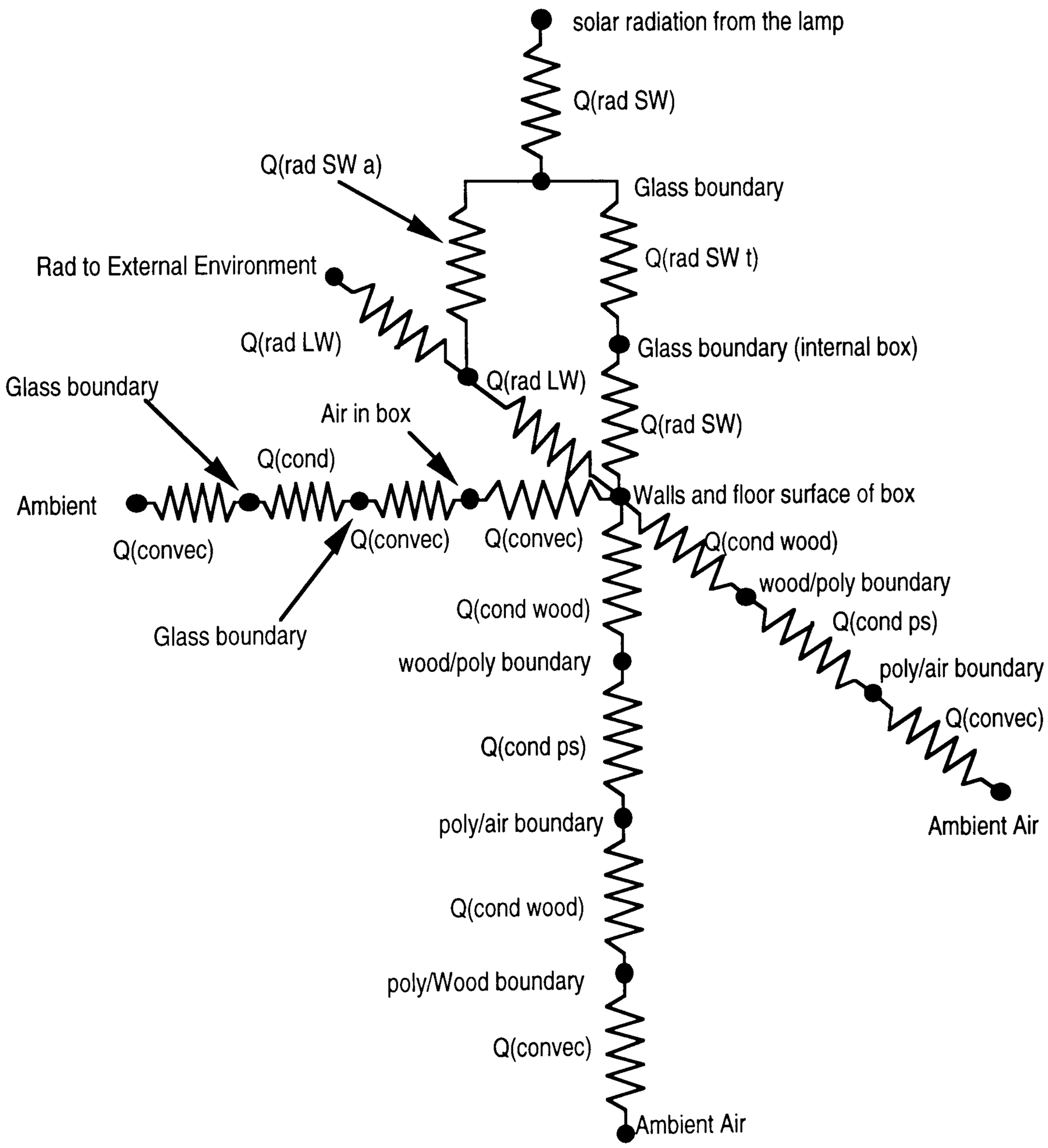

Fig. 4.1 A schematic diagram of the thermal processes in the experimental rig

The resistance model having been established, a flow chart was constructed to determine the various energy paths which would need to be established within the model. Below is a flow-diagram of how the program is set up to determine heat flow, Figure 4.2.

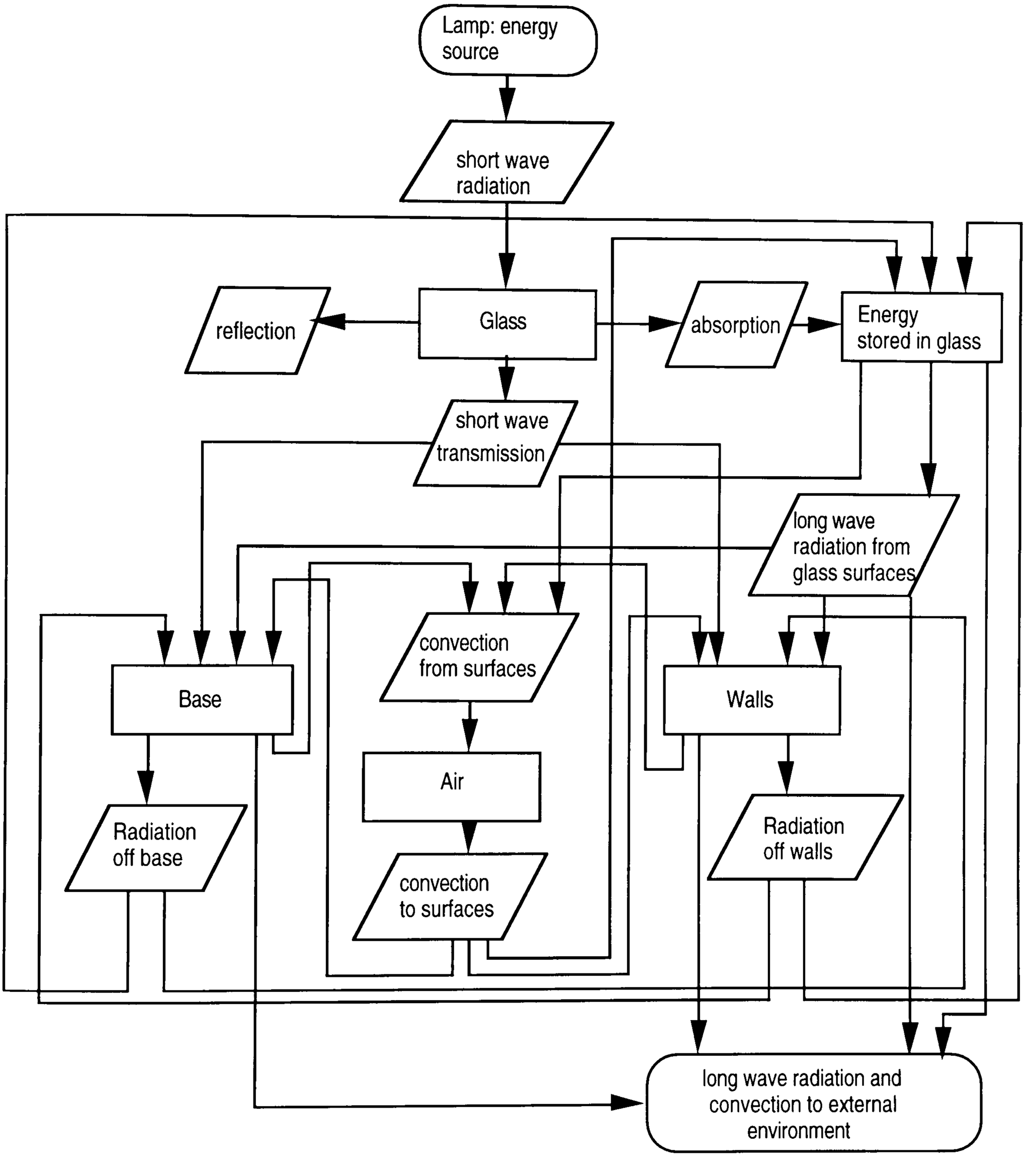

Fig. 4.2 Schematic diagram of how the first model dealt with heat flow

The radiant energy transfer from the lamp to the box was considered, using shape factors. The same process was used for radiant thermal energy transfer between

surfaces in the box. Heat radiation transfer coefficients were used where possible, in order to eliminate the T^4 terms from the equations, thus making the computations easier to resolve, that is, all temperatures being then considered in terms of T. Where short wave heat transfer from the lamp is included as an input, this is represented by the lamp intensity, modified by the shape factor, area of the surface and any other operations, for example, absorption and transmittance, for that particular surface.

A series of energy balances was set up which reflect the schematic diagram, Figure 4.2. The energy source is the lamp which transmits its energy to the box via the glass. At the glass surface the light is split into three components, a) the reflected energy Q_ρ, b) the transmitted energy Q_τ, and c) absorbed energy, Q_α. The reflected component is lost to the external environment, the energy entering the glass is therefore $Q_{(1-\rho)}$; a part of this is absorbed by the glass as a result of the processes discussed earlier (see Chapter 1). The energy then passes through the inner glass/air boundary where further reflection within the glass will occur. The transmitted energy is still in a short wave form and is absorbed by the walls and the floor of the box. The directly transmitted solar radiation is determined using the Equations (2.24) and (2.25) in Chapter 2, Section 2.3. The radiant energy reaching the internal surfaces of the box is therefore dependent upon, a) the radiant energy emitted by the lamp, b) the amount of energy which is transmitted through the glass, including the directly transmitted short wave radiation and a component of the short wave radiation which is absorbed by the glass and then radiated inwards, c) the short wave emissivity of the receiving surface and d) the shape factor, which is a measure of how much of the radiation leaving one surface is received by another surface and is defined by Siegel and Howell (1980).

The model contains a number of nodes at which the temperature is determined. At each node an energy balance is determined using the principle of the conservation of energy and the three forms of heat transfer; radiation, convection and conduction.

4.2 Radiation, Convection and Conduction

Conduction through a material is dependent upon the its thermal conductivity, its area and thickness, and the temperature difference between the two surfaces, see Equation (4.1).

$$q_{cond} = \frac{A_s k}{x} \Delta T \qquad (4.1)$$

where A_s is the area, k is the thermal conductivity, x is the thickness and ΔT is the temperature difference across the material.

Convection away from a surface is similar to conduction, however the thermal resistance of the surface air film needs to be taken into account. This is known as the convection heat transfer coefficient. The convective heat transfer coefficient, h_c, of all the surfaces of the model, changes with respect to the surface temperature and thermophysical properties of the air, which are themselves dependent upon the air temperature. The convective heat transfer coefficient is determined by the Nusselt number, Nu, the thermal conductivity of the fluid, k_f, and the characteristic length of the surface L see Equation (4.2).

$$h_c = \frac{Nu k_f}{L} \tag{4.2}$$

Within the boundaries of the model it has been assumed that only free convection takes place. Taking into account this assumption, the Nusselt number can be calculated from the Rayleigh number, Ra. The formula to calculate the Nusselt number is dependent upon the orientation of the surface as shown by Incopera and de Witt (1981). The different equations are outlined below:

Upper Surface of Heated Plate or Lower Surface of Cooled Plate

$$Nu = 0.54 Ra_L^{1/4} \qquad (10^4 \sim < Ra_L \sim < 10^7) \tag{4.3}$$

$$Nu = 0.15 Ra_L^{1/3} \qquad (10^7 \sim < Ra_L \sim < 10^{11}) \tag{4.4}$$

Lower Surface of Heated Plate or Upper Surface of Cooled Plate

$$Nu = 0.27 Ra_L^{1/4} \qquad (10^5 \sim < Ra_L \sim < 10^{10}) \tag{4.5}$$

The Rayleigh number is the product of the Grashof and Prandtl numbers. For horizontal plates the Rayleigh number is

$$Ra_L = Gr.Pr = \frac{g\beta(T_s - T_\infty)L^3}{\nu\psi} \tag{4.6}$$

where g is the acceleration due to gravity, T_s is the surface temperature and T_∞ is the fluid temperature. The physical properties of the fluid are β, the volumetric thermal

expansion coefficient, ν, the kinematic viscosity and ψ, the thermal diffusivity. L is the characteristic length of the surface which is defined as

$$L = \frac{A_s}{P} \tag{4.7}$$

where A_s and P are the plate surface area and perimeter, respectively.

For vertical surfaces, the Nusselt number can be determined using Equation (4.8):

$$Nu = 0.68 + \frac{0.670 Ra_L^{1/6}}{\left[1 + \left(\frac{0.492}{Pr}\right)^{9/16}\right]^{4/9}} \quad (0<Ra_L<10^9) \tag{4.8}$$

The Rayleigh number for a vertical surface is determined using Equation (4.5), replacing the characteristic length, L, with the height of the surface, x.

The fluid properties vary for different fluid temperatures. A series of graphs was produced, to derive algorithms from which the properties could be determined for a known temperature. The data used to plot the graphs were taken from tables of air properties in Incopera and de Witt (1981). Once the graphs were plotted, a curve-fitting program was used to derive equations for the individual properties, over the range of temperatures required.

The algorithms of thermophysical properties of air which were determined, are the kinematic viscosity, ν, the thermal conductivity, k_f, the thermal diffusivity, ψ and the Prandtl number, Pr. See Figures 4.3 to 4.6.

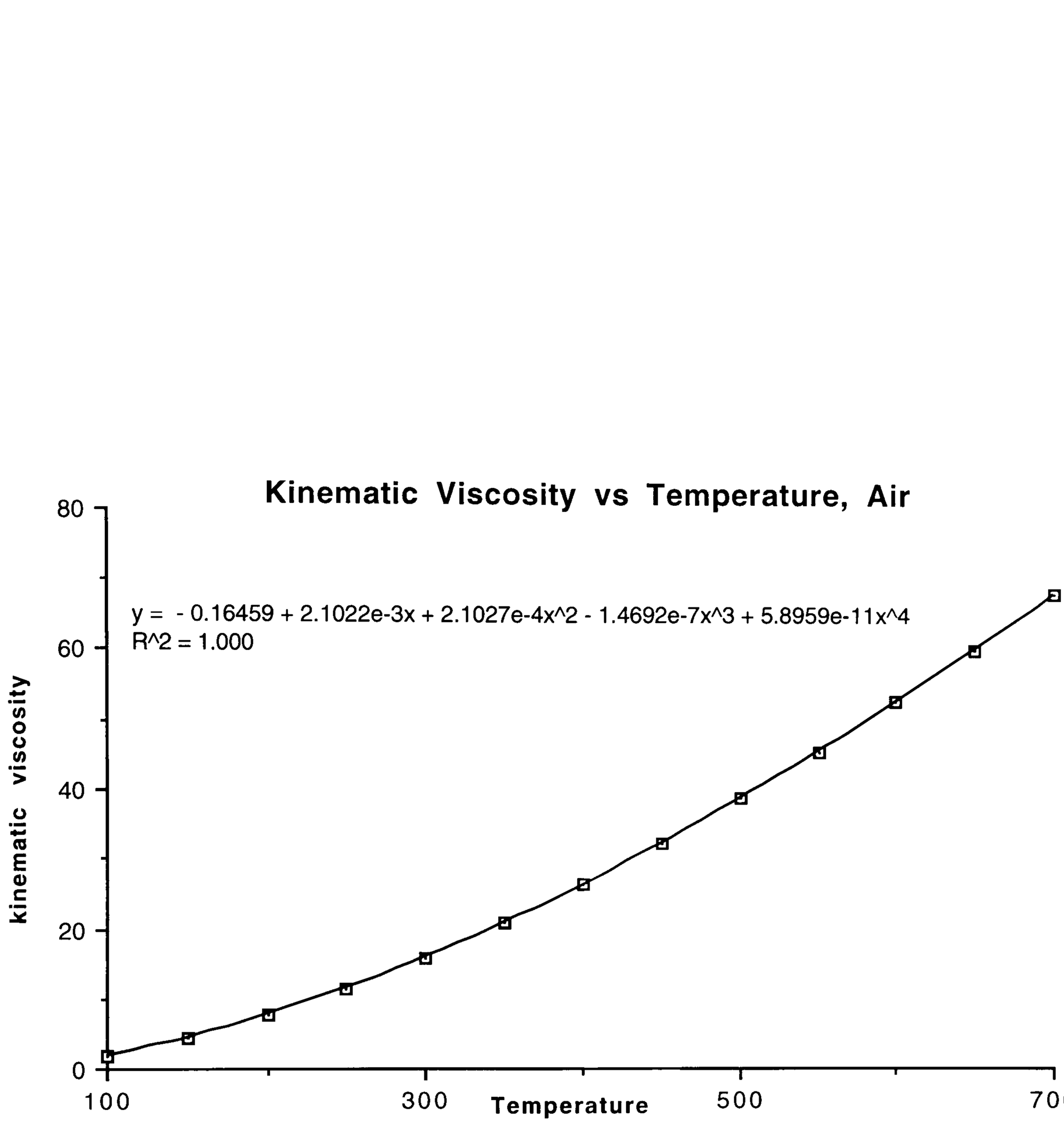

Fig. 4.3 Kinematic viscosity ($\times 10^{-6}$ m^2/s) of air vs temperature (K)

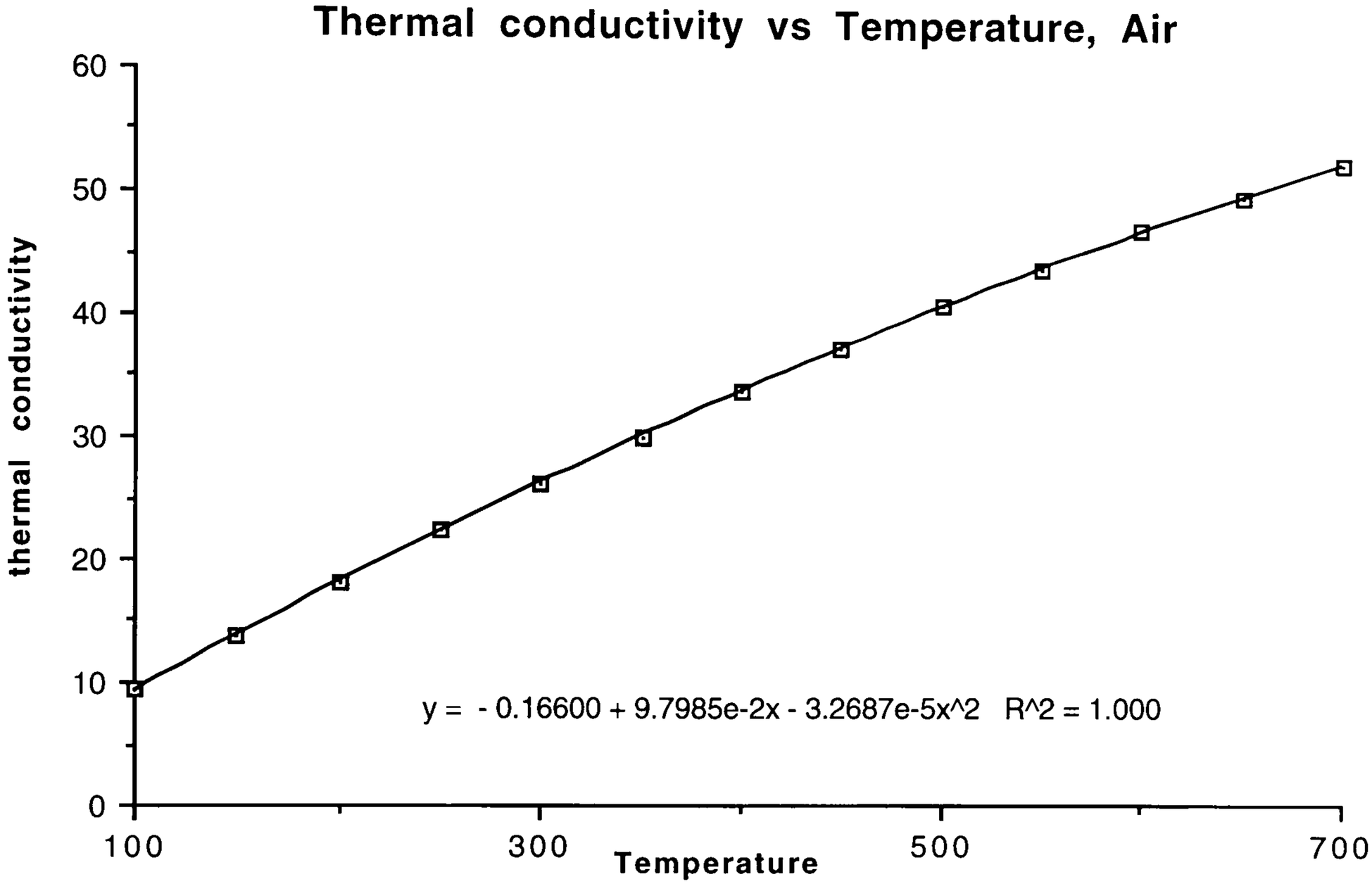

Fig. 4.4 Thermal conductivity ($\times 10^{-3}$ W/mK) of air vs temperature (K)

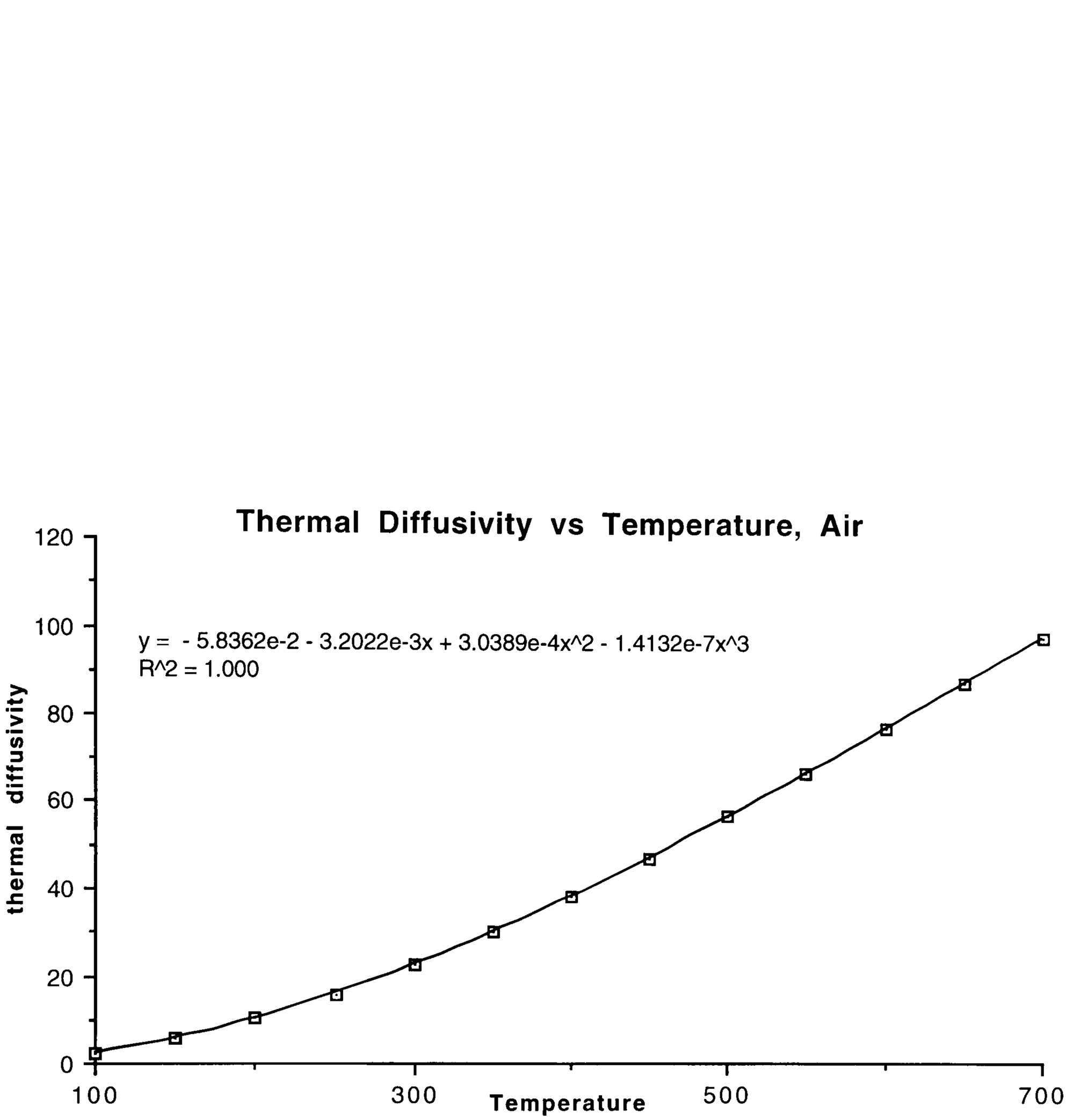

Fig. 4.5 Thermal diffusivity ($\times 10^{-6}$ m^2/s) of air vs temperature (K)

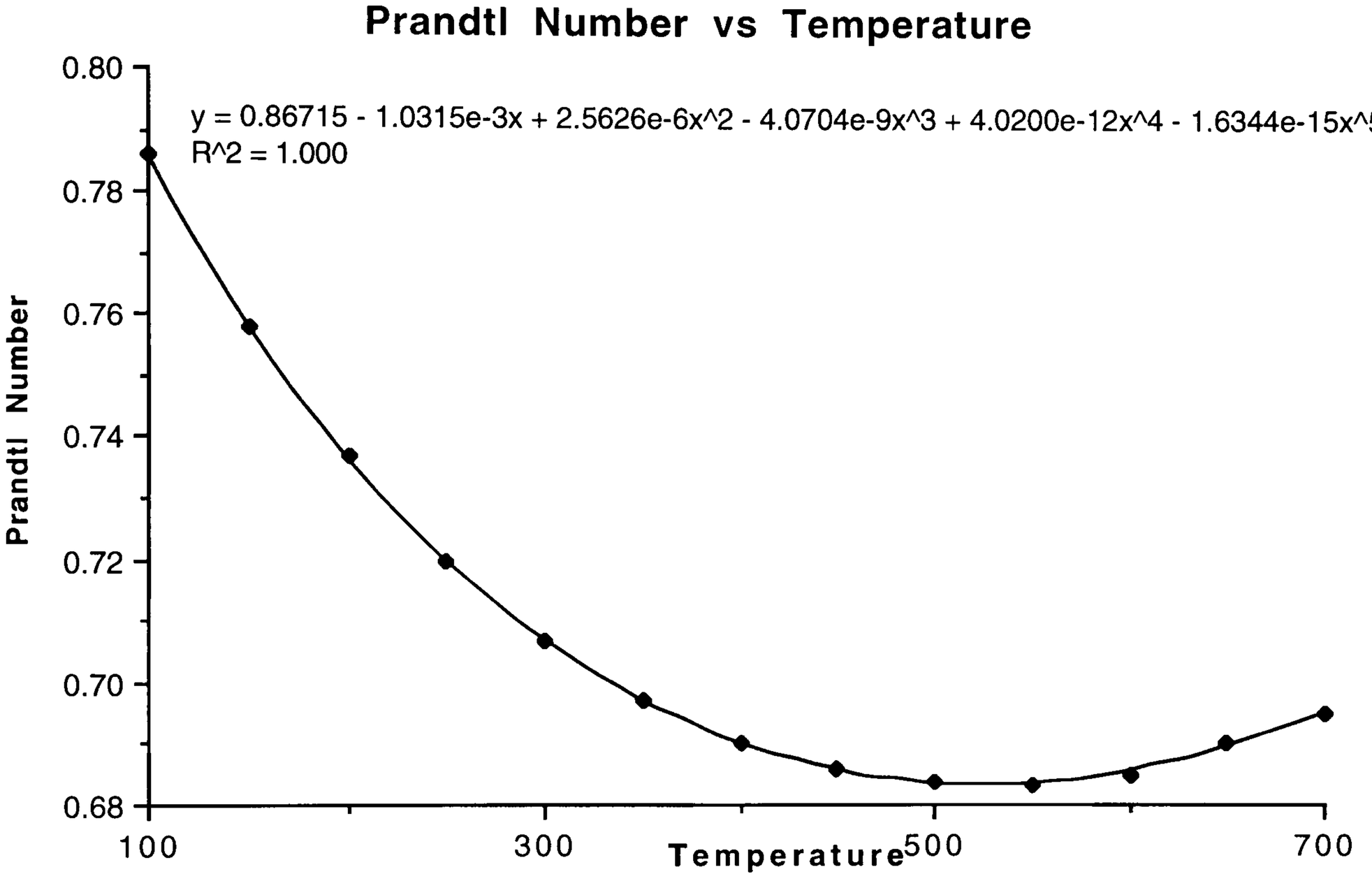

Fig. 4.6 Prandtl Number if air vs temperature (K)

For each curve-fit a regression analysis was carried out, and for each curve a 99% fit was achieved making them acceptable for the purpose in hand. The resulting algorithms derived were:

Prandtl number:

$$\mathrm{Pr} = \begin{pmatrix} 0.86715 - 1.0315\times10^{-3}\mathrm{T}_{air} + 2.5626\times10^{-6}\mathrm{T}_{air}^{2} \\ -4.0704\times10^{-9}\mathrm{T}_{air}^{3} + 4.02\times10^{-12}\mathrm{T}_{air}^{4} - 1.6344\times10^{-15}\mathrm{T}_{air}^{5} \end{pmatrix} \qquad (4.9)$$

Thermal diffusivity:

$$\psi = \begin{pmatrix} -5.8362\times10^{-2} - 3.2022\times10^{-3}\mathrm{T}_{air} \\ +3.0389\times10^{-4}\mathrm{T}_{air}^{2} - 1.4132\times10^{-7}\mathrm{T}_{air}^{3} \end{pmatrix} \times 10^{-6} \qquad (4.10)$$

Thermal conductivity:

$$k_f = \left(-0.166 + 9.7985\times10^{-2}\mathrm{T}_{air} - 3.2687\times10^{-5}\mathrm{T}_{air}^{2}\right)\times10^{-3} \qquad (4.11)$$

Kinematic Viscosity:

$$\nu = \begin{pmatrix} -0.16459 + 2.1022\times10^{-3}\mathrm{T}_{air} + 2.1027\times10^{-4}\mathrm{T}_{air}^{2} \\ -1.4692\times10^{-7}\mathrm{T}_{air}^{3} + 5.8959\times10^{-11}\mathrm{T}_{air}^{4} \end{pmatrix} \times 10^{-6} \qquad (4.12)$$

These were then used to determined the convective heat transfer coefficients over the range of air temperatures which existed in the experimentation.

Radiation between surfaces is determined by the Equation (4.13).

$$q_{rad} = F_{12}A_1\sigma\varepsilon_1\left(T_1^4 - T_2^4\right) \qquad (4.13)$$

where F is the shape factor of the interchange between the two surfaces (a percentage of the radiation leaving one surface which is incident upon another), σ is the Stefan-Boltzmann's constant and ε is the emissivity of the emitting surface. To avoid using any T^4 terms a radiative heat transfer coefficient was determined.

Radiative heat transfer coefficients were determined using two formulas.

It was decided to set the shape factor for the radiation from the external surfaces to the ambient environment to one, to simplify the calculation, otherwise a complicated integral would have been needed to calculate the various energy flows to the various room surfaces. Therefore, Equation (4.14) was used for all external surfaces.

$$h_r = \sigma \varepsilon A_s \left(T_s + T_\infty\right)\left(T_s^2 + T_\infty^2\right) \qquad (4.14)$$

where σ is the Stefan-Boltzmann's constant and ε is the emissivity of the emitting surface.

For the internal surfaces, the radiative heat transfer coefficient was determined by the shape factor, F_{12}, and the emissivity and the area, A, of both the emitting and receiving surfaces respectively. Therefore, Equation (4.15) was used for all the internal surfaces.

$$h_r = \frac{\sigma\left(T_s + T_\infty\right)\left(T_s^2 + T_\infty^2\right)}{\left(\frac{1-\varepsilon_1}{\varepsilon_1 A_1} + \frac{1}{A_1 F_{12}} + \frac{1-\varepsilon_2}{\varepsilon_2 A_2}\right)} \qquad (4.15)$$

Using these basic formulas heat balances were established for each node.

Finally, a routine was developed to obtain the shape factors for the radiation heat transfer, between the lamp and the hot box, with respect to the angle of incidence of the lamp to the glass surface. It was decided that the cross-string method should be used. To start with, the distances between the box surfaces and the lamp were measured, see Figure 4.7, for angles of incidence between 0 and 80°.

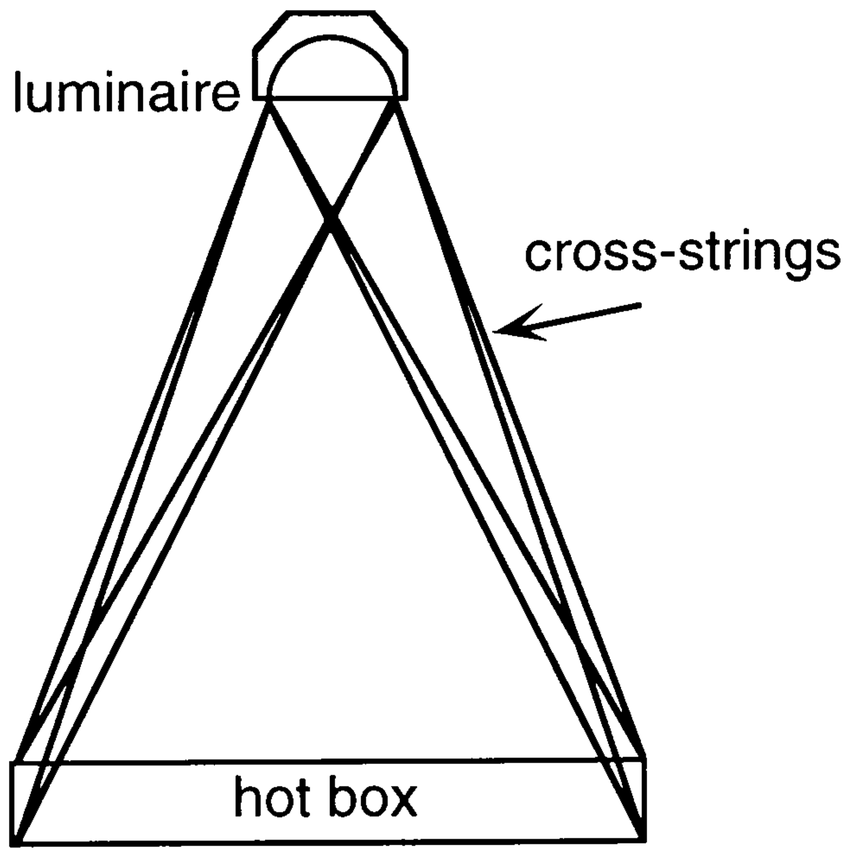

Fig 4.7 The cross-strings between the luminaire and the hot box.

These measurements were then plotted on a graph and curves produced for each string, see Figure 4.8. Next, curves were fitted to these strings and the curve-fit equations were used in a program which produced shape-factors for angles of incidence between 0 and 80°, see Equations (4.16-23).

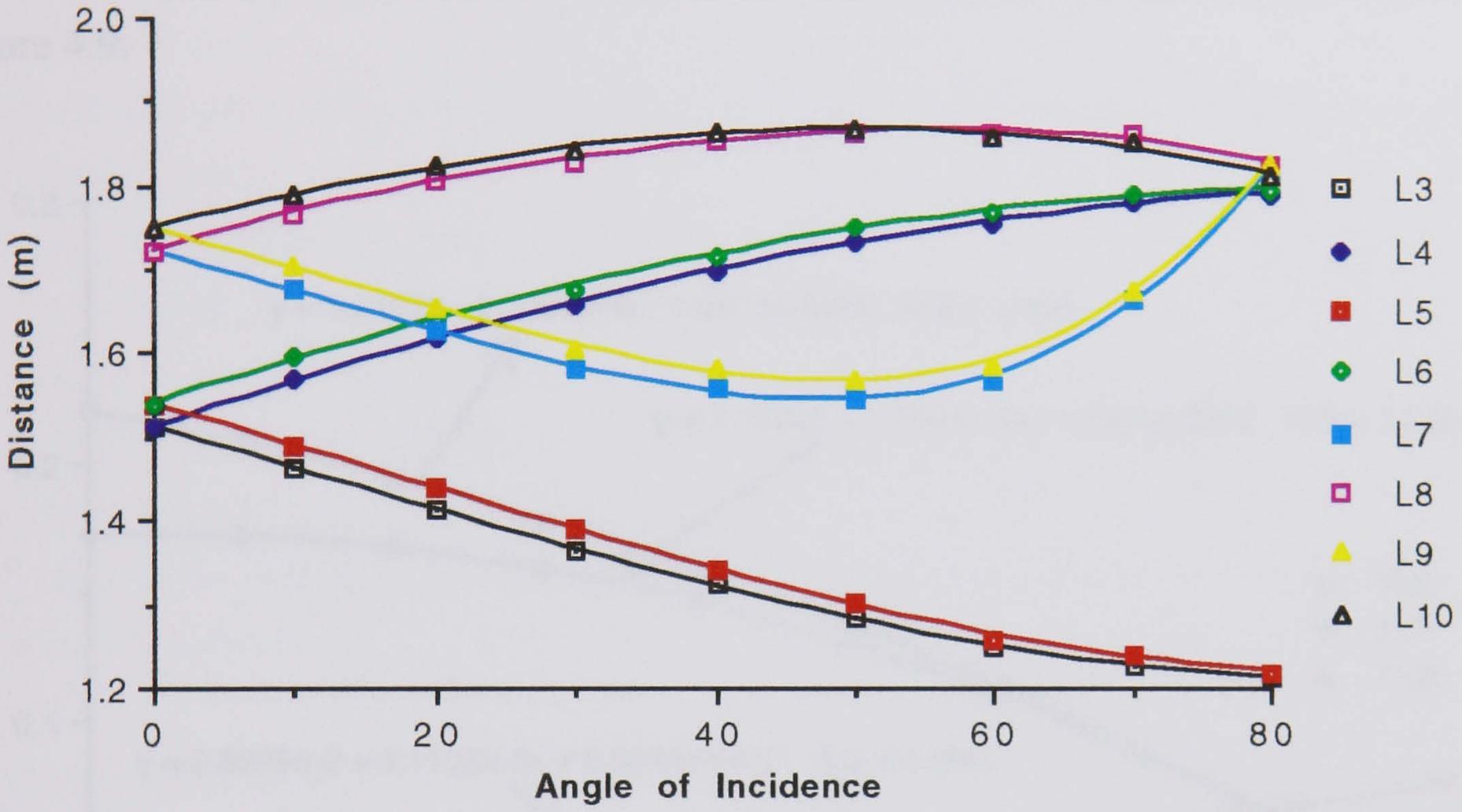

Fig 4.8 Length of cross-strings vs angle of incidence.

The equations obtained from the curves for each cross-string were:

$$L10 = \begin{pmatrix} 1.748 + 5.1322\times10^{-3}\theta - 8.3566\times10^{-5}\theta^2 \\ +9.3706\times10^{-7}\theta^3 - 6.993\times10^{-9}\theta^4 \end{pmatrix} \quad (4.16)$$

$$L9 = \begin{pmatrix} 1.7485 - 4.4937\times10^{-3}\theta - 8.5004\times10^{-6}\theta^2 \\ -2.015\times10^{-7}\theta^3 + 1.4685\times10^{-8}\theta^4 \end{pmatrix} \quad (4.17)$$

$$L8 = \begin{pmatrix} 1.7215 + 5.4867\times10^{-3}\theta - 7.6053\times10^{-5}\theta^2 \\ +7.7752\times10^{-7}\theta^3 - 5.8275\times10^{-9}\theta^4 \end{pmatrix} \quad 4.18)$$

$$L7 = \begin{pmatrix} 1.7221 - 4.6045\times10^{-3}\theta - 6.0917\times10^{-6}\theta^2 \\ -1.4038\times10^{-7}\theta^3 + 1.4219\times10^{-8}\theta^4 \end{pmatrix} \quad (4.19)$$

$$L6 = \begin{pmatrix} 1.5415 + 5.4918\times10^{-3}\theta \\ -2.3117\times10^{-5}\theta^2 - 6.0606\times10^{-8}\theta^3 \end{pmatrix} \quad (4.20)$$

$$L5 = \begin{pmatrix} 1.54 - 4.6836\times10^{-3}\theta \\ -1.938\times10^{-5}\theta^2 + 3.5017\times10^{-7}\theta^3 \end{pmatrix} \quad (4.21)$$

$$L4 = \begin{pmatrix} 1.5131 + 5.7891\times10^{-3}\theta \\ -2.627\times10^{-5}\theta^2 - 2.1886\times10^{-8}\theta^3 \end{pmatrix} \quad (4.22)$$

$$L3 = \begin{pmatrix} 1.5123 - 4.7868 \times 10^{-3}\theta \\ -1.0981 \times 10^{-5}\theta^2 + 2.9966 \times 10^{-7}\theta^3 \end{pmatrix} \tag{4.23}$$

Finally, the data from this program was used to produce a graph of shape factor vs angle of incidence for the surfaces which would be receiving the radiant energy, that is, the external glass surface, FLG, the floor of the box, FLF, and the side walls, FLW, see Figure 4.9.

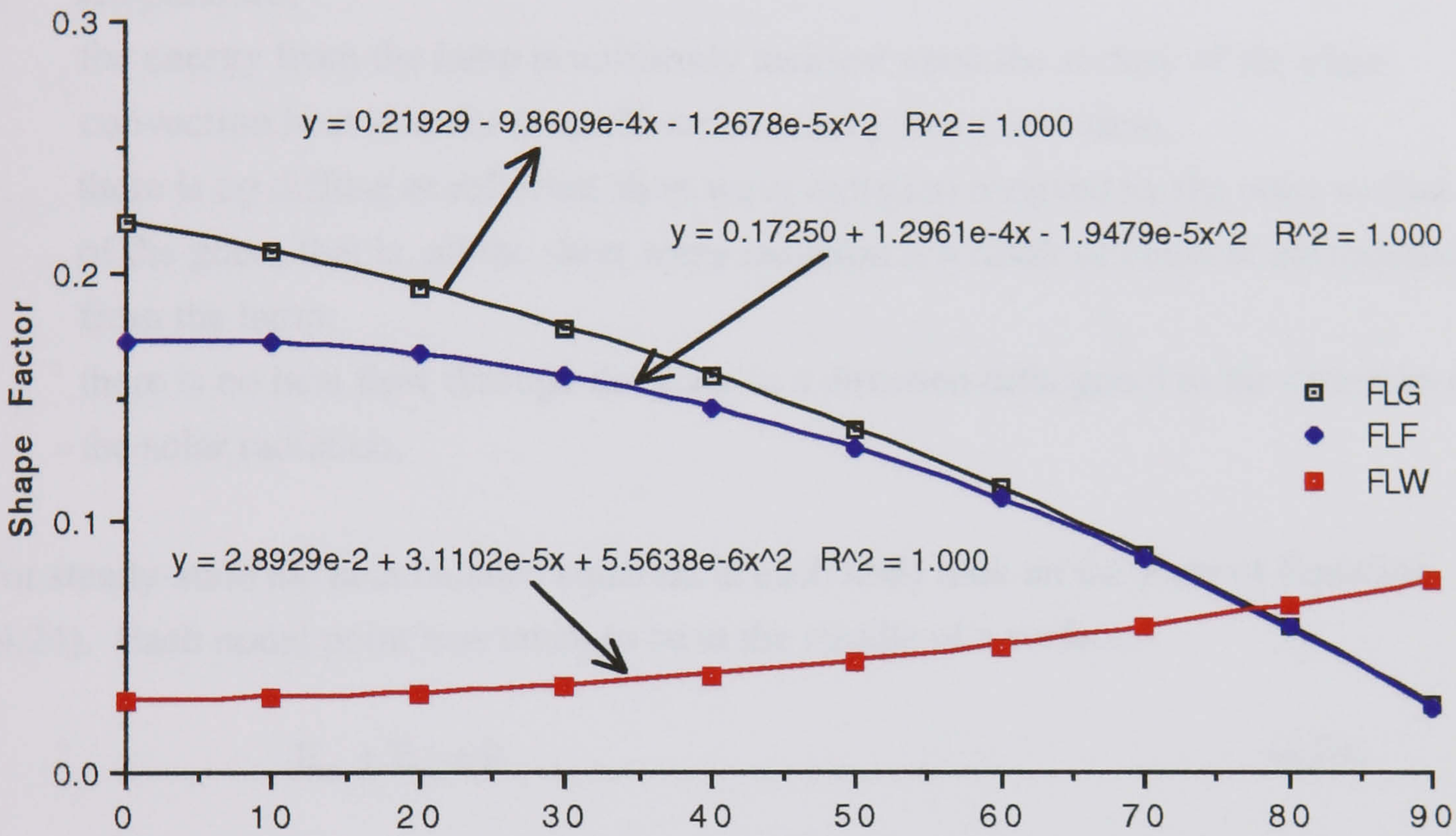

Fig 4.9 Shape Factors verses angle of incidence

From Figure 4.9, equations were obtained for the curves. These equations were used within the computer-based simulation to provide the shape factors for any angle of incidence between 0 and 80°. A regression analysis for each curve was also undertaken, see the R^2 numbers at the end of each equation. This analysis gave excellent results in each case. A similar process was undertaken to obtain data for the shadows which were cast by the walls of the hot box on the floor and the other walls. This data was then used to determine the amount of energy that was incident upon the internal surfaces of the hot box.

Therefore with the various physics of the heat transfer paths established, two models were developed; a steady-state model and a transient model.

4.3 Steady-State Model

Several assumptions were made before the steady-state model was constructed. These assumptions were:

Steady-state one-dimensional heat flow, for each of the rig constructional components;
constant properties, that is, the properties of the said components do not vary with temperature;
the energy from the lamp is uniformly incident upon the surface of the glass;
convection heat transfer from all surfaces is by free convection;
there is no diffuse or reflected short wave radiation received by the outer surface of the glass, that is, all the short wave radiation is a result of direct beam radiation from the lamp;
there is no heat flow through the glass in a direction orthogonal to the direction of the solar radiation.

For steady-state the heat balance equation at each node took on the form of Equation (4.24). Each nodal point was taken to be at the middle of a surface.

$$E_{in} + E_g = 0 \qquad (4.24)$$

where E_{in} is the net energy into the node, E_g is the energy generated, for example by absorption. Energy which flows out of the node is included as a negative value within the E_{in} variable.

The experimental rig consisted of a box with an open lid, see Figure 3.1. Using the known thermophysical properties of the materials used, a network of equations was built up to describe the thermal behaviour of the system. Using these equations, an iterative was used to determine the temperatures under steady state conditions.

Nodal points were established on all the surfaces of the hot box including the glass, where two materials were adjacent, for example, within the wall and floor components, and in the middle of the glass. Two other nodal points were established for the internal and external air. Known temperatures included, the external environment temperature and the lamp temperature.

By utilising the energy flows in Figure 4.2, an energy balance was determined for each node. The resultant equations are laid out below.

Figure 4.10 shows how energy interacts with the glass surface node $\mathbf{T_{ge}}$. This diagram shows the energy paths into and out of the node, see Equation (4.25). These energy paths include heat exchange with the external environment via convective heat transfer and radiative heat transfer from the surface of the glass, conduction through the glass and short wave radiation absorption. The absorption includes one portion which is absorbed directly from the lamp, and a second which is reflected, that is, not absorbed, by the internal surfaces of the box.

Therefore the energy balance for the node on the external surface of the box is: convection heat transfer at the surface + long wave radiative heat transfer at the surface + the heat transfer via conduction from the internal glass node + the absorbed short wave radiation equals zero.

$$\left(\begin{array}{c} h_{cge}A_g\left(T_{ae}-T_{ge}\right)+h_{rge}\left(T_{ae}-T_{ge}\right)+ \\ h_{rLg}T_L A_{LA}F_{LgT}\left(T_L-T_{ge}\right)+\frac{A_g k_g}{\Delta x_g}\left(T_{go}^p-T_{ge}^p\right)+ \\ I_s A_g \alpha\left(F_{L-g}+\tau\left(1-\alpha_{sab}\right)\left(A_f F_{gf} F_{Lf} S_f+4A_w F_{wg} F_{Lw} S_w\right)\right)\frac{\Delta x_g}{2} \end{array}\right)=0 \qquad (4.25)$$

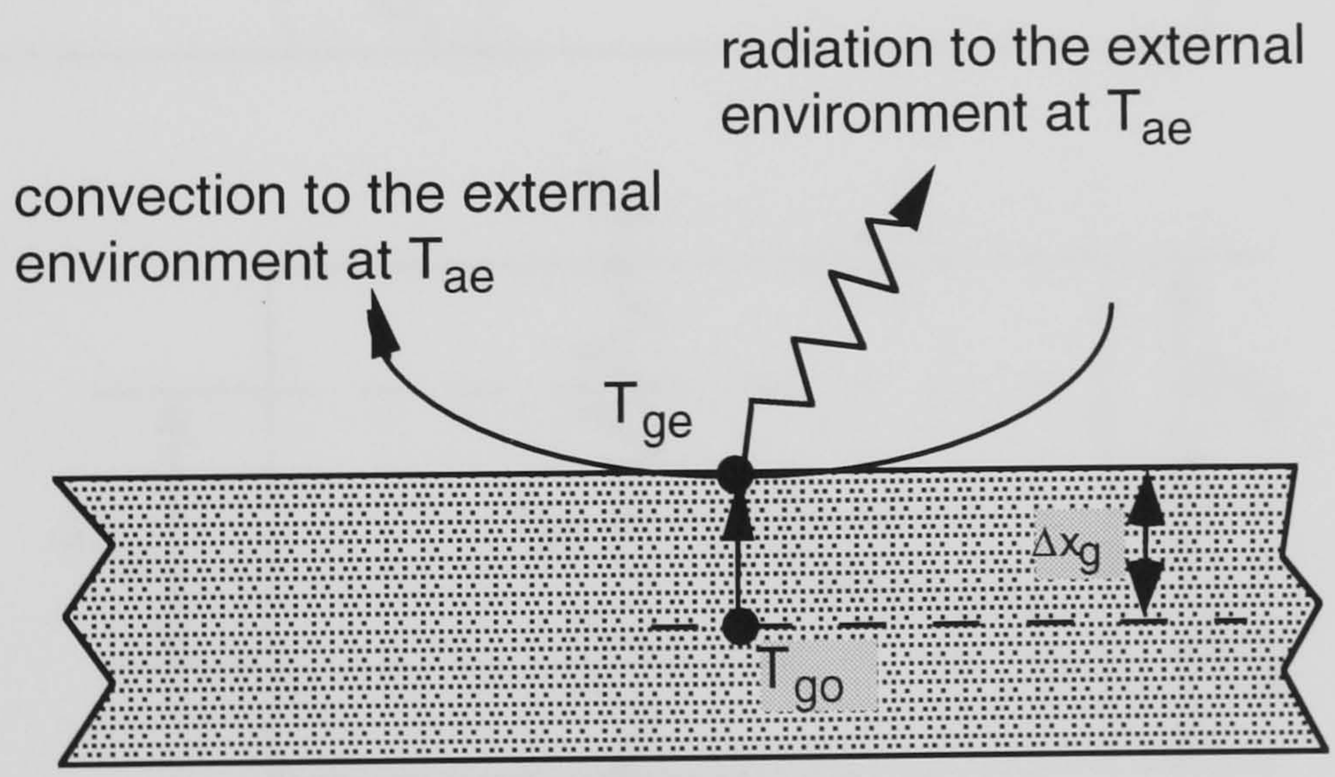

Fig. 4.10 Energy interactions which affect T_{ge}.

By rearranging Equation (4.25) an equation to determine T_{ge} can be obtained, see Equation (4.26).

$$\frac{\left(\begin{array}{c}\left(h_{cge}A_g + h_{rge}\right)T_{ae}^{p} + h_{rLg}T_L A_{LA}F_{LgT}\left(T_L\right) + \frac{A_g k_g}{\Delta x_g}\left(T_{go}^{p}\right) + \\ I_s A_g \alpha\left(F_{L-g} + \tau\left(1-\alpha_{sab}\right)\left(A_f F_{gf} F_{Lf} S_f + 4A_w F_{wg} F_{Lw} S_w\right)\right)\frac{\Delta x_g}{2}\end{array}\right)}{\left(h_{rge} + h_{cge}A_g + h_{rLg}T_L A_{LA}F_{LgT} + \frac{A_g k_g}{\Delta x_g}\right)} = T_{ge}^{p} \qquad (4.26)$$

There are three components for the inner glass node, $\mathbf{T_{go}}$. Two of the components are the same; these are, the conduction from each surface, and the absorbed radiation component, see Figure 4.11.

$$\left(\begin{array}{c}\frac{A_g k_g}{\Delta x_g}\left(T_{ge}^{p} - T_{go}^{p}\right) + \frac{A_g k_g}{\Delta x_g}\left(T_{gi}^{p} - T_{go}^{p}\right) + \\ I_s A_g \alpha\left(F_{L-g} + \tau\left(1-\alpha_{sab}\right)\left(A_f F_{gf} F_{Lf} S_f + 4A_w F_{wg} F_{Lw} S_w\right)\right)\Delta x_g\end{array}\right) = 0 \qquad (4.27)$$

Equation (4.27) can be rearranged to achieve an expression for T_{go}, Equation (4.28).

$$\frac{\left(\begin{array}{c}\frac{A_g k_g}{\Delta x_g}\left(T_{ge}^{p} + T_{gi}^{p}\right) + \\ I_s A_g \alpha\left(F_{L-g} + \tau\left(1-\alpha_{sab}\right)\left(A_f F_{gf} F_{Lf} S_f + 4A_w F_{wg} F_{Lw} S_w\right)\right)\Delta x_g\end{array}\right)}{\left(2\frac{A_g k_g}{\Delta x_g}\right)} = T_{go}^{p} \qquad (4.28)$$

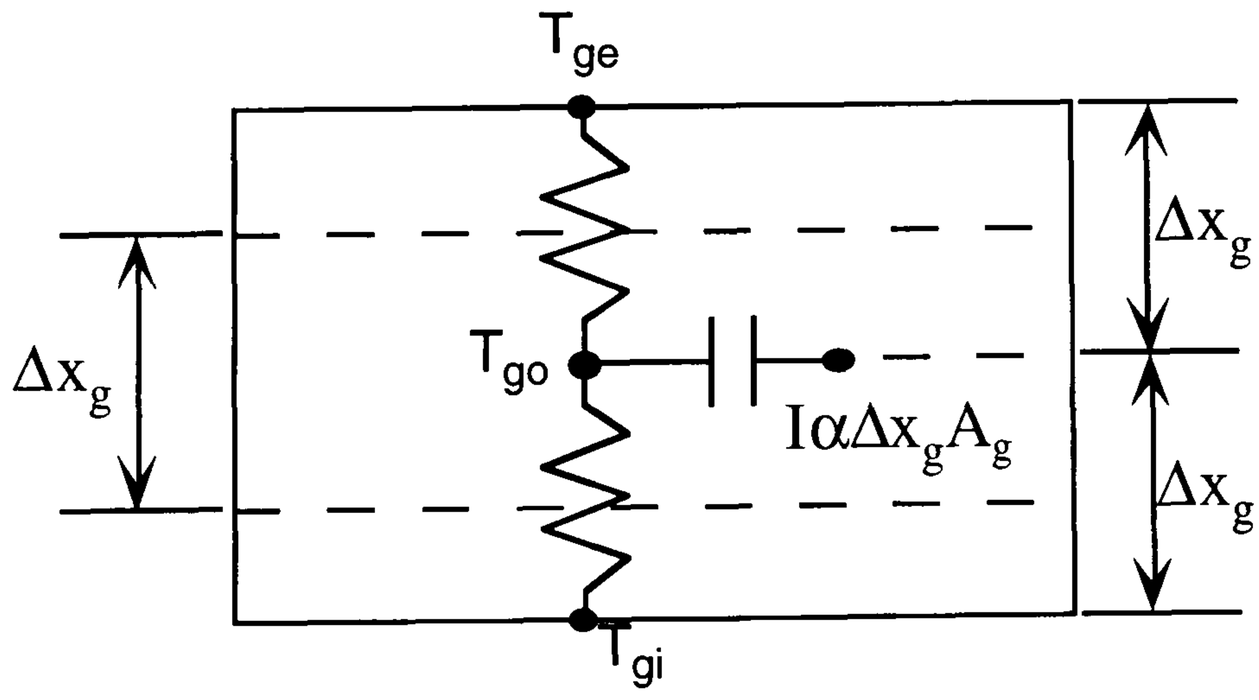

Fig. 4.11 Operations upon T_{go}.

For the internal surface of the glass, $\mathbf{T_{gi}}$, the nodal equation was developed using the same theory for the upper surface. However, this node is 'seen' by the five internal surfaces of the box, see Figure 4.12. Therefore a number of radiation heat transfer coefficients need to be taken into account, as each of the surfaces will be at different temperatures, especially when the lamp is inclined away from normal incidence. The energy balance for this node is shown in Equation (4.29), once again taking into account the absorbed solar radiation.

$$\left(\begin{array}{c}\dfrac{k_g A_g}{\Delta x}\left(T_{go}^p - T_{gi}^p\right) + h_{cgi}A_g\left(T_{ai}^p - T_{gi}^p\right) + h_{rwwg}\left(T_{wwi}^p - T_{gi}^p\right) + \\ h_{rwng}\left(T_{wni}^p - T_{gi}^p\right) + h_{rwsg}\left(T_{wsi}^p - T_{gi}^p\right) + \\ h_{rweg}\left(T_{wei}^p - T_{gi}^p\right) + h_{rfig}\left(T_{fi}^p - T_{gi}^p\right) + \\ I_s A_g \alpha\left(F_{L-g} + \tau\left(1-\alpha_{sab}\right)\left(A_f F_{gf} F_{Lf} S_f + 4A_w F_{wg} F_{Lw} S_w\right)\right)\dfrac{\Delta x_g}{2}\end{array}\right) = 0 \qquad (4.29)$$

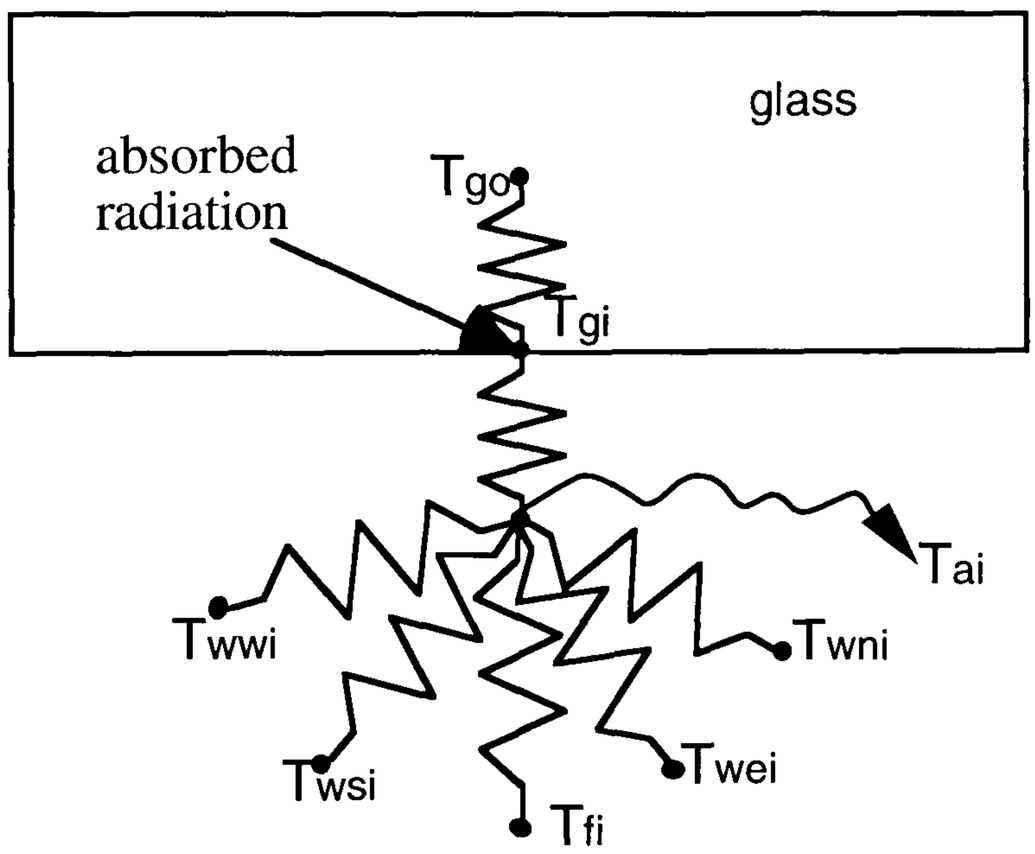

Fig. 4.12 Internal surface glass node and its operands.

Again Equation 4.29 can be rearranged to derive an expression for T_{gi}, see Equation (4.30).

$$\frac{\left(\begin{array}{c}\dfrac{k_g A_g}{\Delta x}T_{go}^p + h_{cgi}A_g T_{ai}^p + h_{rwwg}T_{wwi}^p + \\ h_{rwng}T_{wni}^p + h_{rwsg}T_{wsi}^p + h_{rweg}T_{wei}^p + h_{rfig}T_{fi}^p + \\ I_s A_g \alpha\left(F_{L-g} + \tau\left(1-\alpha_{sab}\right)\left(A_f F_{gf} F_{Lf} S_f + 4A_w F_{wg} F_{Lw} S_w\right)\right)\dfrac{\Delta x_g}{2}\end{array}\right)}{\left(\dfrac{k_g A_g}{\Delta x} + h_{cgi}A_g + h_{rwwg} + h_{rwng} + h_{rwsg} + h_{rweg} + h_{rfig} + \right)} = T_{gi}^p \qquad (4.30)$$

For the floor node, $\mathbf{T_{fi}}$, the inputs include, convection from the internal air, radiation from the lamp, radiation to and from the walls and the glass, and conduction through the floor, see Figure 4.13. The energy balance is shown in Equation (4.31).

$$\left(\begin{array}{l}\dfrac{k_f A_f}{\Delta x_f}\left(T_{fi1}^p - T_{fi}^p\right) + h_{cfi}A_f\left(T_{ai}^p - T_{fi}^p\right) + h_{rfg}\left(T_{gi}^p - T_{fi}^p\right) \\ \quad + I_s\tau\left(F_{L-f}S_f A_f\alpha_{sab} + 4\left(1-\alpha_{sab}\right)A_w F_{wf}F_{Lw}S_w\right) \\ \qquad + h_{rwwf}\left(T_{wwi}^p - T_{fi}^p\right) + h_{rwef}\left(T_{wei}^p - T_{fi}^p\right) \\ \qquad + h_{rwnf}\left(T_{wni}^p - T_{fi}^p\right) + h_{rwsf}\left(T_{wsi}^p - T_{fi}^p\right)\end{array}\right) = 0 \qquad (4.31)$$

Once again, by rearranging the terms, an expression for the temperature at this node can be obtained, see Equation (4.32).

$$\frac{\left(\begin{array}{l}\dfrac{k_f A_f}{\Delta x_f}T_{fi1}^p + h_{cfi}A_f T_{ai}^p + h_{rfg}T_{gi}^p \\ + h_{rwwf}T_{wwi}^p + h_{rwef}T_{wei}^p + h_{rwnf}T_{wni}^p + h_{rwsf}T_{wsi}^p \\ + I_s\tau\left(F_{L-f}S_f A_f\alpha_{sab} + 4\left(1-\alpha_{sab}\right)A_w F_{wf}F_{Lw}S_w\right)\end{array}\right)}{\left(\dfrac{k_f A_f}{\Delta x_f} + h_{cfi}A_f + h_{rfg} + h_{rwwf} + h_{rwef} + h_{rwnf} + h_{rwsf}\right)} = T_{fi}^p \qquad (4.32)$$

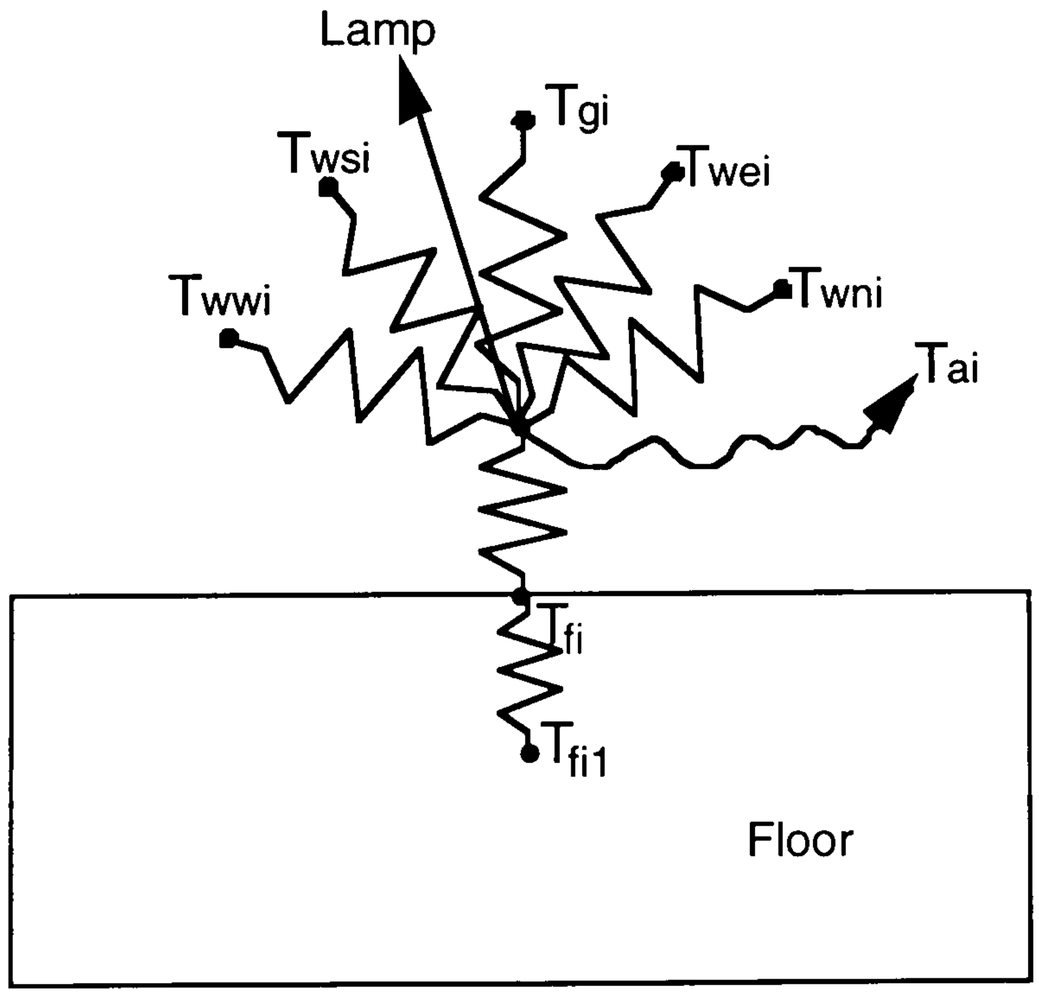

Fig 4.13 Floor node.

The materials which make up the floor and the walls are opaque. Therefore the temperatures for the nodal points through these structures, are based upon the heat flow in, and the heat flow out, as there is no internal heat generation. The energy balance for the nodal temperature, $\mathbf{T_{fi1}}$, the interface between the box floor and the floor interface, is shown in Equation (4.33), where the subscript f refers to the properties of the floor of the box which is made of wood, and p refers to the properties of the insulation, which in this case is polystyrene.

$$\frac{k_f A_f}{x_f}\left(T_{fi} - T_{fi1}\right) + \frac{k_p A_p}{x_p}\left(T_{fi2} - T_{fi1}\right) = 0 \qquad (4.33)$$

The area of the floor and the insulation are equal. Therefore Equation (4.33) can be simplified to give an expression for $\mathbf{T_{fi1}}$, see Equation (4.34).

$$\boxed{\frac{\frac{k_f}{x_f}T_{fi} + \frac{k_p}{x_p}T_{fi2}}{\frac{k_f}{x_f} + \frac{k_p}{x_p}} = T_{fi1}} \qquad (4.34)$$

Equation (4.34) can be developed to provide an expression for the temperature at the interface between the insulation and the base, $\mathbf{T_{fi2}}$.

The expression for the temperature of the external floor node, $\mathbf{T_{fo}}$, is similar to the external glass node, minus the solar radiation input. This surface also faces a cool floor, of temperature T_{earth}, which is a heat sink for the thermal radiation. The energy balance for this node can be seen in Equation (4.35).

$$\frac{k_b A_b}{\Delta x_b}\left(T^p_{fi2} - T^p_{fe}\right) + h_{cfe}A_b\left(T^p_{ae} - T^p_{fe}\right) + h_{rfe}A_b\left(T^p_{earth} - T^p_{fe}\right) = 0 \qquad 4.35$$

Once again, by rearranging the energy balance an equation for the external temperature of the floor, $\mathbf{T_{fe}}$, can be determined, see Equation (4.36).

$$\boxed{\frac{\frac{k_b}{\Delta x_b}T^p_{fi21} + h_{cfe}T^p_{ae} + h_{rfe}T^p_{earth}}{\frac{k_b}{\Delta x_b} + h_{cfe} + h_{rfe}} = T^p_{fe}} \qquad 4.36$$

The same basic equation can be used to determine the temperature for all the walls. Figure 4.14 shows the interactions of the east wall with other nodal points. The

equations for the west, south and north walls are the same. However, as the angle of incidence moves away from normal incidence, the amounts of direct solar radiation which a surface intercepts changes. Hence an S factor is used, which is a measure of the shading that takes place on that particular wall. The temperature of the west wall, $\mathbf{T_{wwi}}$, is derived from the energy balance shown in Equation (2.37).

$$\left(\begin{array}{c}\dfrac{k_w A_w}{\Delta x_w}\left(T^p_{wx+1}-T^p_{wwi}\right)+h_{cwi}A_w\left(T^p_{ai}-T^p_{wwi}\right)\\ +h_{rfiw}\left(T^p_{gi}-T^p_{wwi}\right)+h_{rgw}\left(T^p_{gi}-T^p_{wwi}\right)\\ I_s\tau\left(F_{L-w}S_wA_w\alpha_{sab}+\left(1-\alpha_{sab}\right)\left(A_fF_{fw}F_{Lf}S_f+3A_wF_{ww}F_{Lw}S_w\right)\right)\\ +h_{rwew}\left(T^p_{wei}-T^p_{wwi}\right)+h_{rwnw}\left(T^p_{wni}-T^p_{wwi}\right)+h_{rwsw}\left(T^p_{wsi}-T^p_{wwi}\right)\end{array}\right)=0 \qquad (4.37)$$

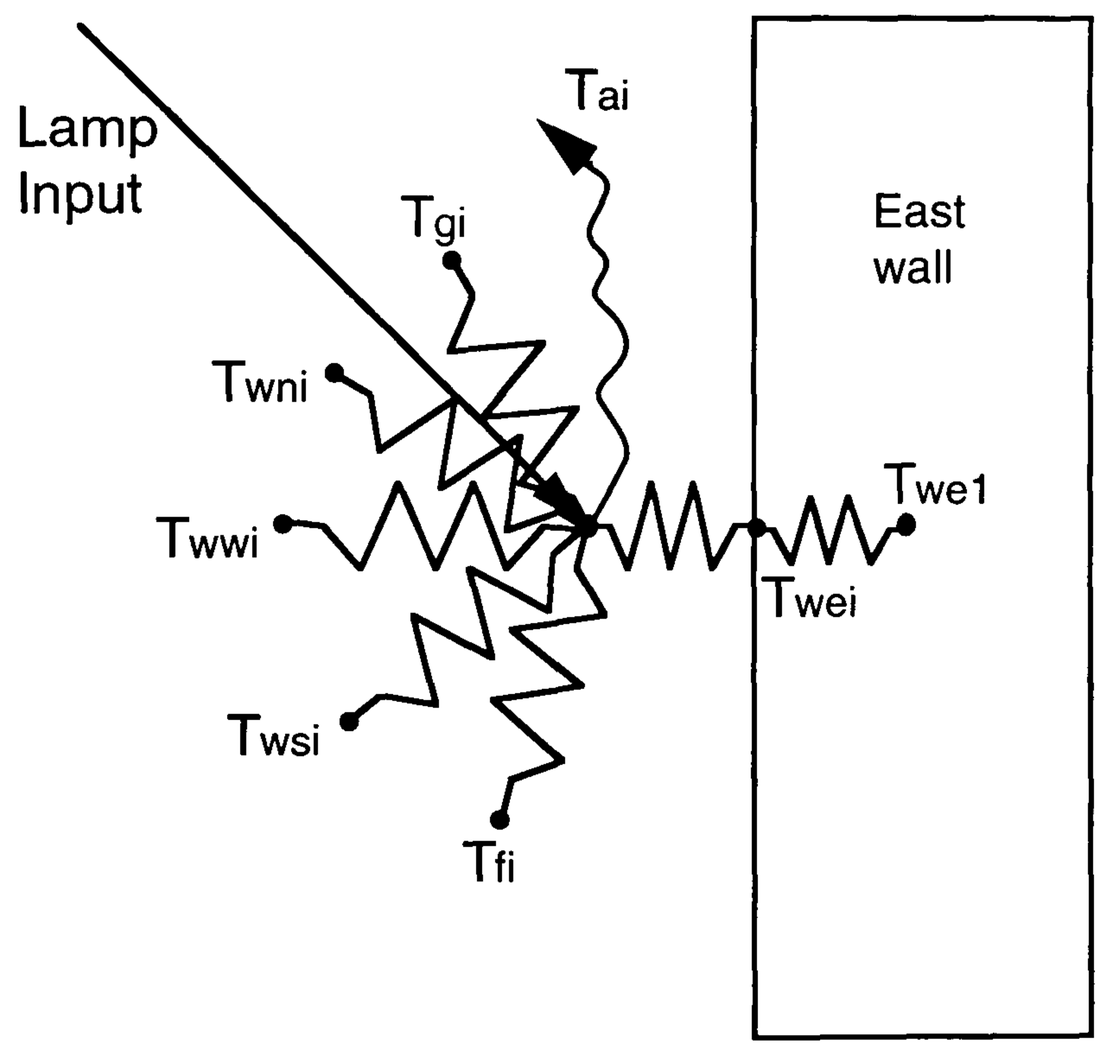

Fig 4.14 The East wall node.

Rearranging this equation gives an expression for $\mathbf{T_{wwi}}$.

$$\frac{\left(\begin{array}{c}\dfrac{k_w A_w}{\Delta x_w}T^p_{ww+1}+h_{cwi}A_wT^p_{ai}+h_{rfiw}T^p_{fi}\\ +h_{rgw}T^p_{gi}+h_{rwew}T^p_{wei}+h_{rwnw}T^p_{wni}+h_{rwsw}T^p_{wsi}\\ I_s\tau\left(F_{L-w}S_wA_w\alpha_{sab}+\left(1-\alpha_{sab}\right)\left(A_fF_{fw}F_{Lf}S_f+3A_wF_{ww}F_{Lw}S_w\right)\right)\end{array}\right)}{\left(\dfrac{k_w A_w}{\Delta x_w}+h_{cwi}A_w+h_{rwew}+h_{rwnw}+h_{rwsw}+h_{rfiw}+h_{rgw}\right)}=T^p_{wwi} \qquad (4.38)$$

As stated earlier, the equations for the east, north and south walls are the same. Furthermore, the temperature nodes for the wall-insulation interface can be determined

using equations similar to Equation (4.33). The energy balance for one of the external surfaces is shown in Equation (4.39). Once again this can be rearranged to give the temperature for that node, see Equation (4.40).

$$\frac{k_p A_p}{x_p}\left(T^p_{ww1} - T^p_{wwe}\right) + h_{cwwe} A_p \left(T^p_{ae} - T^p_{wwe}\right) + h_{rwwe} A_p \left(T^p_{ae} - T^p_{wwe}\right) = 0 \qquad (4.39)$$

$$\frac{\dfrac{k_p}{x_p} T^p_{ww1} + \left(h_{cwwe} + h_{rwwe}\right) T^p_{ae}}{\dfrac{k_p}{x_p} + h_{cwwe} + h_{rwwe}} = T^p_{wwe} \qquad (4.40)$$

The internal air temperature node, $\mathbf{T_{ai}}$, is calculated as follows:

$$\left(\begin{array}{c} h_{cfi} A_f \left(T_{fi} - T_{ai}\right) + h_{cgi} A_g \left(T_{gi} - T_{ai}\right) + h_{cwwi} A_w \left(T_{wwi} - T_{ai}\right) + \\ h_{cwei} A_w \left(T_{wei} - T_{ai}\right) + h_{cwni} A_w \left(T_{wni} - T_{ai}\right) + h_{cwsi} A_w \left(T_{wsi} - T_{ai}\right) \end{array}\right) = 0 \qquad (4.41)$$

Finally, by rearranging Equation (4.41), an expression for T_{ai}, can be obtained:

$$\boxed{\frac{\left(\begin{array}{c} A_g \left(h_{cfi} T_{fi} + h_{cgi} T_{gi}\right) + \\ A_w \left(h_{cwei} T_{wei} + h_{cwwi} T_{wwi} + h_{cwni} T_{wni} + h_{cwsi} T_{wsi}\right) \end{array}\right)}{\left(\begin{array}{c} A_g \left(h_{cfi} + h_{cgi}\right) + \\ A_w \left(h_{cwwi} + h_{cwei} + h_{cwni} + h_{cwsi}\right) \end{array}\right)} = T_{ai}} \qquad (4.42)$$

With the algorithms developed for the nodal points, a steady-state program was written, Figure 4.15 shows a flow diagram for the program.

The first part of the program comprises the array statements so that the computer can allocate memory for the data produced by the algorithms. This is followed by a number of procedures which establish the physical properties of the materials used, for example, the dimensions and the thermal conductivity. In the next procedure several inputs are required, these being, the angle of incidence of the solar radiation, the refractive index and absorptive coefficient of the material under test. Once this is inputted, the shape factors and the optical properties are calculated. The next procedure then establishes the initial temperatures for every node in the model. Once the temperatures have been assigned, an iterative process can begin to determine the node temperatures. The determination of the temperatures at each node within the iteration takes place within a loop. Within this loop a number of procedures take place. The

first procedure determines the convective and radiative heat transfer coefficients for each surface to air and surface to surface interchange. This is followed by the determination of the temperatures for each nodal point. When all the new nodal temperatures have been obtained the computer program determines the difference between the new temperatures, T_i, and the previous temperatures, T_{i-1}. Only when the difference between T_i and T_{i-1} is less than 0.0001 does the loop finish. Finally, the temperatures at time i are written to a file and displayed on the computer screen.

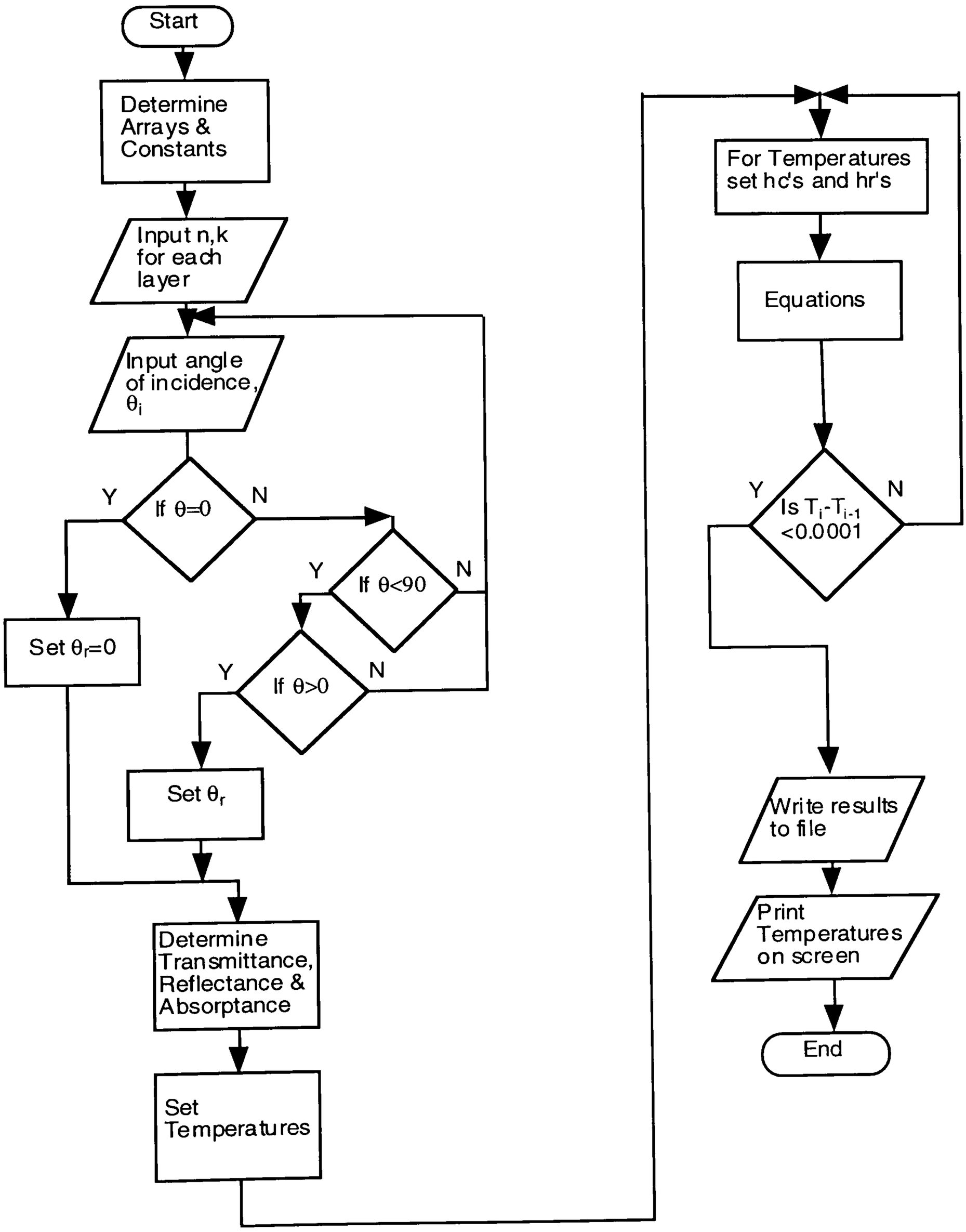

Fig 4.15 Flow diagram for Steady-state model

4.4 Transient Model

The initial investigation of the transient model concerned the glass only. The lumped capacitance method was initially considered but this was only useful for single layered glass, such as clear float or absorption glass which has its absorption medium placed within the glass during the manufacturing process. The route finally chosen was a Finite-Difference method as demonstrated by Incopera and de Witt, (1981) and Bejan (1993).

There are various finite-difference methods which would be useful for this investigation. It was decided that a method of energy balances upon nodal points, would be employed to simplify the process and therefore reduce the computing power needed. For each nodal point the equation below was used,

$$E_{in} + E_g = E_{st} \tag{4.43}$$

where E_{in} represents energy into the node, E_g, energy generated in the node, and E_{st}, energy stored in the node. Once again energy flowing out of the node was represented by negative values of E_{in}. This is the same principle as used under steady-state operations. The difference between steady-state and transient conditions concerns the heat storage, E_{st}. Steady-state by its own name, assumes that the temperatures are not changing with time. In a transient situation, the temperatures are changing and each node has the capacity for energy storage. Therefore, E_{st} represents the rate of energy stored within in the volume per time interval, and can be shown as a change in temperature over time as below.

$$\frac{\partial E_{st}}{\partial t} = \rho c V \frac{\partial T}{\partial t}\bigg|_x \tag{4.44}$$

The above equation shows that the heat stored within the volume per unit of time, is determined by its density, ρ, and the specific heat capacity, c. Using this information a series of equations was built up using an explicit technique. Two new variables were introduced to aid in the production of the nodal equations,

$$Fo = \frac{\psi \Delta t}{(\Delta x)^2} \tag{4.45}$$

where $\psi = \frac{k}{\rho c}$ (4.46)

and $Bi = \frac{h\Delta x}{k}$ (4.47)

where Fo is the Fourier number, ψ is the thermal diffusivity and Bi, is the Biot number. The Biot number is a dimensionless parameter and plays an important role in conduction problems which have surface convection effects. It is a measure of the temperature drop in the solid relative to the temperature difference between the surface and the fluid. The Fourier number is a dimensionless time, and is used to determine time differential under transient conditions.

Using the equation above and following the pattern used for the steady-state study, a series of equations was developed for each node. During the development of the model, it was seen that there was a need for a greater number of nodes, specifically within the solid structures. The extra nodes were needed to give a better representation of what was happening at the material interfaces. By using more nodes and hence smaller Δx's, the volume where the thermal conductivity was averaged, was reduced. Patankar (1980), put forward a method by which the effective thermal conductivity of two solids, adjacent to one-another, could be determined. However, this method does not allow nodal points to exist on the interface and therefore was not used in this study.

Once again several assumptions were made before the model was constructed. These assumptions were based on those used for the steady-state version. These assumptions were:

one-dimensional heat flow for each of the rig constructional components;
constant properties, that is, the properties of the solid components do not vary with temperature;
the energy from the lamp is uniformly incident upon the surface of the glass;
convection heat-transfer from all surfaces is by free convection;
there is no diffuse or reflected short wave radiation received by the outer surface of the glass, that is, all the short wave radiation is a result of direct beam radiation from the lamp;
there is no heat flow through the glass, in a direction orthogonal to the direction of the solar radiation.

As for the steady-state, the transient model was set up using the known thermophysical properties of the materials used. With this information, along with the dimensions of the illuminated hot box, a set of equations was built up. An iterative method was used to determine the temperatures, from the equations, under transient conditions.

Outer Glass Surface node, $\mathbf{T_{ge}}$

$$\left(\begin{array}{c} h_{cge}A_g\left(T_{ae}^p - T_{ge}^p\right) + h_{rge}\left(T_{ae}^p - T_{ge}^p\right) + \\ h_{rLg}T_L A_{LA}F_{LgT}\left(T_L - T_{ge}\right) + \dfrac{A_g k_g}{\Delta x_g}\left(T_{go}^p - T_{ge}^p\right) + \\ I_s A_g \alpha\left(F_{L-g} + \tau\left(1-\alpha_{sab}\right)\left(\begin{array}{c} A_f F_{gf} F_{Lf} S_f \\ +4A_w F_{wg} F_{Lw} S_w \end{array}\right)\right)\dfrac{\Delta x_g}{2} \end{array}\right) = \frac{\rho c A_g \Delta x_g}{2\Delta t}\left(T_{ge}^{p+1} - T_{ge}^p\right) \quad (4.48)$$

$$\left(\begin{array}{c} Bi_g\left(T_{ae}^p - T_{ge}^p\right) + \dfrac{h_{rge}\Delta x_g}{A_g k_g}\left(T_{ae}^p - T_{ge}^p\right) + \\ \dfrac{\Delta x_g h_{rLg} T_L A_{LA} F_{LgT}}{A_g k_g}\left(T_L - T_{ge}\right) + \left(T_{go}^p - T_{ge}^p\right) + \\ I_s \alpha\left(F_{L-g} + \tau\left(1-\alpha_{sab}\right)\left(\begin{array}{c} A_f F_{gf} F_{Lf} S_f \\ +4A_w F_{wg} F_{Lw} S_w \end{array}\right)\right)\dfrac{\left(\Delta x_g\right)^2}{2k_g} \end{array}\right) = \frac{1}{2Fo_g}\left(T_{ge}^{p+1} - T_{ge}^p\right) \quad (4.49)$$

$$\left(\begin{array}{c} 2Fo_g\left(\begin{array}{c} T_{go}^p + \left(Bi_g + \dfrac{h_{rge}\Delta x_g}{A_g k_g}\right)T_{ae}^p + \dfrac{\Delta x_g h_{rLg} T_L A_{LA} F_{LgT}}{k_g A_g} T_L + \\ I_s \alpha\left(F_{L-g} + \tau\left(1-\alpha_{sab}\right)\left(A_f F_{gf} F_{Lf} S_f + 4A_w F_{wg} F_{Lw} S_w\right)\right)\dfrac{\left(\Delta x_g\right)^2}{2k_g} \end{array}\right) \\ + \left(1 - 2Fo_g\left(1 + Bi_g + \dfrac{\Delta x_g}{A_g k_g}\left(h_{rLg} T_L A_{LA} F_{LgT} + h_{rge}\right)\right)\right)T_{ge}^p \end{array}\right) = T_{ge}^{p+1} \quad (4.50)$$

Unlike the steady-state model, the explicit transient model can be unstable. In a transient program, the solution for the nodal temperatures should continuously approach steady-state values with increasing time. However, with the explicit method, this solution may be characterised by numerically induced oscillations, which are physically impossible. If the oscillations become unstable, then the solution will diverge from steady-state. Thus to prevent instability, the value of Δt must be maintained below a limit. This limit depends upon the nodal separations and other

parameters. Incopera and De Witt (1981), stated that the criterion for stability 'is determined by requiring that the coefficient associated with the node of interest at the previous time is greater than or equal to zero'. This is done by collecting the terms, involving in this case T_{ge}. This then gives a relation involving the Fourier number from which a maximum value of Δt may be determined. In the case of the external glass node, stability depends upon,

$$\left(1-2Fo_g\left(1+Bi_g+\frac{\Delta x_g}{A_g k_g}\left(h_{rLg}T_L A_{LA}F_{LgT}+h_{rge}\right)\right)\right)\geq 0 \qquad (4.51)$$

This can be rearranged to give an expression for Δt.

$$\frac{\rho_g c_g(\Delta x)^2}{2k_g\left(1+Bi_g+\frac{\Delta x_g}{A_g k_g}\left(h_{rLg}T_L A_{LA}F_{LgT}+h_{rge}\right)\right)}\geq \Delta t \qquad (4.52)$$

The glass internal node, $\mathbf{T_{go}}$, is determined using the simple balance of heat in ,via conduction and solar absorption, which must be equal to the heat stored within the glass and the heat which flows out by conduction.

$$\left(\begin{array}{c}\frac{A_g k_g}{\Delta x_g}\left(T_{ge}^p-T_{go}^p\right)+\frac{A_g k_g}{\Delta x_g}\left(T_{gi}^p-T_{go}^p\right)+\\ I_s A_g\alpha\left(F_{L-g}+\tau\left(1-\alpha_{sab}\right)\left(\begin{array}{c}A_f F_{gf}F_{Lf}S_f\\ +4A_w F_{wg}F_{Lw}S_w\end{array}\right)\right)\Delta x_g\end{array}\right)=\frac{\rho c A_g\Delta x_g}{\Delta t}\left(T_{go}^{p+1}-T_{go}^p\right) \qquad (4.53)$$

$$\left(\begin{array}{c}\left(T_{ge}^p-T_{go}^p\right)+\left(T_{gi}^p-T_{go}^p\right)+\\ I_s\alpha\left(F_{L-g}+\tau\left(1-\alpha_{sab}\right)\left(A_f F_{gf}F_{Lf}S_f+4A_w F_{wg}F_{Lw}S_w\right)\right)\frac{\left(\Delta x_g\right)^2}{k_g}\end{array}\right)=\frac{1}{Fo_g}\left(T_{go}^{p+1}-T_{go}^p\right) \qquad (4.54)$$

$$\boxed{Fo_g\left(\begin{array}{c}T_{ge}^p+T_{gi}^p+\\ I_s\alpha_{sab}\left(F_{L-g}+t\left(1-\alpha_{sab}\right)\left(\begin{array}{c}A_f F_{gf}F_{Lf}S_f\\ +4A_w F_{wg}F_{Lw}S_w\end{array}\right)\right)\frac{\left(\Delta x_g\right)^2}{k_g}\end{array}\right)+\left(1-2Fo_g\right)T_{go}=T_{go}^{p+1}} \qquad (4.55)$$

Again, the stability can be determined by examining the expression $(1\text{-}2Fo_g)\geq 0$. By determining expressions for Δt at each nodal point, the value of Δt which is lowest will be the one under which the whole system will be stable.

The glass inner node, $\mathbf{T_{gi}}$, is similar to the external surface however it interacts with the surfaces within the box via radiation as well as convection to the air, and so is more complex.

$$\left(\begin{array}{c}\frac{k_g A_g}{\Delta x}\left(T_{go}^p - T_{gi}^p\right)+ \\ h_{cgi}A_g\left(T_{ai}^p - T_{gi}^p\right)+h_{rwwg}\left(T_{wwi}^p - T_{gi}^p\right)+ \\ h_{rwng}\left(T_{wni}^p - T_{gi}^p\right)+h_{rwsg}\left(T_{wsi}^p - T_{gi}^p\right)+ \\ h_{rweg}\left(T_{wei}^p - T_{gi}^p\right)+h_{rfig}\left(T_{fi}^p - T_{gi}^p\right)+ \\ I_s A_g \alpha\left(F_{L-g}+\tau\left(1-\alpha_{sab}\right)\left(\begin{array}{c}A_f F_{gf} F_{Lf} S_f \\ +4A_w F_{wg} F_{Lw} S_w\end{array}\right)\right)\frac{\Delta x_g}{2}\end{array}\right) = \frac{\rho c A_g \Delta x_g}{2\Delta t}\left(T_{gi}^{p+1} - T_{gi}^p\right) \quad (4.56)$$

$$\left(\begin{array}{c}\left(T_{go}^p - T_{gi}^p\right)+\frac{\Delta x_g h_{cgi}}{k_g}\left(T_{ai}^p - T_{gi}^p\right)+\frac{h_{rfig}\Delta x_g}{A_g k_g}\left(T_{fi}^p - T_{gi}^p\right)+ \\ \frac{\Delta x_g}{A_g k_g}\left(\begin{array}{c}h_{rwwg}\left(T_{wwi}^p - T_{gi}^p\right)+h_{rwng}\left(T_{wni}^p - T_{gi}^p\right) \\ +h_{rwsg}\left(T_{wsi}^p - T_{gi}^p\right)+h_{rweg}\left(T_{wei}^p - T_{gi}^p\right)\end{array}\right)+ \\ I_s\alpha\left(F_{L-g}+\tau\left(1-\alpha_{sab}\right)\left(A_f F_{gf} F_{Lf} S_f + 4A_w F_{wg} F_{Lw} S_w\right)\right)\frac{\left(\Delta x_g\right)^2}{2}\end{array}\right) = \frac{1}{2Fo_g}\left(T_{gi}^{p+1} - T_{gi}^p\right) \quad (4.57)$$

$$\left(\begin{array}{c}2Fo_g\left(T_{go}^p+\frac{\Delta x_g}{k_g}\left(\begin{array}{c}h_{cgi}T_{ai}^p+\frac{1}{A_g}\left(\begin{array}{c}h_{rfig}T_{fi}^p+h_{rwwg}T_{wwi}^p+h_{rwng}T_{wni}^p \\ +h_{rwsg}T_{wsi}^p+h_{rweg}T_{wei}^p\end{array}\right)+ \\ \alpha I_s\frac{\Delta x_g}{2}\left(F_{L-g}+\tau\left(1-\alpha_{sab}\right)\left(\begin{array}{c}A_f F_{gf} F_{Lf} S_f \\ +4A_w F_{wg} F_{Lw} S_w\end{array}\right)\right)\end{array}\right)\right) \\ +T_{gi}^p\left(1-2Fo_g\left(1+\frac{\Delta x_g}{k_g}\left(h_{cgi}+\frac{1}{A_g}\left(\begin{array}{c}h_{rfig}+h_{rwwg} \\ +h_{rwng}+h_{rwsg}+h_{rweg}\end{array}\right)\right)\right)\right)\end{array}\right) = T_{gi}^{p+1} \quad (4.58)$$

The floor inner node, $\mathbf{T_{fi}}$, is again, similar to that of the external glass.

$$\left(\begin{array}{c}\frac{k_f A_f}{\Delta x_f}\left(T_{fi1}^p - T_{fi}^p\right)+h_{cfi}A_f\left(T_{ai}^p - T_{fi}^p\right)+h_{rfg}\left(T_{gi}^p - T_{fi}^p\right) \\ +I_s\tau\left(F_{L-f}S_f A_f\alpha_{sab}+4\left(1-\alpha_{sab}\right)A_w F_{wf} F_{Lw} S_w\right) \\ +h_{rwwf}\left(T_{wwi}^p - T_{fi}^p\right)+h_{rwef}\left(T_{wei}^p - T_{fi}^p\right) \\ +h_{rwnf}\left(T_{wni}^p - T_{fi}^p\right)+h_{rwsf}\left(T_{wsi}^p - T_{fi}^p\right)\end{array}\right) = \frac{\rho c A_f \Delta x_f}{2\Delta t}\left(T_{fi}^{p+1} - T_{fi}^p\right) \quad (4.59)$$

$$\left(\begin{array}{l}\left(T_{fi1}^{p}-T_{fi}^{p}\right)+\dfrac{h_{cfi}A_f\Delta x_f}{A_f k_f}\left(T_{ai}^{p}-T_{fi}^{p}\right)+\dfrac{h_{rfg}\Delta x_f}{A_f k_f}\left(T_{gi}^{p}-T_{fi}^{p}\right)\\ +\dfrac{\Delta x_f I_s \tau}{A_f k_f}\left(F_{L-f}S_f A_f \alpha_{sab}+4\left(1-\alpha_{sab}\right)A_w F_{wf} F_{Lw} S_w\right)\\ +\dfrac{\Delta x_f}{A_f k_f}\left(\begin{array}{l}h_{rwwf}\left(T_{wwi}^{p}-T_{fi}^{p}\right)+h_{rwsf}\left(T_{wsi}^{p}-T_{fi}^{p}\right)\\ +h_{rwef}\left(T_{wei}^{p}-T_{fi}^{p}\right)+h_{rwnf}\left(T_{wni}^{p}-T_{fi}^{p}\right)\end{array}\right)\end{array}\right)=\frac{1}{2Fo_f}\left(T_{fi}^{p+1}-T_{fi}^{p}\right) \qquad (4.60)$$

$$\left(\begin{array}{l}2Fo_f\left(T_{fi1}^{p}+\dfrac{\Delta x_f}{A_f k_f}\left(\begin{array}{c}h_{cfi}A_f T_{ai}^{p}+h_{rfg}T_{gi}^{p}+h_{rwwf}T_{wwi}^{p}\\ +h_{rwsf}T_{wsi}^{p}+h_{rwef}T_{wei}^{p}+h_{rwnf}T_{wni}^{p}\\ +I_s\tau\left(\begin{array}{c}F_{L-f}S_f A_f \alpha_{sab}\\ +4\left(1-\alpha_{sab}\right)A_w F_{wf} F_{Lw} S_w\end{array}\right)\end{array}\right)\right)\\ +\left(1-2Fo_f\left(1+\dfrac{\Delta x_f}{A_f k_f}\left(\begin{array}{c}h_{cfi}A_f+h_{rfg}+h_{rfg}\\ +h_{rwwf}+h_{rwsf}+h_{rwef}+h_{rwnf}\end{array}\right)\right)\right)T_{fi}^{p}\end{array}\right)=T_{fi}^{p+1} \qquad (4.61)$$

The nodes within the floor and walls are similar to that for the middle of the glass. However, unlike the glass, the floor and walls are opaque. This simplifies the nodal equations to energy balances concerning conduction and heat storage depending upon the thermal properties of the material. The distance between the nodes is small so that the effective thermal conductivity of the interface node does not greatly effect the temperature gradient, as was discussed earlier. Figure 4.16 shows the nodal points through part of the floor. The nodal points are the same distance apart and they give a mean temperature value for the volume A*Δx.

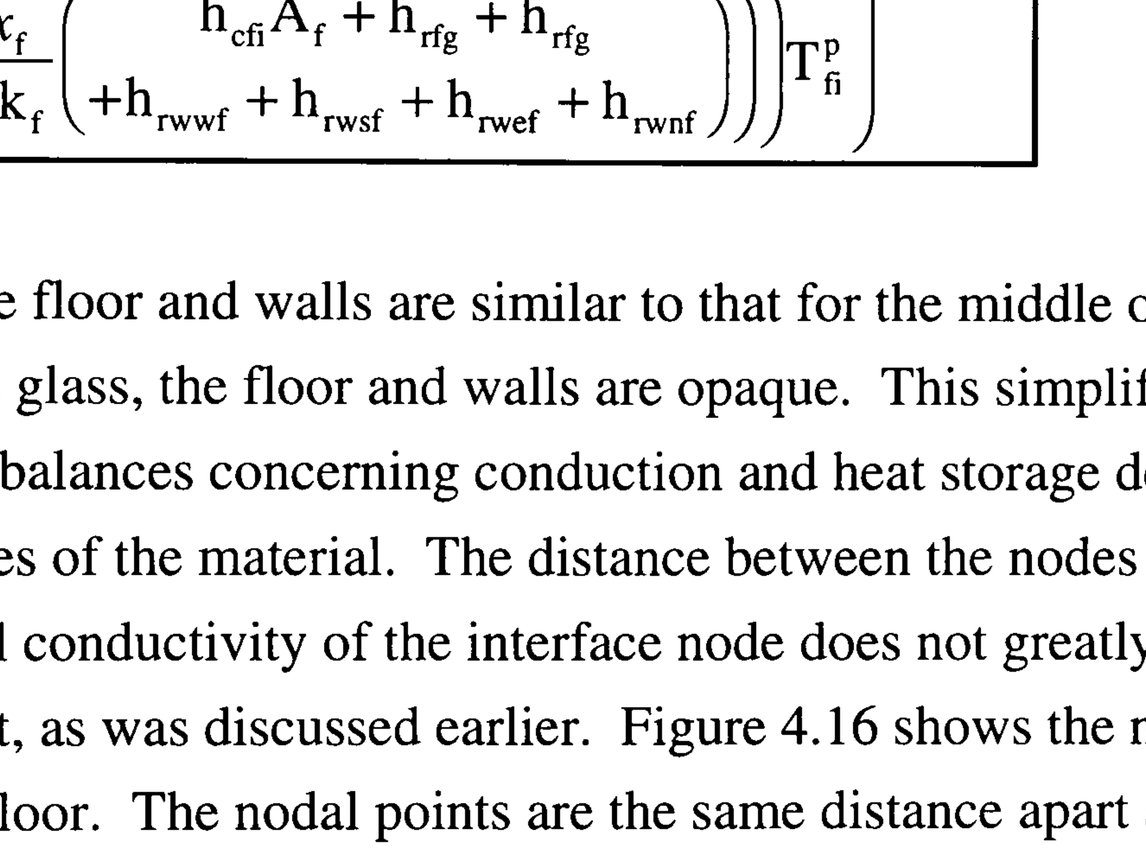

Fig 4.16 Schematic floor construction showing the nodal points.

Therefore by performing an energy balance upon the floor internal node, $\mathbf{T_{fi1}}$, the following expression can be determined, and from it an equation expressing the new temperature, T^{p+1}.

$$\frac{k_f A_f}{\Delta x_f}\left(T_{fi}^{p} - T_{fi1}^{p}\right) + \frac{k_f A_f}{\Delta x_f}\left(T_{fi2}^{p} - T_{fi1}^{p}\right) = \frac{\rho c A_f \Delta x}{\Delta t}\left(T_{fi1}^{p+1} - T_{fi1}^{p}\right) \qquad (4.62)$$

$$Fo_f\left(T_{fi}^{p} - T_{fi1}^{p}\right) + Fo_f\left(T_{fi2}^{p} - T_{fi1}^{p}\right) - T_{fi1}^{p} = T_{fi1}^{p+1} \qquad (4.63)$$

$$Fo_f\left(T_{fi}^{p} + T_{fi2}^{p}\right) + T_{fi1}^{p}\left(1 - 2Fo_f\right) = T_{fi1}^{p+1} \qquad (4.64)$$

The nodes at the material interfaces, for example, $\mathbf{T_{fix}}$, involve the thermal properties of both materials. The equations below show how an expression for the new temperature at the interface was determined. The subscripts f and p represent the wooden floor of the box and the polystyrene underneath it.

$$\frac{k_f A_f}{\Delta x_f}\left(T_{x-1}^{p} - T_{x}^{p}\right) + \frac{k_p A_p}{\Delta x_p}\left(T_{x+1}^{p} - T_{x}^{p}\right) = \left(\frac{\rho_f c_f A_f \Delta x_f}{2\Delta t} + \frac{\rho_p c_p A_p \Delta x_p}{2\Delta t}\right)\left(T_{x}^{p+1} - T_{x}^{p}\right) \qquad (4.65)$$

$$\frac{k_f}{\Delta x_f}\left(T_{x-1}^{p} - T_{x}^{p}\right) + \frac{k_p}{\Delta x_p}\left(T_{x+1}^{p} - T_{x}^{p}\right) = \left(\frac{\rho_f c_f \Delta x_f}{2\Delta t} + \frac{\rho_p c_p \Delta x_p}{2\Delta t}\right)\left(T_{x}^{p+1} - T_{x}^{p}\right) \qquad (4.66)$$

$$\frac{k_f}{\Delta x_f} T_{x-1}^{p} + \frac{k_p}{\Delta x_p} T_{x+1}^{p} + \left(\begin{array}{c} \frac{\rho_f c_f \Delta x_f}{2\Delta t} + \frac{\rho_p c_p \Delta x_p}{2\Delta t} \\ -\frac{k_f}{\Delta x_f} - \frac{k_p}{\Delta x_p} \end{array}\right) T_{x}^{p} = \left(\frac{\rho_f c_f \Delta x_f}{2\Delta t} + \frac{\rho_p c_p \Delta x_p}{2\Delta t}\right) T_{x}^{p+1} \qquad (4.67)$$

$$\boxed{\frac{\frac{k_f}{\Delta x_f} T_{x-1}^{p} + \frac{k_p}{\Delta x_p} T_{x+1}^{p}}{\left(\frac{\rho_f c_f \Delta x_f}{2\Delta t} + \frac{\rho_p c_p \Delta x_p}{2\Delta t}\right)} + T_{x}^{p}\left(1 - \frac{\frac{k_f}{\Delta x_f} - \frac{k_p}{\Delta x_p}}{\left(\frac{\rho_f c_f \Delta x_f}{2\Delta t} + \frac{\rho_p c_p \Delta x_p}{2\Delta t}\right)}\right) = T_{x}^{p+1}} \qquad (4.68)$$

The expressions for the nodes at the material interface and inside the material are the same throughout the floor and for the walls.

The floor external node, T_{fie}, is again similar to the surface node of the glass, with the radiation off the base, being received by the floor of the room, which is classed as "earthed".

$$\begin{pmatrix} \frac{k_b A_b}{\Delta x_b}\left(T^p_{fe-1} - T^p_{fe}\right) \\ +h_{cfe}A_b\left(T^p_{ae} - T^p_{fe}\right) + h_{rfe}A_b\left(T^p_{earth} - T^p_{fe}\right) \end{pmatrix} = \frac{\rho_b c_b A_b \Delta x_b}{2\Delta t}\left(T^{p+1}_{fe} - T^p_{fe}\right) \qquad (4.69)$$

$$k_b\left(T^p_{fe-1} - T^p_{fe}\right) + \frac{h_{cfe}\Delta x_b}{k_b}\left(T^p_{ae} - T^p_{fe}\right) + \frac{h_{rfe}\Delta x_b}{k_b}\left(T^p_{earth} - T^p_{fe}\right) = \frac{1}{2Fo_b}\left(T^{p+1}_{fe} - T^p_{fe}\right) \qquad (4.70)$$

$$\boxed{2Fo_b\left(T^p_{fe-1} + \frac{\Delta x_b}{k_b}T^p_{ae}\left(h_{cfe} + h_{rfe}\right)\right) + \left(1 - 2Fo_b\left(1 + \frac{\Delta x_b}{k_b}\left(h_{cfe} + h_{rfe}\right)\right)\right)T^p_{fe} = T^{p+1}_{fe}} \qquad (4.71)$$

The four walls are similar to the floor node. Again an energy balance is determined taking into account direct gain, reflected solar radiation, thermal radiation off the other surfaces, conduction from within the wall and convection to the internal air. To distinguish between the walls and to input the amount of solar radiation which it receives, a shadow factor is used as in the case of the floor. From the energy balance the wall surface node $\mathbf{T_{wxi}}$ is,

$$\begin{pmatrix} \frac{k_w A_w}{\Delta x_w}\left(T^p_{wx+1} - T^p_{wwi}\right) + h_{cwi}A_w\left(T^p_{ai} - T^p_{wwi}\right) \\ +h_{rfiw}\left(T^p_{gi} - T^p_{wwi}\right) + h_{rgw}\left(T^p_{gi} - T^p_{wwi}\right) \\ I_s\tau\left(F_{L-w}S_w A_w\alpha_{sab} + \left(1-\alpha_{sab}\right)\left(\begin{matrix} A_f F_{fw} F_{Lf} S_f \\ +3A_w F_{ww} F_{Lw} S_w \end{matrix}\right)\right) \\ +h_{rwew}\left(T^p_{wei} - T^p_{wwi}\right) + h_{rwnw}\left(T^p_{wni} - T^p_{wwi}\right) \\ +h_{rwsw}\left(T^p_{wsi} - T^p_{wwi}\right) \end{pmatrix} = \frac{\rho_w c_w A_w \Delta x_w}{2\Delta t}\left(T^{p+1}_{wwi} - T^p_{wwi}\right) \qquad (4.72)$$

$$\left(\begin{array}{c}\left(T^{p}_{wx1}-T^{p}_{wwi}\right)+h_{cwi}\dfrac{\Delta x_w}{k_w}\left(T^{p}_{ai}-T^{p}_{wwi}\right)\\ +h_{rfiw}\dfrac{\Delta x_w}{k_w A_w}\left(T^{p}_{gi}-T^{p}_{wwi}\right)+h_{rgw}\dfrac{\Delta x_w}{k_w A_w}\left(T^{p}_{gi}-T^{p}_{wwi}\right)\\ +\dfrac{I_s\tau\Delta x_w}{A_w k_w}\left(F_{L-w}S_w A_w\alpha_{sab}+\left(1-\alpha_{sab}\right)\left(\begin{array}{c}A_f F_{fw}F_{Lf}S_f\\ +3A_w F_{ww}F_{Lw}S_w\end{array}\right)\right)\\ +\dfrac{\Delta x_w}{k_w A_w}\left(\begin{array}{c}h_{rwew}\left(T^{p}_{wei}-T^{p}_{wwi}\right)\\ +h_{rwnw}\left(T^{p}_{wni}-T^{p}_{wwi}\right)+h_{rwsw}\left(T^{p}_{wsi}-T^{p}_{wwi}\right)\end{array}\right)\end{array}\right)=\frac{1}{2Fo_w}\left(T^{p+1}_{wwi}-T^{p}_{wwi}\right) \quad (4.73)$$

$$\left(\begin{array}{l}2Fo_w\left(T^{p}_{wx1}+\dfrac{\Delta x_w}{k_w}\left(h_{cwi}T^{p}_{ai}+\dfrac{1}{A_w}\left(\begin{array}{c}h_{rwnw}T^{p}_{wni}+h_{rwsw}T^{p}_{wsi}\\ +h_{rfiw}T^{p}_{gi}+h_{rgw}T^{p}_{gi}+h_{rwew}T^{p}_{wei}\\ +I_s\tau F_{L-w}S_w A_w\alpha_{sab}\\ +I_s\tau\left(1-\alpha_{sab}\right)\left(\begin{array}{c}A_f F_{fw}F_{Lf}S_f\\ +3A_w F_{ww}F_{Lw}S_w\end{array}\right)\end{array}\right)\right)\right)\\ \quad+\left(1-2Fo_w\left(1+\dfrac{\Delta x_w}{k_w}\left(h_{cwi}+\dfrac{1}{A_w}\left(\begin{array}{c}h_{rfiw}+h_{rwew}+\\ h_{rgw}+h_{rwnw}+h_{rwsw}\end{array}\right)\right)\right)\right)T^{p}_{wwi}\end{array}\right)=T^{p+1}_{wwi} \quad (4.74)$$

The external surfaces of the walls will have energy balances similar to the floor node.

The air node will respond very quickly to heat inputs and outputs. By analysing its density and specific heat capacity, it can be assumed that an instantaneous flux occurs and an air node similar to that used for the steady-state air node can be used.

$$T_{ai}=\frac{\left(A_g\left(h_{cfi}T_{fi}+h_{cgi}T_{cgi}\right)+h_{cwi}A_w\left(T_{wwi}+T_{wni}+T_{wei}+T_{wsi}\right)\right)}{\left(A_g\left(h_{cfi}+h_{cgi}\right)+4h_{cwi}A_w\right)} \quad (4.75)$$

Using these equations a transient computer program was constructed.

Figure 4.17 shows a flow diagram of the transient program. (A copy of the program can be found in the Appendix.) The layout of the transient program is similar to that for the steady-state program, especially in the first stage where the computer determines all the constants either from data already within the program or, as in the case of the solar optical properties, by calculation. Once the temperatures have been established for all the nodal points, the computer program begins a procedure to determine the change in temperature for each node over time. At each time step in this procedure, the heat transfer coefficients are determined as in the steady-state model, and then the nodal

temperatures are calculated from previous values. This procedure is run for a required time at which point the temperatures are written to a file. The procedure is then continued until the program has simulated the time required, usually four hours, at which point the program writes the final set of data to the computer file and the temperatures at this point are outputted to the computer screen.

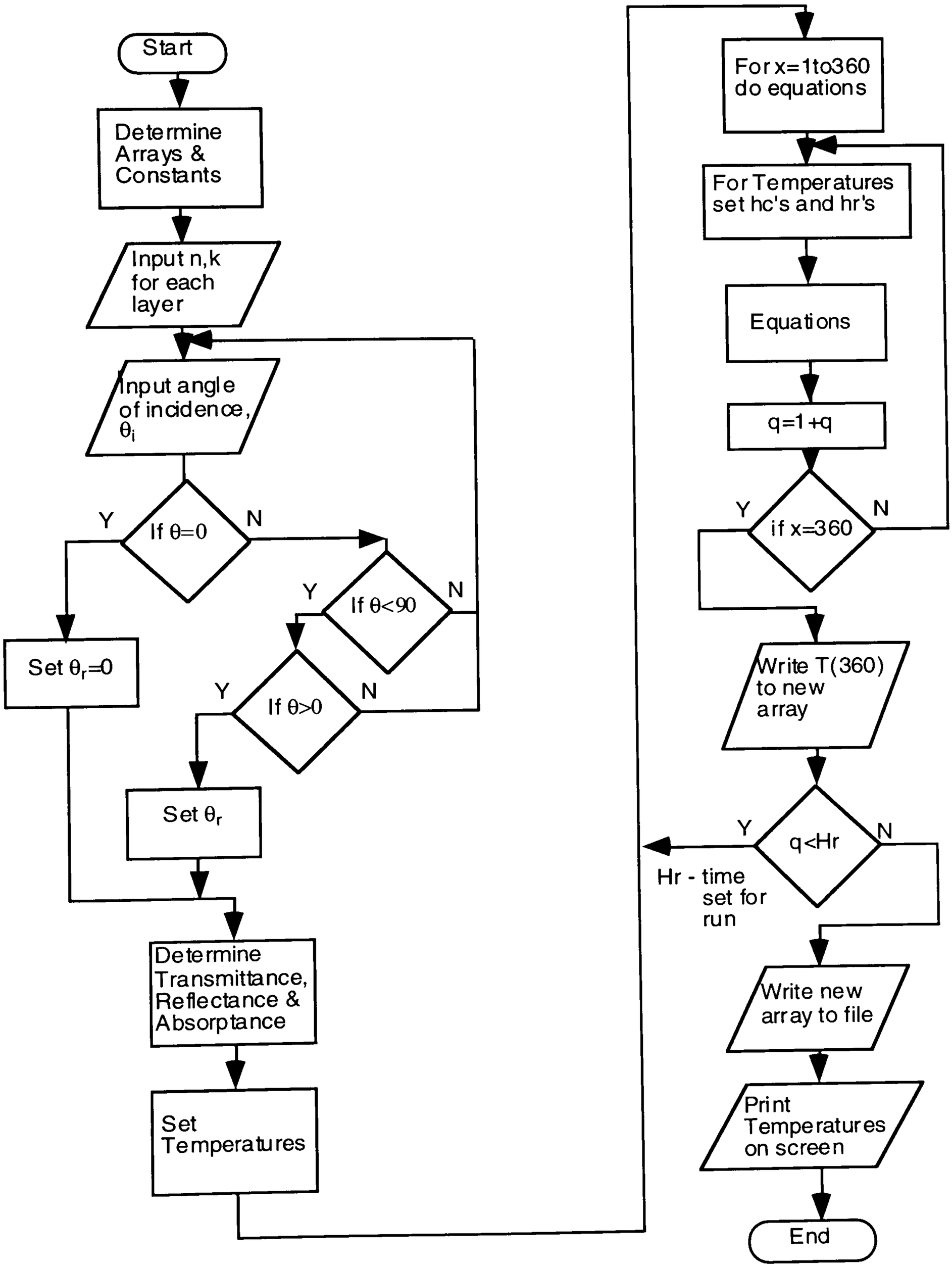

Fig 4.17 A flow diagram of the transient program.

Chapter 5 Experimental Results

5.1 Introduction

A set of samples of solar-control films was acquired from three manufacturers, Madico, Courtaulds and 3M. Two sets of results were obtained, as described in Chapter 3. These were, i) the total solar energy and the daylight transmittance, and, ii) the temperature rise over a 4 hour period. Table 5.1 outlines the films tested.

Manufacturer	Code	Type	Colour
Madico	RS 330	Reflective	Silver
	RS 220	Reflective	Silver
	SB 340	Insulation	Bronze
	SB 550	Insulation	Bronze
	AG 51	Tinted (absorption)	Grey
	AG 36	Tinted (absorption)	Grey
	TG 21	Absorption	Grey
	RB 321	Reflective	Bronze
	RG 321	Reflective	Silver
Courtaulds (Llumar)	E 1220	Insulation	Silver
	E 1235	Insulation	Bronze
	AT 35	Tinted (absorption)	Bronze
	AT 50	Tinted (absorption)	Bronze
	AT 70	Tinted (absorption)	Amber
	RB 35	Reflective	Silver
	R 30	Reflective	Gold
	R 20	Reflective	Silver
3M	NR 20	Absorption	Smoke
	RE 35	Absorption	Neutral
	IN 50	Insulation	Bronze
	P 34	Insulation	Silver
	P 19	Reflective	Silver
	P 12	Reflective	Smoke

Table 5.1 The Solar-Control Films used in the present tests

Clear 4mm thick float glass was chosen, on which to mount the films. This is because it is commonly used as window glass in many buildings. Films were mounted on the inside surface of the glass. They are applied using a water activated adhesive first developed by 3M (Thiessen, 1968)

The solar and daylight transmittance of all the films were measured using a solarimeter and a lux meter, Figures 5.1 to 5.4, while four sets of experiments were carried out to determine the temperature change over time for specific film types. Within each set of experiments, the temperature change was monitored over 4 hours for angles of

incidence from 0 to 80°. These four sets were: clear float, Figures 5.5 to 5.13; reflective film - RS220, Figures 5.26 to 5.34; insulating film - SB340, Figures 5.47 to 5.55; and tinted film - AT50, Figures 5.68 to 5.76.

The results of the experiments undertaken using the illuminated hot box, were compared with a series of computer based simulations using the physical model developed. These results can be seen in the sections which follow the experimental data. These results were obtained using the transient model, the development of which was described in Chapter 4. The results obtained using a steady-state model, also described in Chapter 4, bore no relation to those obtained experimentally. When the steady-state program was used to simulate the clear float glass, it predicted temperatures of around 50°C. The code was investigated, and the data referring to the physical properties of the materials used was checked for any mistakes, but no answer was found to explain why the results were not as expected. A possible answer to this problem could lie in the solving method used. Finally, after lengthy analysis of the code and data used, it was decided to leave the steady-state model, and instead concentrate on the transient model.

Figures 5.1 to 5.4 show the light and energy transmittance verses angle of incidence for a selection of the films tested. Compared to earlier work on the measurement of these figures (Griffiths et.al 1992), these results showed a closer correlation with those proposed by Markus and Morris (1980) and Duffie and Beckman (1991). Figure 5.1 is a graph showing the results obtained for the tests on clear float glass. From this graph it can be seen that the transmittance only varies slightly, up until an angle of incidence of 60°, and then rapidly decreases. This pattern was replicated for all the films, see Figures 5.2 to 5.4.

Figure 5.2 shows the solarimeter and light meter tests results for tinted films. These films were taken to be absorptive films throughout the time of the experimentation and the computer modelling, due to high levels of absorptance stated by the manufacturers within trade literature. It was not until after the experimentation was completed that it was discovered that Courtaulds classified these as tinted films (Spence 1994). For the rest of this study, these films will be referred to as absorptive films to avoid confusion. The ability of these films to reduce light transmittance can be clearly seen in Figure 5.2, with the results of light transmittance being lower than that of the total solar energy transmittance, with the exception of the AT70 film. The insulating and reflective films show a tendency similar to that of clear glass, that is, they allow a greater proportion of

light through, compared to solar energy. This is a result of the nature and purpose of these films as discussed in Chapter 1. The insulating film is designed to allow light through while reflecting long wave thermal radiation back into the room, whereas, the purpose of the reflective film is to keep energy out of the room. The problem with comparing the changes in transmittance of solar energy and visible light, is that these figures represent the proportion of light transmitted through the film/glass to the detectors compared to the readings obtained without any "obstructions". Therefore, while the proportion of the transmitted light is greater than that measured for total solar energy, the amount of solar energy transmitted is greater. This is quite obvious as visible light is a part of the total solar energy. However, by distinguishing between total solar energy transmitted and the visible light transmitted, a degree of understanding of the use of the film can be obtained. A film with a light transmittance considerably higher than that measured for total solar energy is one designed to keep unwanted solar energy out, while at the same time providing the maximum amount of daylight.

The results of the transmittance tests for a sample of reflective films are seen in Figure 5.4. These reflective films are designed to reduce the total solar gain and also the visible light transmittance. These films use a reflective metal film to produce a mirror effect. Overall, the results obtained for the total solar energy and light transmittance through the films tested were satisfactory, and compared well with the manufacturers data which was available.

Following the determination of total solar energy and light transmittance, a series of experiments was undertaken to determine the change in temperature within the box with different films and at different angles of incidence. A sheet of 4mm clear float glass was tested first, this being used to examine the system, so that any problems could be removed. The results of these experiments can be seen in Figures 5.5 to 5.13. A series of tests was carried out at 0° angle of incidence so that extraneous light paths and reflecting surfaces could be removed and so that the box and thermocouples could be calibrated, see Chapter 3. The results of the experimentation showed that the box did not reach a thermally steady-state condition during the four hours for which it was tested.

During the experiments where the angle of incidence of the lamp was greater than 0°, it was noted that a significant portion of the energy from the lamp was falling on the external wall surface which faced the lamp. A way of shielding the external walls was

therefore needed. After many ideas were rejected, it was decided to place an external wall around the outside of the box, made from polystyrene, to act as a 'sun' shade. This wall was constructed approximately 10cm away from the outside wall of the box, and was as high as the external walls. However, this then produced a warm and relatively still, body of air between the external wall surfaces and the shading device. This resulted in the external surfaces being hotter than they should have been. After much consideration concerning how to overcome this problem, it was decided to proceed with the experiments and include the shading device within the model. Figures 5.6 to 5.13 show the temperature rise of the box under the new conditions. It is quite evident that the heat flux through the walls was altered by the shading device, however, it was a better result than that achieved without the shading device.

The computer modelling of the heat flow within the box while testing clear float glass was quite successful. The results of this work can be seen in Figures 5.14 to 5.25. Two computer models were used, one where the solar insolation was incident upon the glass surface only, and the other where it was incident upon the sides with a shading wall present. The results of these modelling tests, compared favourably with those achieved during the laboratory experimentation. The computer model results for angles of incidence over 50° did not fit in as well with the experimental results. On examination of the results and those obtained from the experimentation, the conclusions drawn were, that the results were affected by an increasing amount of the lamp's energy being incident upon the external sides of the box as the angle of incidence rose greater than 40°.

The characteristics used to describe the clear float were its surface emissivity, refractive index and absorptive index. As shown in Chapter 2, it was these characteristics which were needed to describe the interaction of energy with transparent media. These characteristics of the films were not available for this research, as the companies were not able or willing to give any data on the absorptive index of the films tested. Therefore the data concerning the films transmittance, obtained during the determination of the total solar energy transmittance, and the values of transmittance, absorptance and reflectance given by the relevant companies, were used for the computer simulations.

The experimental results and the computer modelling results, for the reflective film, can be seen in Figures 5.26 to 5.34 and Figures 5.35 to 5.46 respectively. It is evident when comparing these results, that the thermal gain is not as great within the computer model,

as that observed in the experimental results. Furthermore, the results from the computer program, were far removed from those obtained during the practical experimentation, where insolation from the lamp was incident upon the external surface. This is emphasised by the fact that the predicted temperature of the external wall was very high compared with the other predicted temperatures for the box during simulations which took into account the energy from the lamp, incident upon the external surfaces, see Figures 5.36, 5.38 and 5.41.

While comparing the graphs for the experimental and the modelling results of the reflective film, it was observed that the glass was hotter than the internal surfaces of the box, due to the film being made of a metal, which would absorb and reflect more of the energy than it transmitted. What was also evident from Figure 5.26 was the effect that this had upon the globe temperature of the internal space. Although it was lower than that seen for clear float, see Figure 5.5, it was still higher than the internal wall temperatures. Therefore, even with a low total solar energy transmittance compared with clear float, the reflective film still transmitted a considerable portion of solar energy. This may have been due to greater absorption by and subsequent inward heat flow from the metal film. Similar films produced by Courtaulds have an emissivity of 0.7. An emissivity within this range may account for the high thermal radiation heat transfer to the interior of the box.

In examining the experimental and the computer based simulation results obtained for the insulating film- Figures 5.48 to 5.67, it could be seen that the temperature rise predicted by the computer simulation did not match those observed during the experimentation when using the hot box. However, it was pleasing to note that the glass temperatures predicted by the simulation, were higher than the other predicted temperatures for the rest of the box as was expected. This was also observed in the results obtained from the hot box testing. Once again, the same observations and conclusions, with respect to the reflective film, could be drawn from these results. It was evident from Figures 5.47 to 5.55 that the angle of incidence did not affect the temperature increase until the angle of incidence was greater than 60°.

Finally, the absorptive film was investigated experimentally, using the illuminated hot box, and by means of a the computer based simulation. The resultant graphs can be seen in Figures 5.68 to 5.88. This was the only film tested for which the emissivity was known. However, as the absorption coefficient was unknown, then the subroutine within the program which determined the transmittance and absorption, had to be

overridden. This was also the case with the insulating and reflective films. Instead of relying upon using the absorptive index, the data used, concerning the film's transmittance and absorptance, was obtained from the manufacturer. During all the testing carried out, it was seen that this film, and the other two films used to produce Figure 5.2, gave results which closely matched the manufacturers stated specifications.

The results obtained from the illuminated hot box, once again, showed the flaw in the design of the box in that the temperature of the walls external surfaces rose more rapidly at the start than did the internal surfaces. However, with the exception of the temperatures obtained from the computer simulations being a few of degrees lower than those obtained from the practical experimentation, the shape of the curves and the temperature differentials between the surfaces were the same for both the experimental work and the computer modelling.

Two graphs showing the actual temperatures vs the predicted temperatures were plotted, to gain a better understanding of how the experimental results differed from the results predicted by the computer based simulation. Figure 5.89 is a graph of the actual temperatures vs the predicted temperatures for clear float glass. Also shown on the graph is a line which represented the expected trend if the predicted results from the simulations had matched the actual results from the experimental procedure. The data in Figure 5.89 showed a bias towards the actual temperatures. This illustrated that the temperatures predicted by the computer model were not as high as those obtained from the experiments. This trend could have been the result of higher temperatures being recorded by the thermojunctions on the experimental rig because of radiative heating of the thermojunctions by the lamp. This was highlighted by the floor temperatures being nearer the expected trend compared to the other temperatures. The thermojunctions which measured the floor temperatures were fixed to the floor, using a tape with a emissivity close to that of the internal surfaces of the box. Therefore the measured floor temperature should be nearer the real temperature of the floor, while the measured temperatures for the glass surfaces could be said to be higher than the real temperatures, as a result of the radiative heating of the thermojunctions.

However, the thermojunctions used to measure the internal wall temperatures were applied to the walls in the same way as those applied to the floor. If the hypothesis concerning the radiative heating was correct then the predicted internal wall temperatures should be closer to those measured. Instead, they were clustered with the glass surfaces and air temperatures. This led to the conclusion that even though the

temperatures measured might have been higher than they should have been as a result of the radiative heating of the thermojunctions, there was another factor influencing the results to cause the trend shown.

A second graph was plotted showing the actual vs the predicted results, this time for the absorptive film results, see Figure 5.90. These results show an increased shift away from the expected trend when compared with that seen for clear float glass. Once again, the floor temperature predictions seem to be nearer the expected trend than the other results. During the analysis of these graphs, a hypothesis was suggested that the floor temperatures were not to be relied upon and that the convective model, regarding the heat transfer between the floor and the air, used within the computer based simulation was incorrect. The majority of the heat gain by the internal air was a result of convection heat transfer from the floor which absorbed the greatest amount of the solar energy transmitted through the glass cover. If the convective heat transfer coefficient between the floor and the air used in the model was lower than that existing in reality, then the temperature rise by the air would not be sufficient and the floor temperature would be higher. Furthermore, the heat gain by the walls was dominated by convection from the air when the lamp was at 0° angle of incidence, and with a higher air temperature, the heat flux from the air to the glass would be greater, which might also result in higher glass temperatures within the computer model. By extending this hypothesis, this would result in the air, wall and glass temperatures shifting towards the expected trend, while the floor temperature would move below the expected trend. Therefore any fault within the convective model could cause the shifting of the results away from the expected trend as seen in Figures 5.89 and 5.90.

The experimental rig was designed to minimise the effects of unrepresentative radiative heating of the thermojunctions, exposed to direct gain from the incident radiation. However, this remains as a possible source of error in the measurements made. This is particularly true of the measurement of the internal and external glass surface temperatures. It is not too surprising that the measured values in this case were higher than those predicted. However, the differences between the predicted and the actual air temperatures are more difficult to explain. It has been suggested that this is due to an error in the assessment of the heat transfer coefficients, and the treatment of the floor as a horizontal surface. The dimensions of the hot box suggest that an alternative treatment of the space as an enclosure for the development of heat transfer coefficients might be more valid.

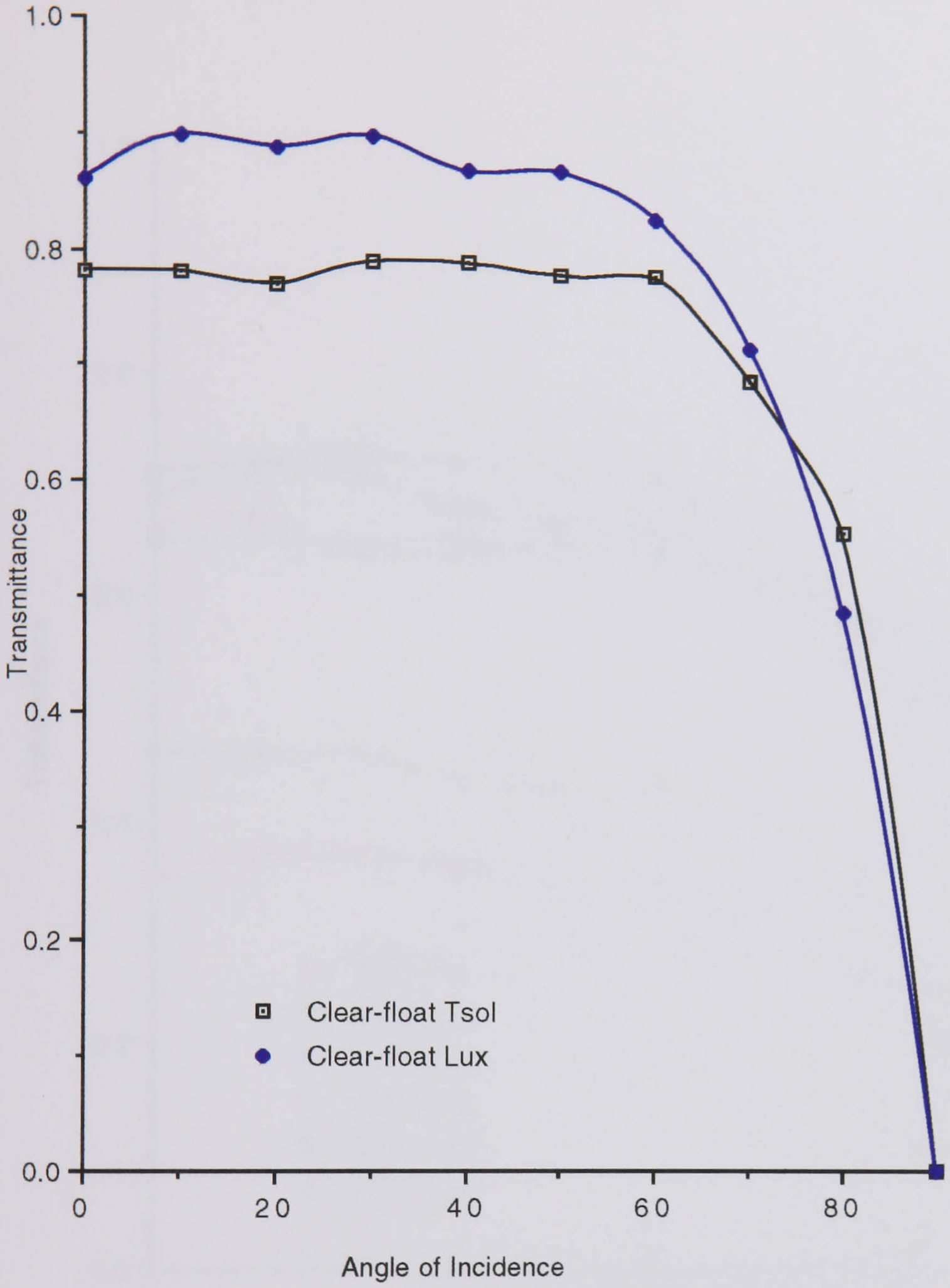

Fig 5.1 Solar and light transmittance through clear glass

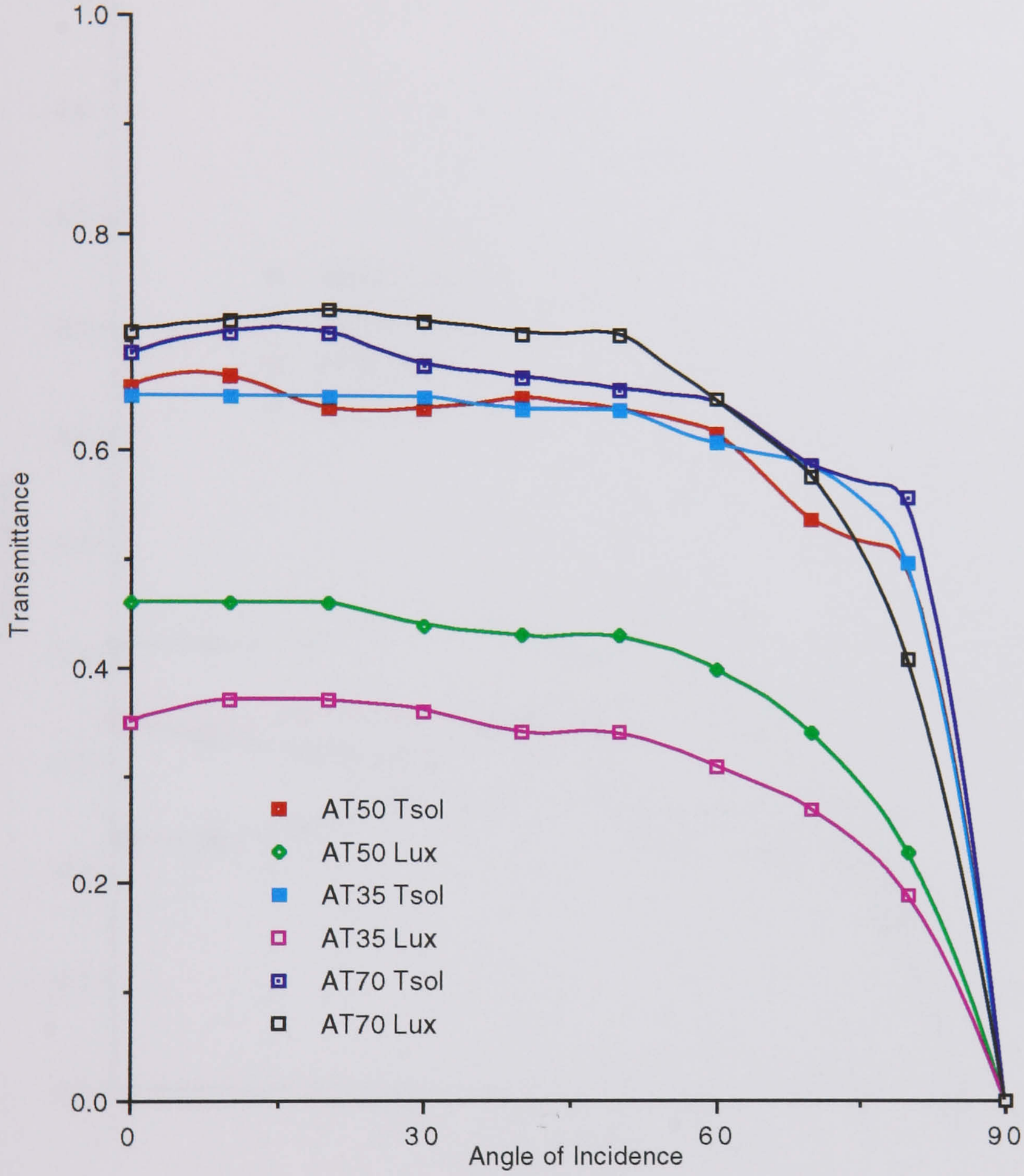

Fig 5.2 Solar and light transmittance for some absorptive films produced by Courtaulds

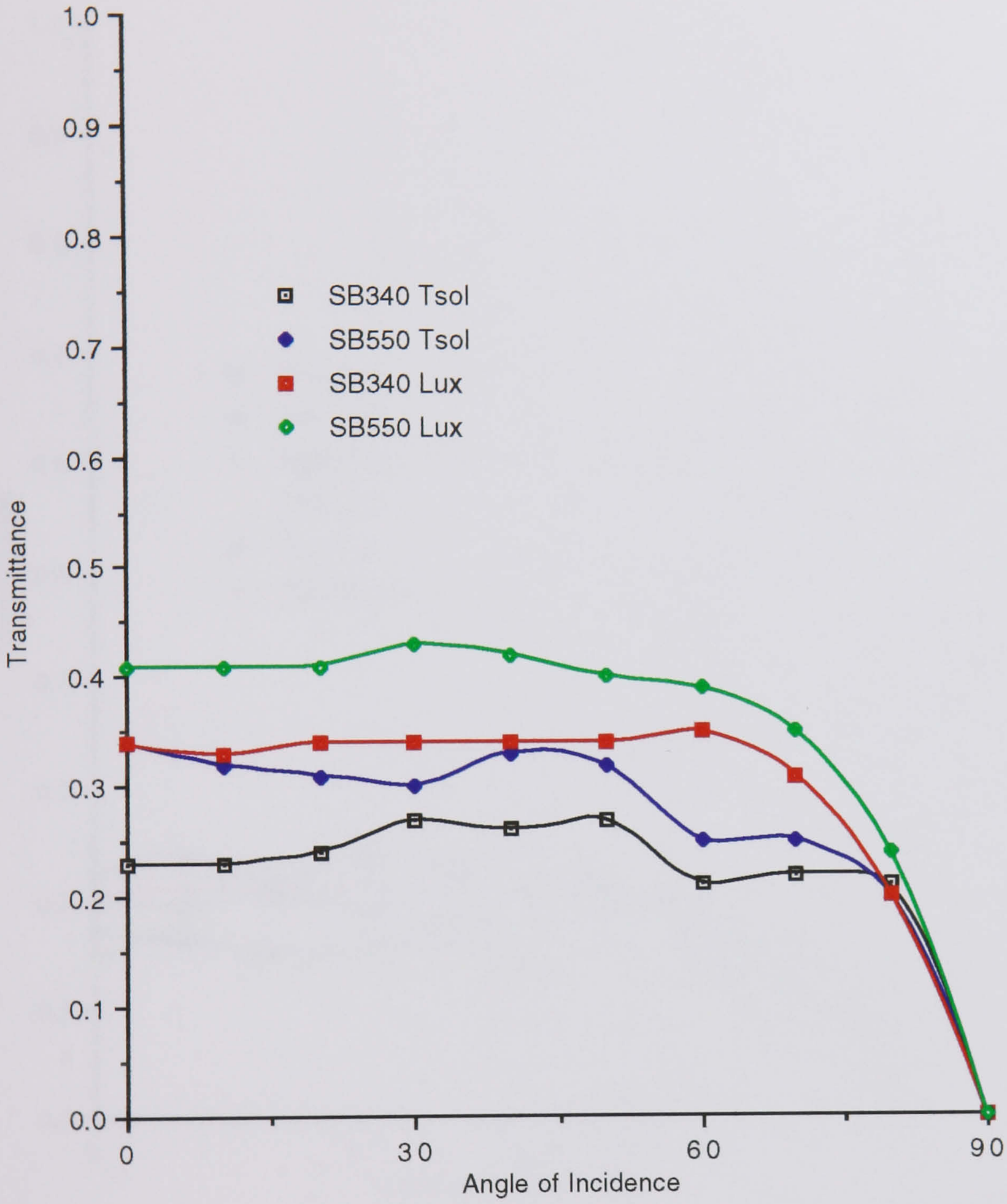

Fig 5.3 Solar and light transmittance for some insulating films produced by Madico

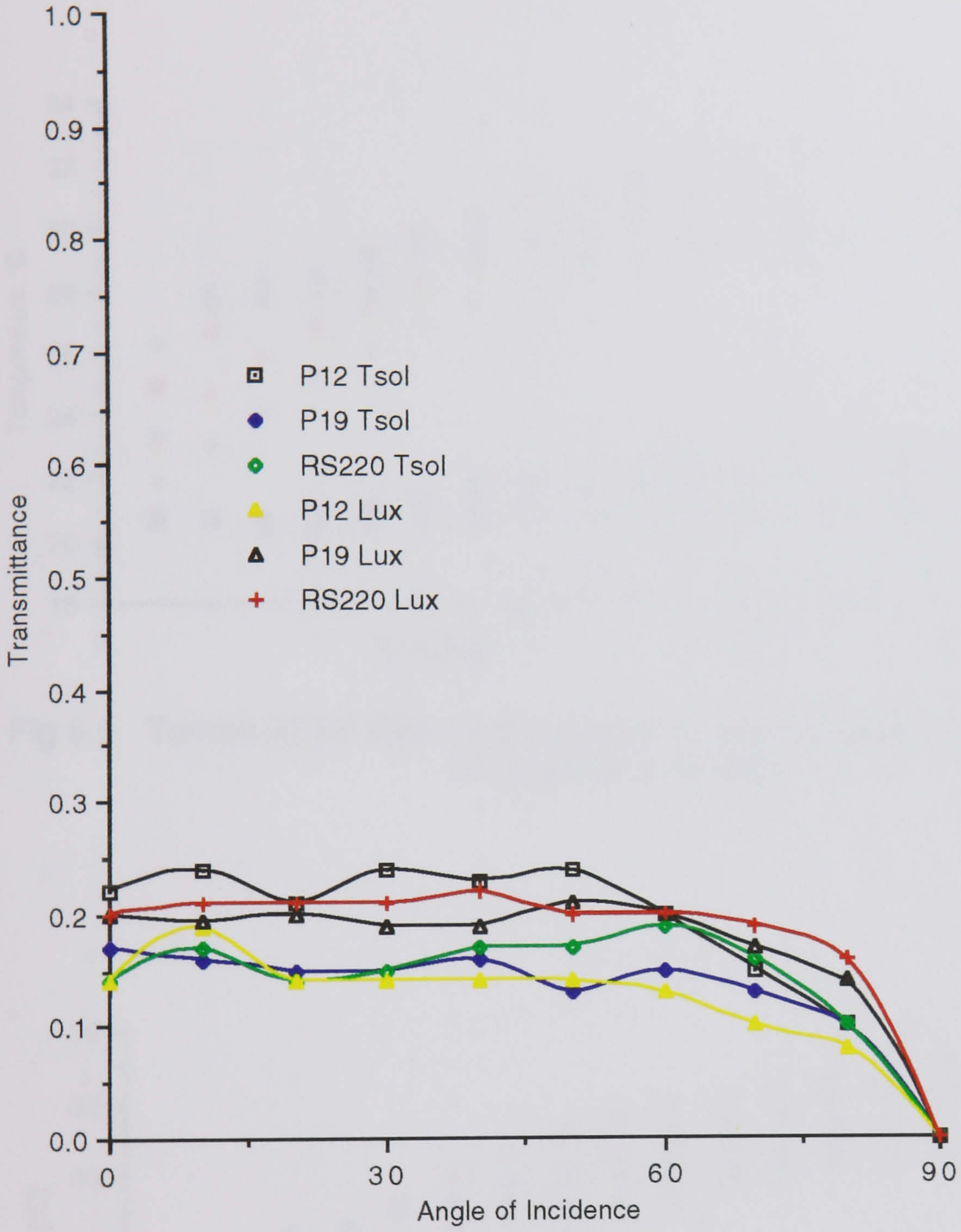

Fig 5.4 Solar and light transmittance for some reflective films produced by Madico (RS220) and 3M (P19, P12)

5.2 Clearfloat glass Results

5.2.1 Experimental Results

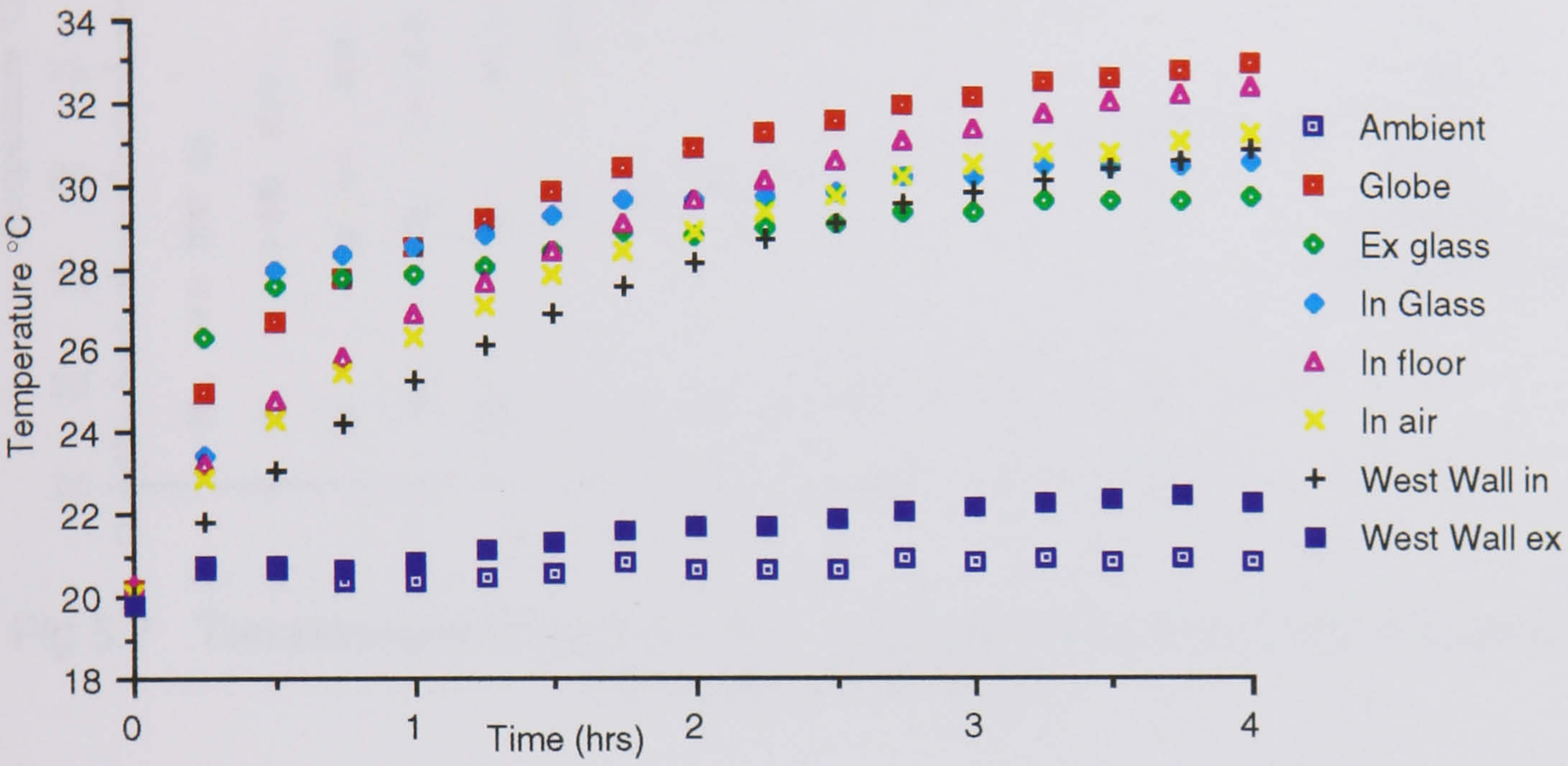

Fig 5.5 Temperature Rise over 4 hours for clear-float glass with insolation at 0° angle of incidence

Fig 5.6 Temperature Rise over 4 hours for clear-float glass with insolation at 10° angle of incidence

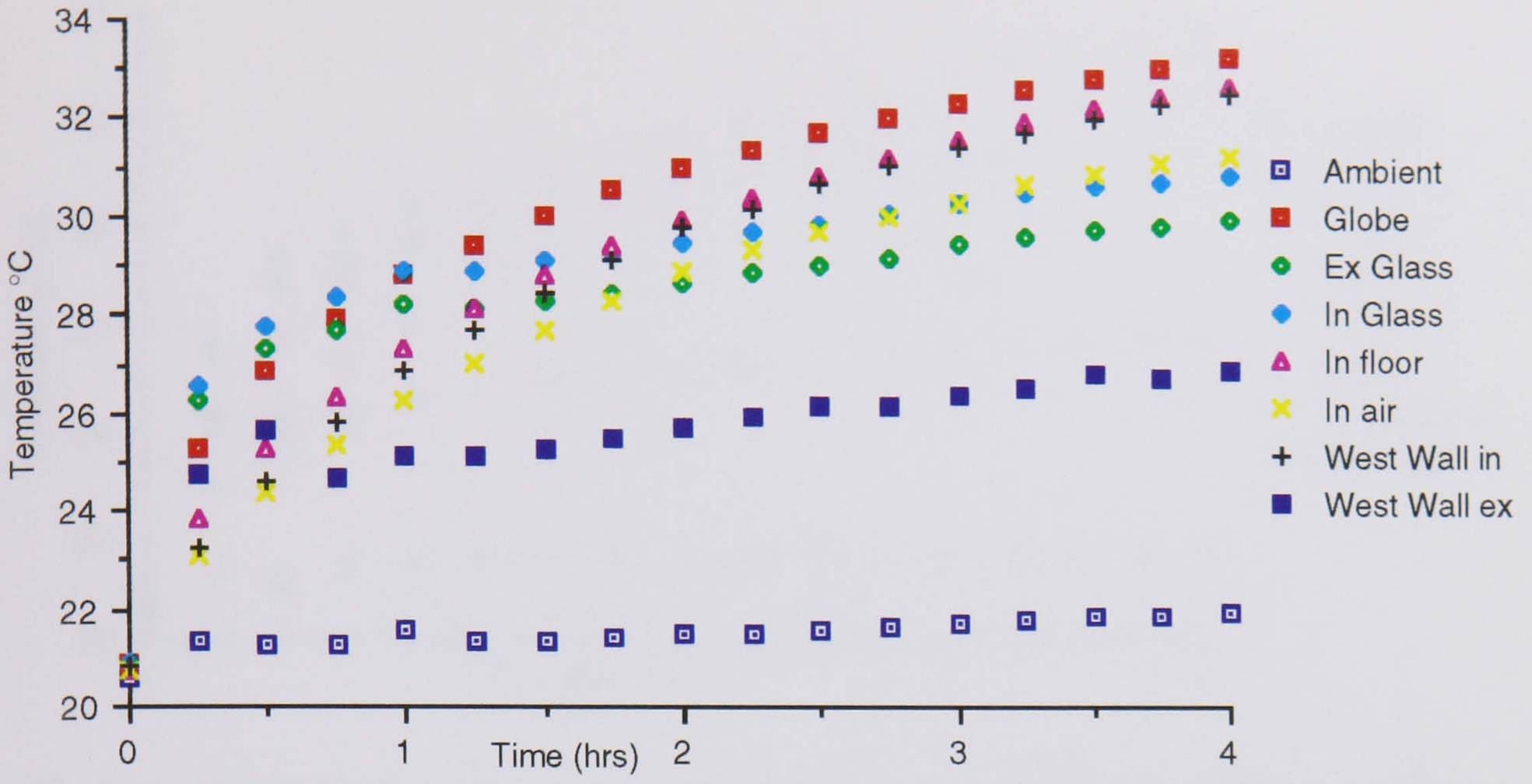

Fig 5.7 Temperature Rise over 4 hours for clear-float glass with insolation at 20° angle of incidence

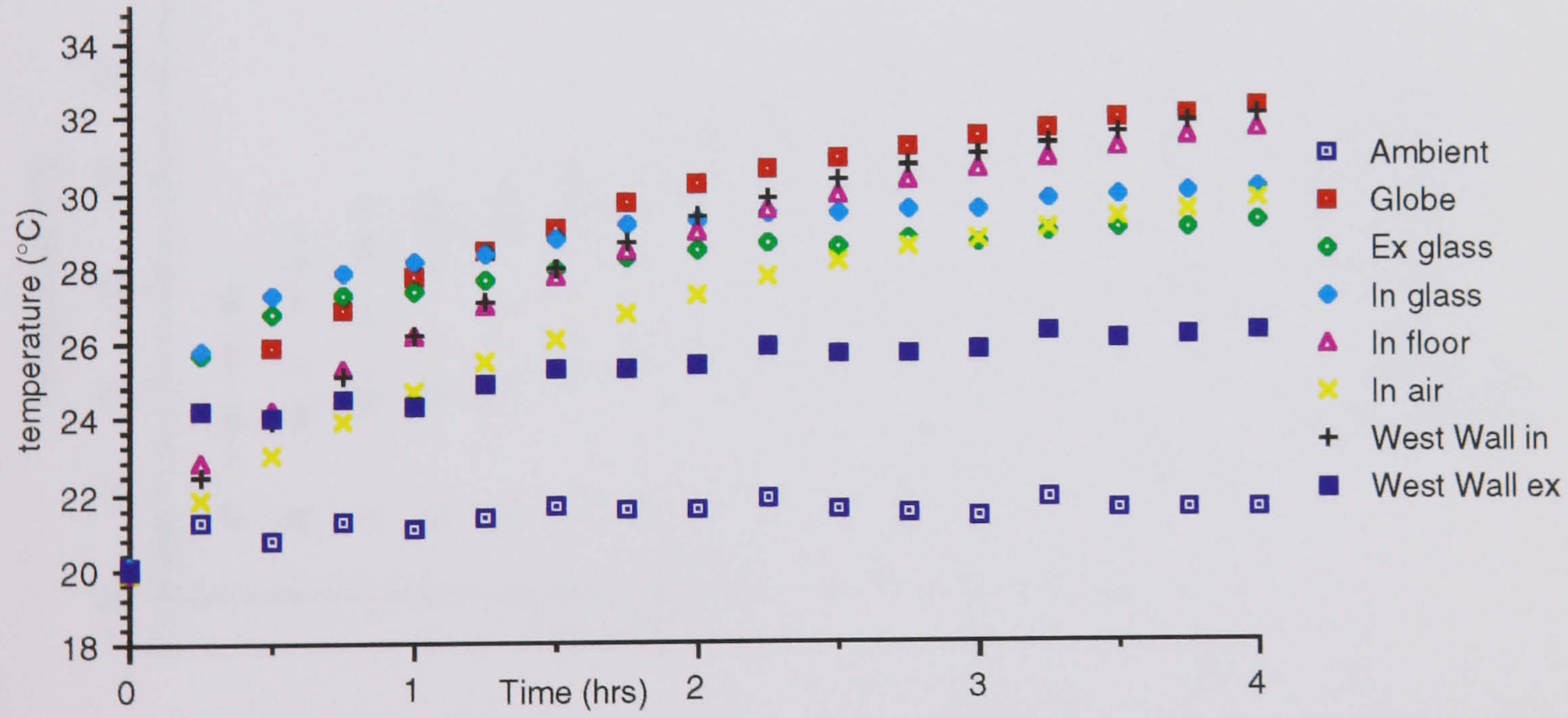

Fig 5.8 Temperature Rise over 4 hours for clear-float glass with insolation at 30° angle of incidence

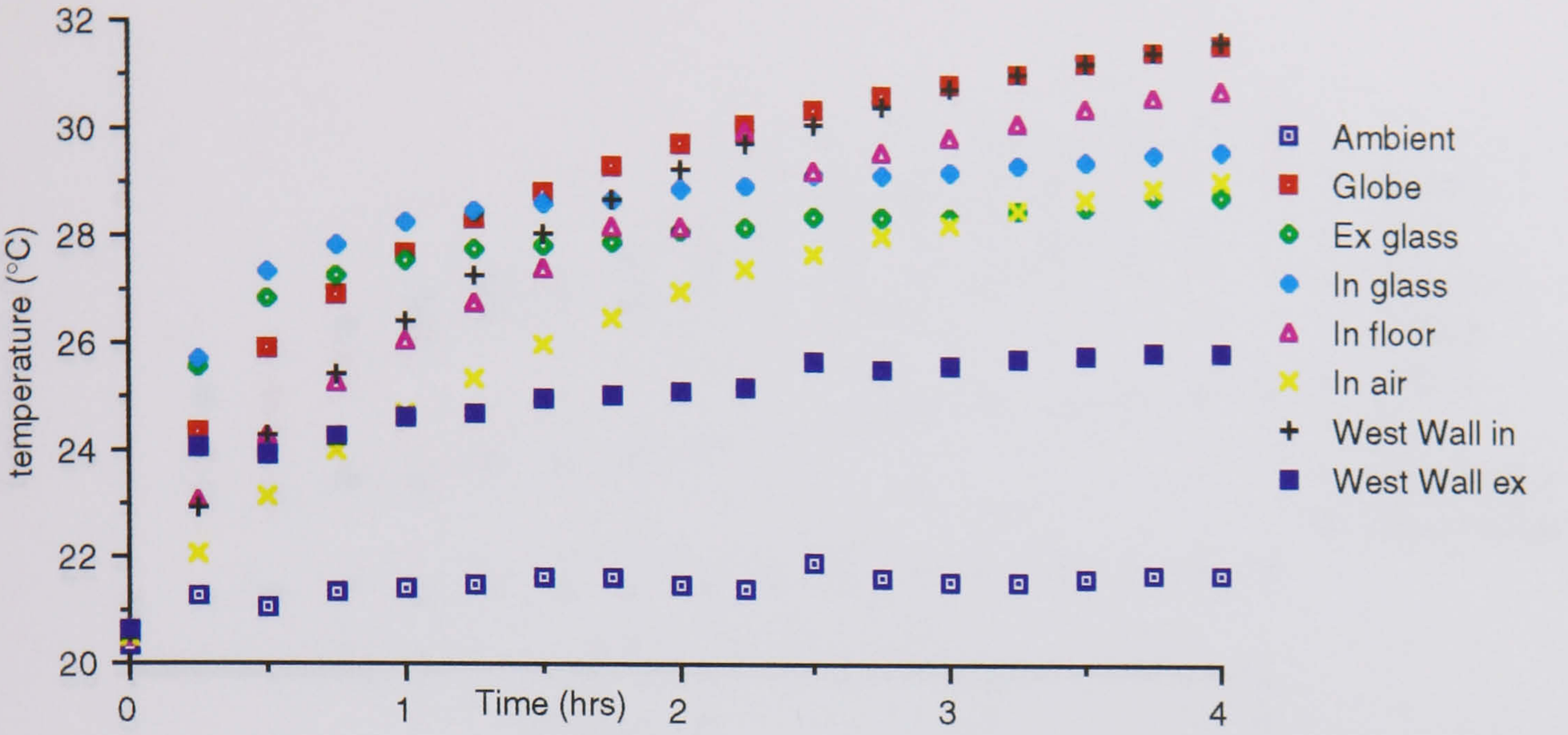

Fig 5.9 Temperature Rise over 4 hours for clear-float glass with insolation at 40° angle of incidence

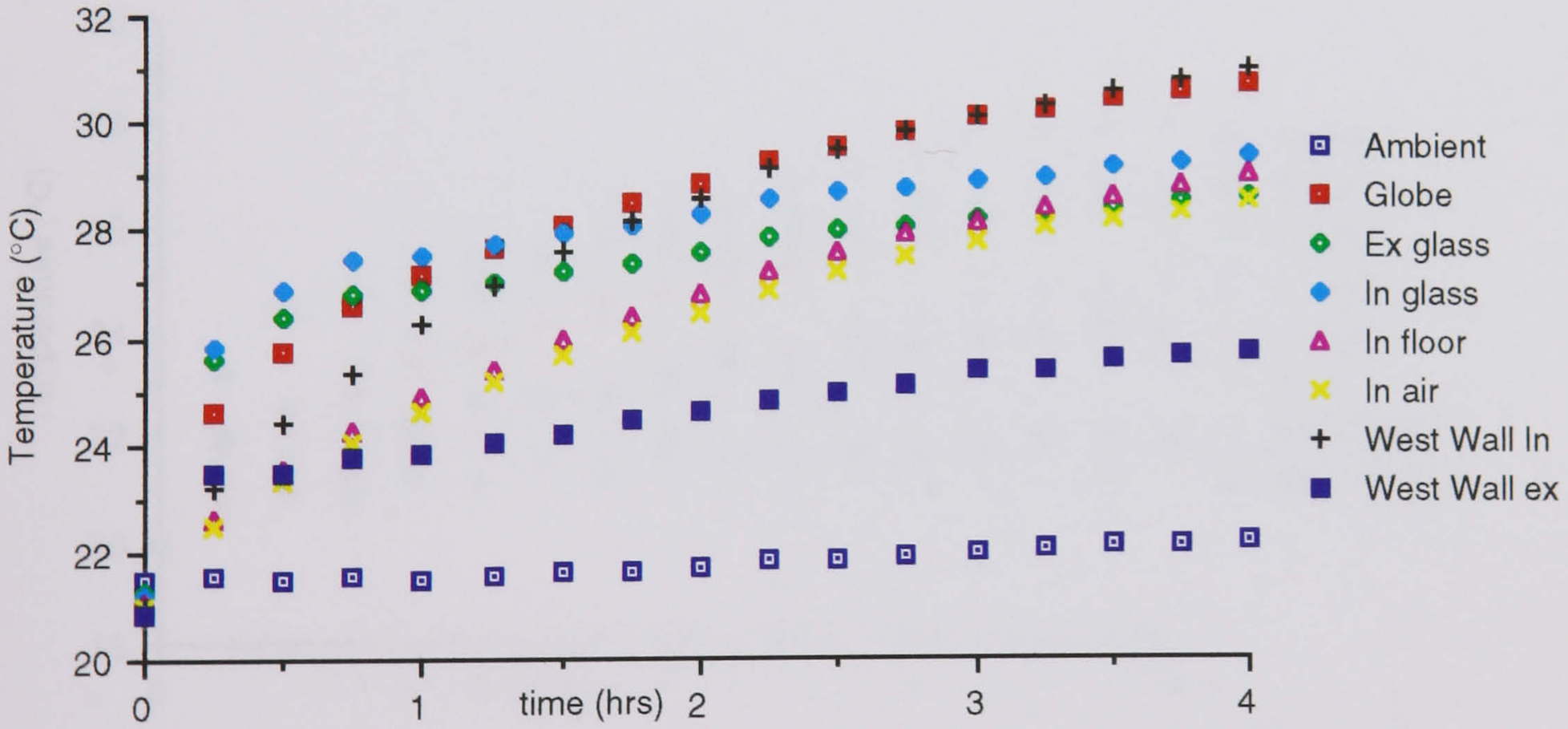

Fig 5.10 Temperature Rise over 4 hours for clear-float glass with insolation at 50° angle of incidence

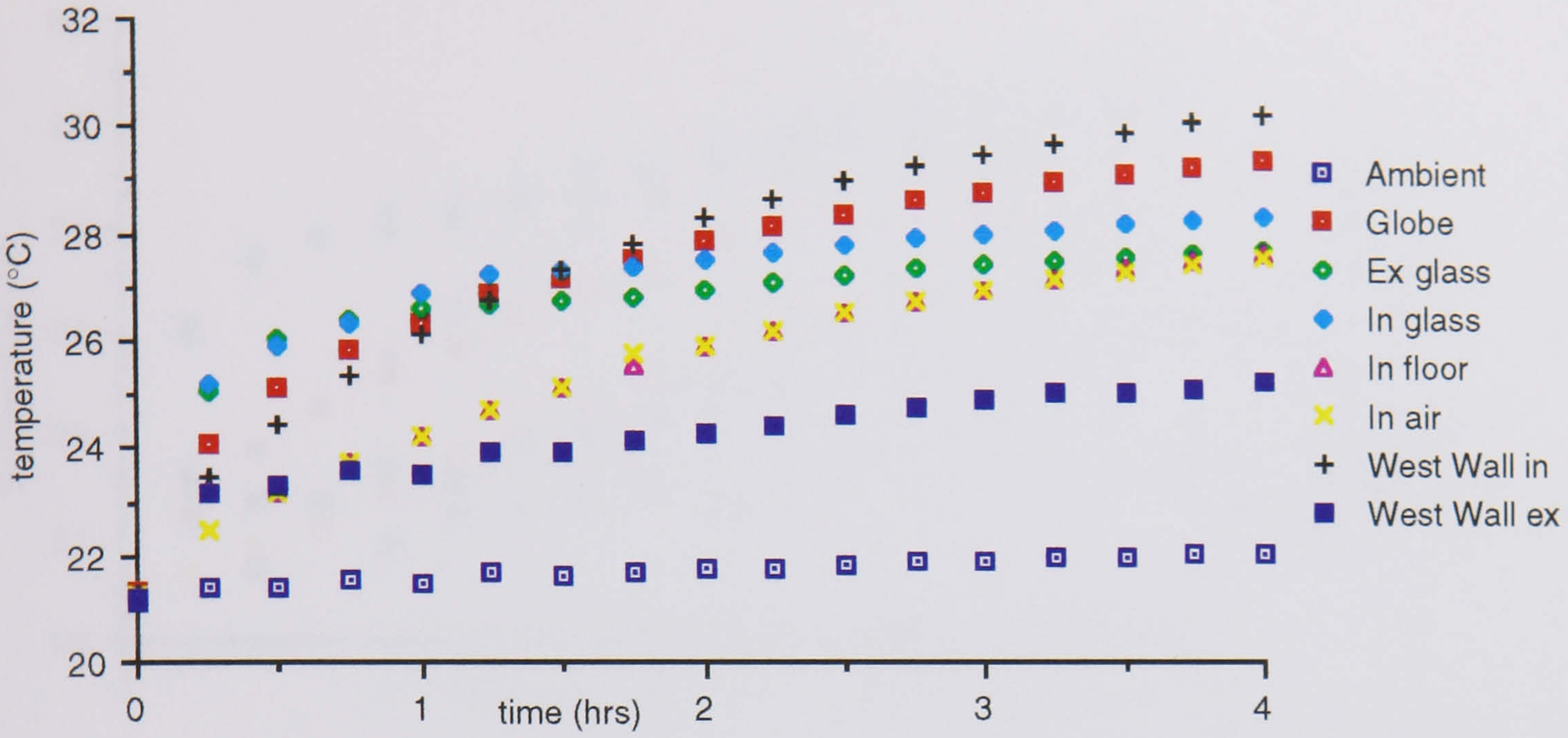

Fig 5.11 Temperature Rise over 4 hours for clear-float glass with insolation at 60° angle of incidence

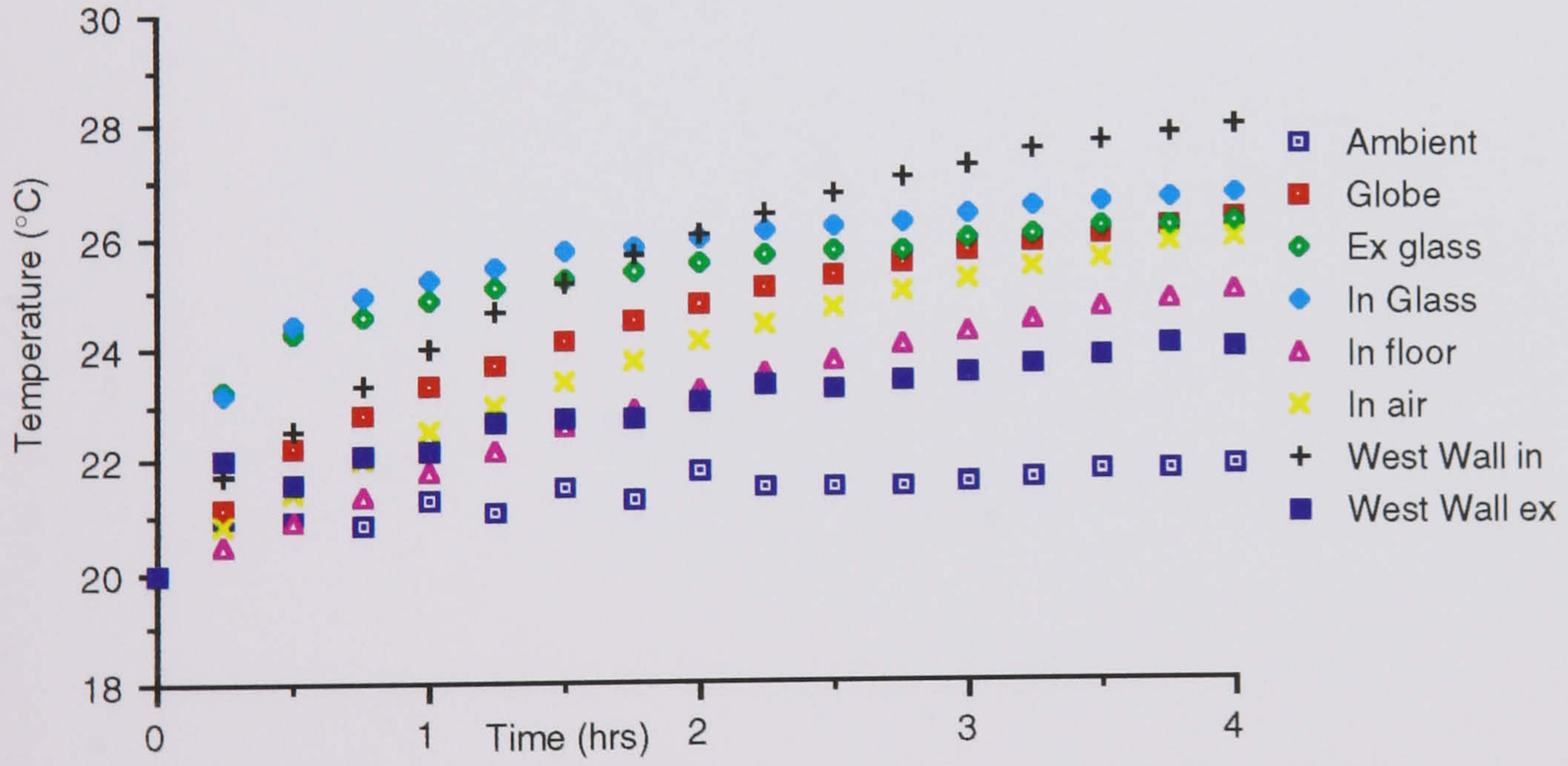

Fig 5.12 Temperature Rise over 4 hours for clear-float glass with insolation at 70° angle of incidence

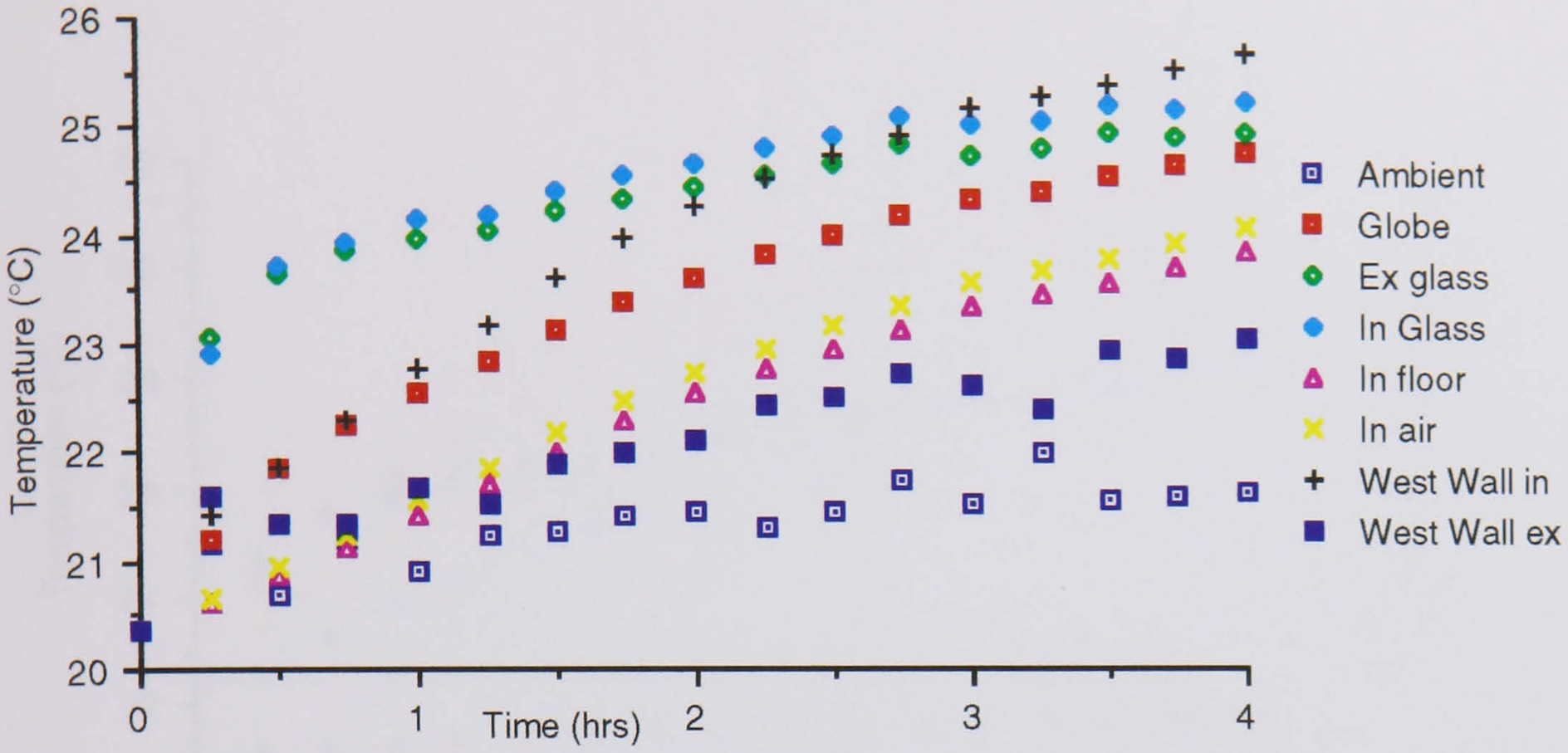

Fig 5.13 Temperature Rise over 4 hours for clear-float glass with insolation at 80° angle of incidence

5.2.2 Computer Model Results

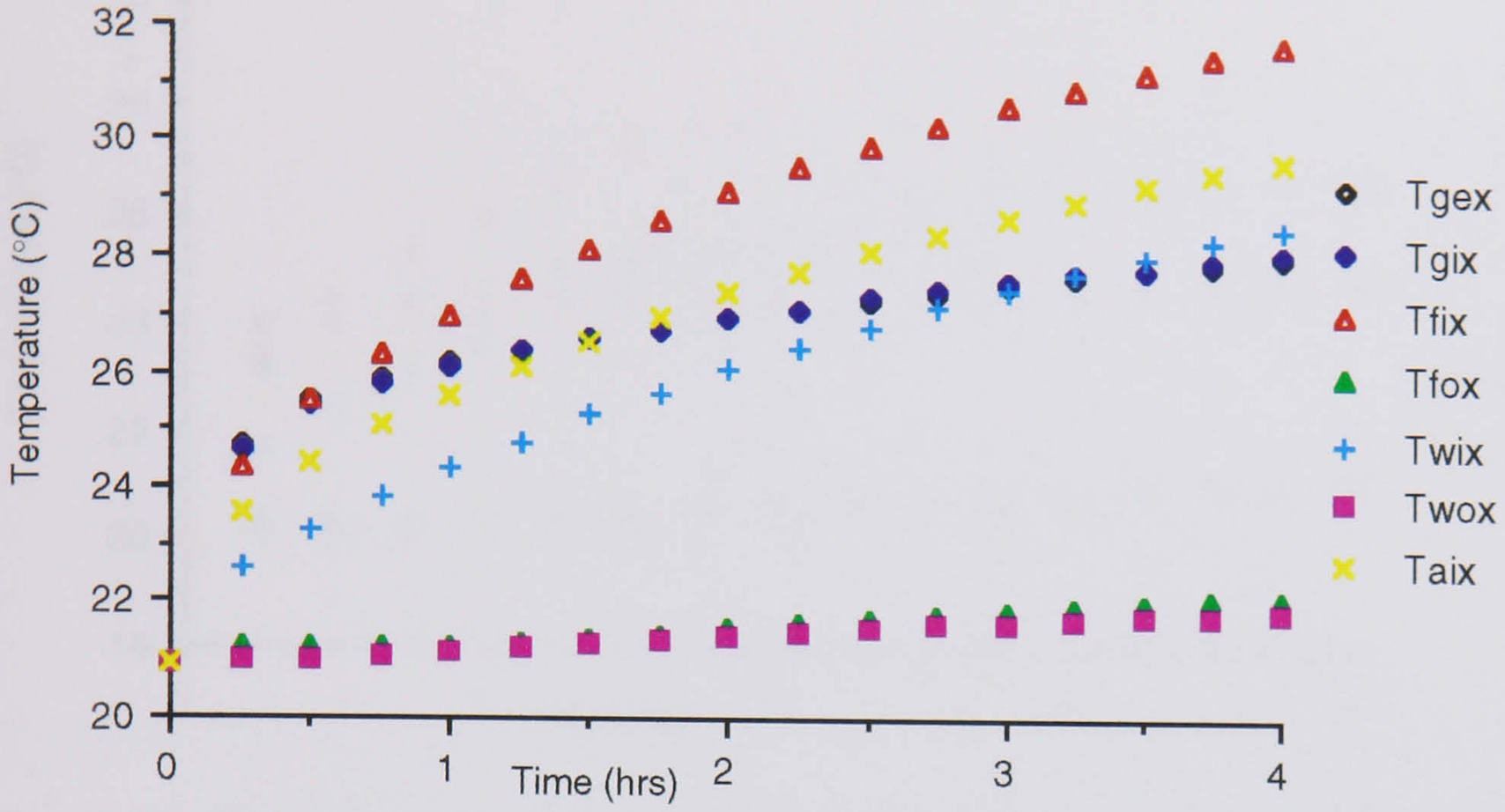

Fig 5.14 The computer model prediction of the temperature rise over 4 hours for clearfloat glass with insolation at 0° angle of incidence

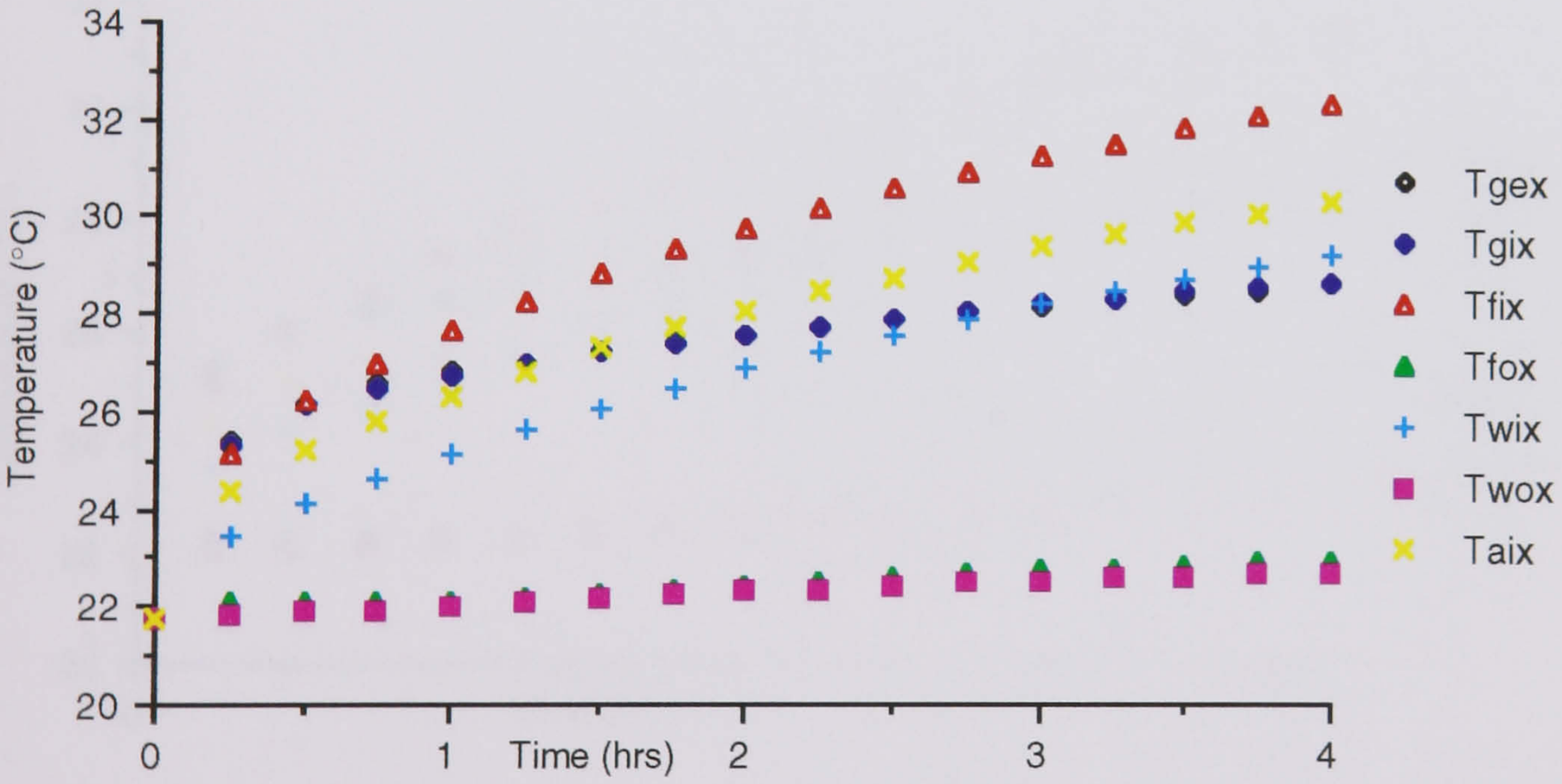

Fig 5.15 The computer model prediction of the temperature rise over 4 hours for clearfloat glass with insolation at 10° angle of incidence

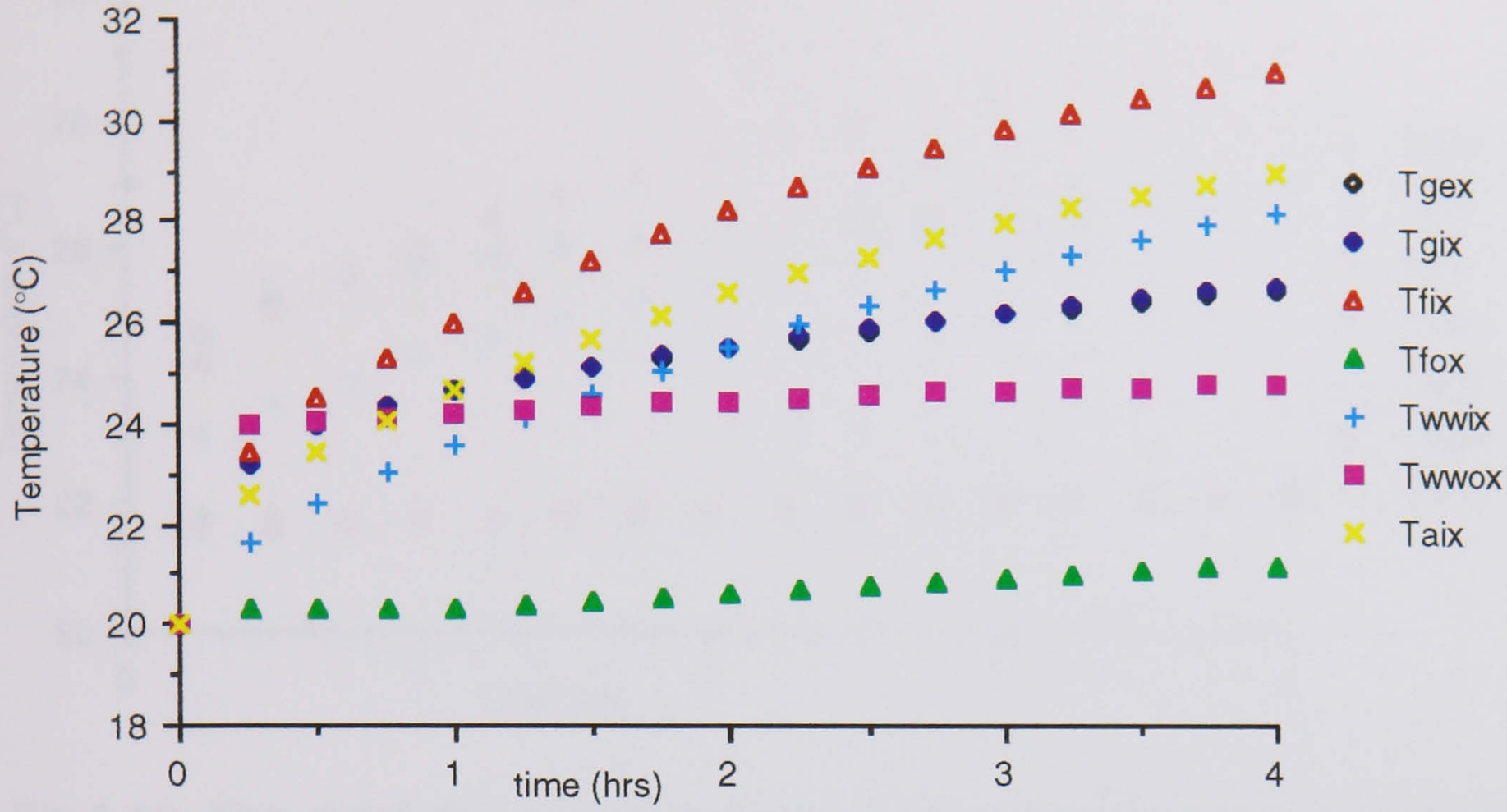

Fig 5.16 The computer model prediction of the temperature rise over 4 hours for clearfloat glass with insolation at 10° angle of incidence where insolation is received by the outside also

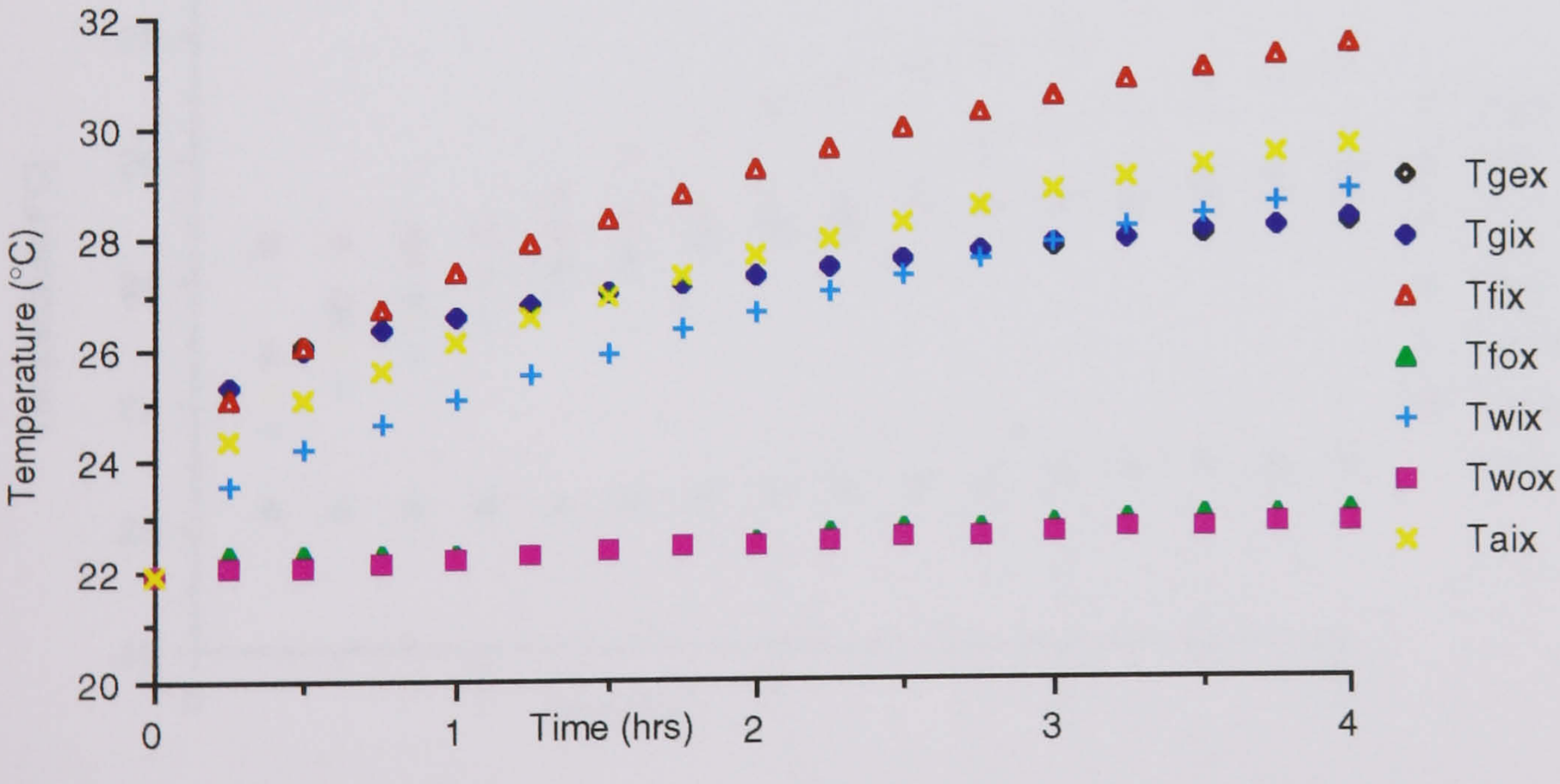

Fig 5.17 The computer model prediction of the temperature rise over 4 hours for clearfloat glass with insolation at 20° angle of incidence

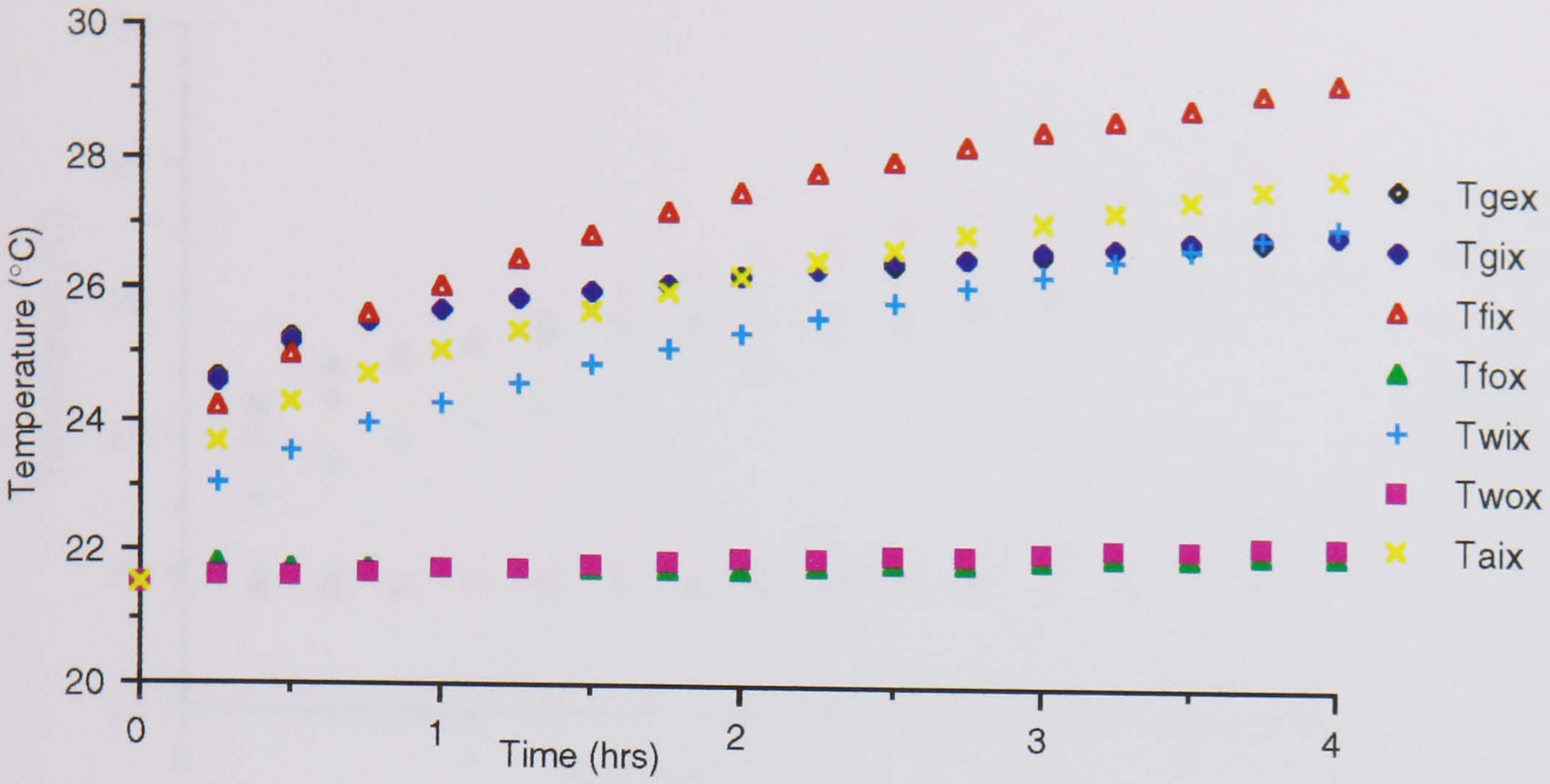

Fig 5.18 The computer model prediction of the temperature rise over 4 hours for clearfloat glass with insolation at 30° angle of incidence

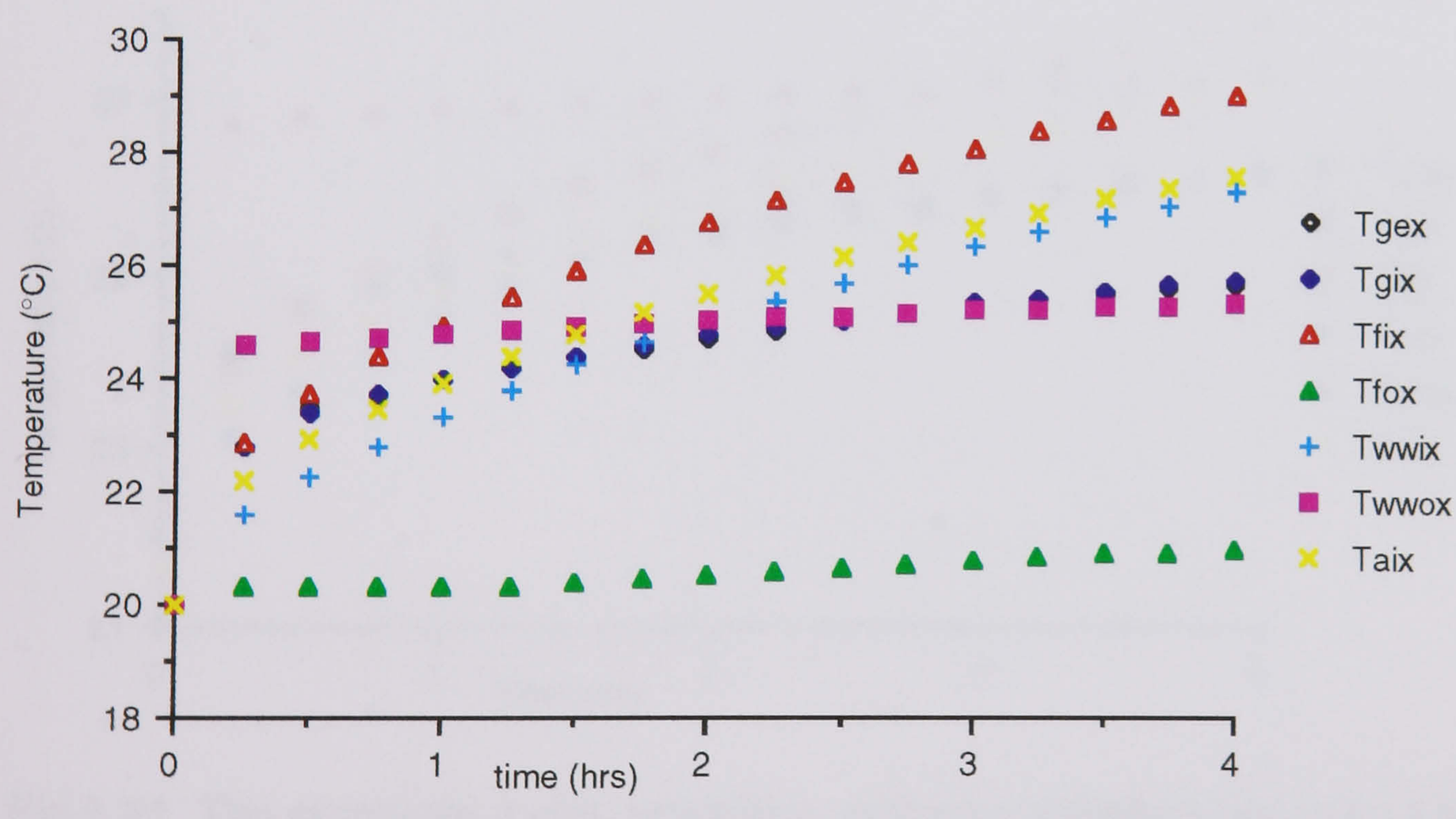

Fig 5.19 The computer model prediction of the temperature rise over 4 hours for clearfloat glass with insolation at 30° angle of incidence where insolation is received by the outside also

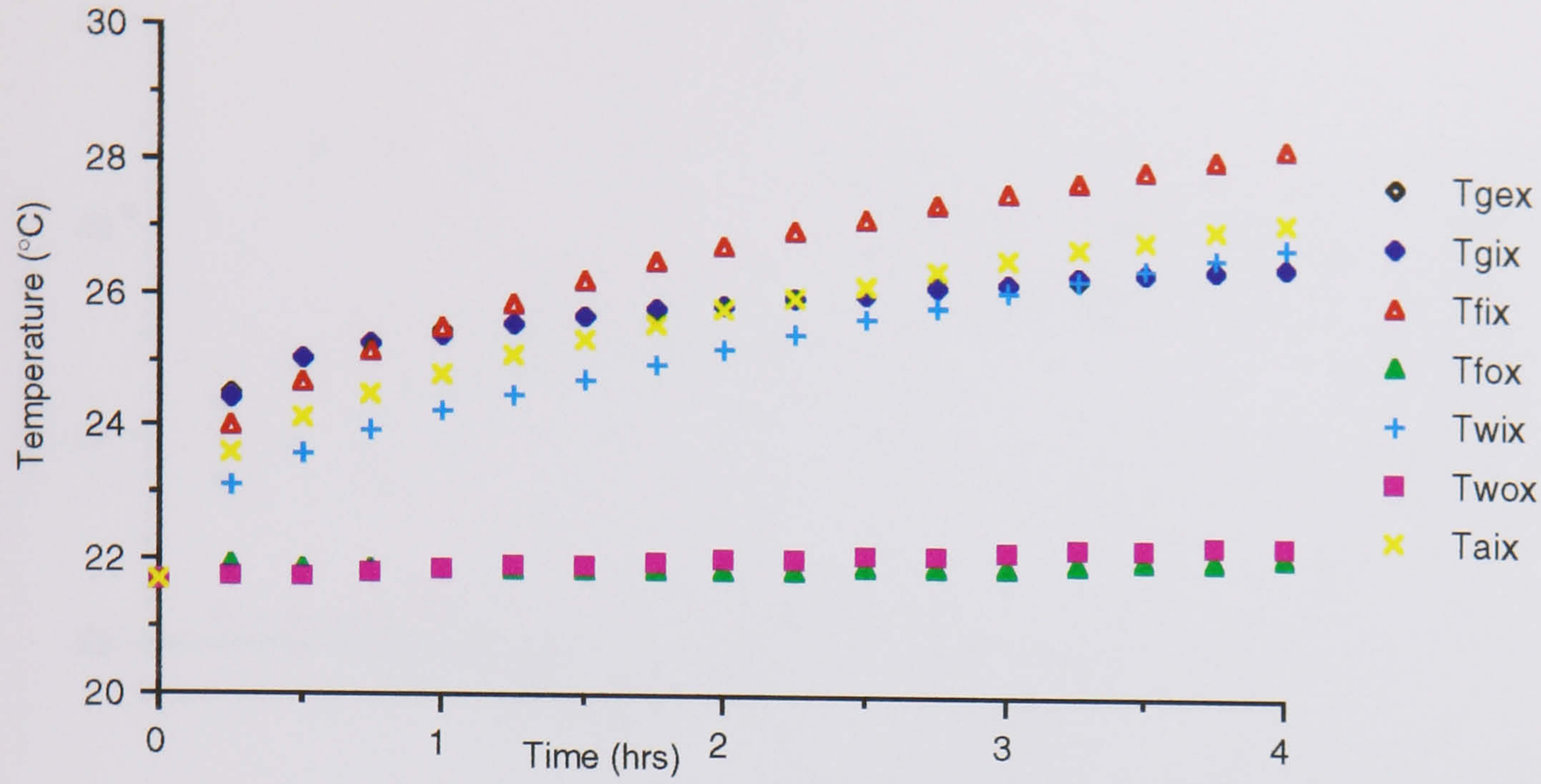

Fig 5.20 The computer model prediction of the temperature rise over 4 hours for clearfloat glass with insolation at 40° angle of incidence

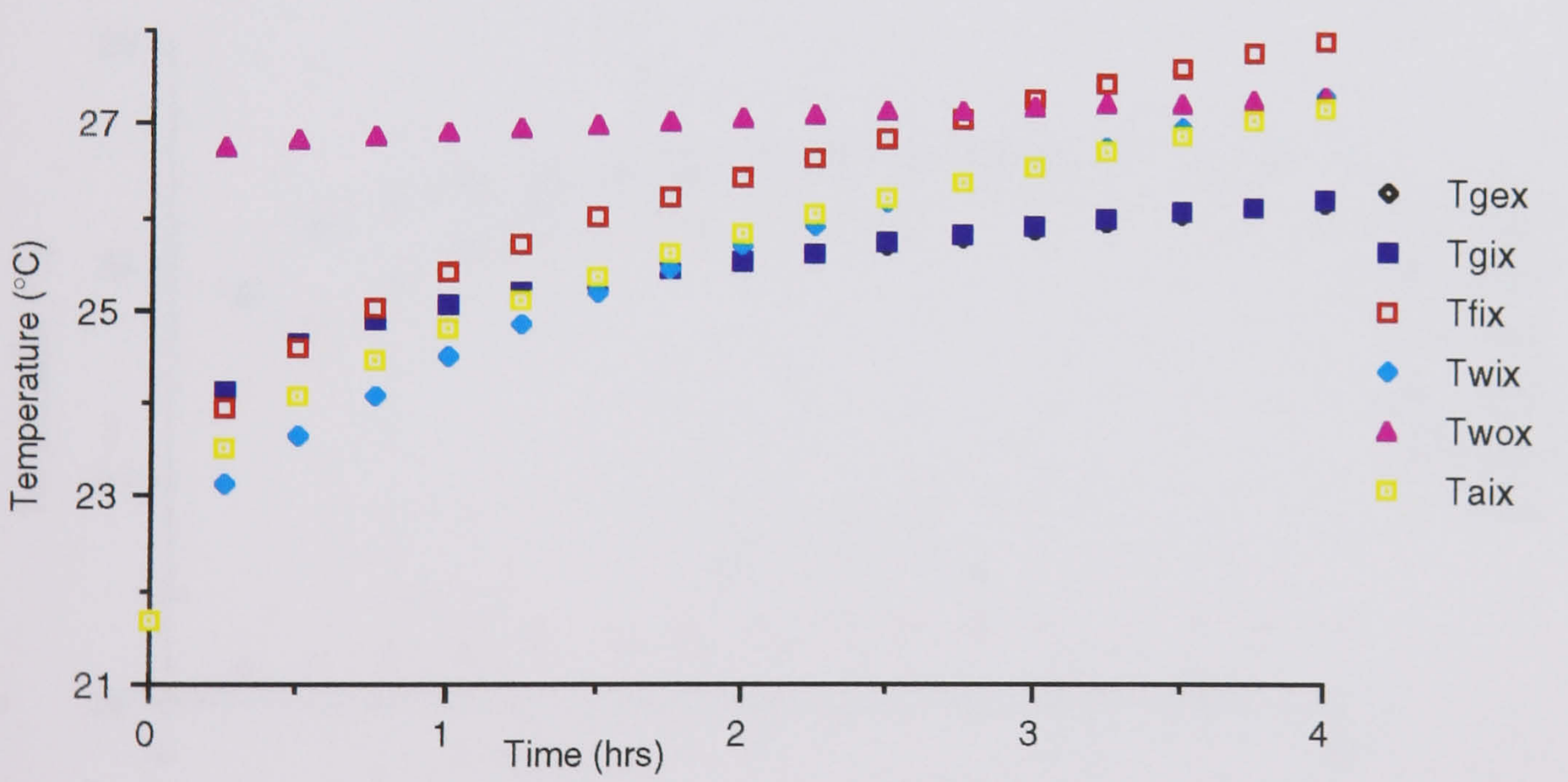

Fig 5.21 The computer model prediction of the temperature rise over 4 hours for clearfloat glass with insolation at 40° angle of incidence where insolation is received by the outside also

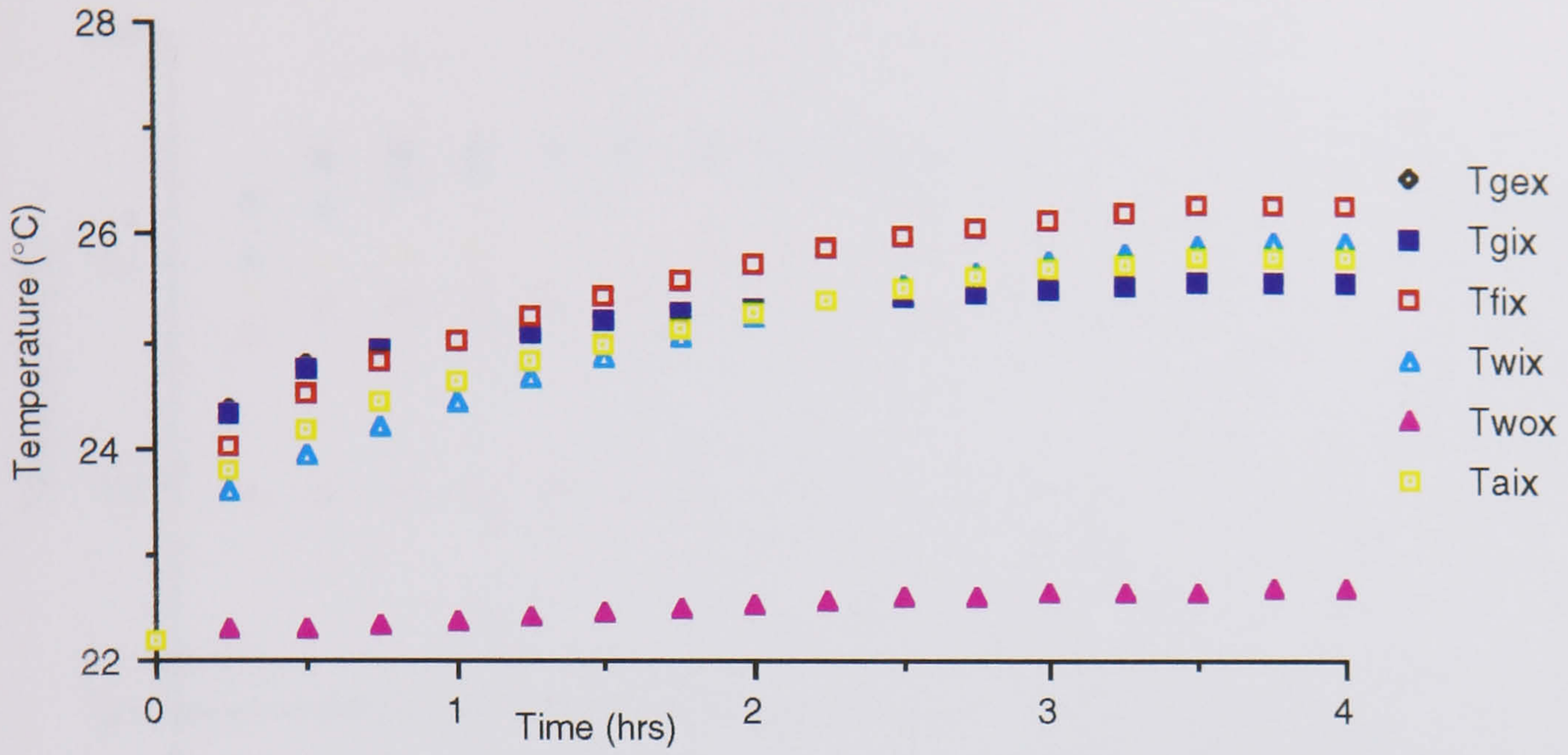

Fig 5.22 The computer model prediction of the temperature rise over 4 hours for clearfloat glass with insolation at 50° angle of incidence

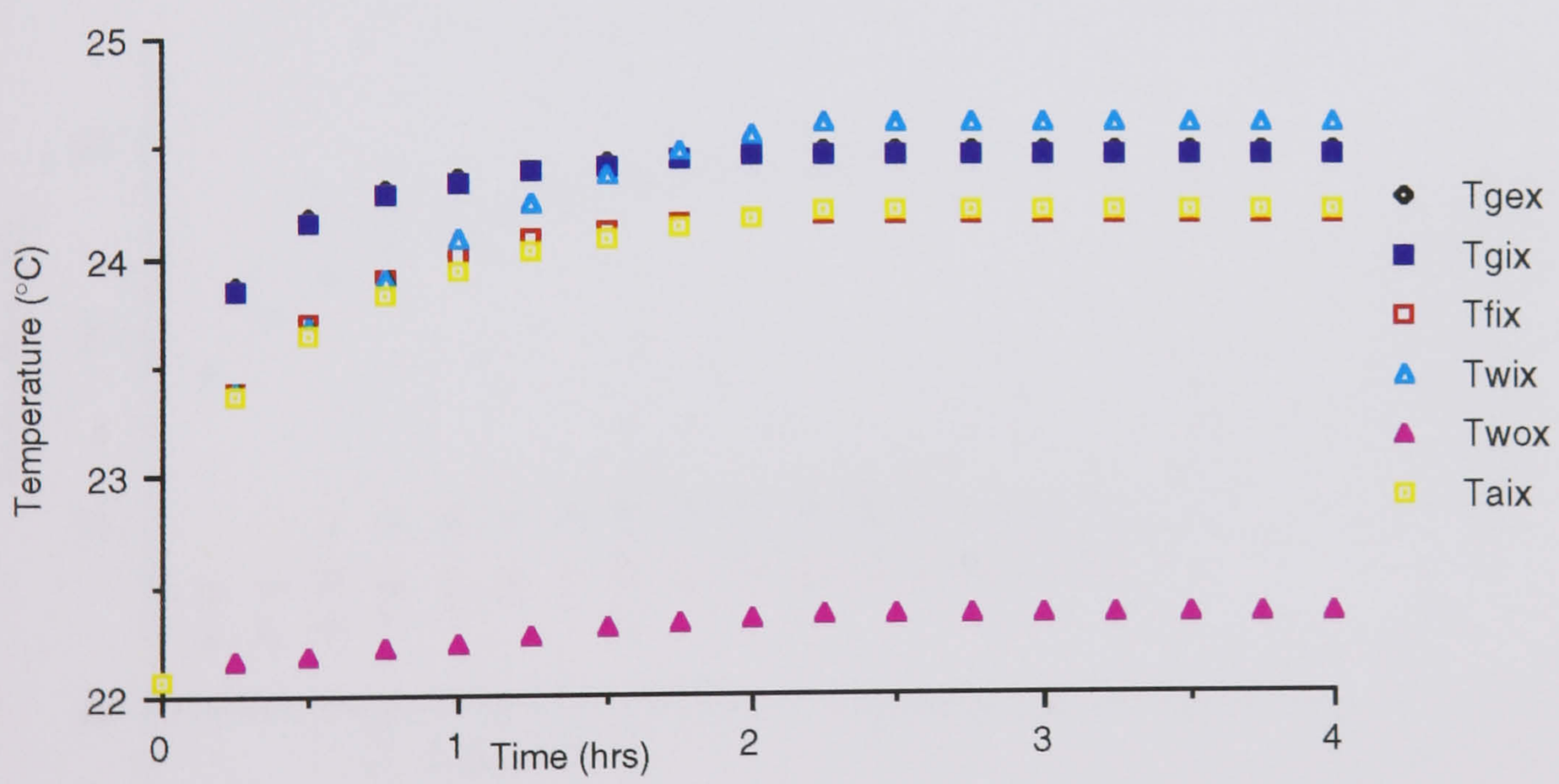

Fig 5.23 The computer model prediction of the temperature rise over 4 hours for clearfloat glass with insolation at 60° angle of incidence

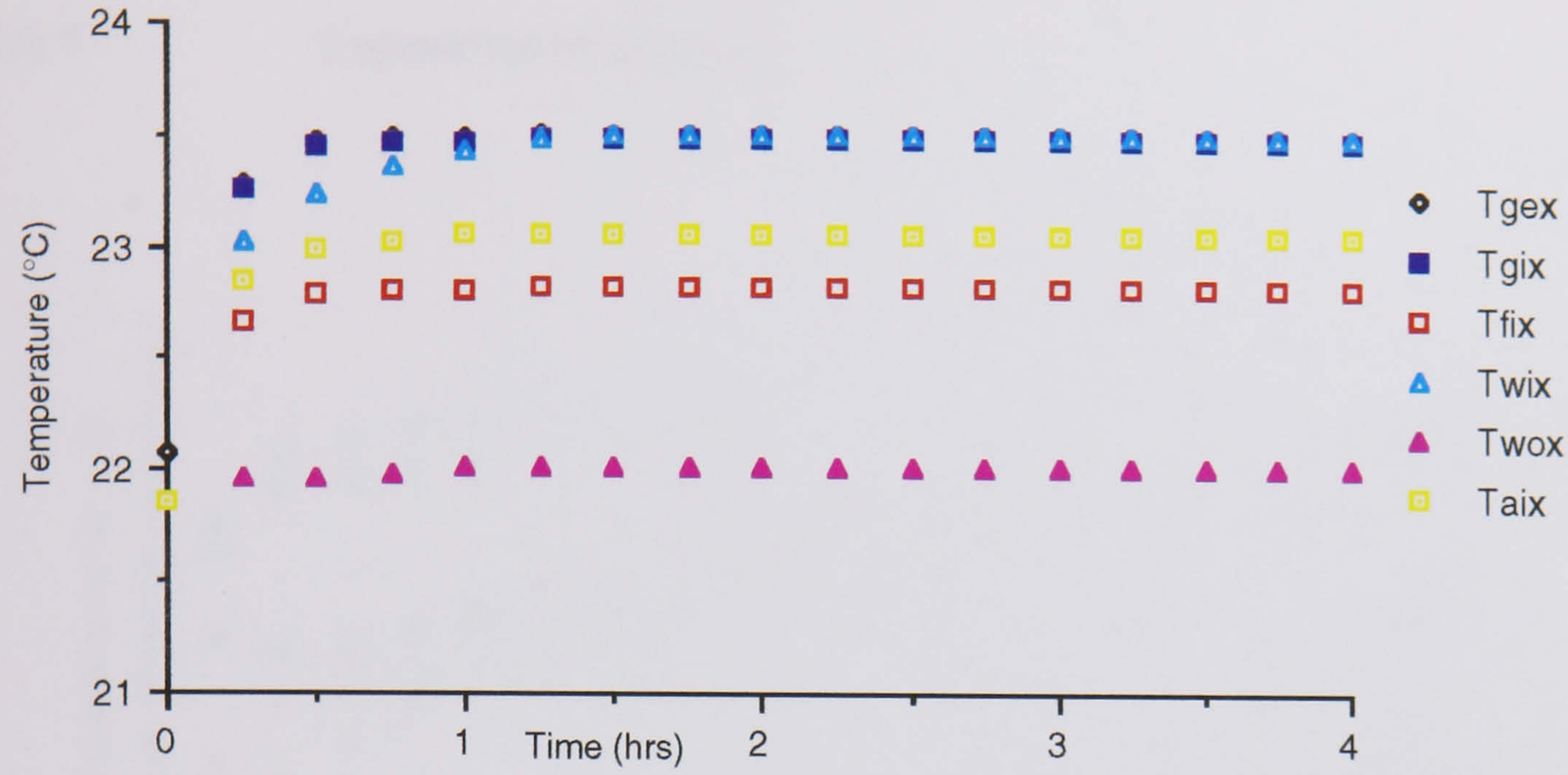

Fig 5.24 The computer model prediction of the temperature rise over 4 hours for clearfloat glass with insolation at 70° angle of incidence

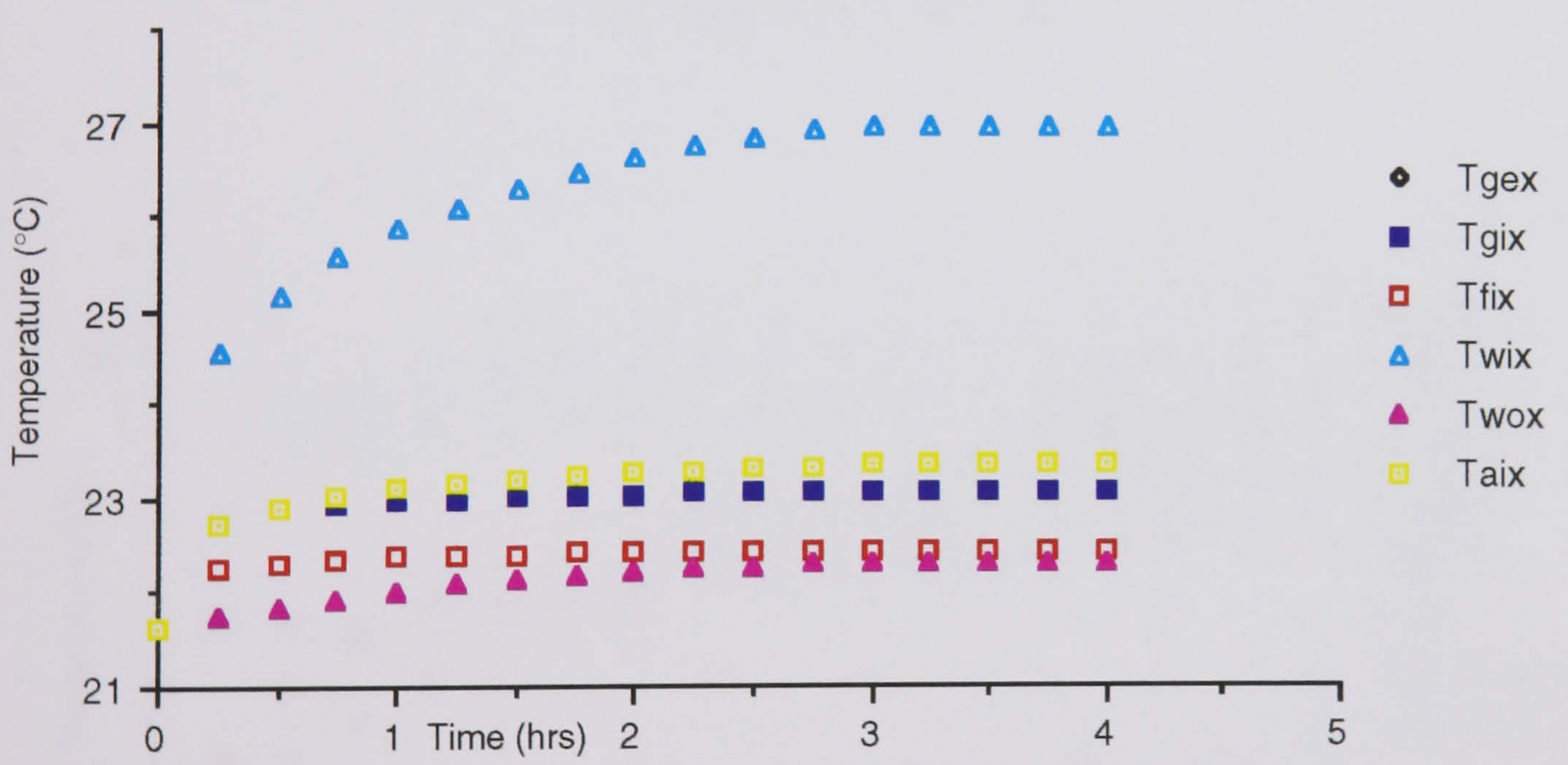

Fig 5.25 The computer model prediction of the temperature rise over 4 hours for clearfloat glass with insolation at 80° angle of incidence

5.3 Reflective Films Results

5.3.1 Experimental Results

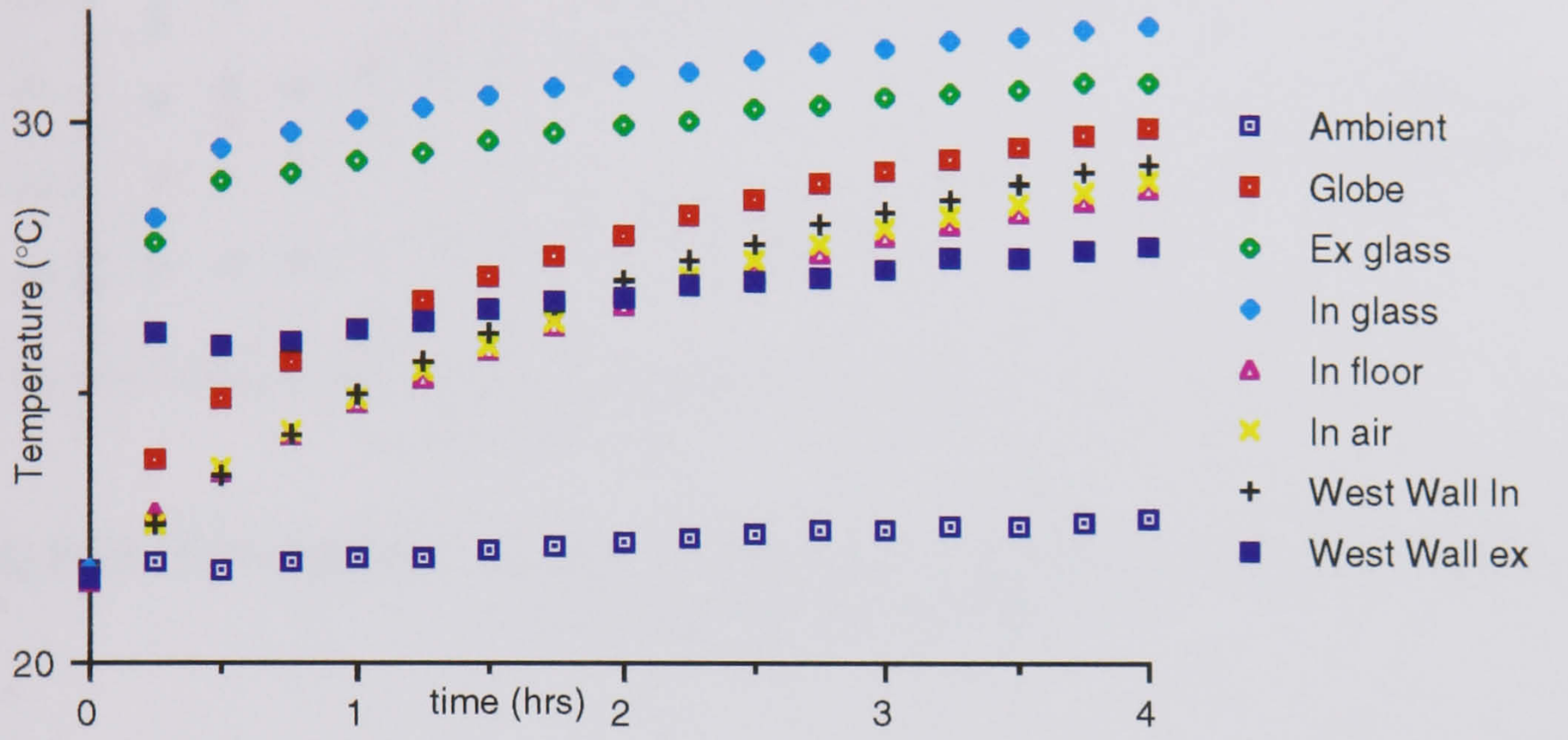

Fig 5.26 Temperature Rise over 4 hours for a reflective film with insolation at 0° angle of incidence

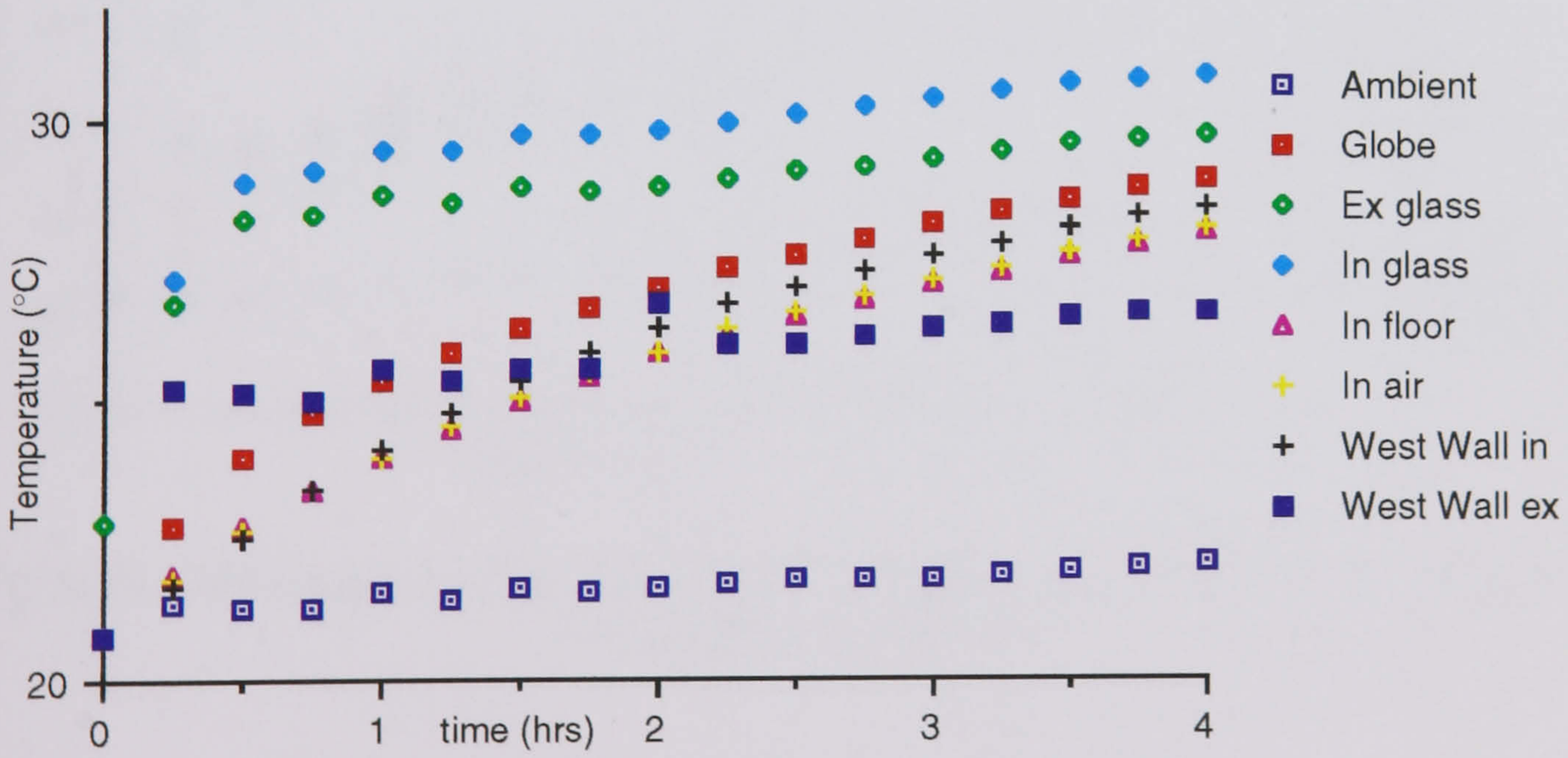

Fig 5.27 Temperature Rise over 4 hours for a reflective film with insolation at 10° angle of incidence

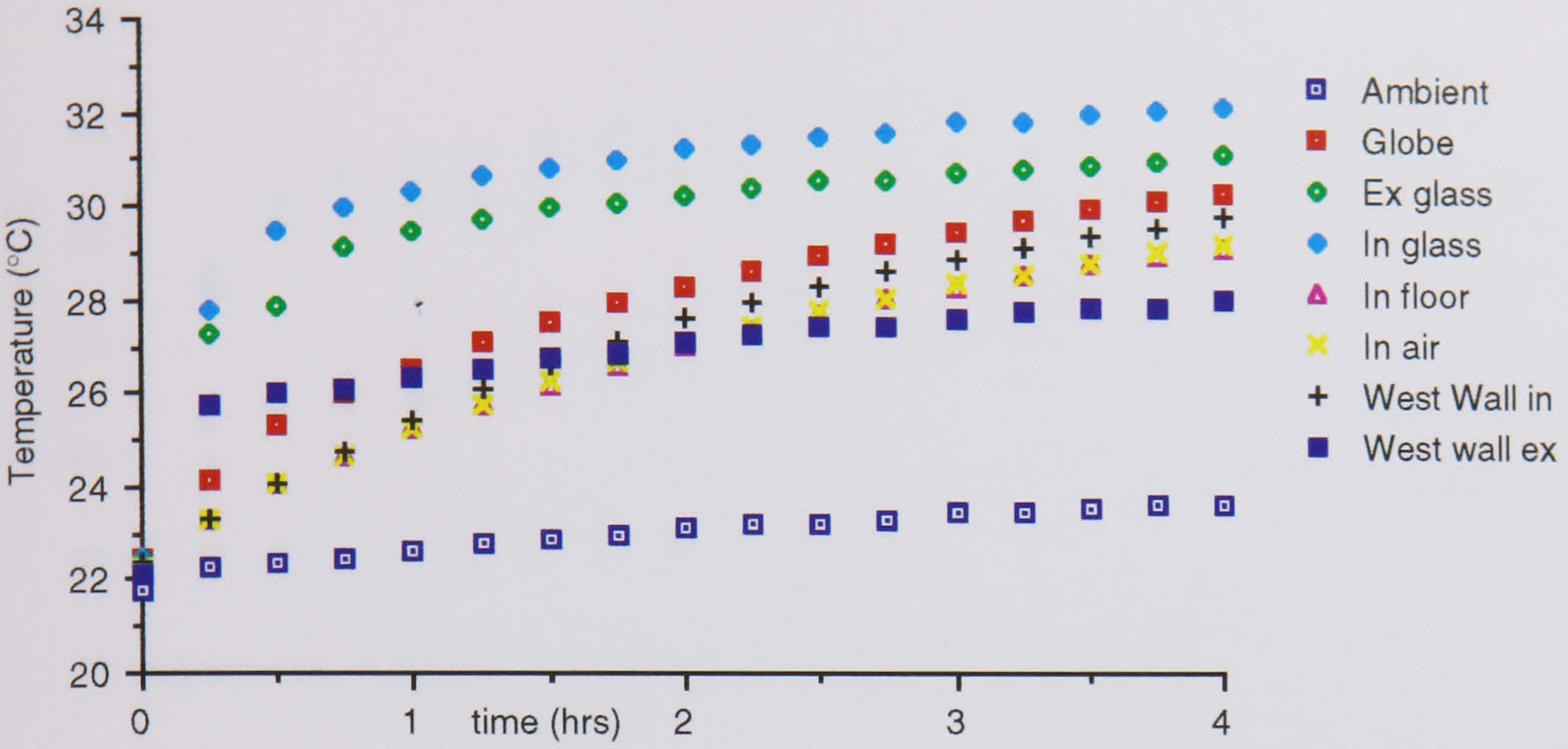

Fig 5.28 Temperature rise over 4 hours for a reflective film with insolation at 20° angle of incidence

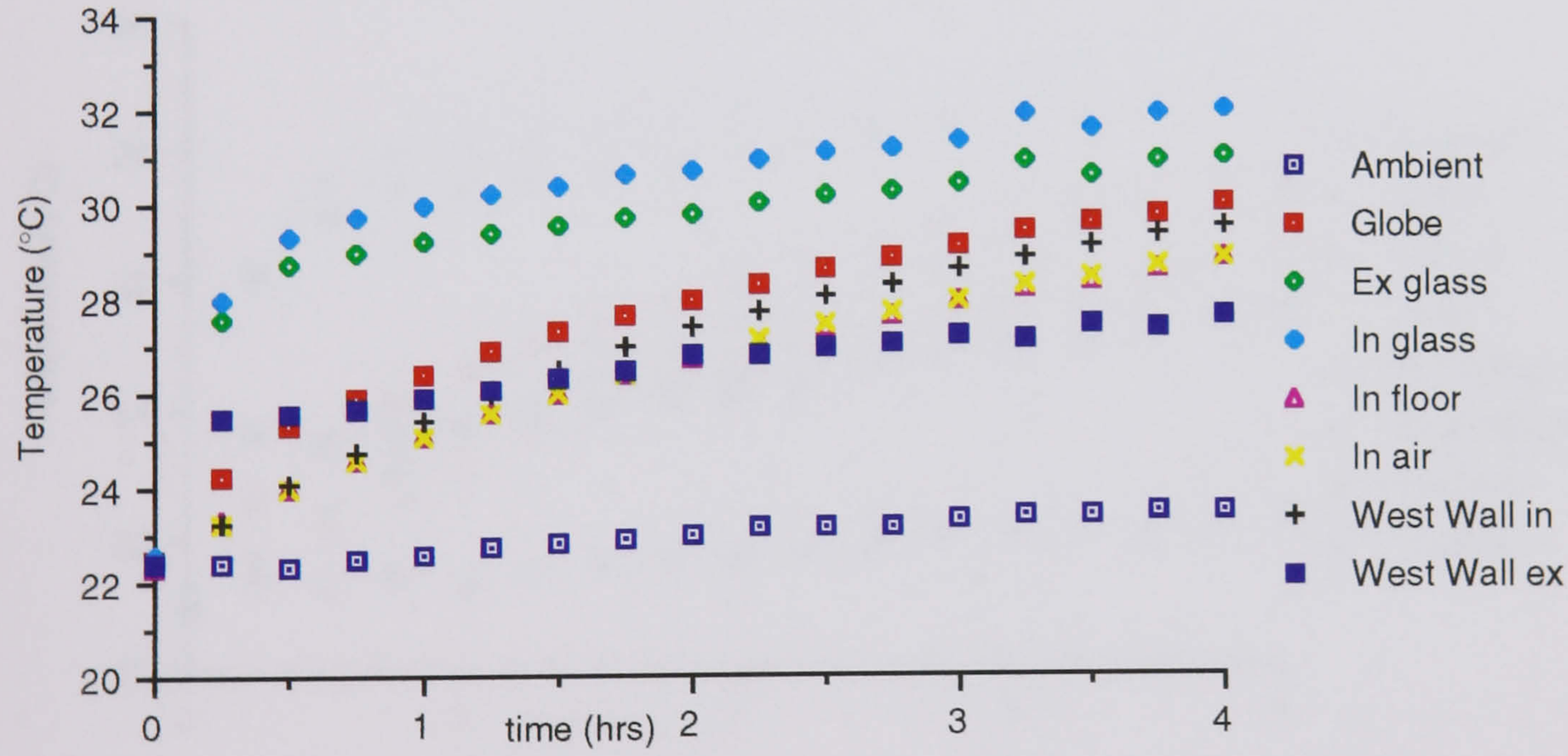

Fig 5.29 Temperature rise over 4 hours for a reflective film with insolation at 30° angle of incidence

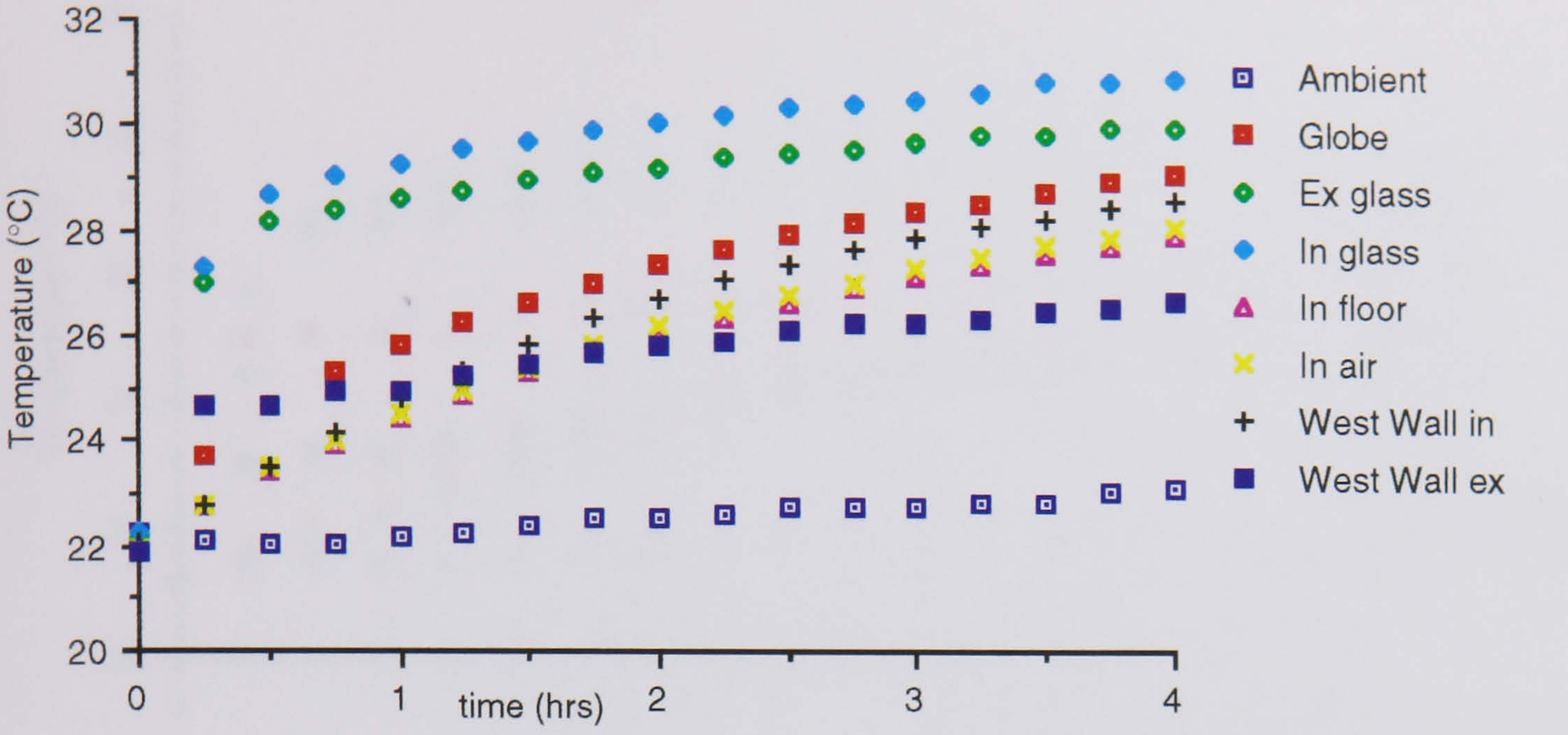

Fig 5.30 Temperature rise over 4 hours for a reflective film with insolation at 40° angle of incidence

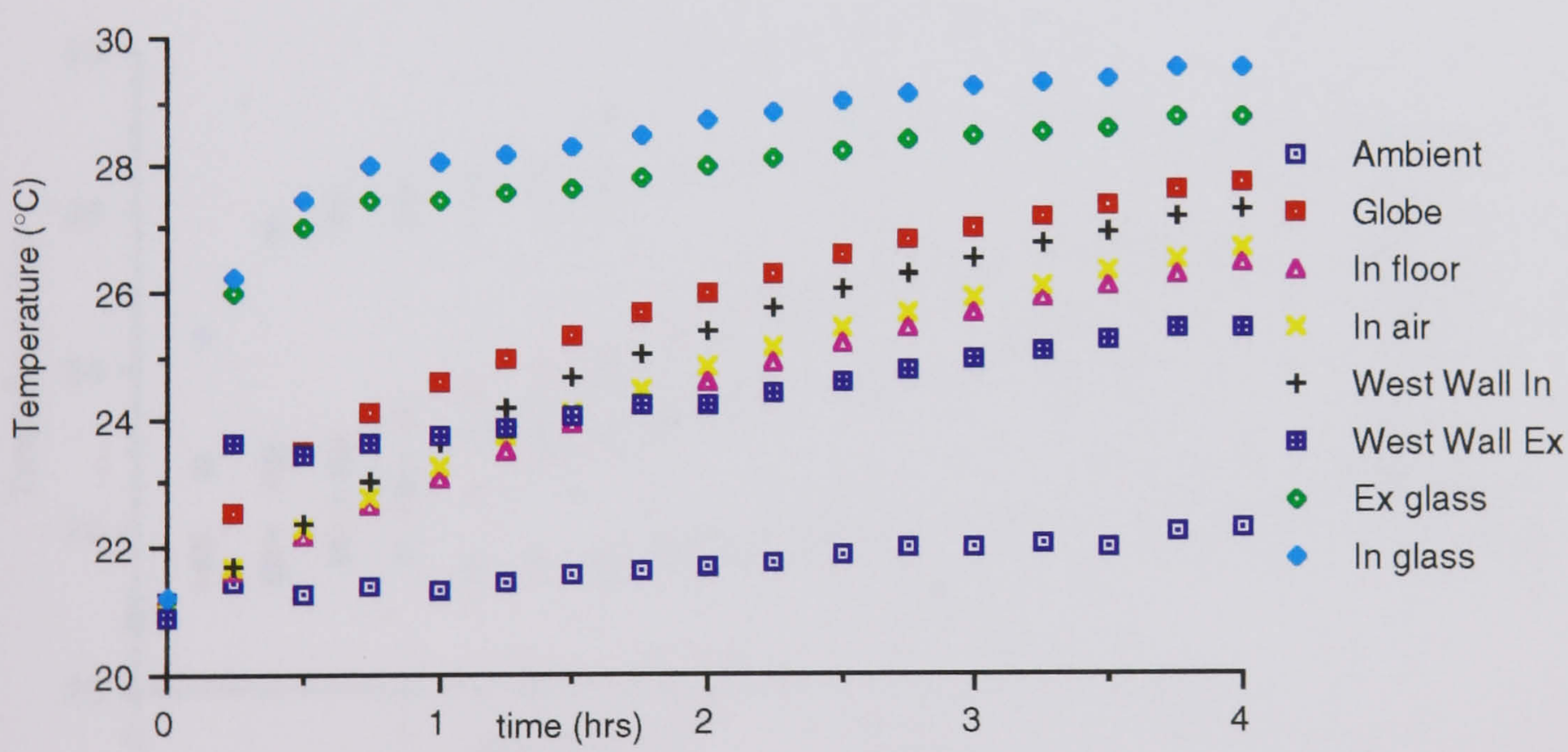

Fig 5.31 Temperature rise over 4 hours for a reflective film with insolation at 50° angle of incidence

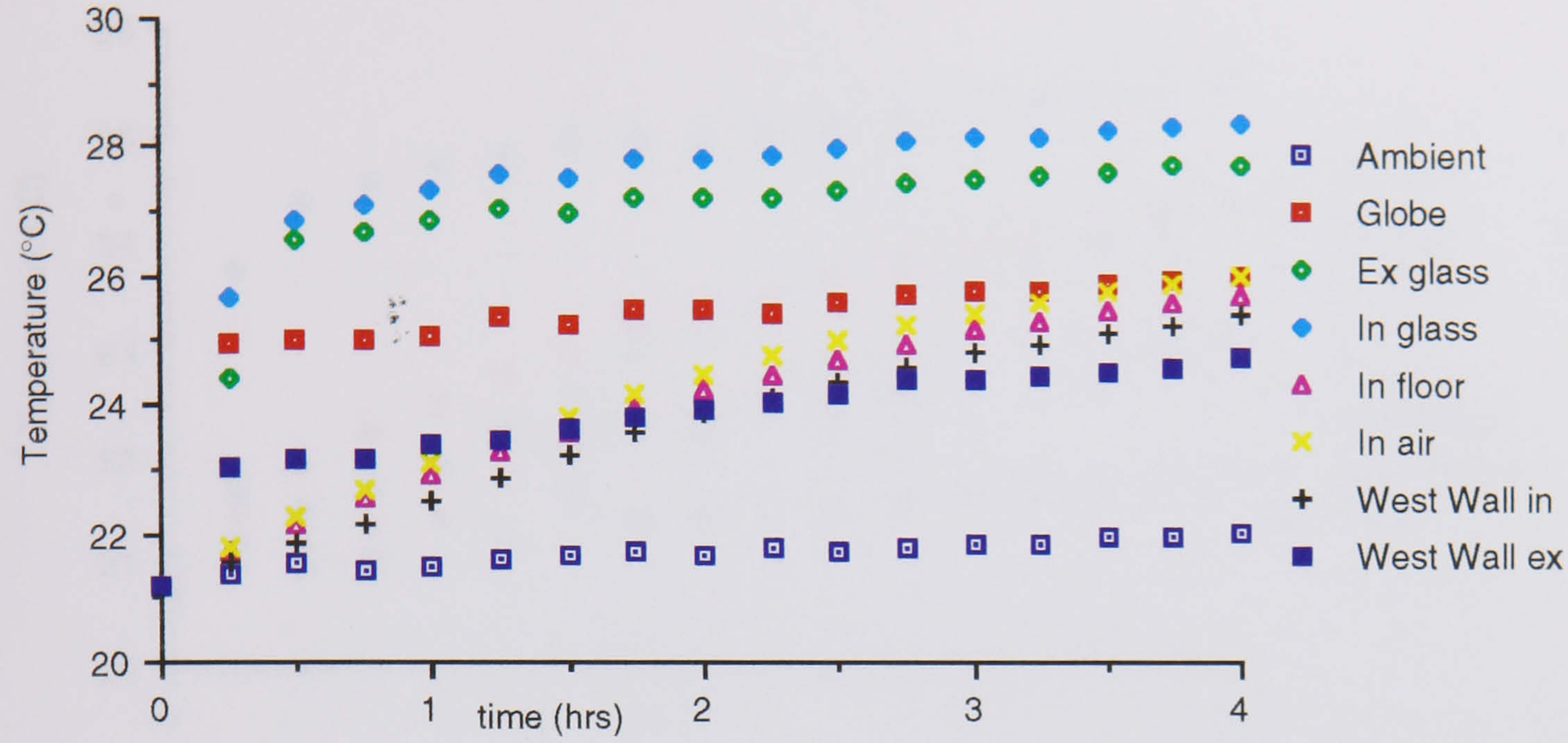

Fig 5.32 Temperature rise over 4 hours for a reflective film with insolation at 60° angle of incidence

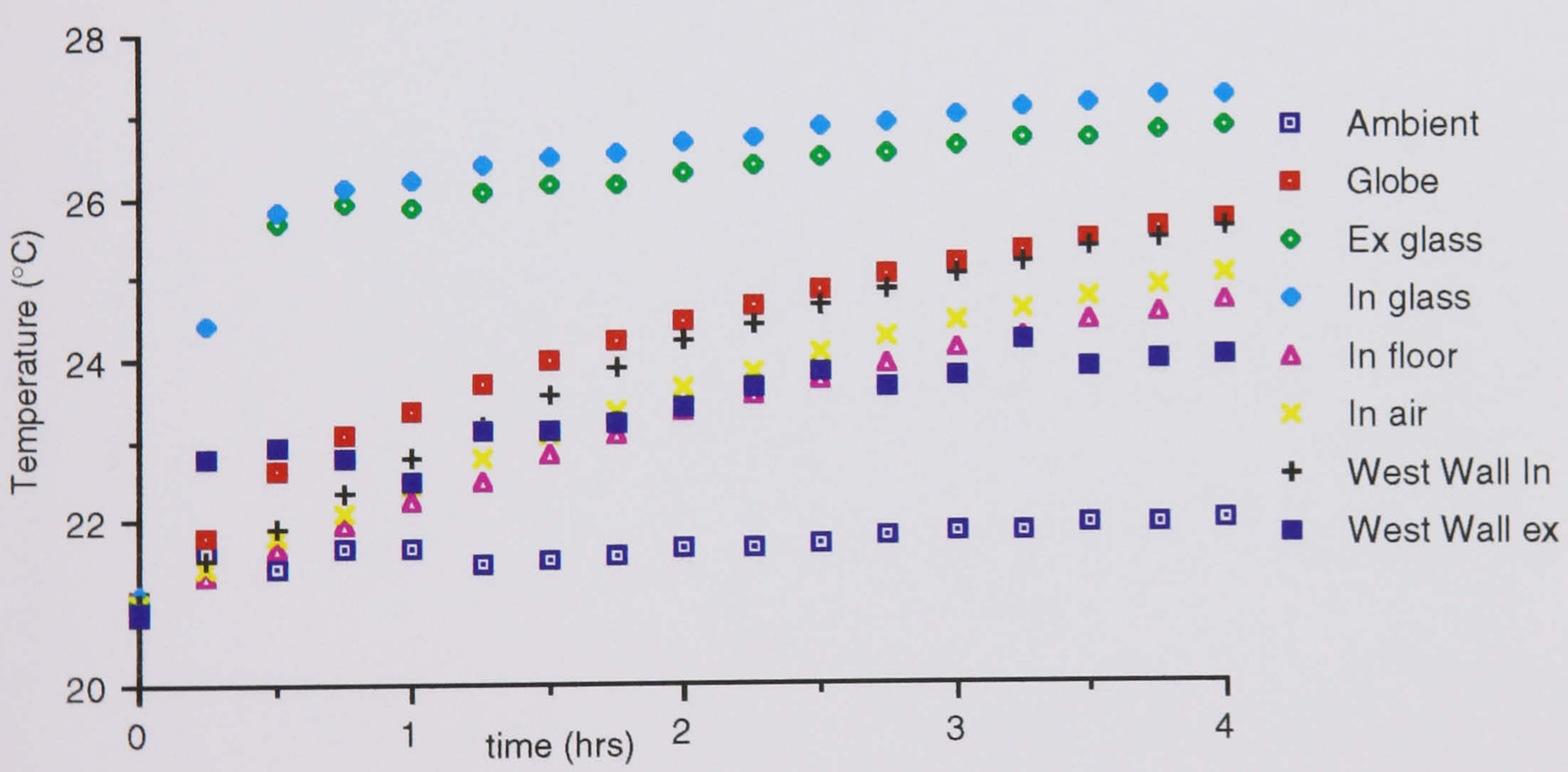

Fig 5.33 Temperature rise over 4 hours for a reflective film with insolation at 70° angle of incidence

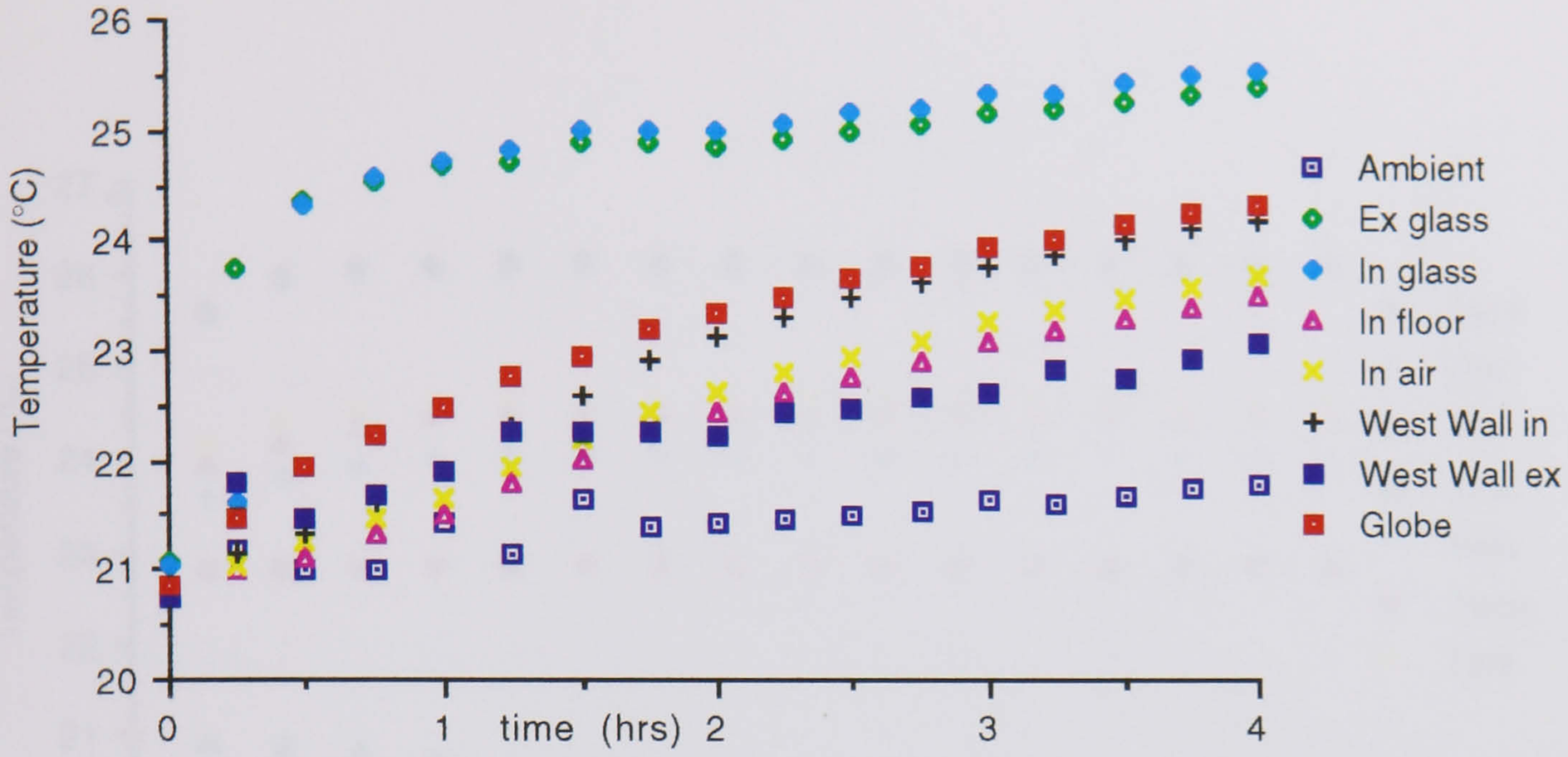

Fig 5.34 Temperature rise over 4 hours for a reflective film with insolation at 80° angle of incidence

5.3.2 Computer Modelling Results

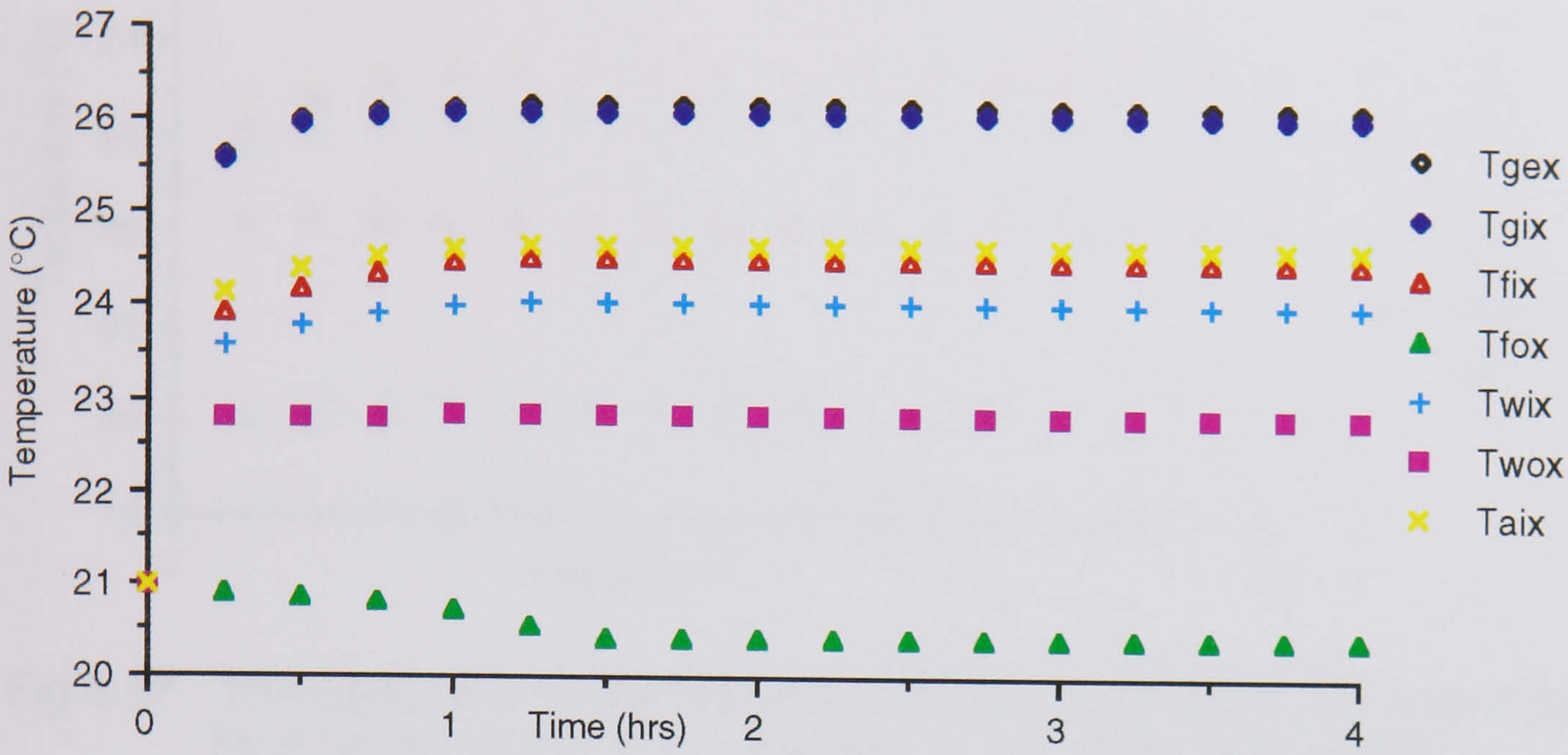

Fig 5.35 The computer model prediction of the temperature rise over 4 hours for a reflective film with insolation at 0° angle of incidence

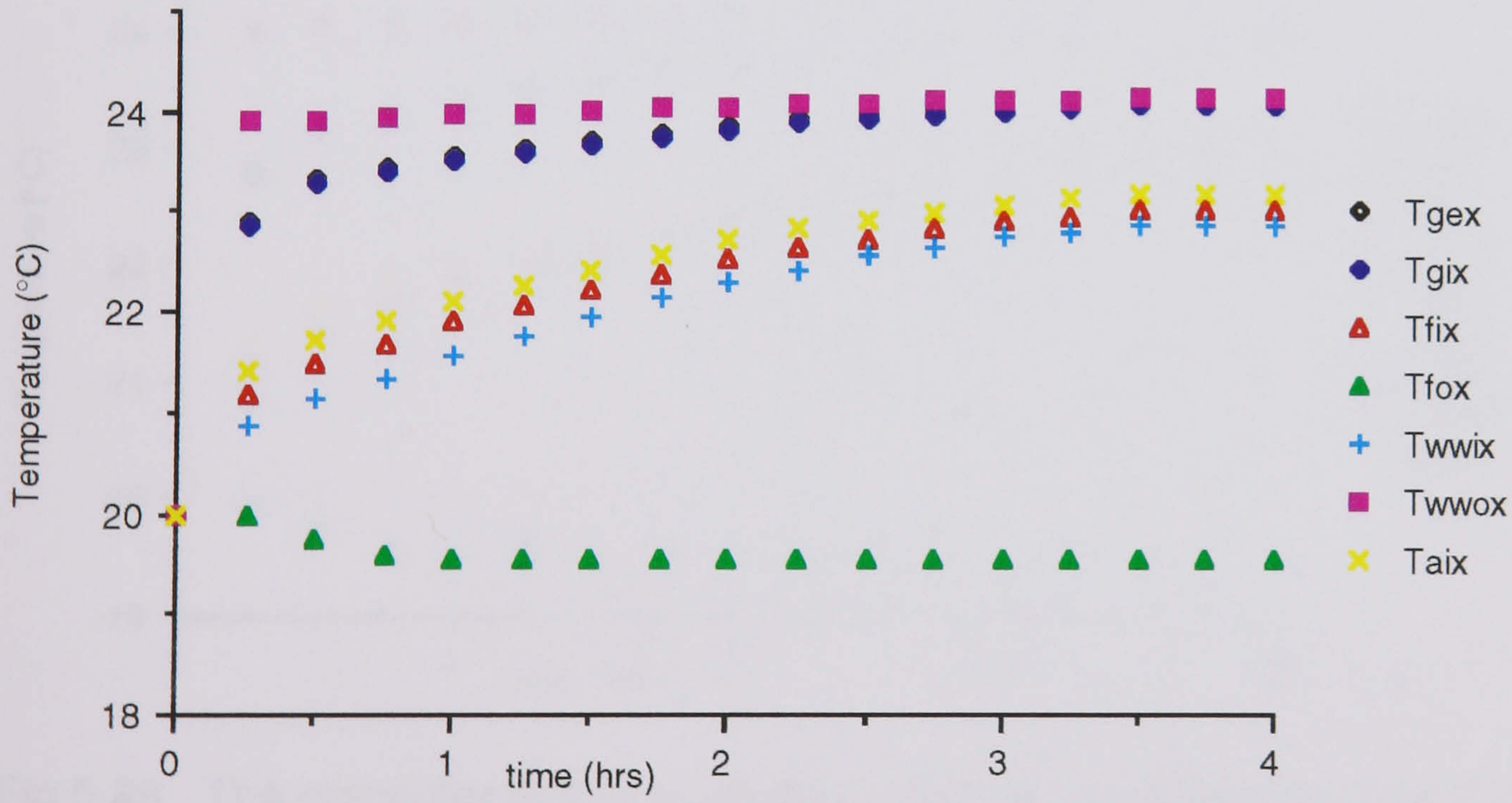

Fig 5.36 The computer model prediction of the temperature rise over 4 hours for a reflective film with insolation at 0° angle of incidence where insolation is received by the outside also

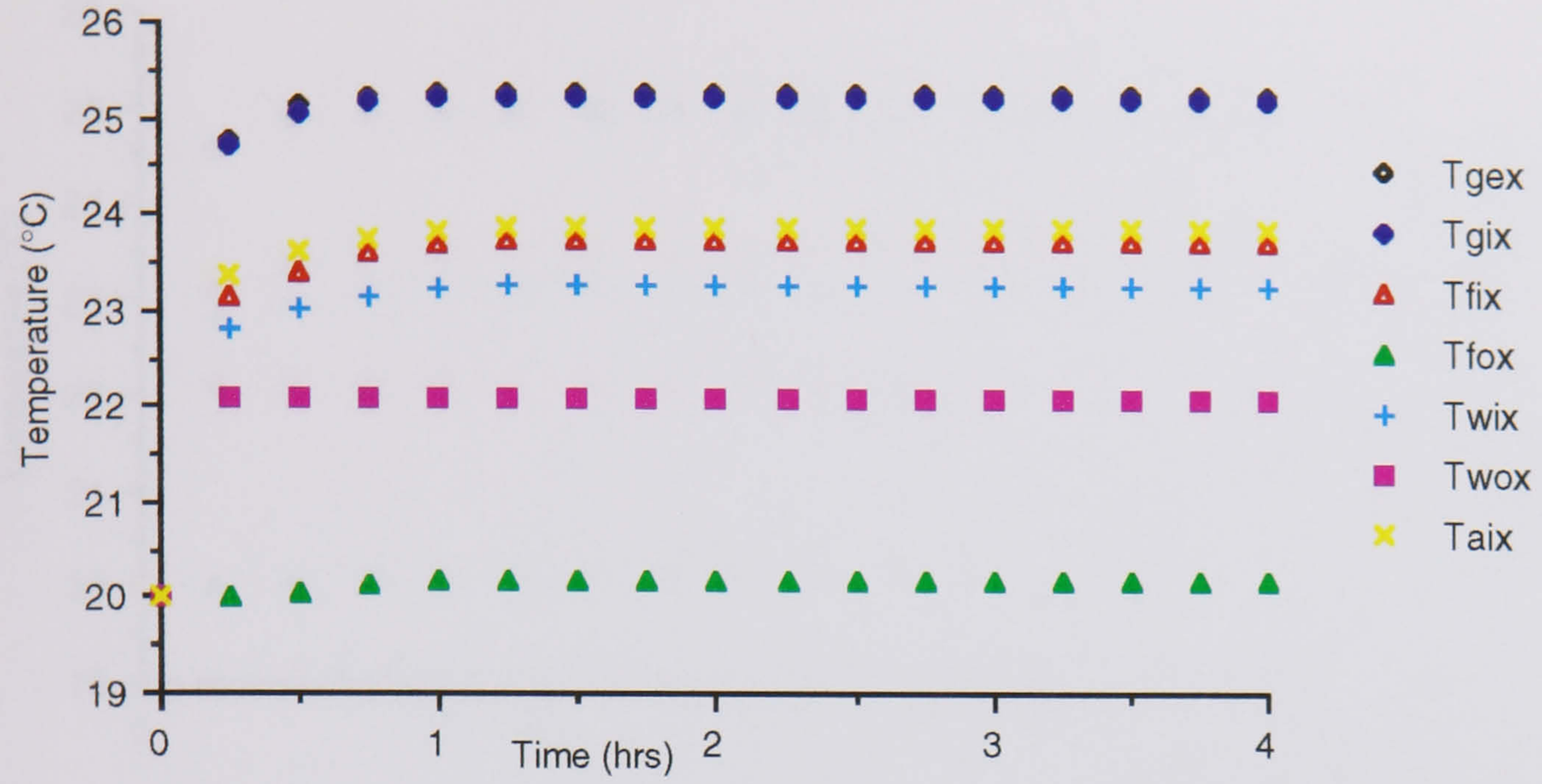

Fig 5.37 The computer model prediction of the temperature rise over 4 hours for a reflective film with insolation at 10° angle of incidence

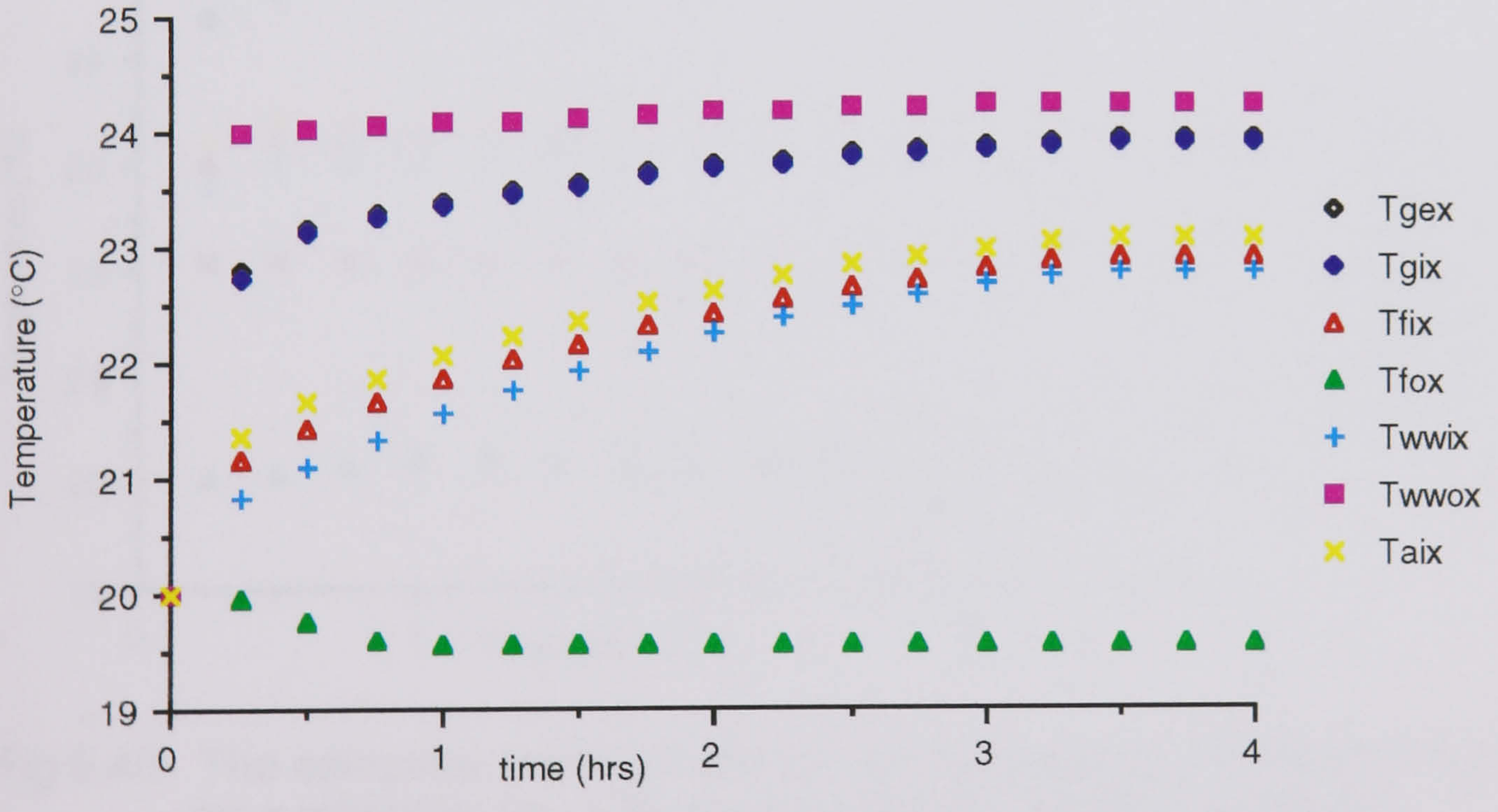

Fig 5.38 The computer model prediction of the temperature rise over 4 hours for a reflective film with insolation at 10° angle of incidence where insolation is received by the outside also

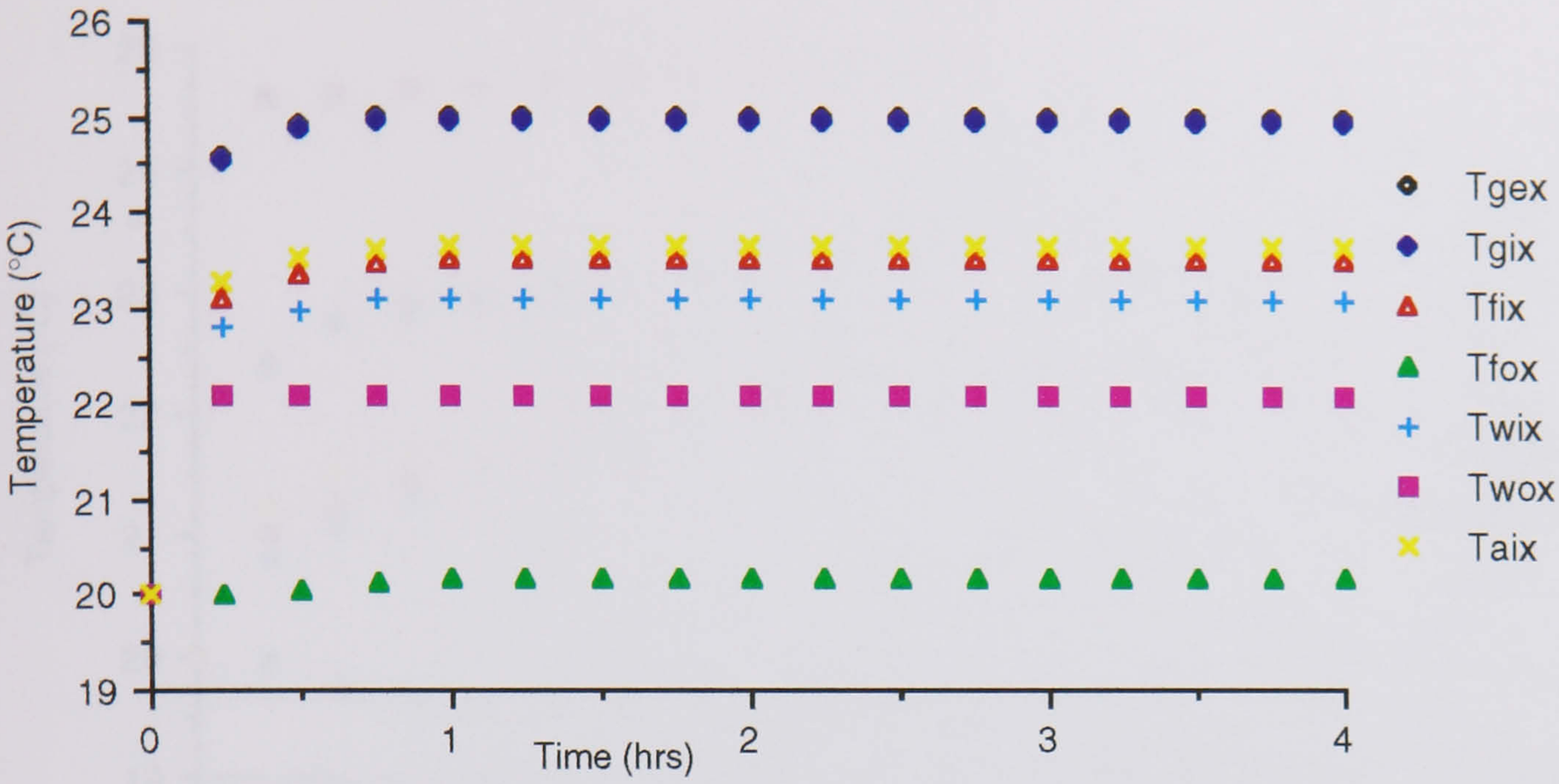

Fig 5.39 The computer model prediction of the temperature rise over 4 hours for a reflective film with insolation at 20° angle of incidence

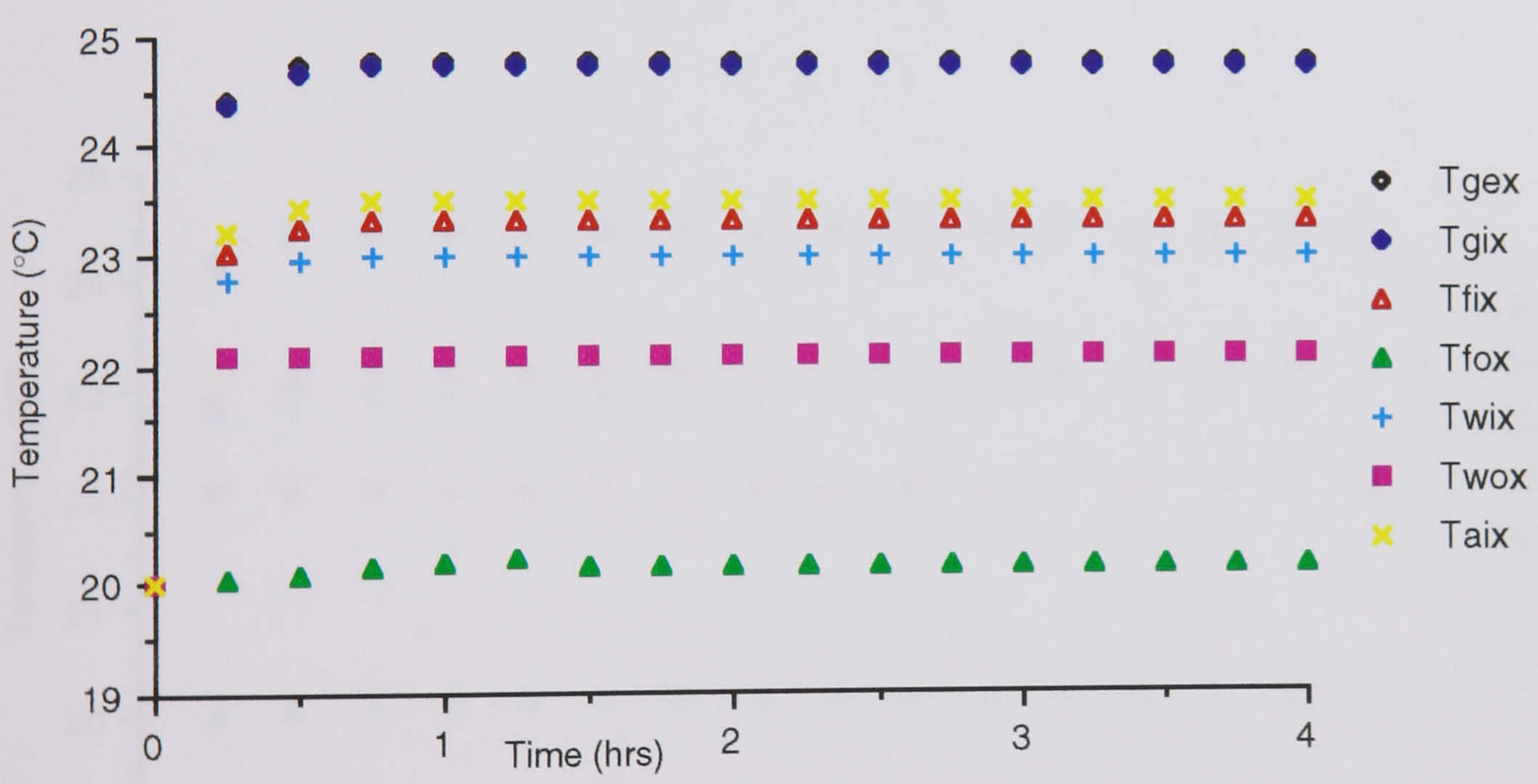

Fig 5.40 The computer model prediction of the temperature rise over 4 hours for a reflective film with insolation at 30° angle of incidence

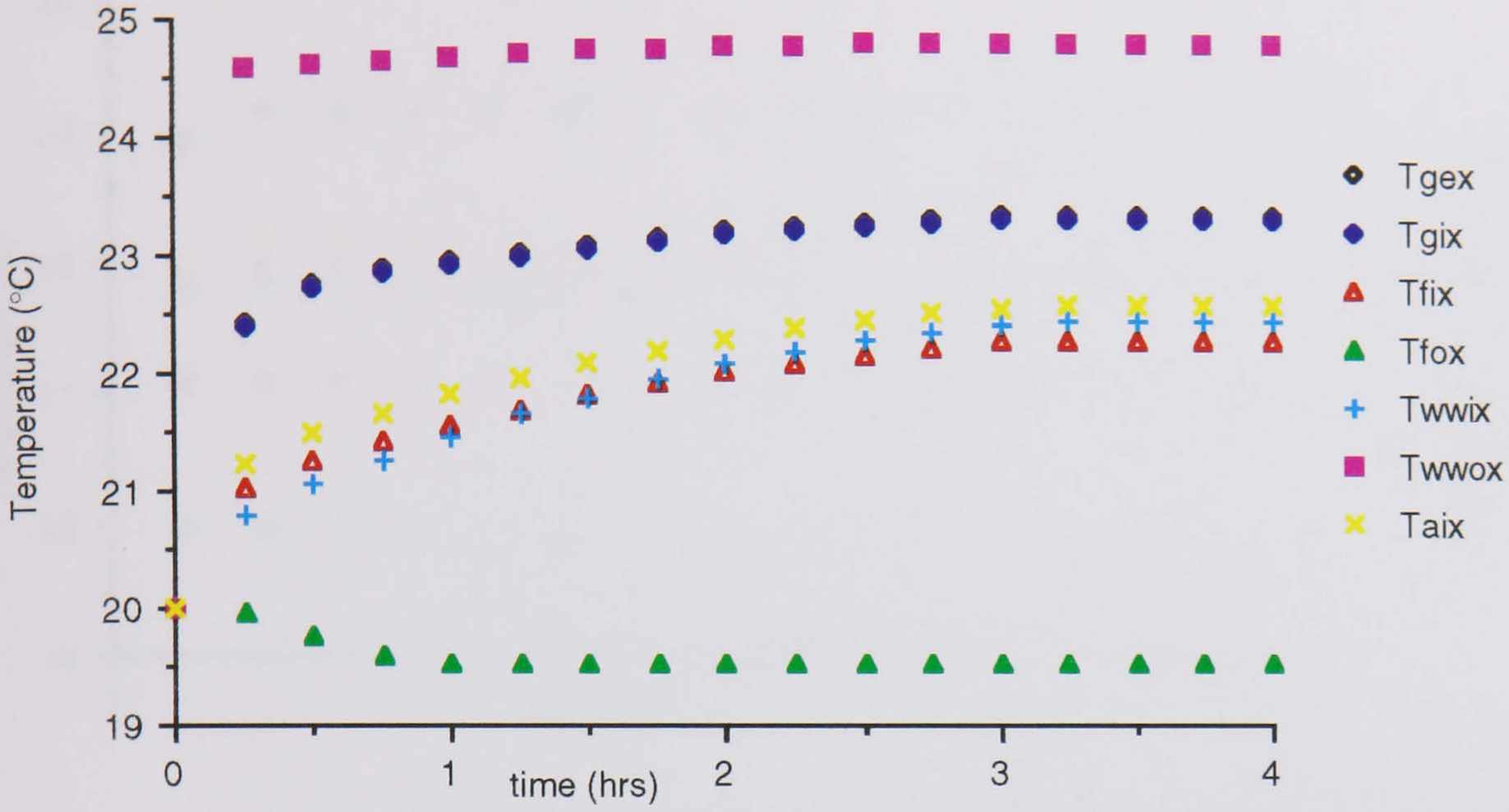

Fig 5.41 The computer model prediction of the temperature rise over 4 hours for a reflective film with insolation at 30° angle of incidence where insolation is received by the outside also

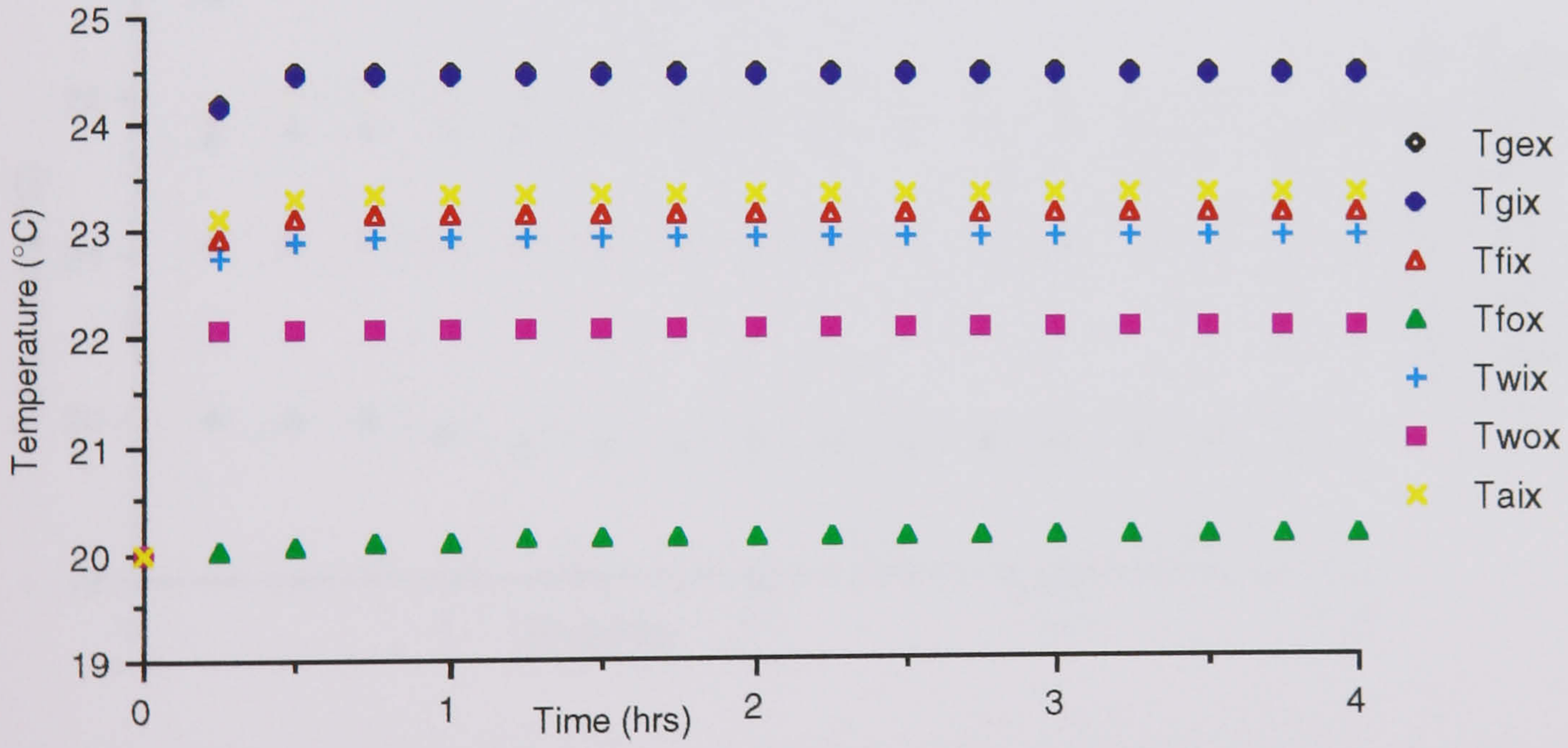

Fig 5.42 The computer model prediction of the temperature rise over 4 hours for a reflective film with insolation at 40° angle of incidence

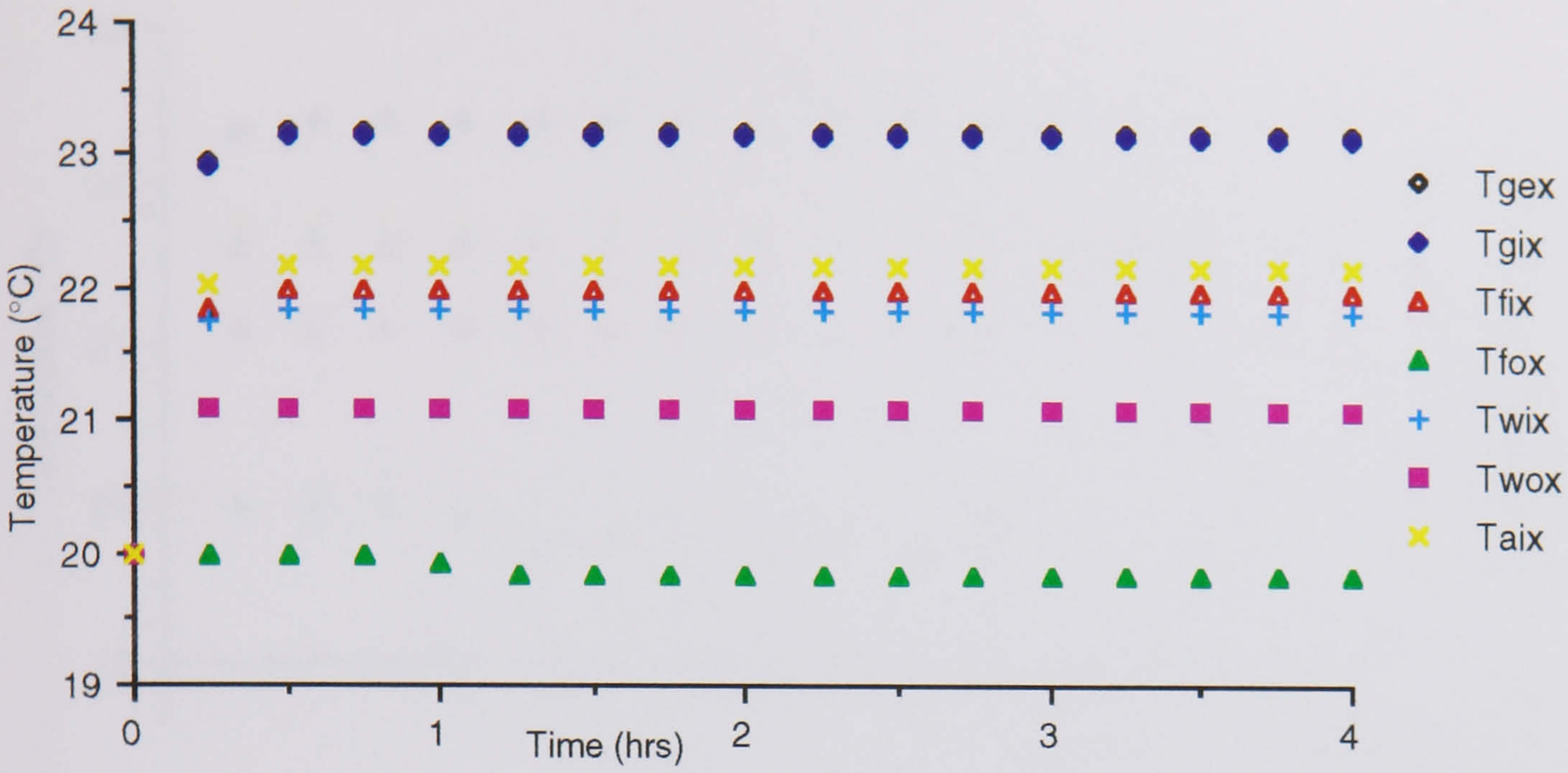

Fig 5.43 The computer model prediction of the temperature rise over 4 hours for a reflective film with insolation at 50° angle of incidence

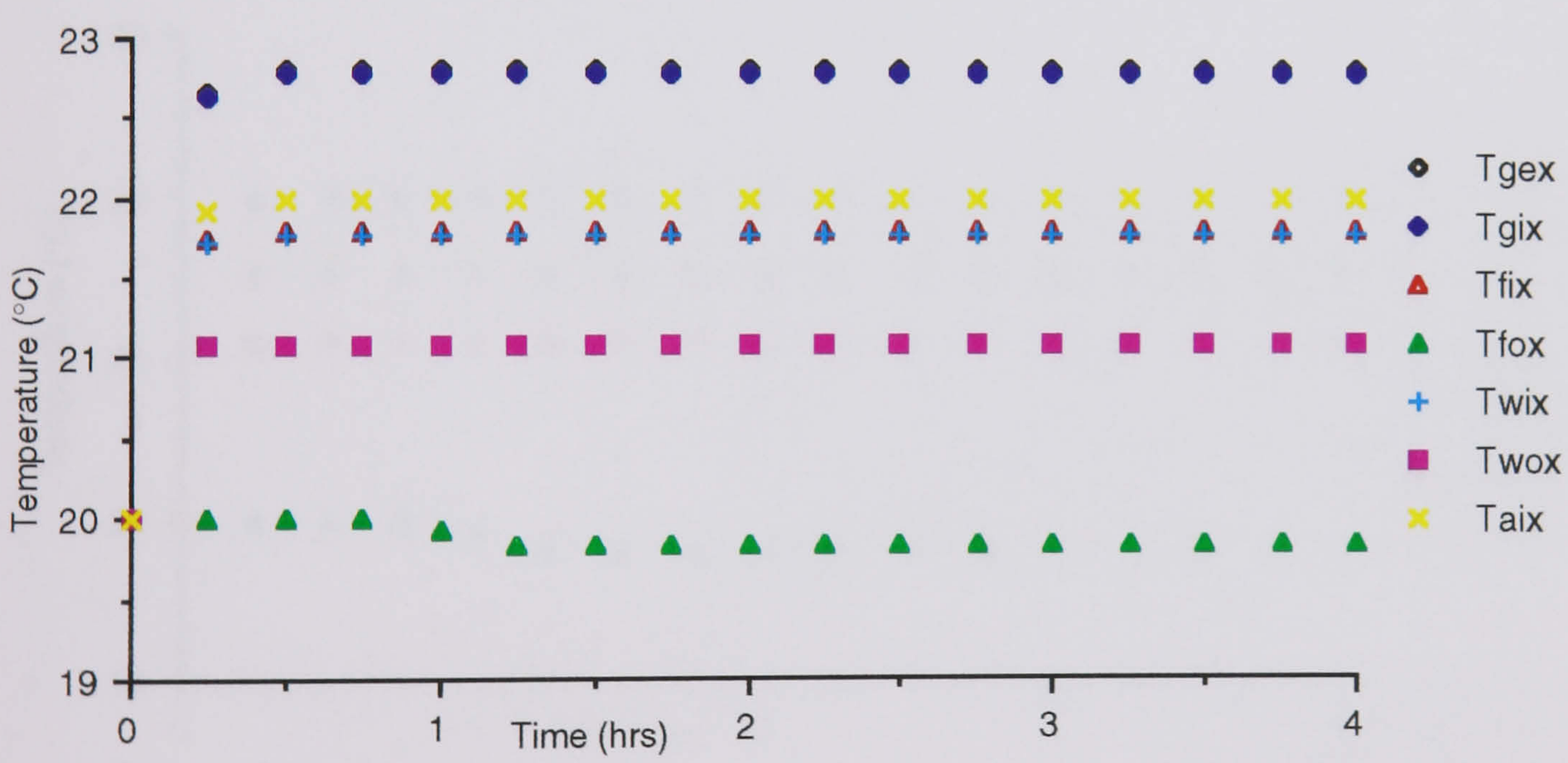

Fig 5.44 The computer model prediction of the temperature rise over 4 hours for a reflective film with insolation at 60° angle of incidence

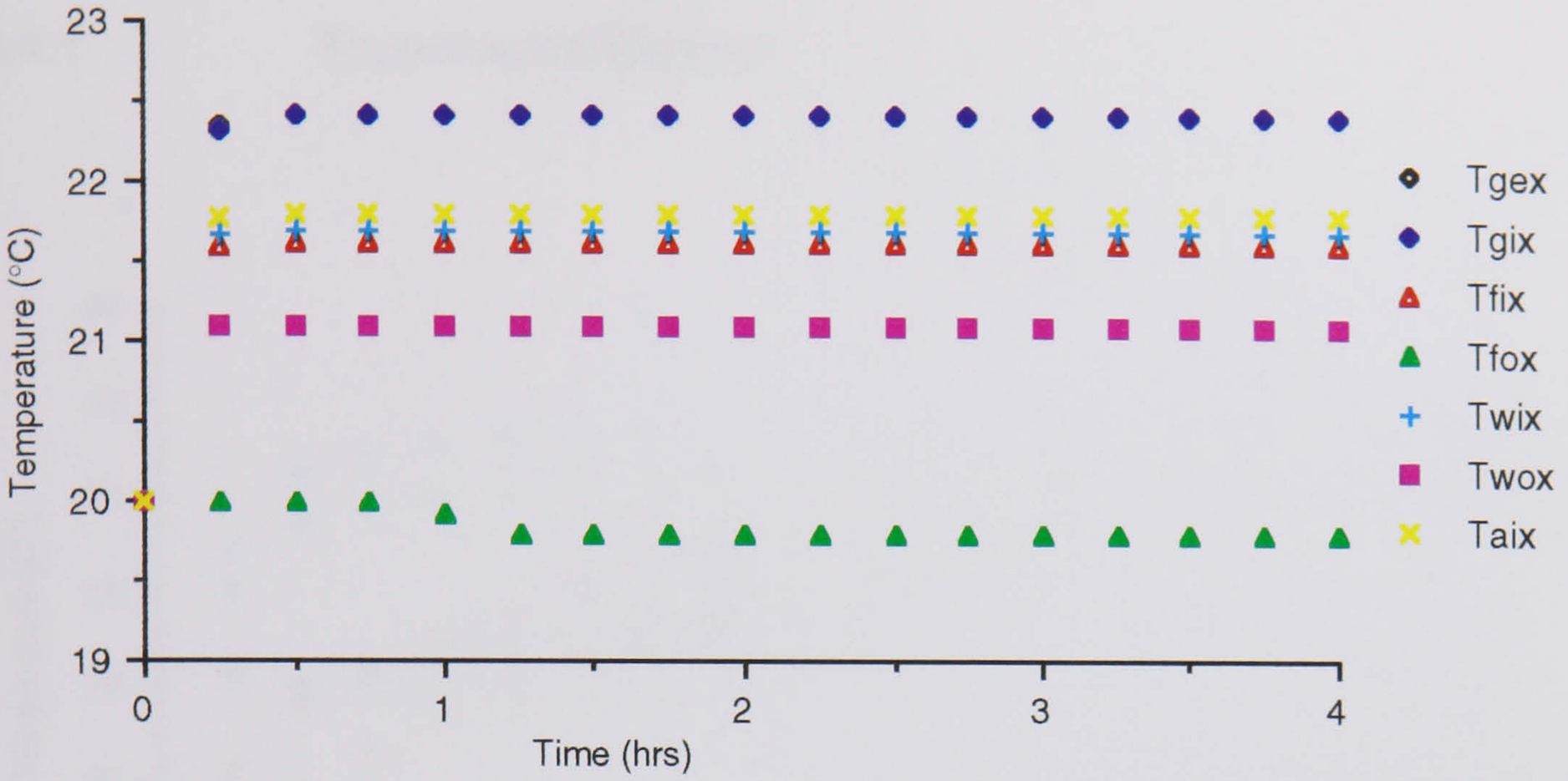

Fig 5.45 The computer model prediction of the temperature rise over 4 hours for a reflective film with insolation at 70° angle of incidence

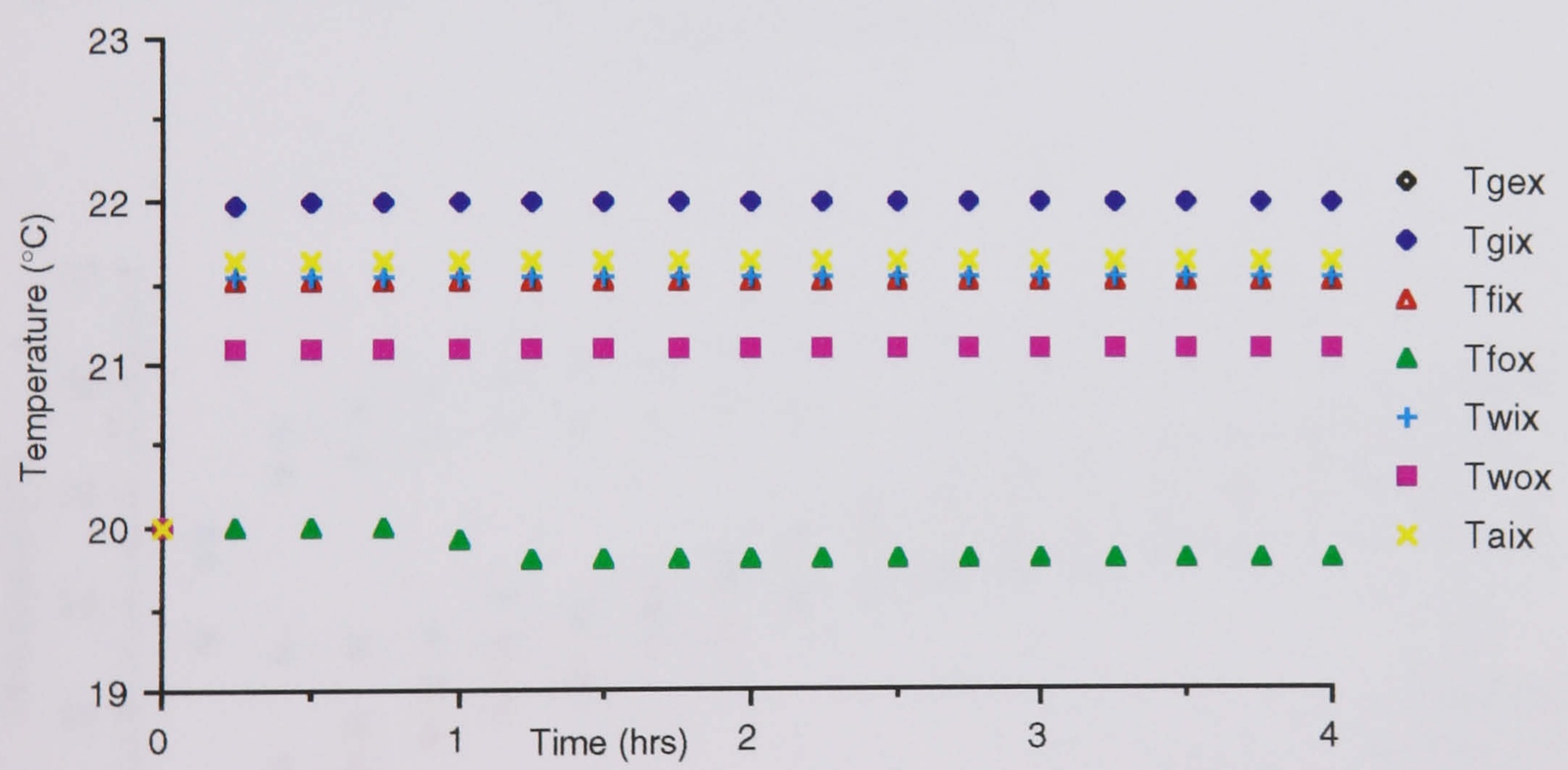

Fig 5.46 The computer model prediction of the temperature rise over 4 hours for a reflective film with insolation at 80° angle of incidence

5.4 Insulating Films Results

5.4.1 Experimental Results

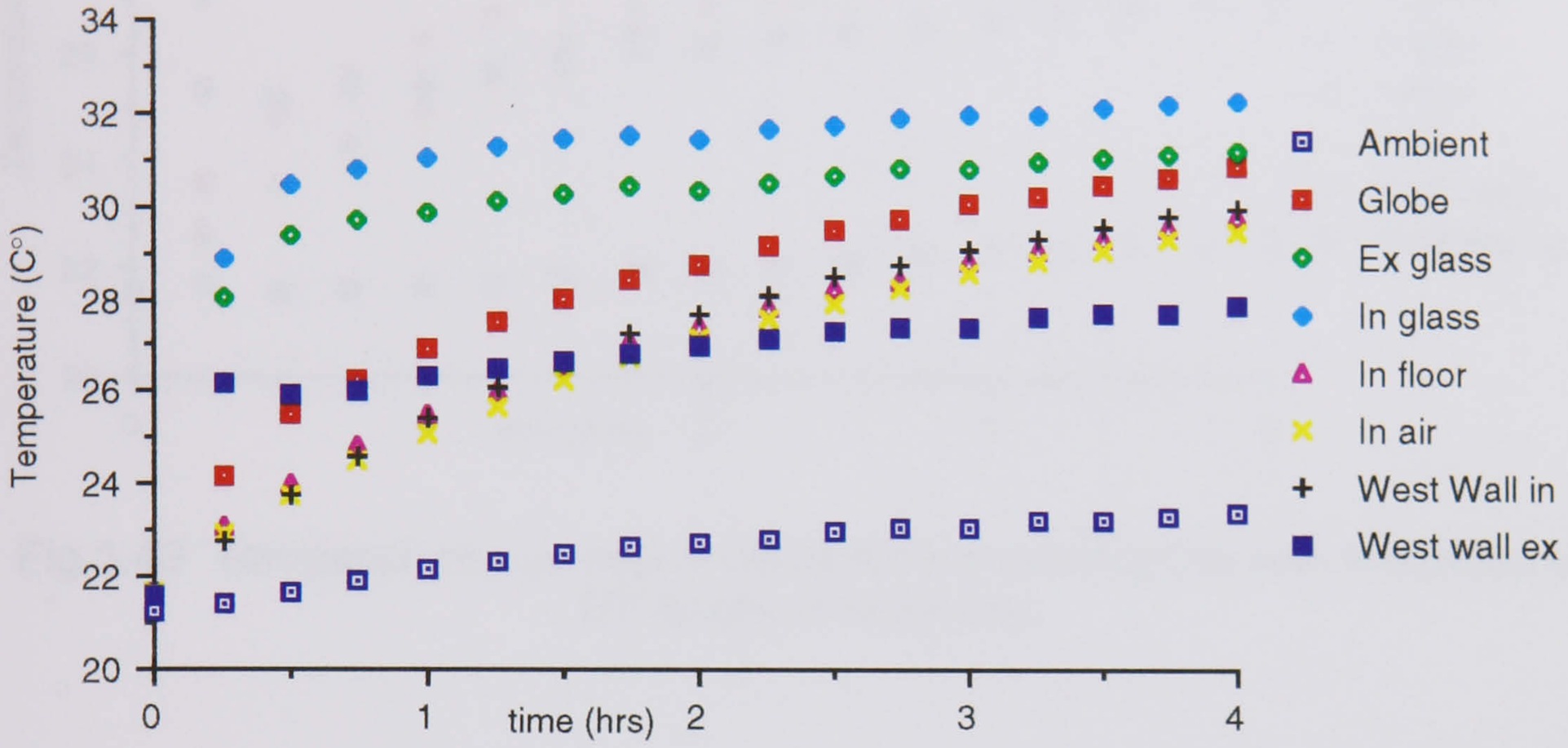

Fig 5.47 Temperature rise over 4 hours for a insulating film with insolation at 0° angle of incidence

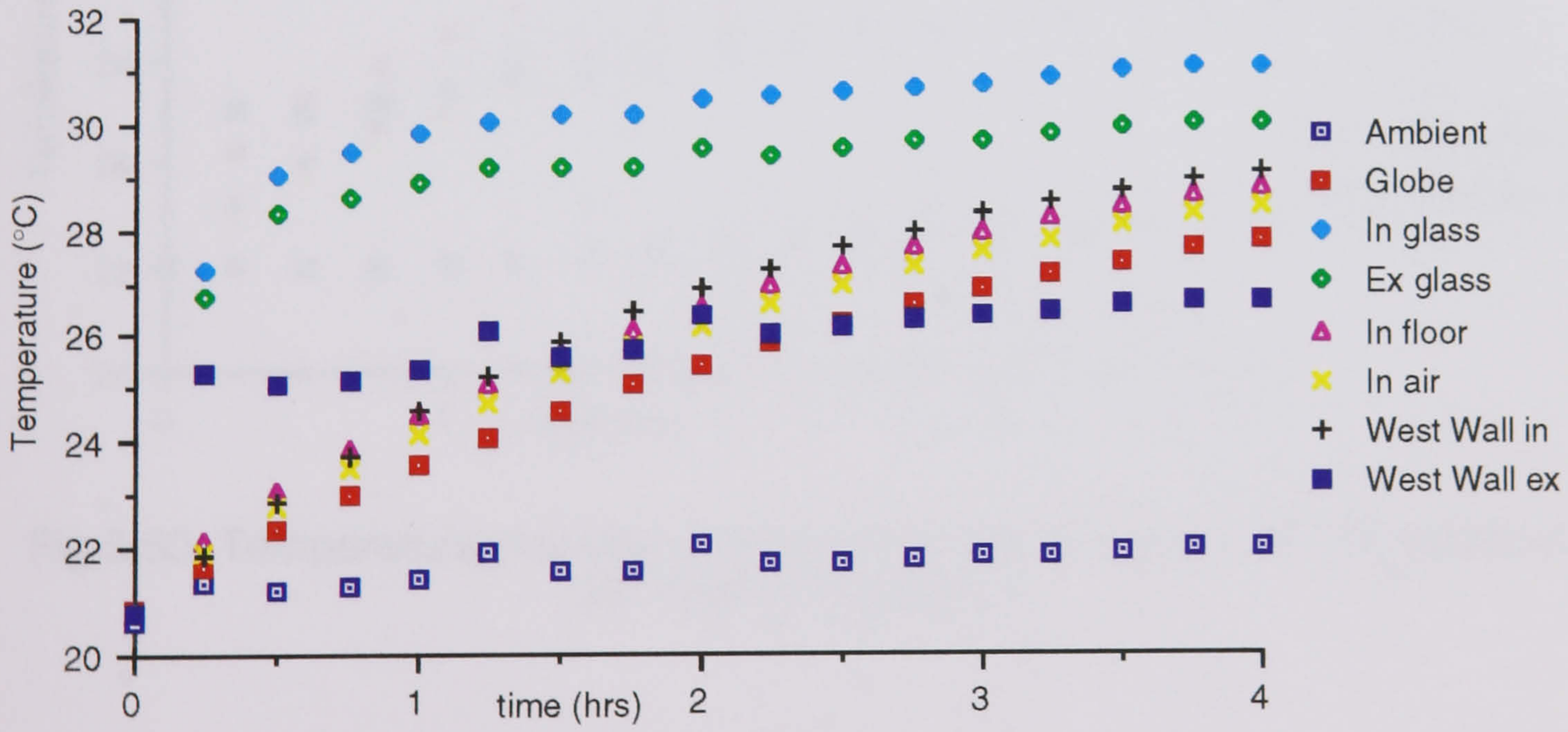

Fig 5.48 Temperature rise over 4 hours for a insulating film with insolation at 10° angle of incidence

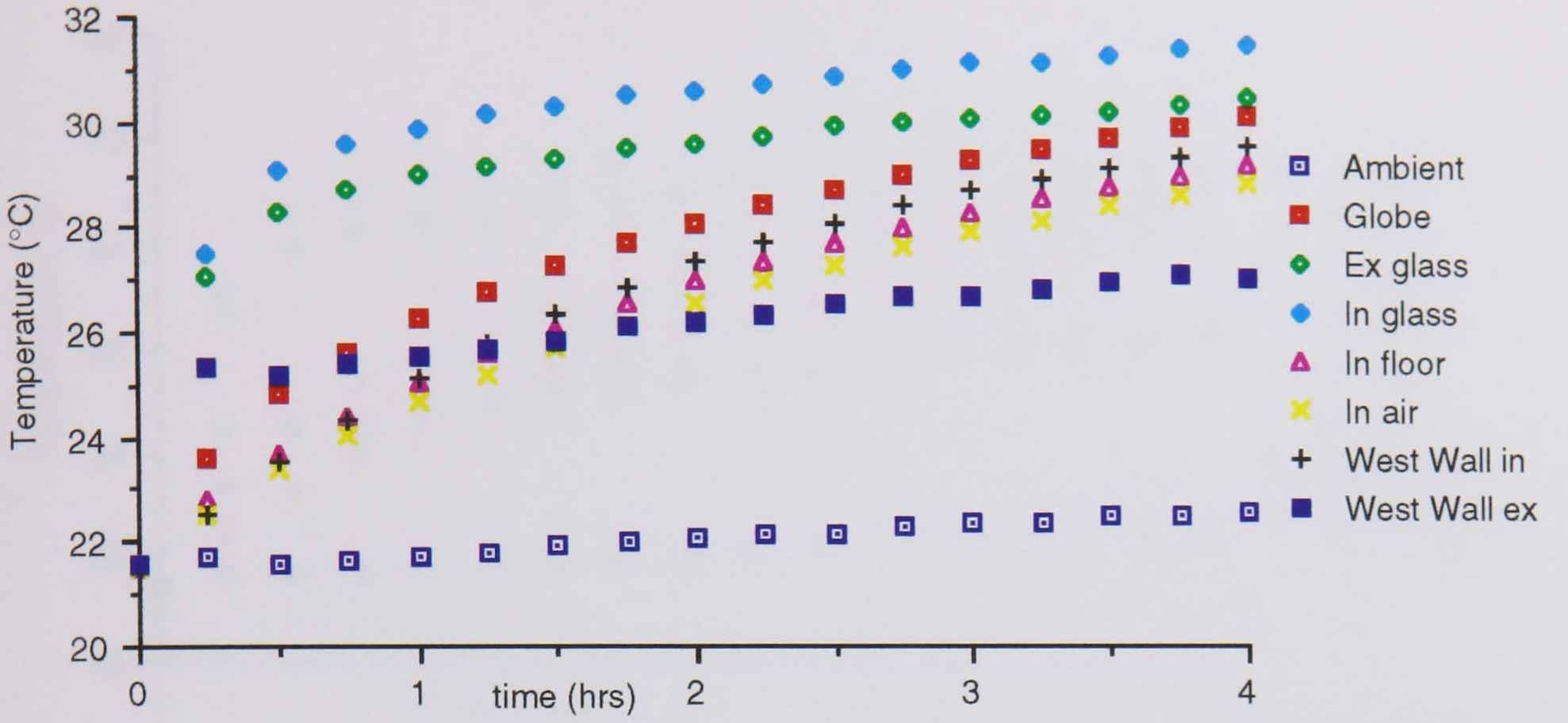

Fig 5.49 Temperature rise over 4 hours for a insulating film with insolation at 20° angle of incidence

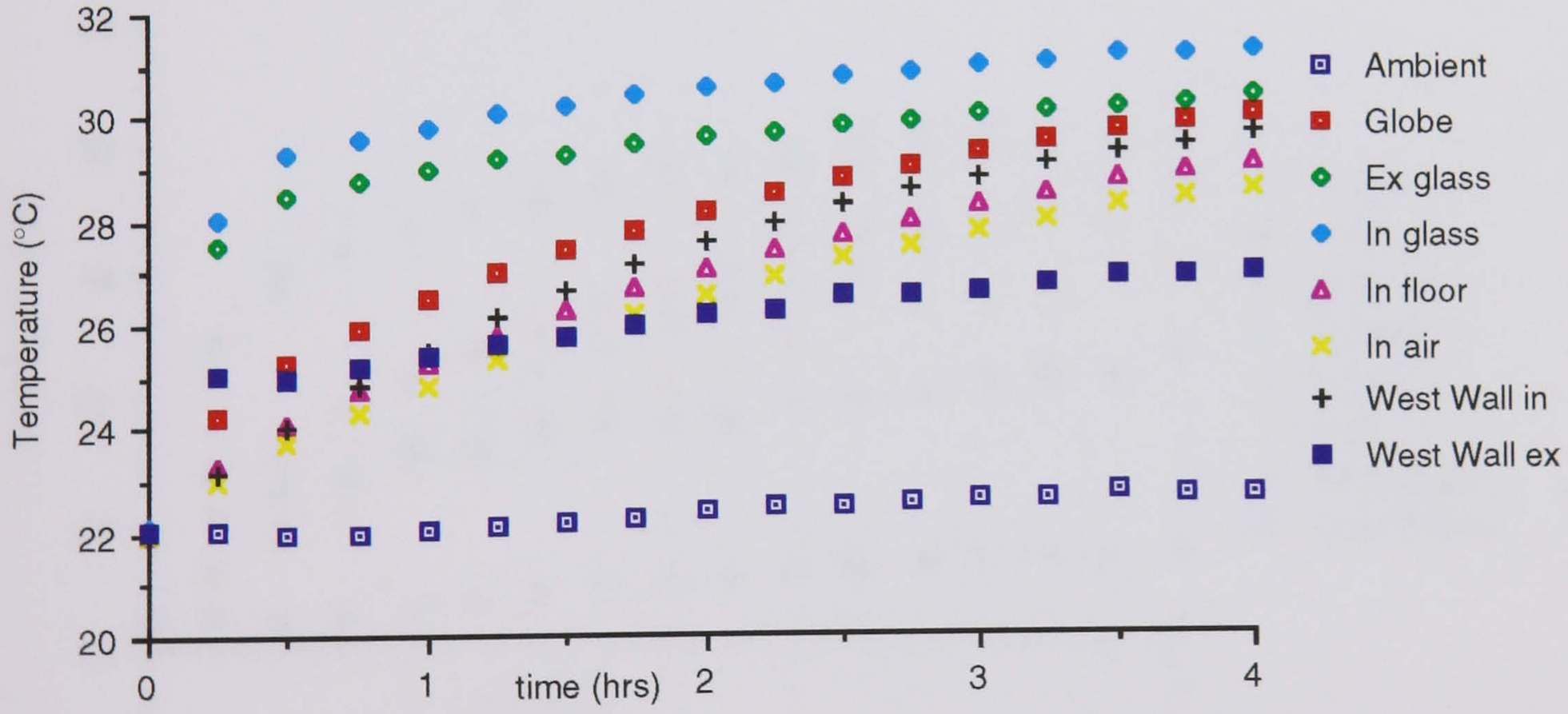

Fig 5.50 Temperature rise over 4 hours for a insulating film with insolation at 30° angle of incidence

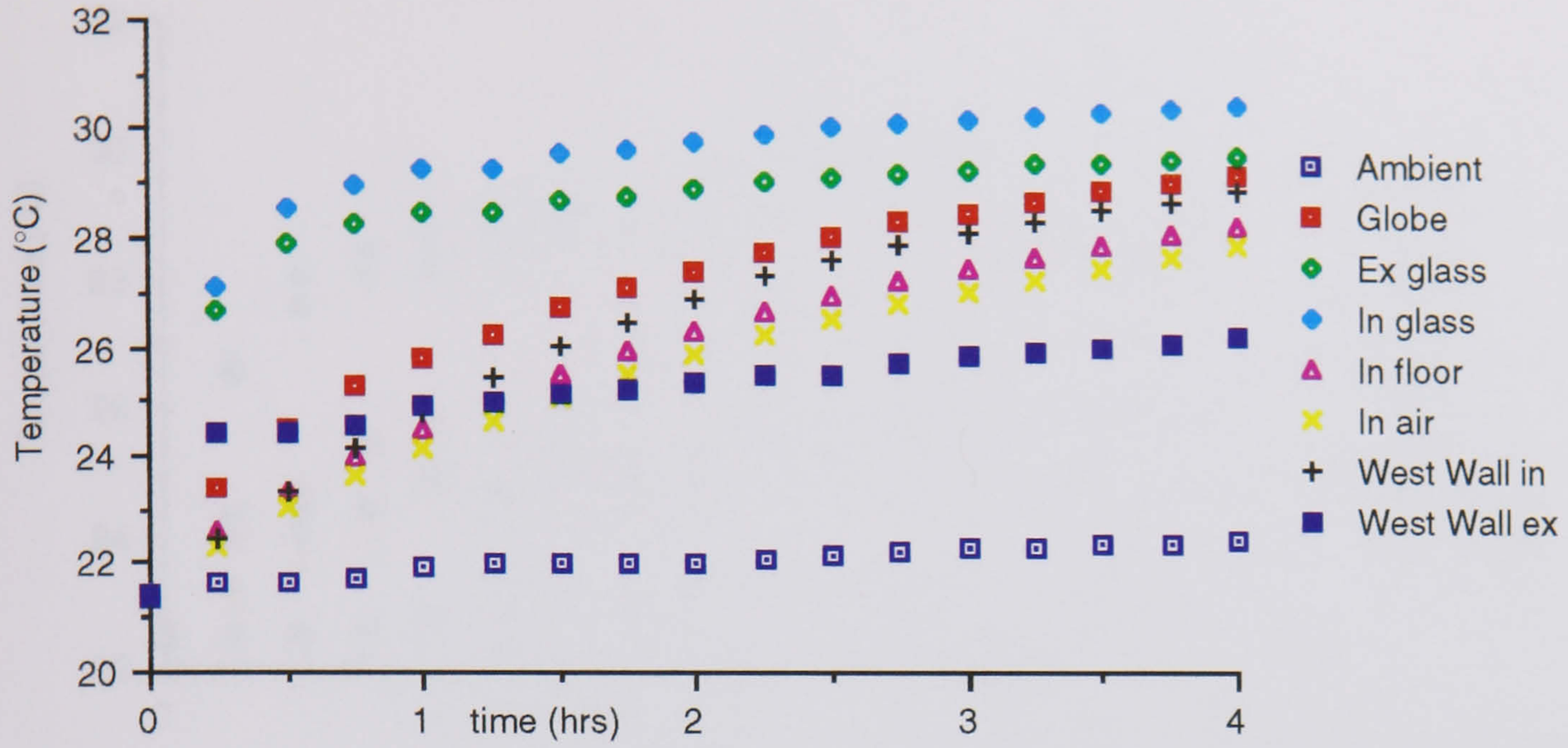

Fig 5.51 Temperature rise over 4 hours for a insulating film with insolation at 40° angle of incidence

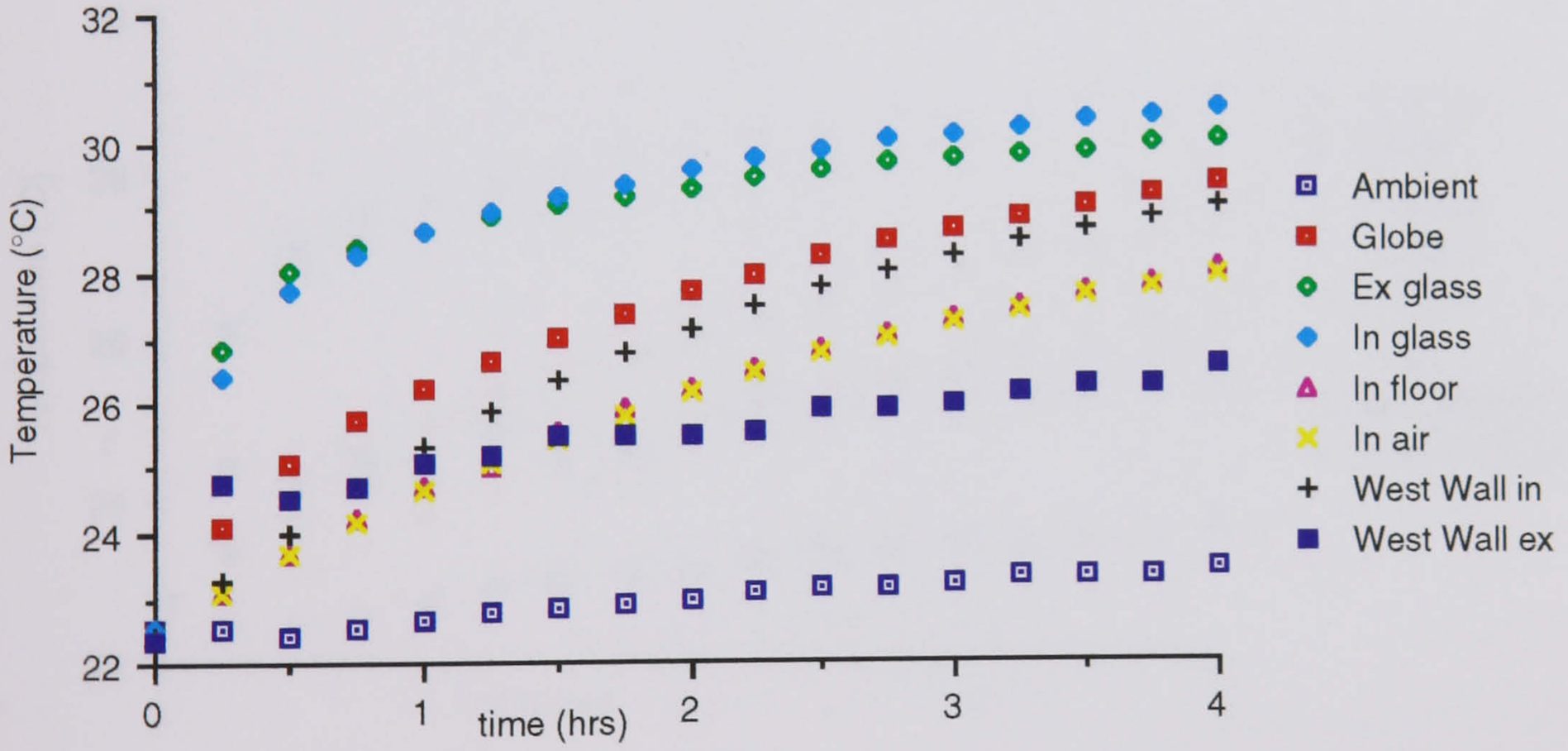

Fig 5.52 Temperature rise over 4 hours for a insulating film with insolation at 50° angle of incidence

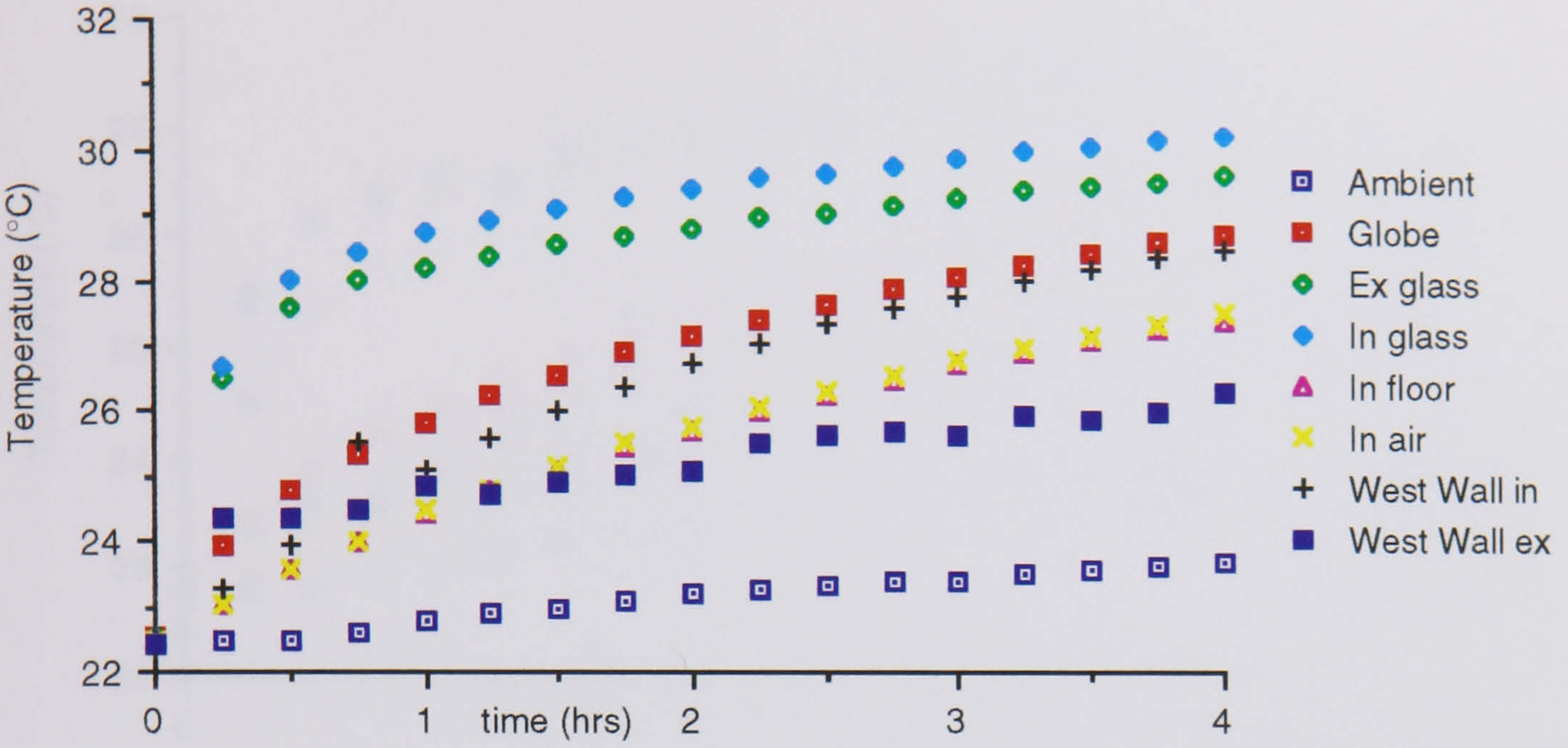

Fig 5.53 Temperature rise over 4 hours for a insulating film with insolation at 60° angle of incidence

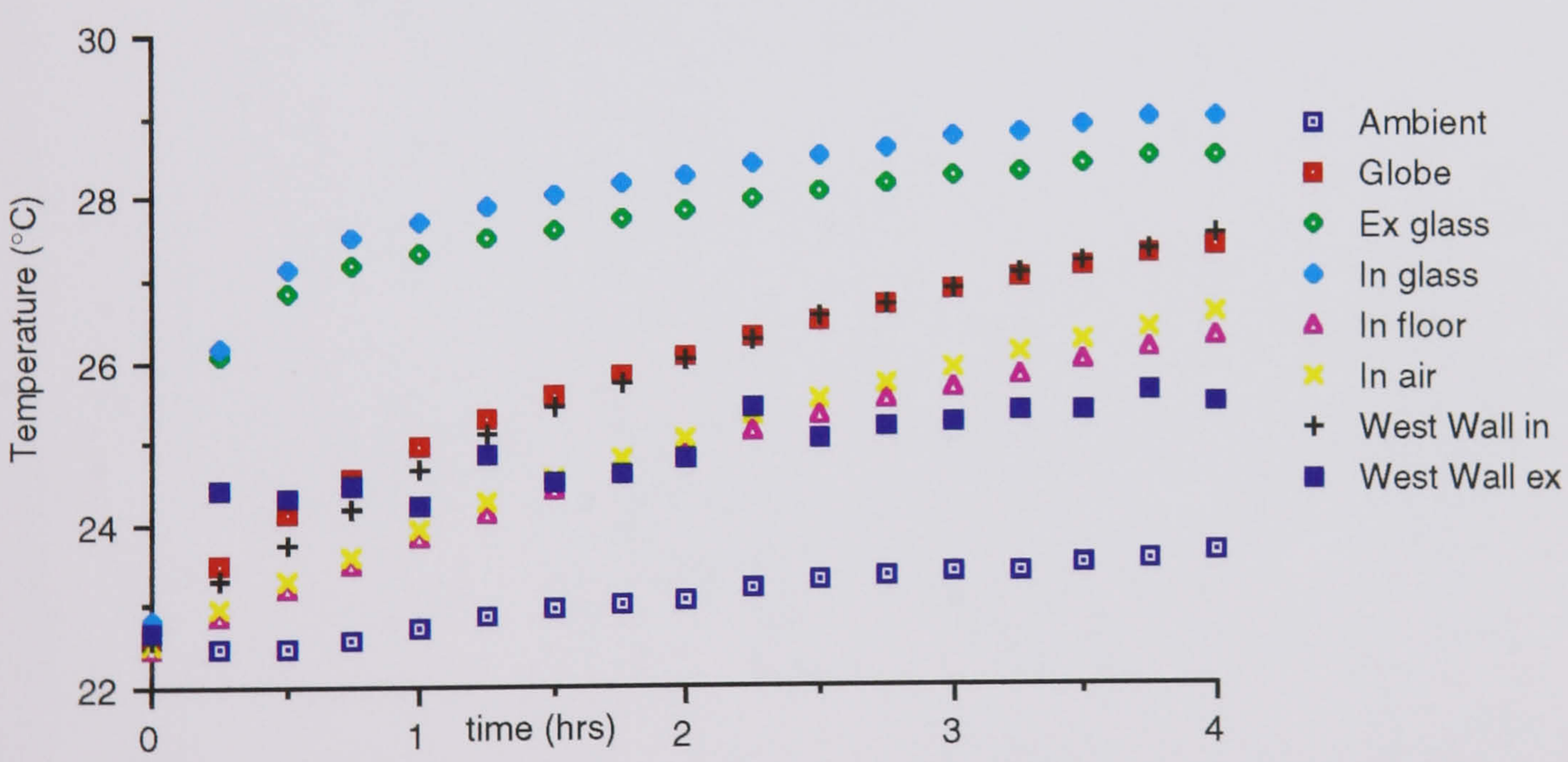

Fig 5.54 Temperature rise over 4 hours for a insulating film with insolation at 70° angle of incidence

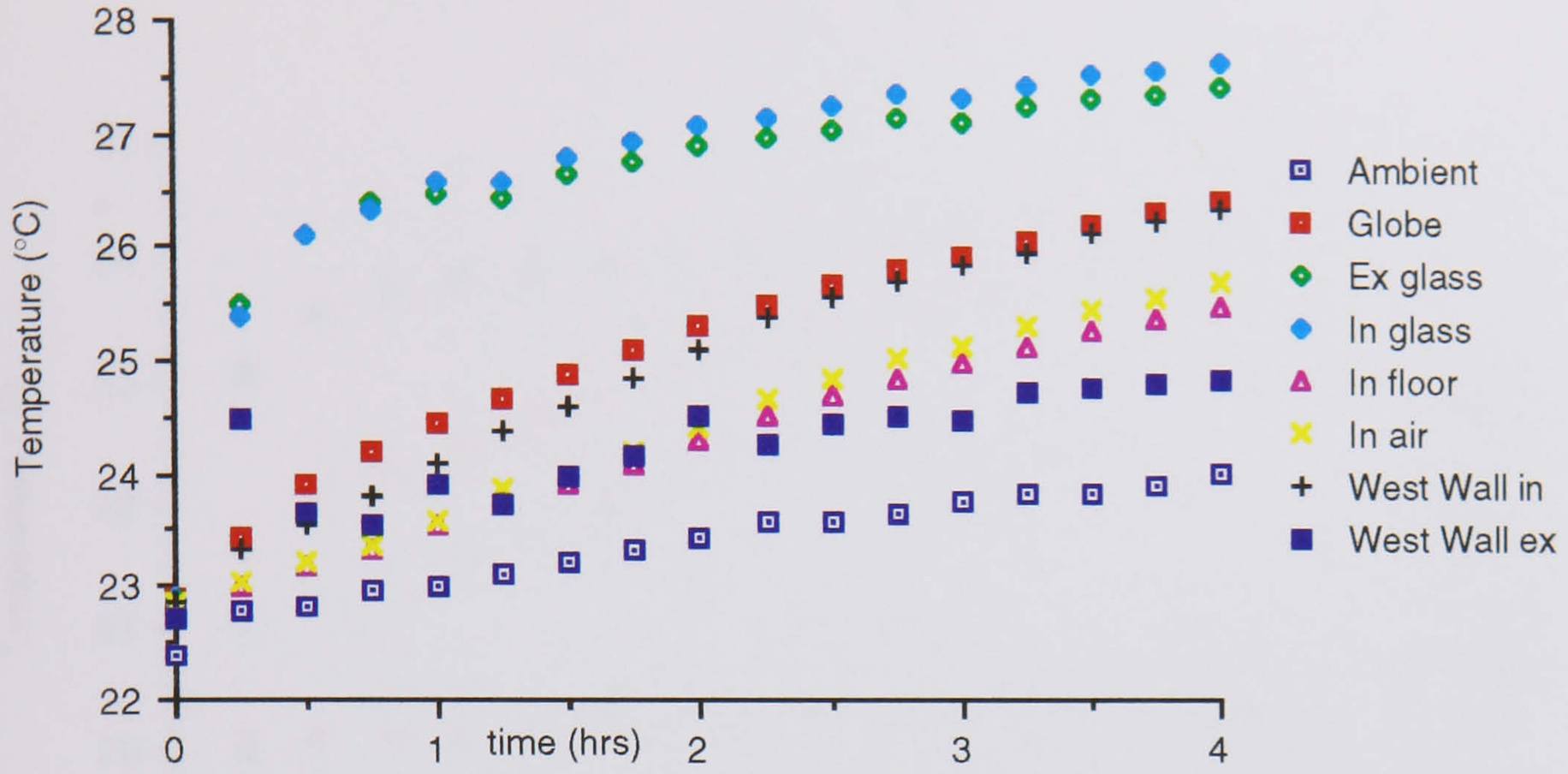

Fig 5.55 Temperature rise over 4 hours for a insulating film with insolation at 80° angle of incidence

5.4.2 Computer Modelling Results

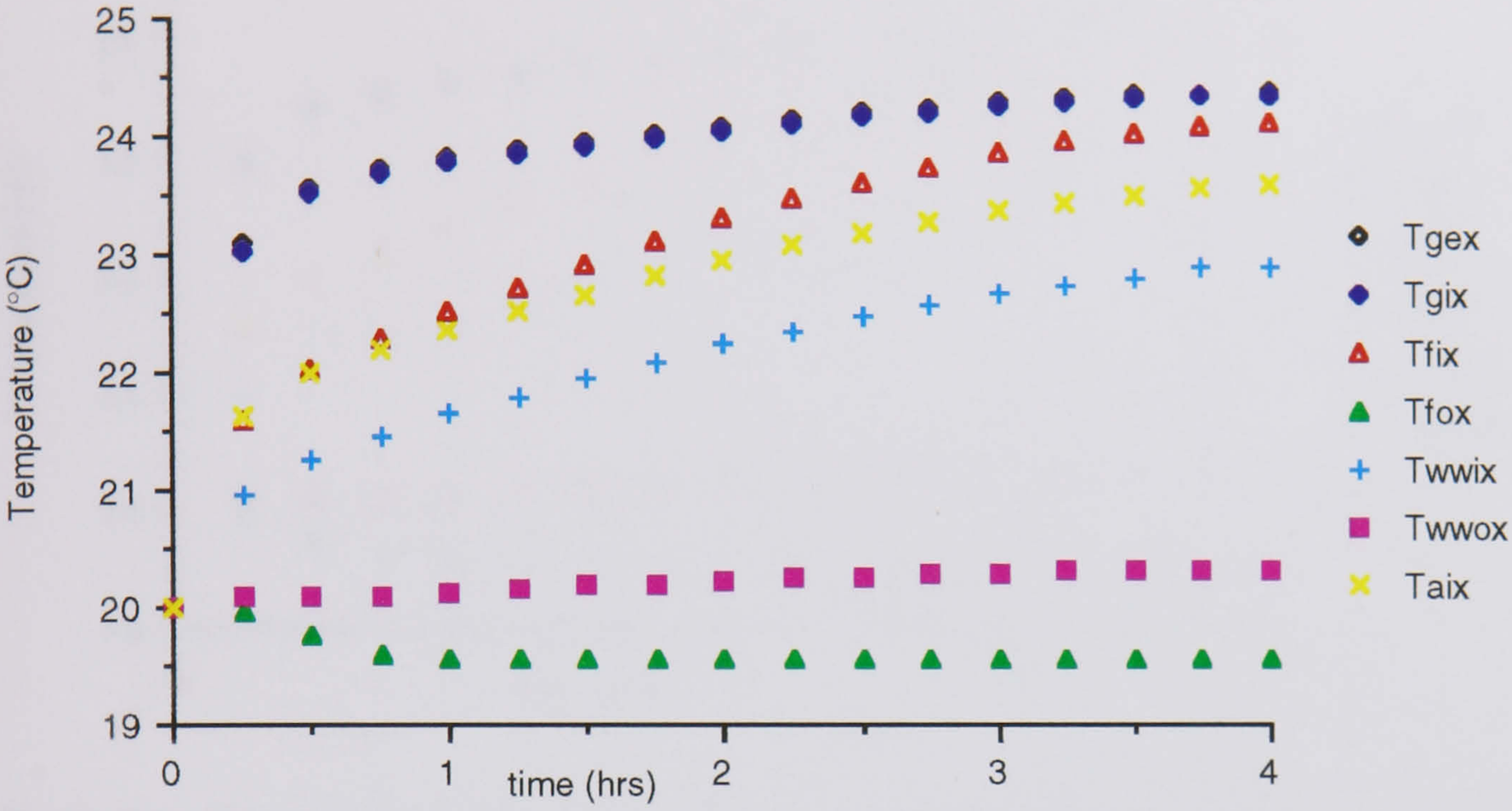

Fig 5.56 The computer model prediction of the temperature rise over 4 hours for a insulating film with insolation at 0° angle of incidence

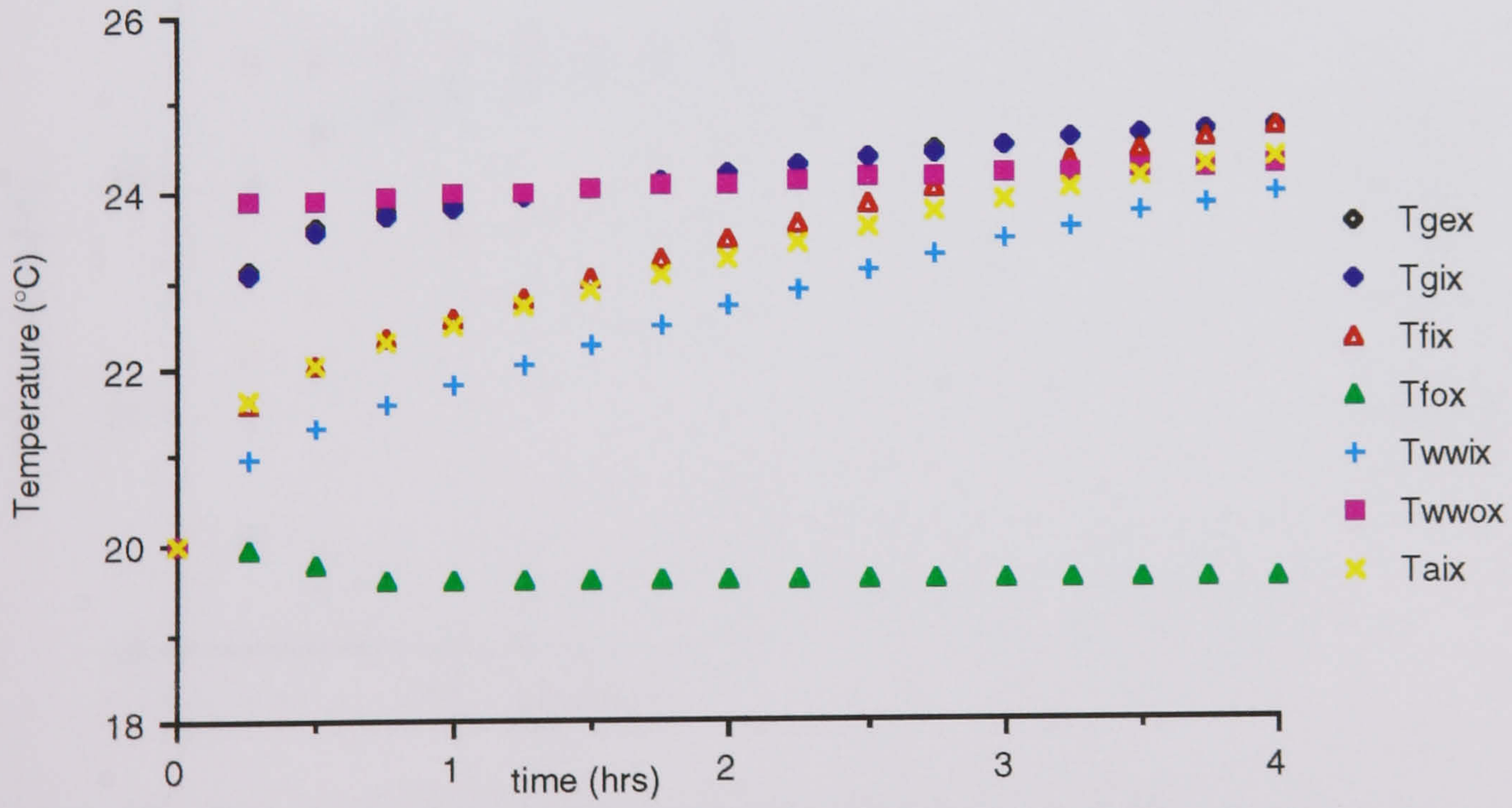

Fig 5.57 The computer model prediction of the temperature rise over 4 hours for a insulating film with insolation at 0° angle of incidence where insolation is received by the outside also

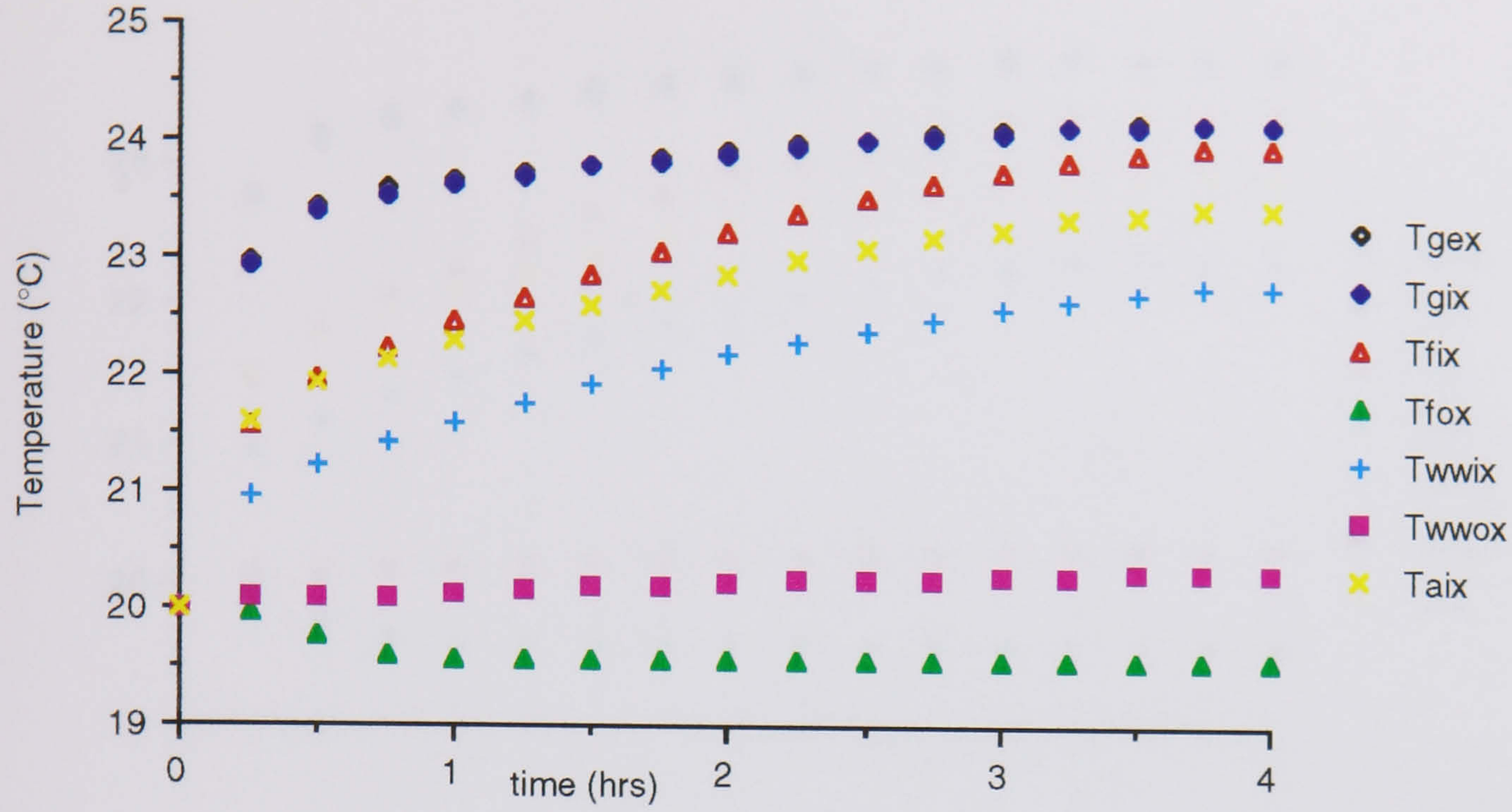

Fig 5.58 The computer model prediction of the temperature rise over 4 hours for a insulating film with insolation at 10° angle of incidence

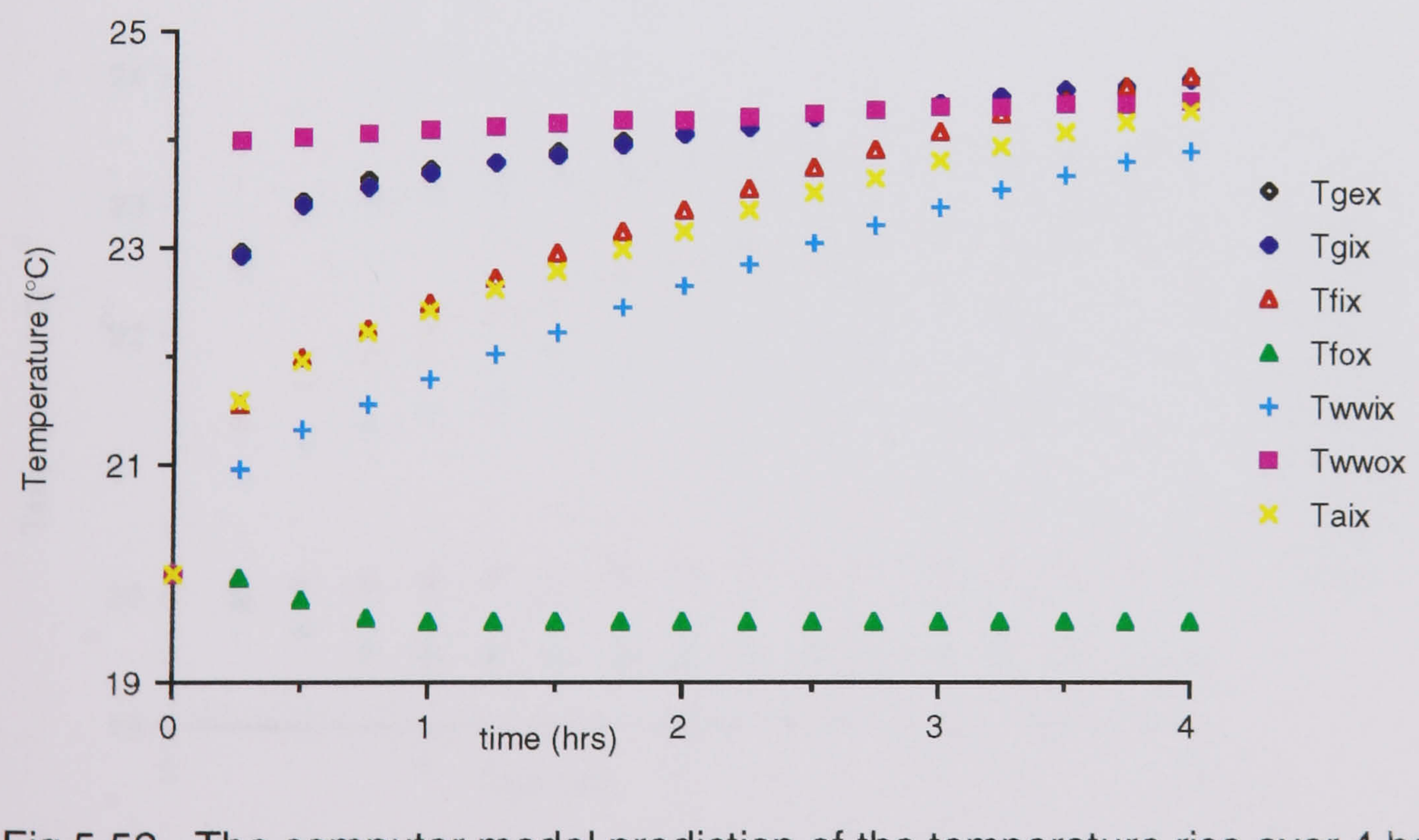

Fig 5.59 The computer model prediction of the temperature rise over 4 hours for a insulating film with insolation at 10° angle of incidence where insolation is received by the outside also

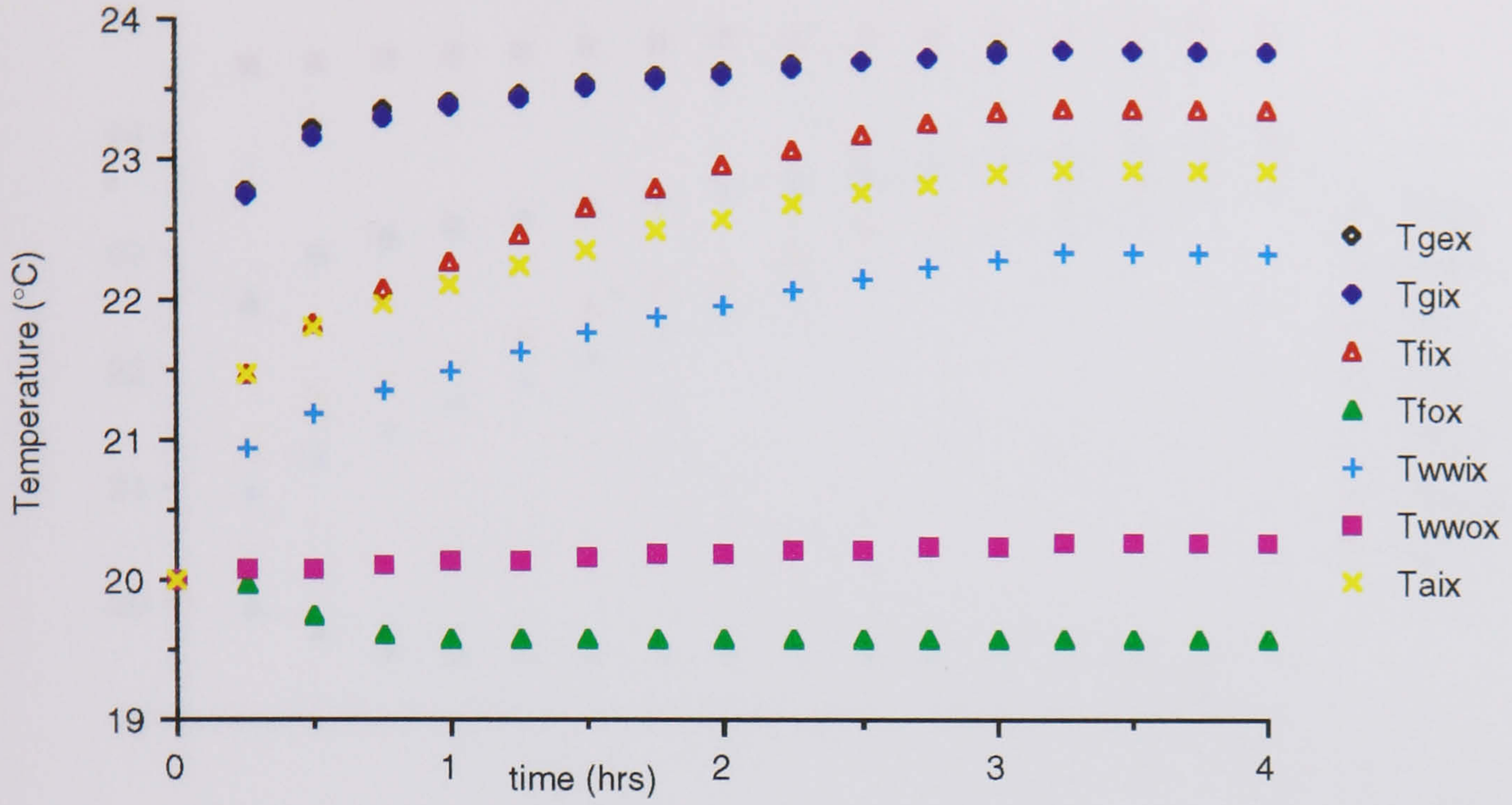

Fig 5.60 The computer model prediction of the temperature rise over 4 hours for a insulating film with insolation at 20° angle of incidence

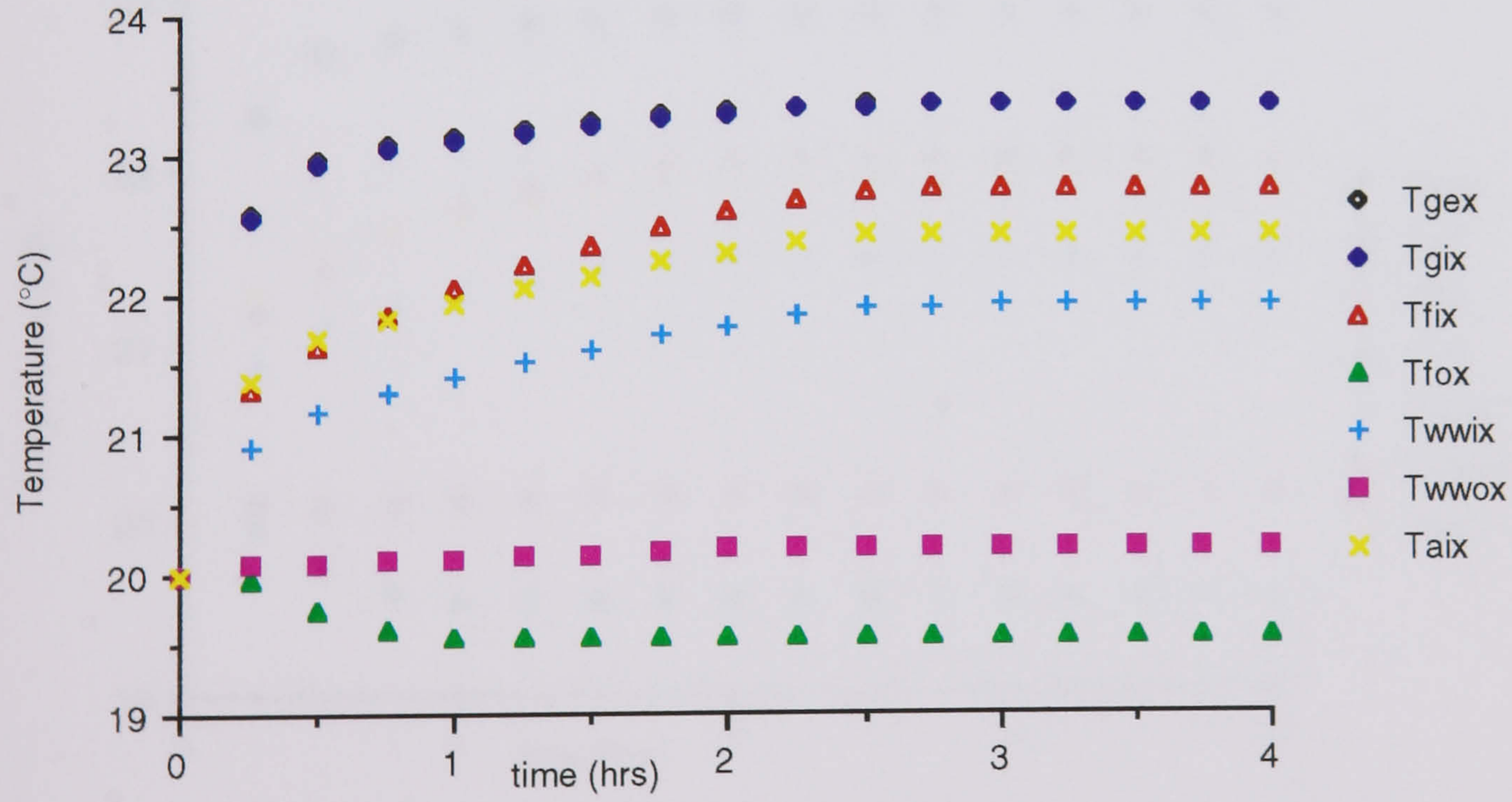

Fig 5.61 The computer model prediction of the temperature rise over 4 hours for a insulating film with insolation at 30° angle of incidence

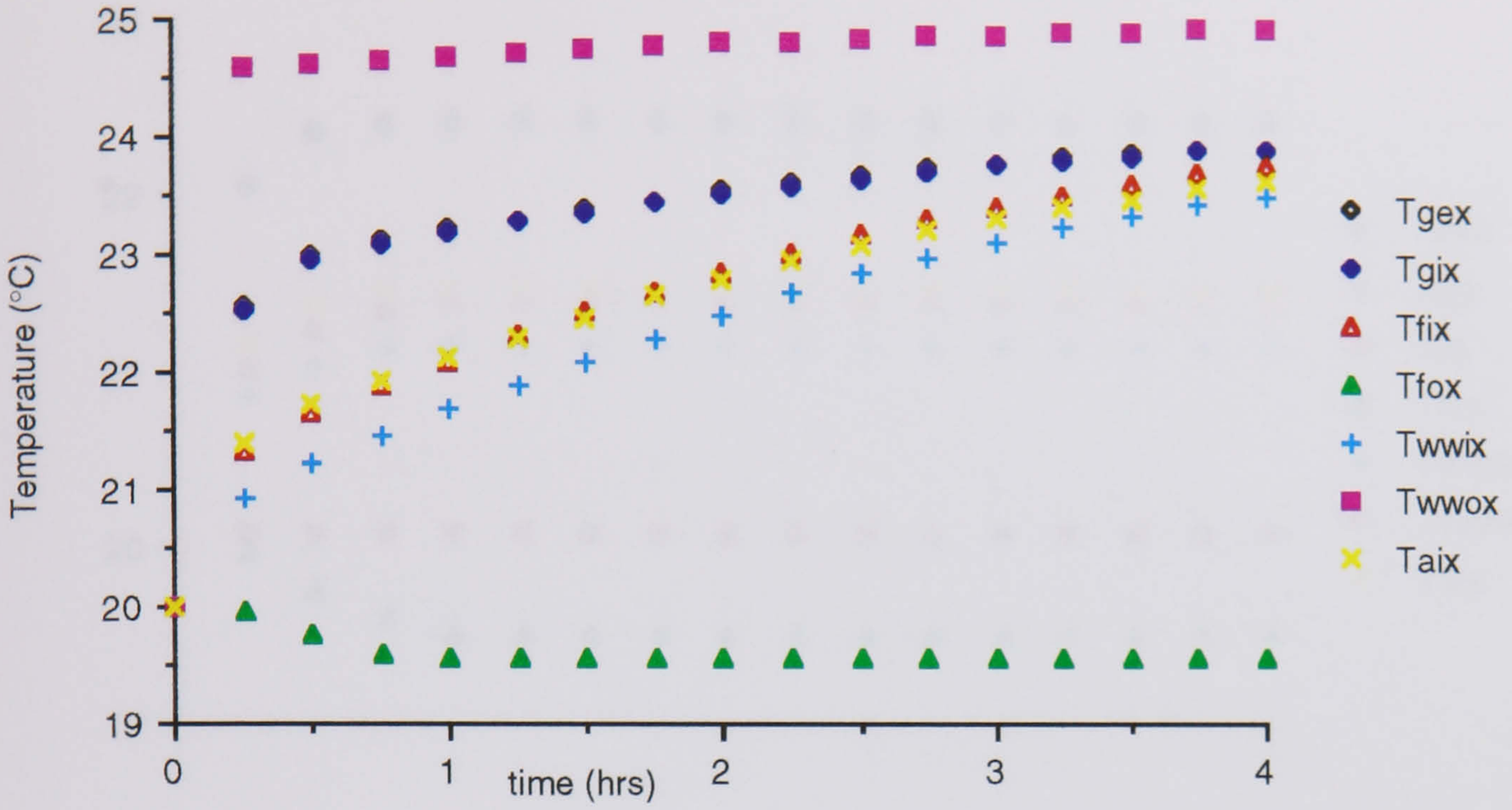

Fig 5.62 The computer model prediction of the temperature rise over 4 hours for a insulating film with insolation at 30° angle of incidence where insolation is received by the outside also

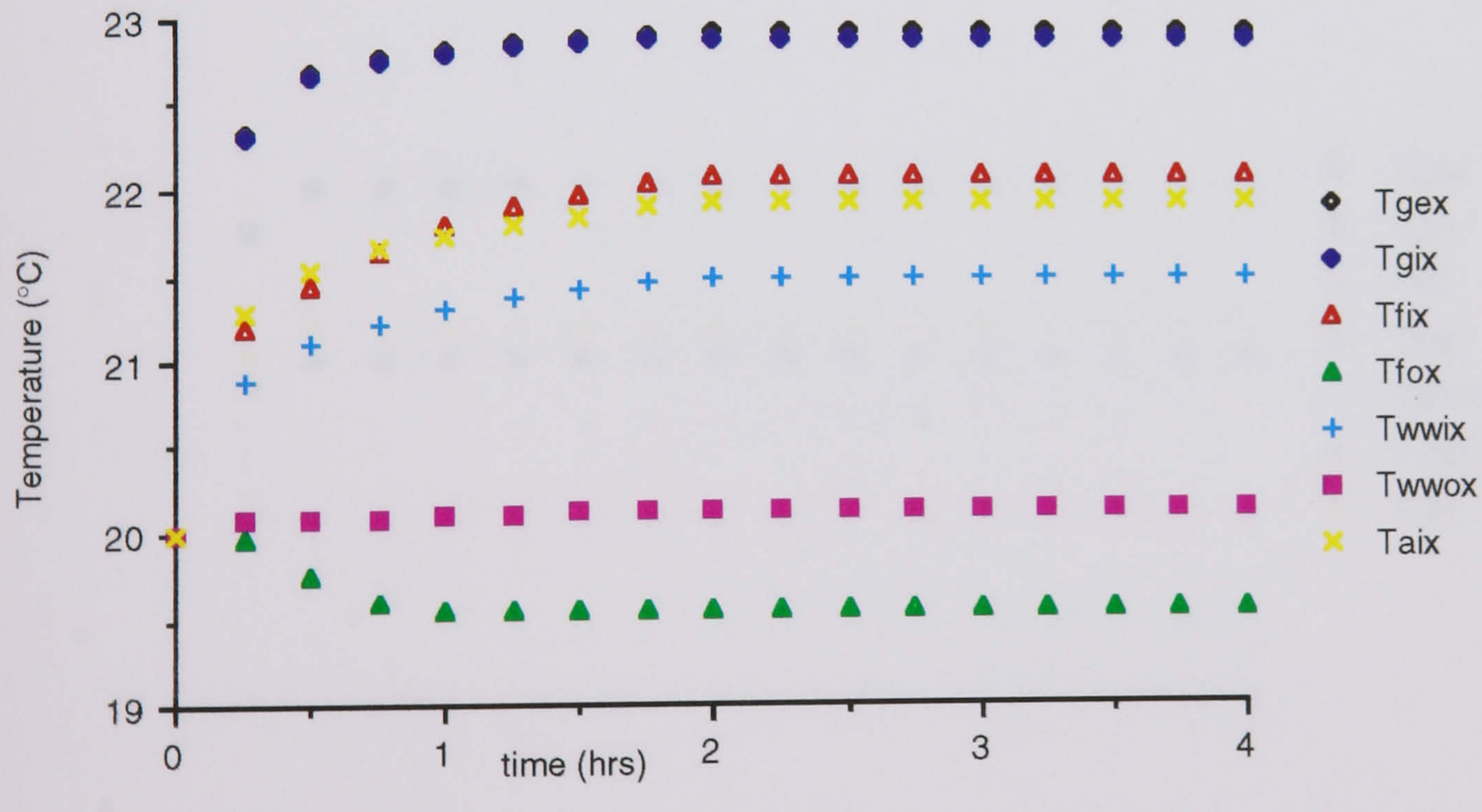

Fig 5.63 The computer model prediction of the temperature rise over 4 hours for a insulating film with insolation at 40° angle of incidence

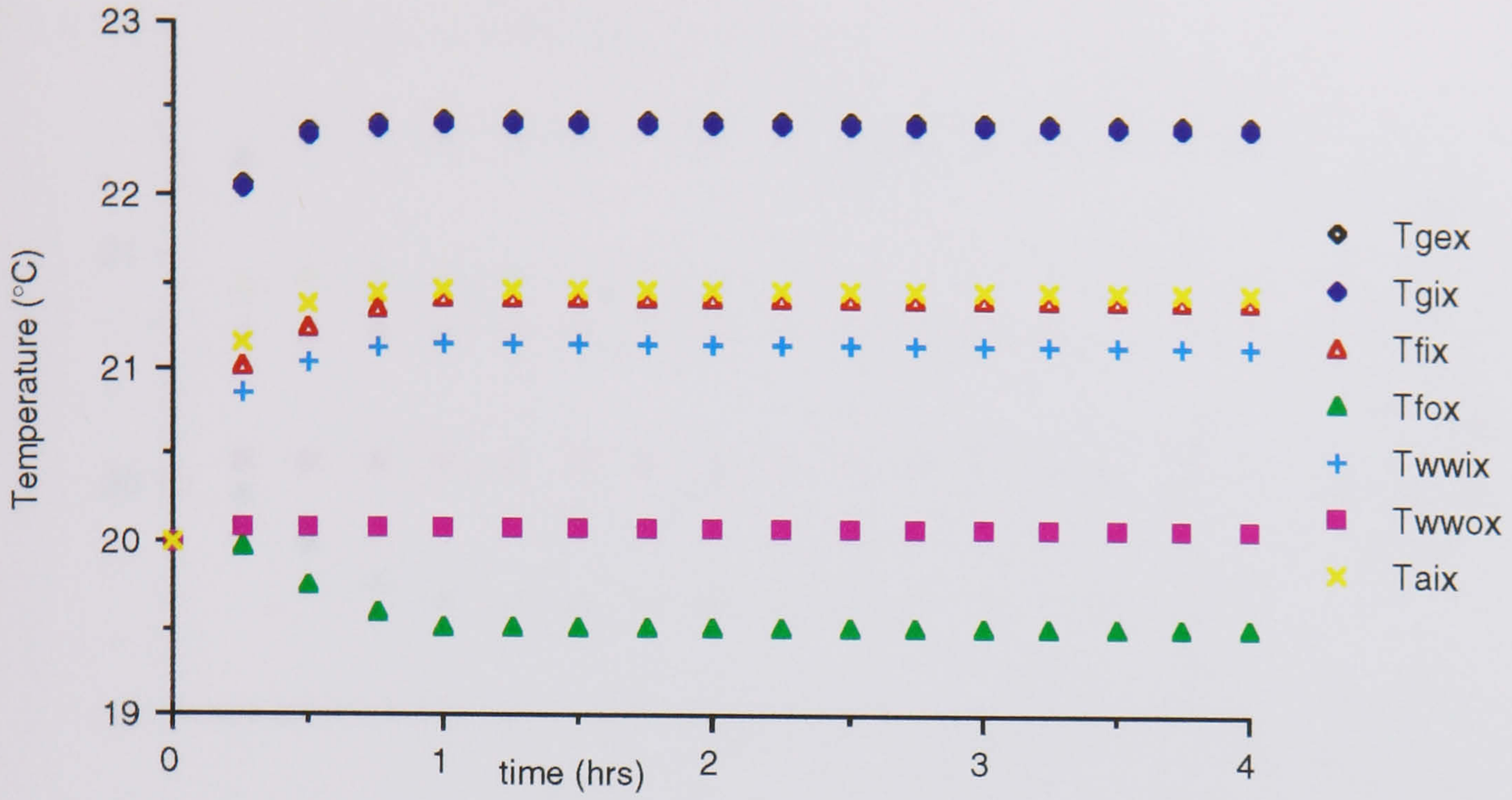

Fig 5.64 The computer model prediction of the temperature rise over 4 hours for a insulating film with insolation at 50° angle of incidence

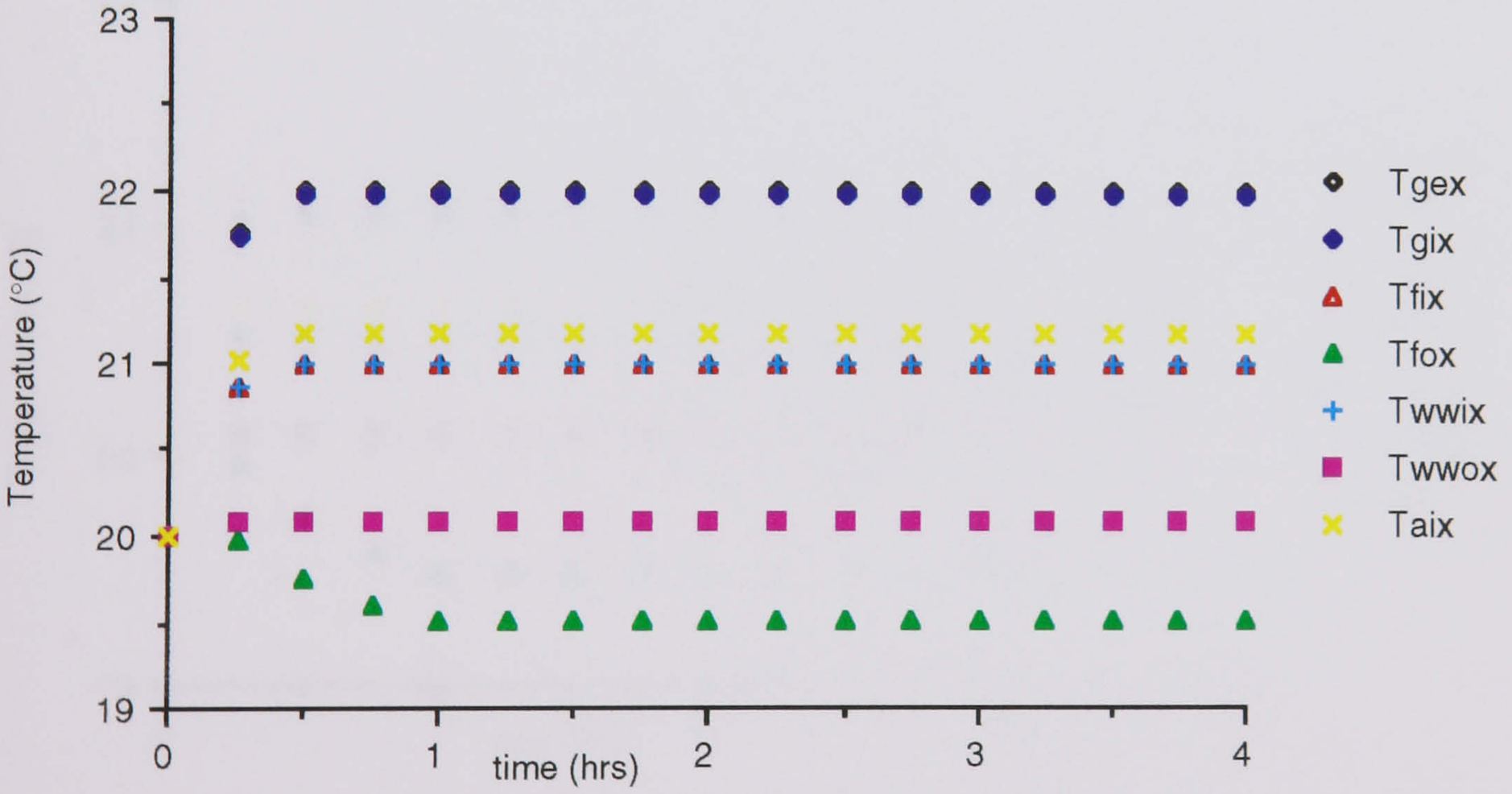

Fig 5.65 The computer model prediction of the temperature rise over 4 hours for a insulating film with insolation at 60° angle of incidence

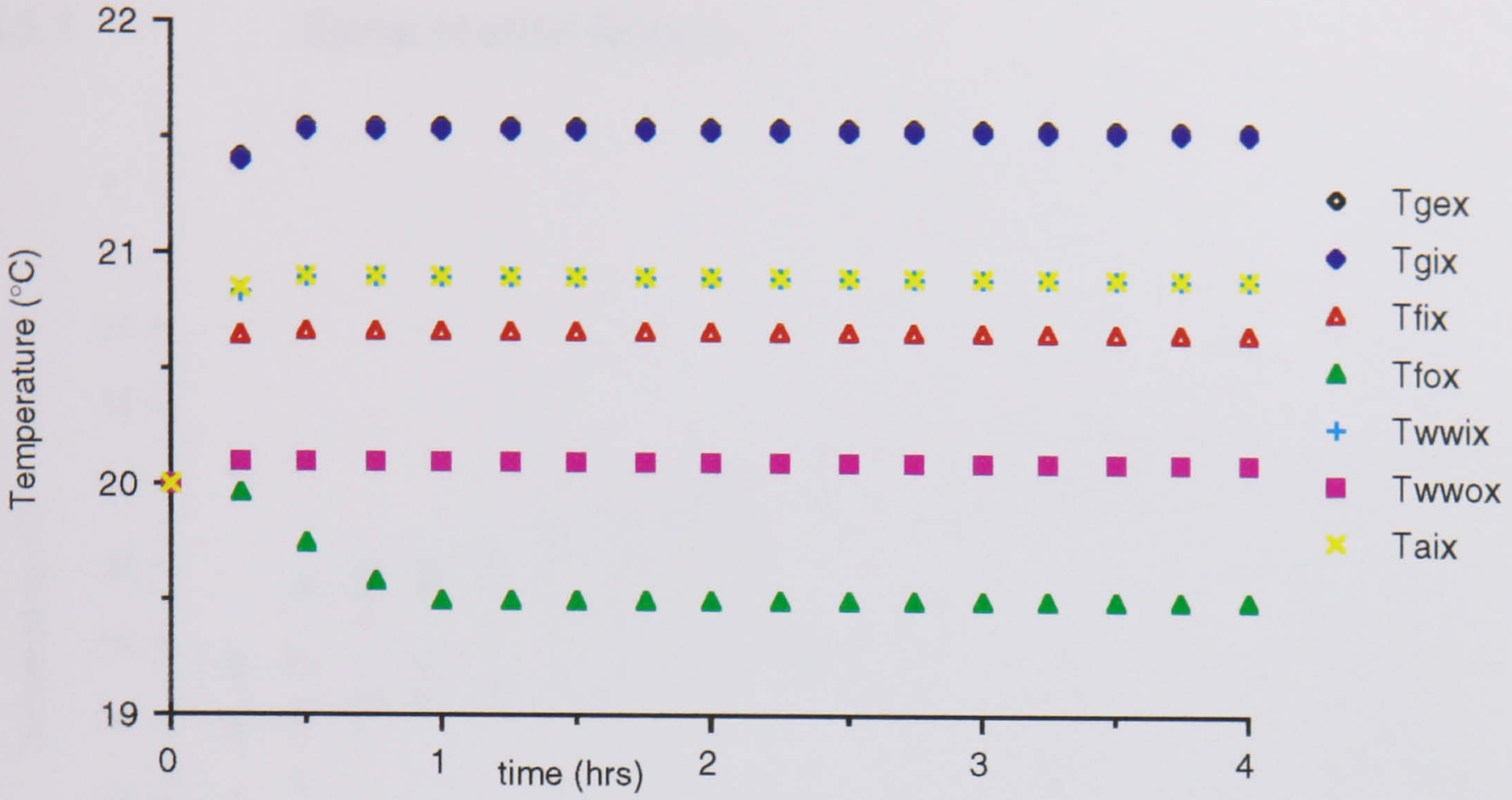

Fig 5.66 The computer model prediction of the temperature rise over 4 hours for a insulating film with insolation at 70° angle of incidence

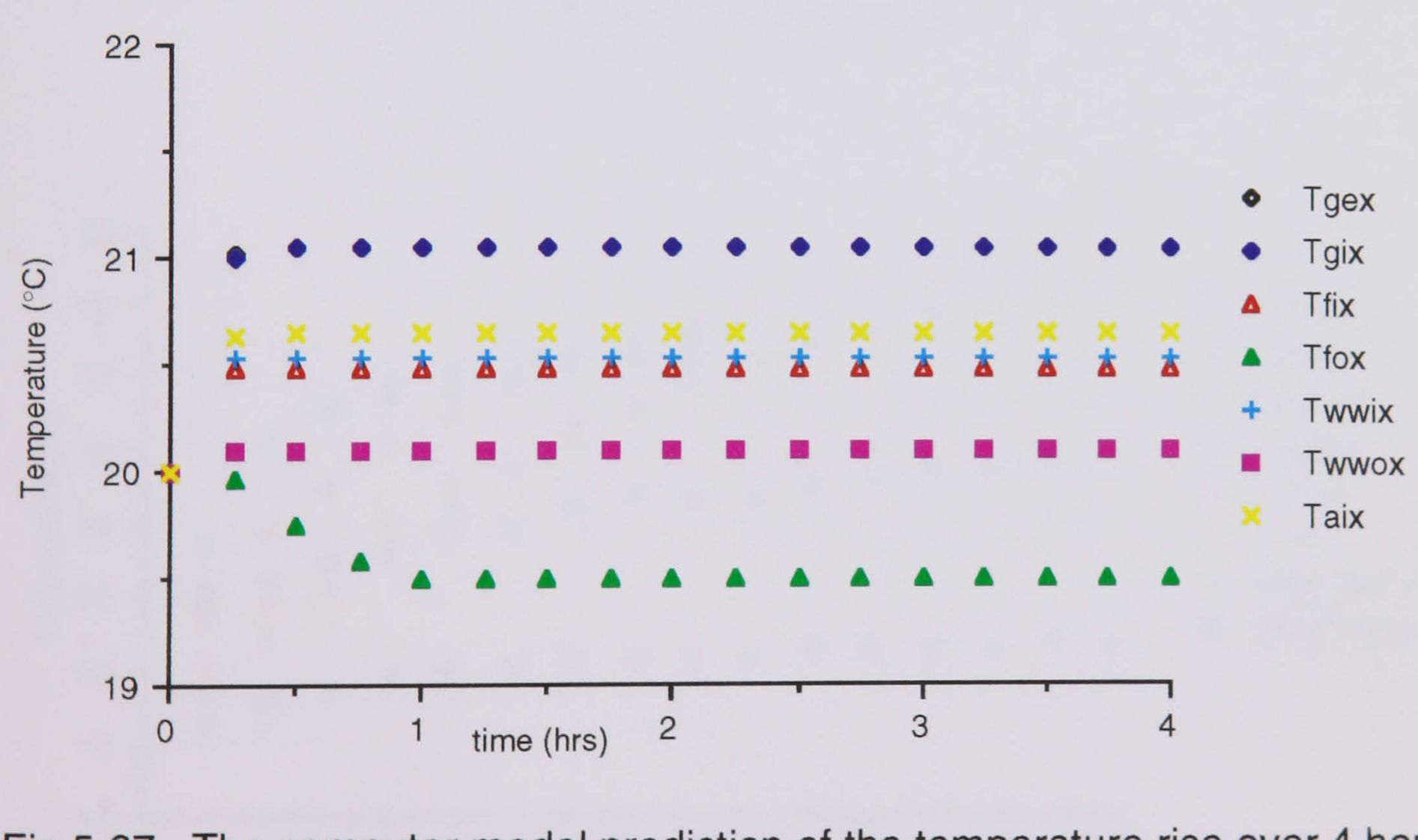

Fig 5.67 The computer model prediction of the temperature rise over 4 hours for a insulating film with insolation at 80° angle of incidence

5.5 Absorptive Films Results

5.5.1 Experimental Results

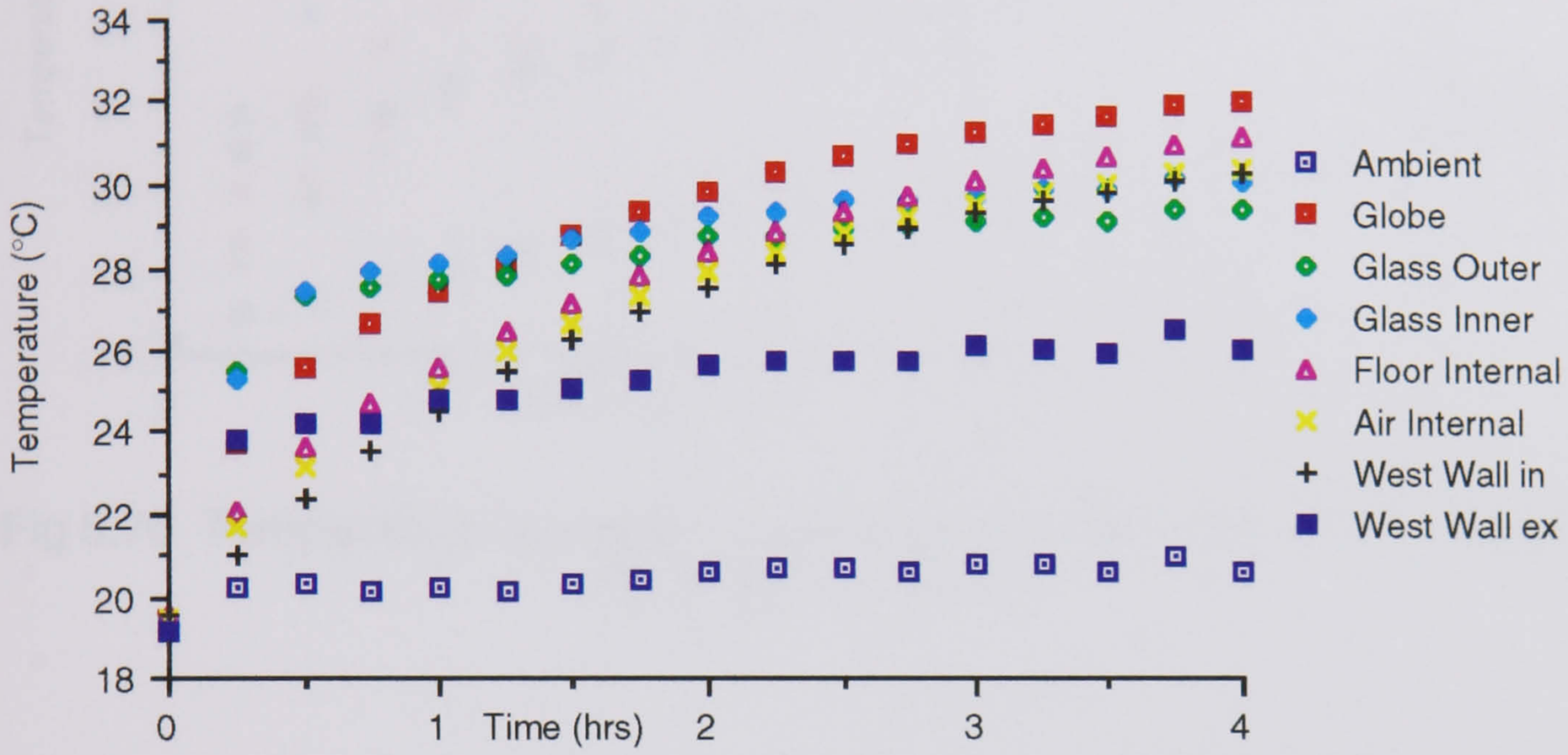

Fig 5.68 Temperature rise over 4 hours for a absorptive film with insolation at 0° angle of incidence

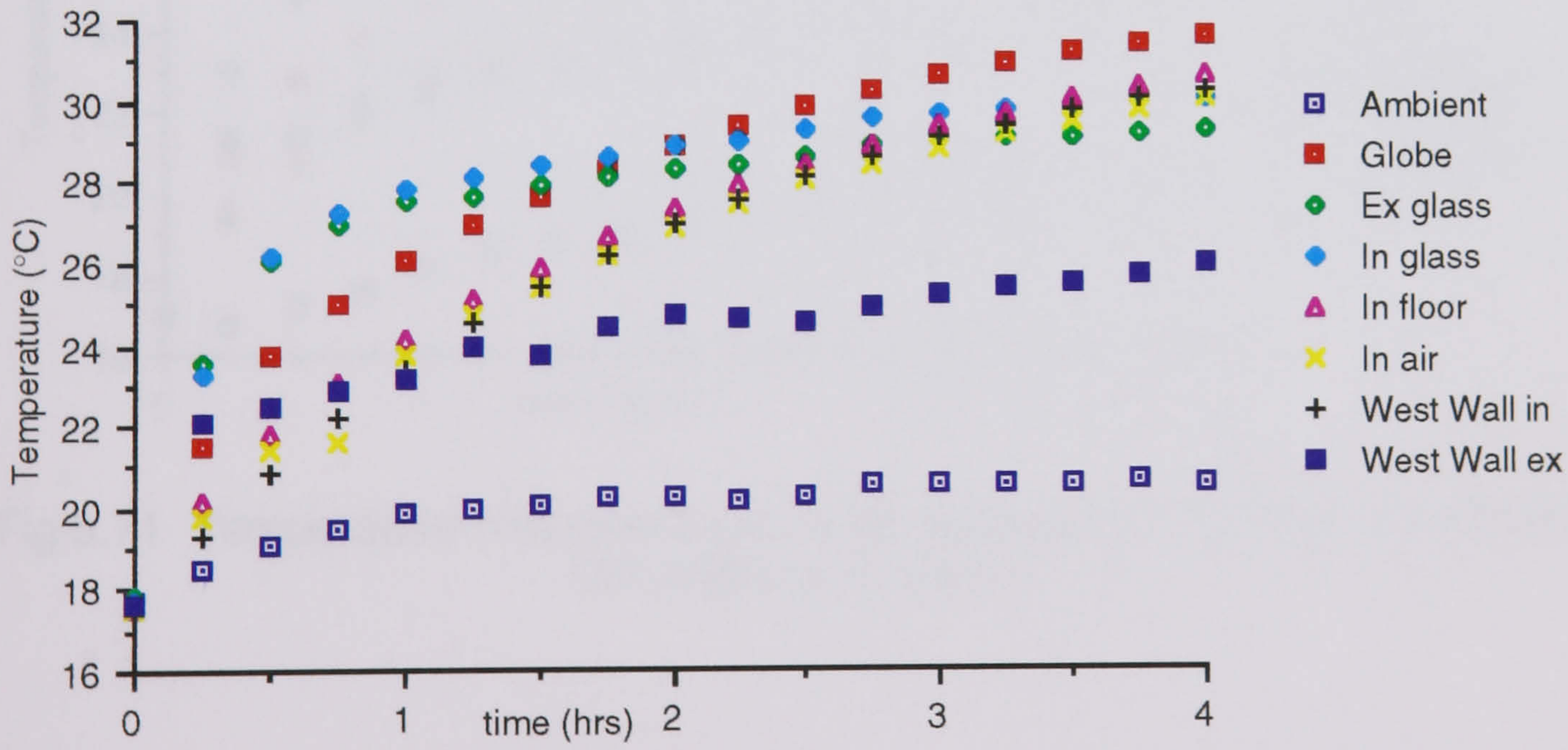

Fig 5.69 Temperature rise over 4 hours for a absorptive film with insolation at 10° angle of incidence

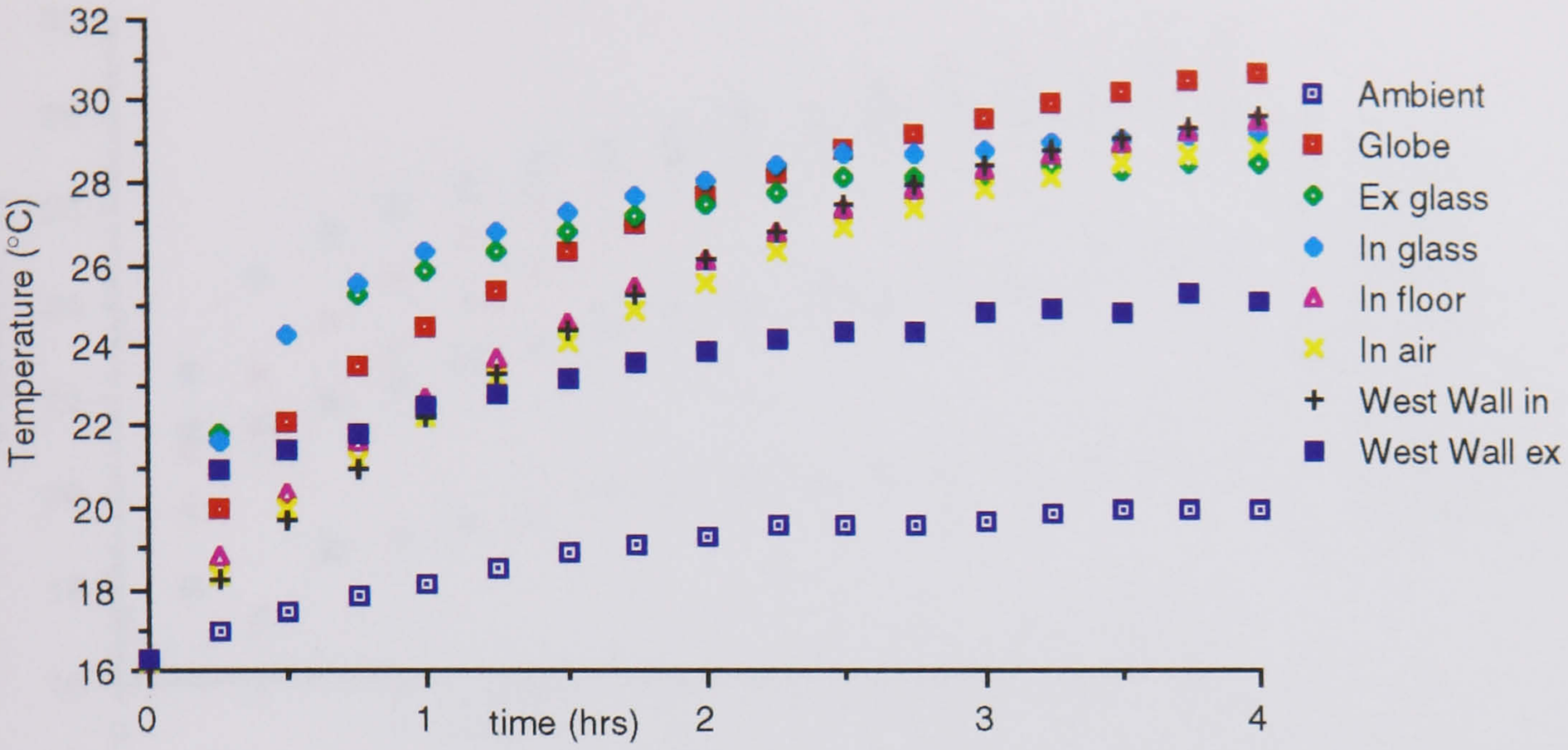

Fig 5.70 Temperature rise over 4 hours for a absorptive film with insolation at 20° angle of incidence

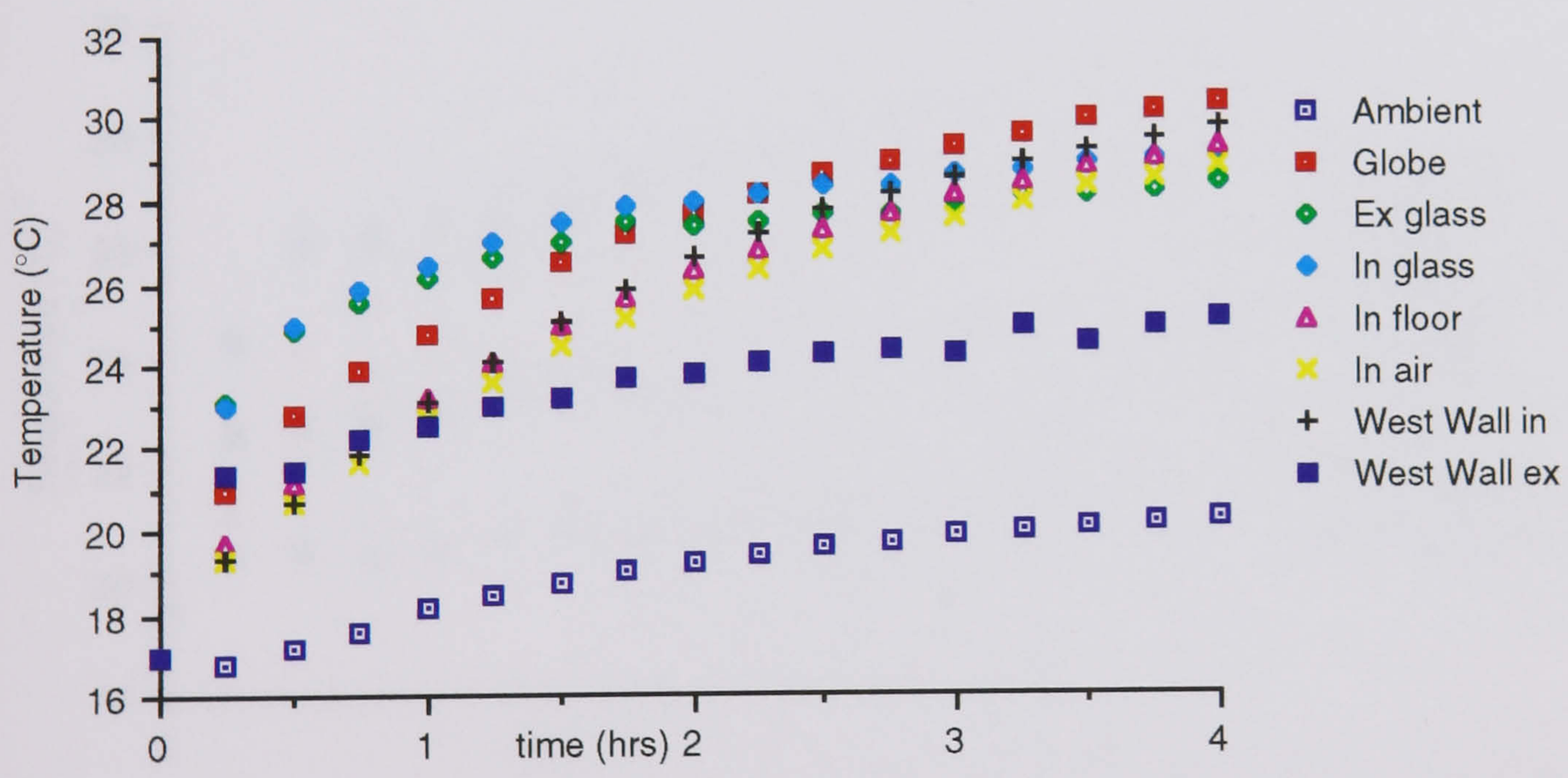

Fig 5.71 Temperature rise over 4 hours for a absorptive film with insolation at 30° angle of incidence

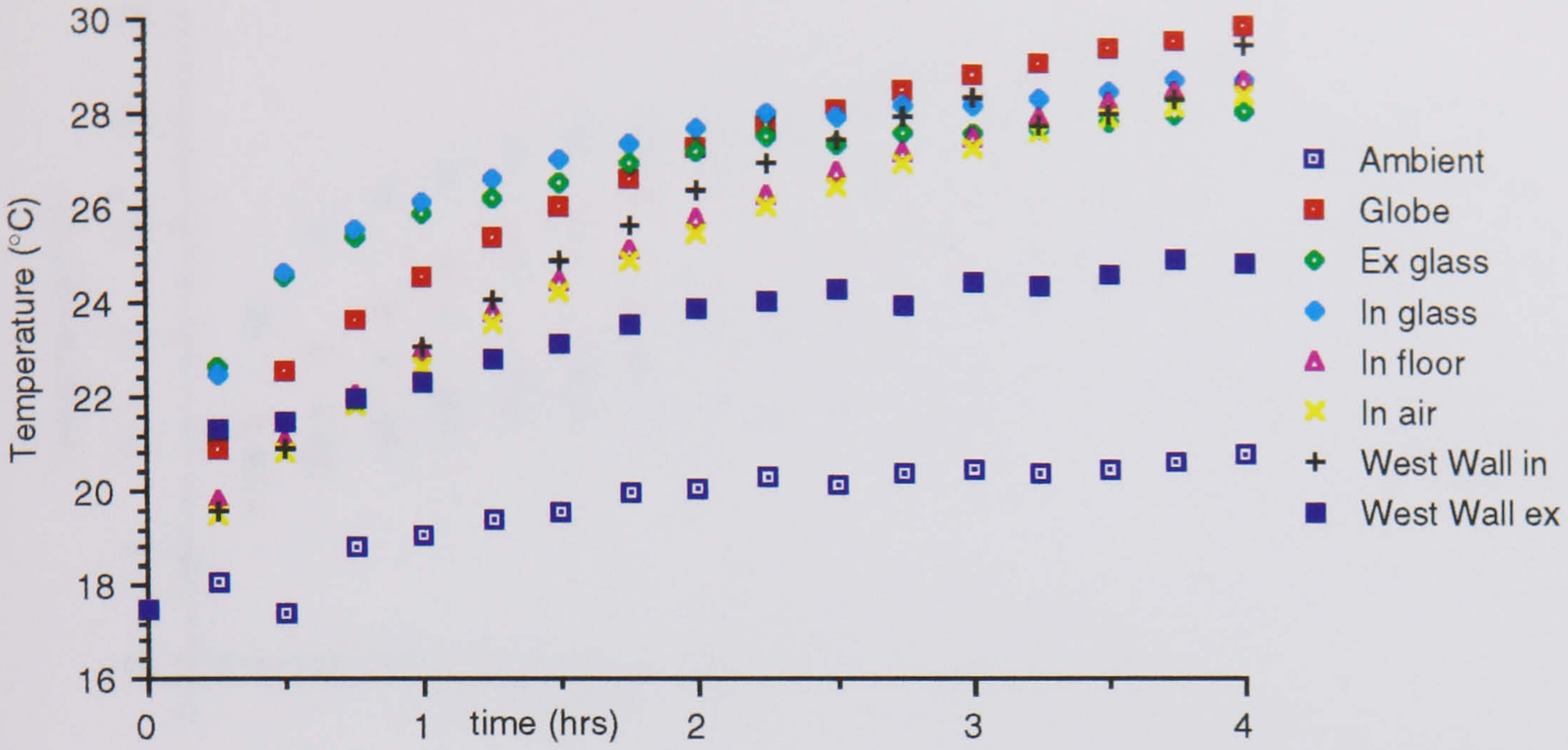

Fig 5.72 Temperature rise over 4 hours for a absorptive film with insolation at 40° angle of incidence

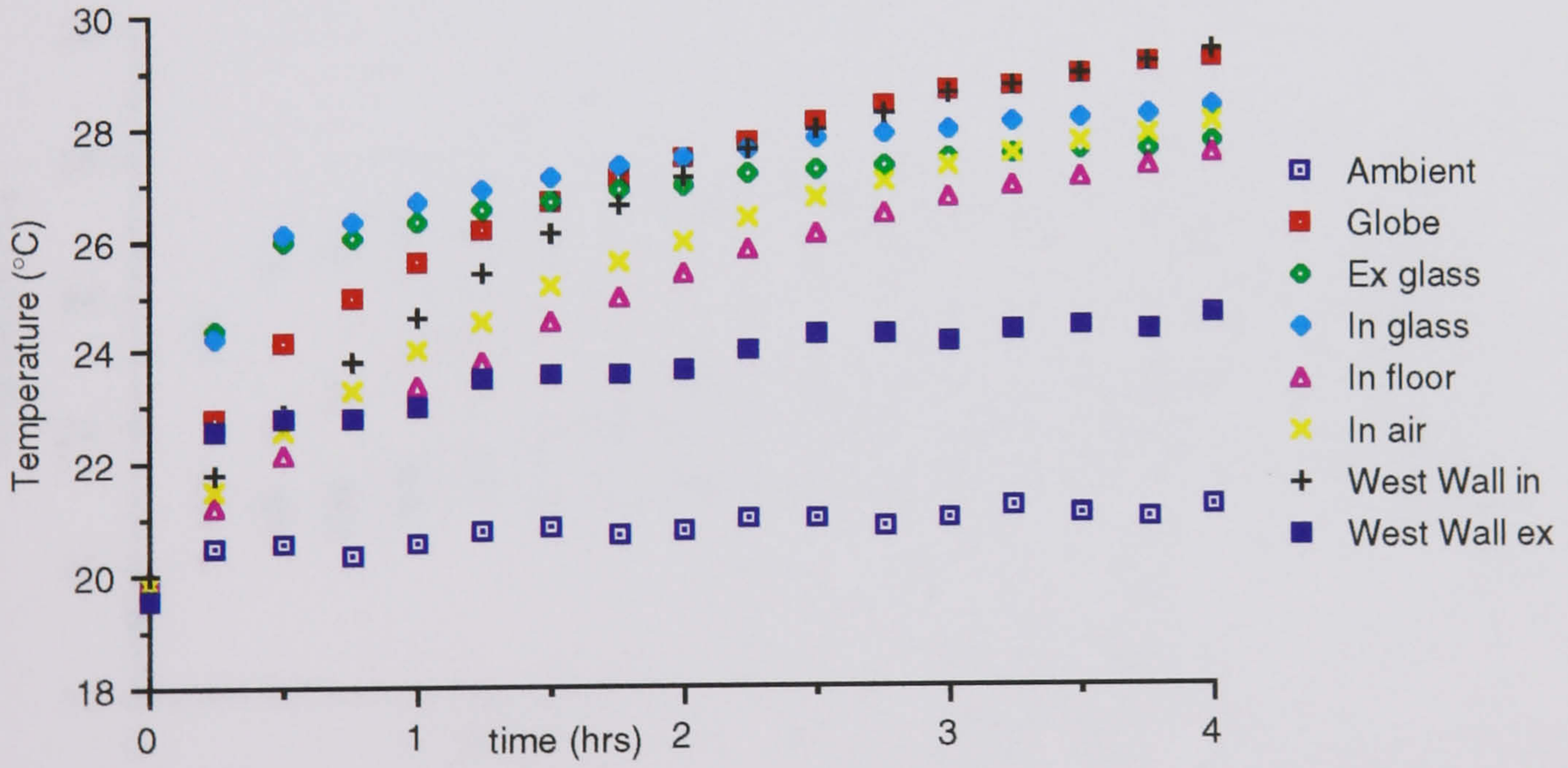

Fig 5.73 Temperature rise over 4 hours for a absorptive film with insolation at 50° angle of incidence

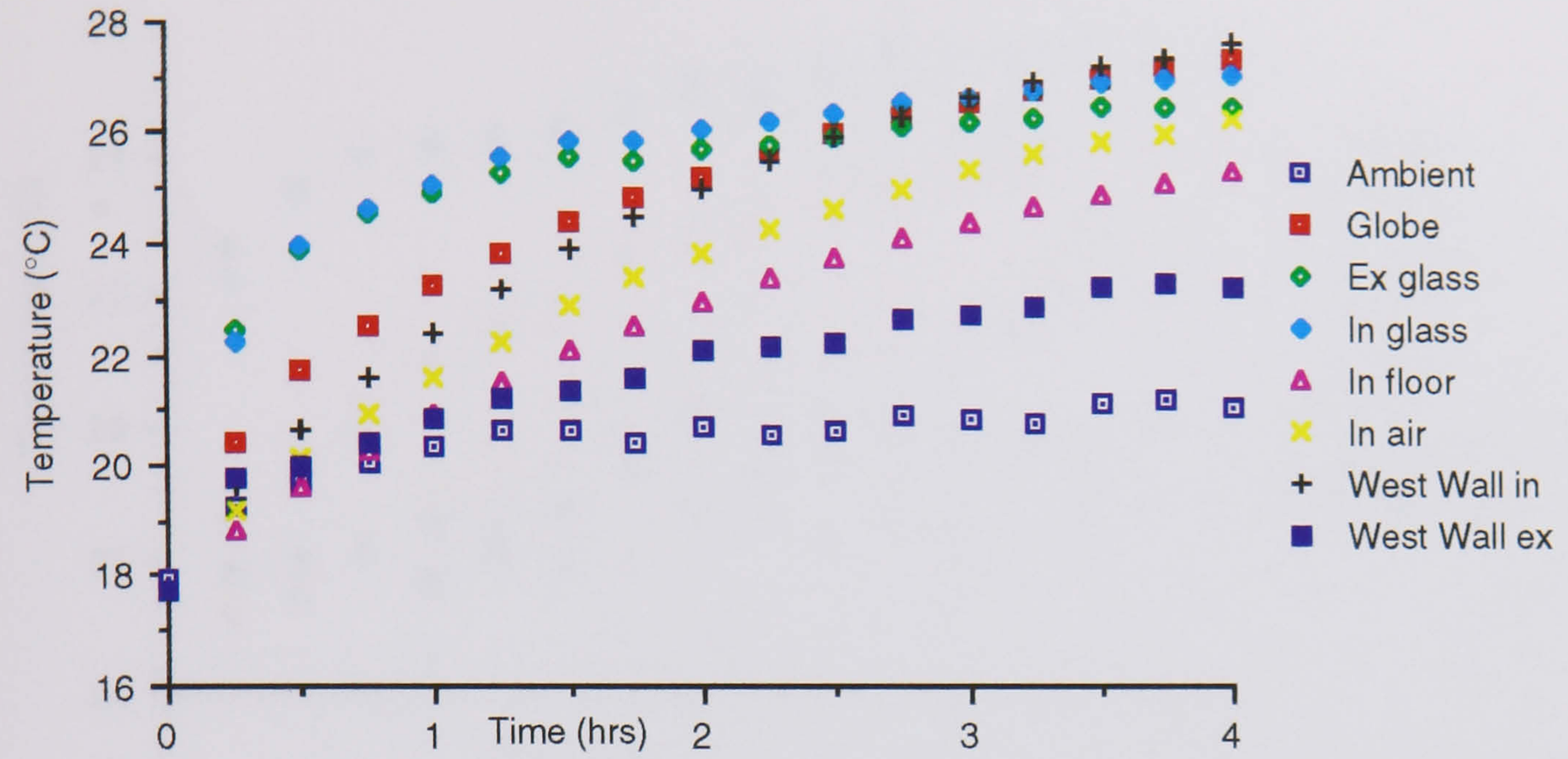

Fig 5.74 Temperature rise over 4 hours for a absorptive film with insolation at 60° angle of incidence

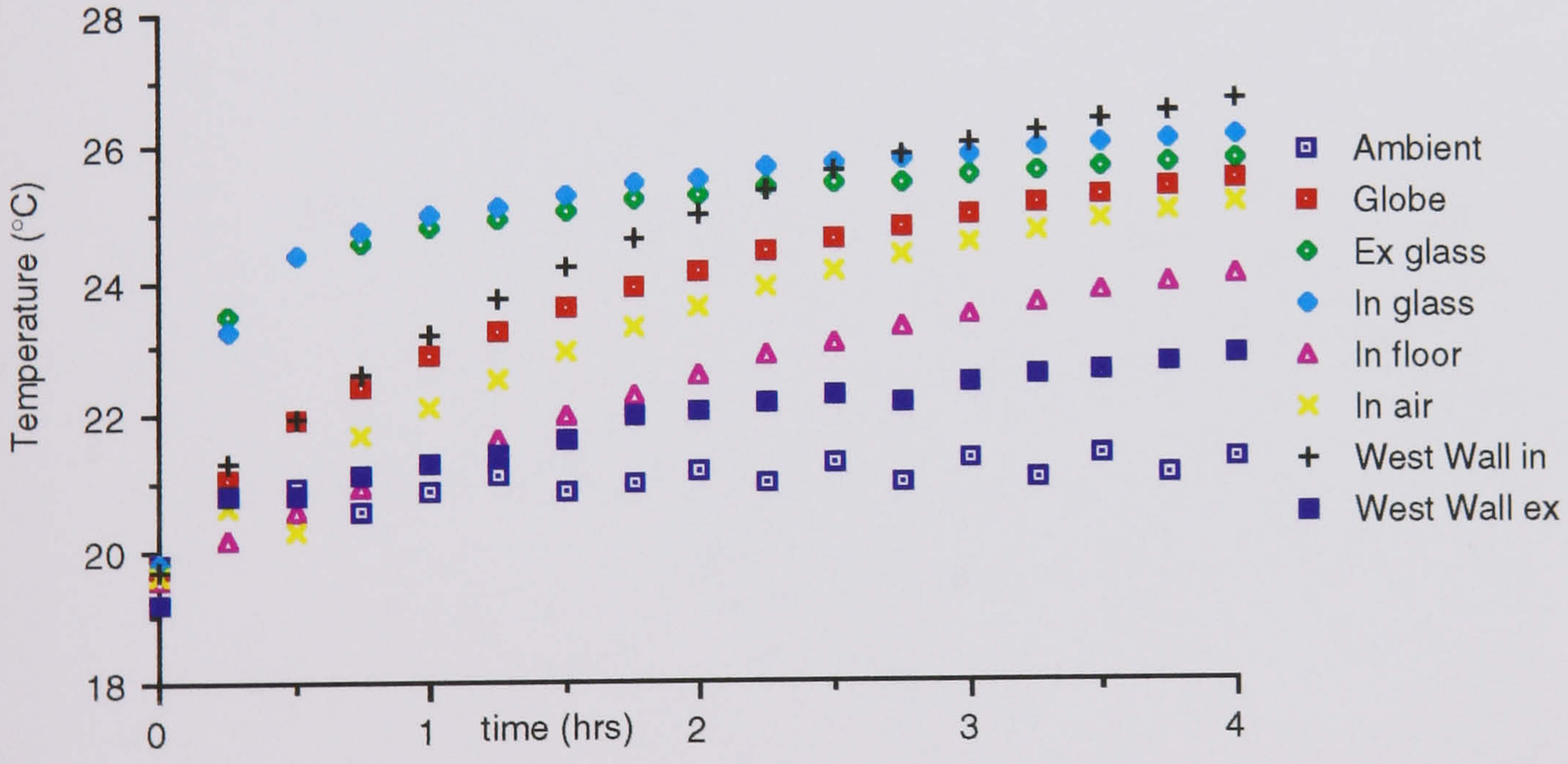

Fig 5.75 Temperature rise over 4 hours for a absorptive film with insolation at 70° angle of incidence

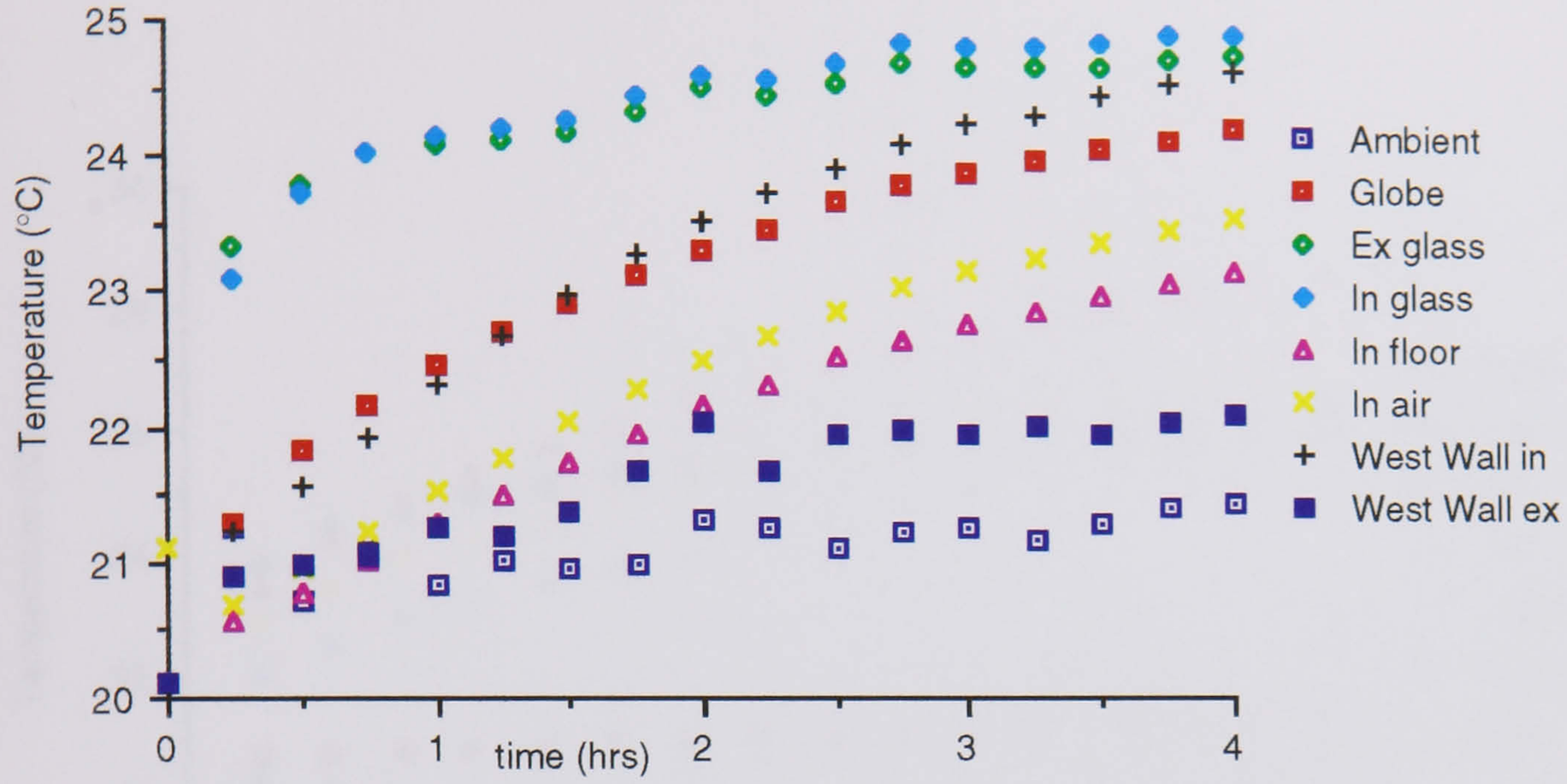

Fig 5.76 Temperature rise over 4 hours for a absorptive film with insolation at 80° angle of incidence

5.5.2 Computer Results

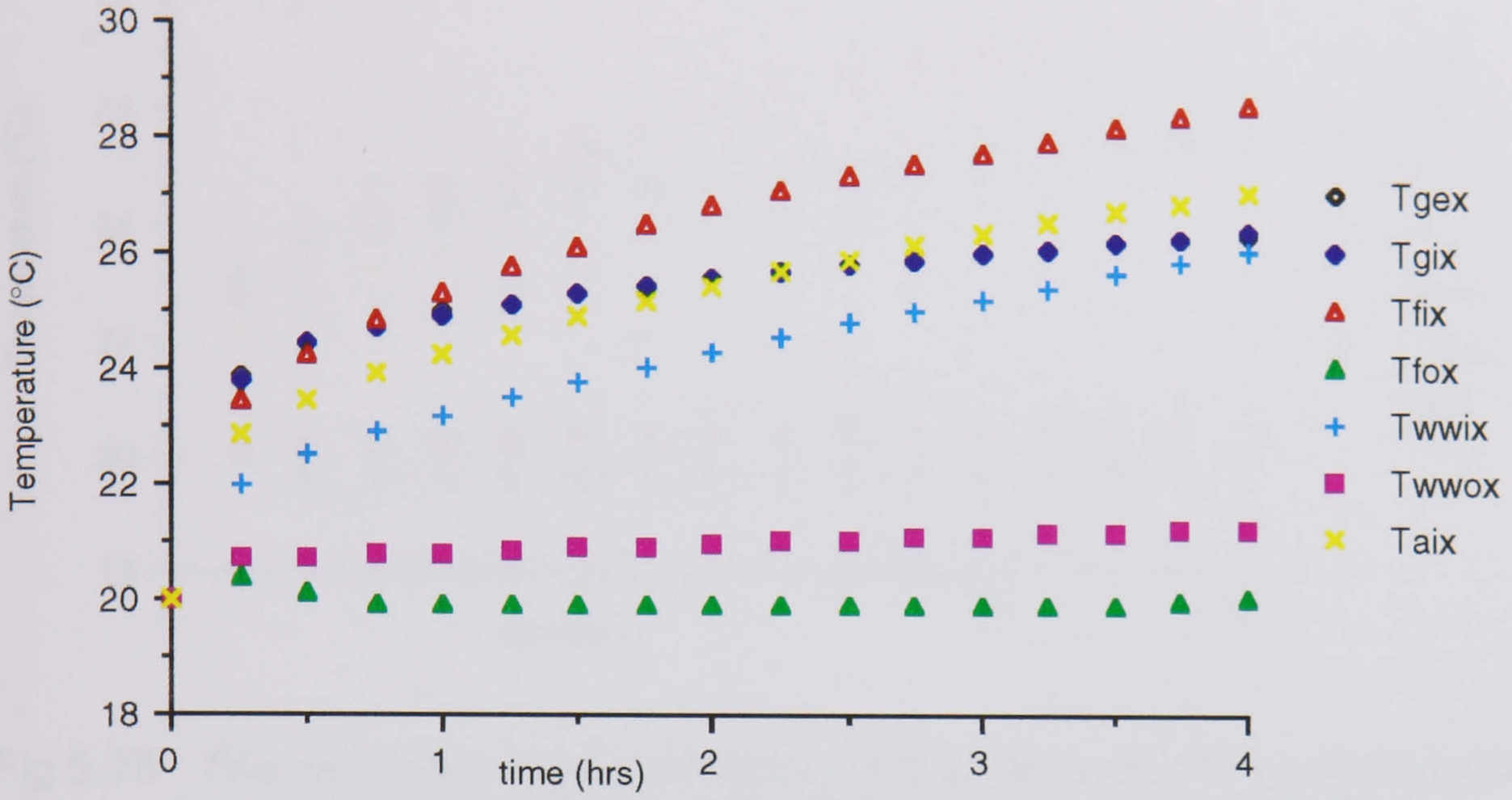

Fig 5.77 The computer model prediction of the temperature rise over 4 hours for a absorptive film with insolation at 0° angle of incidence

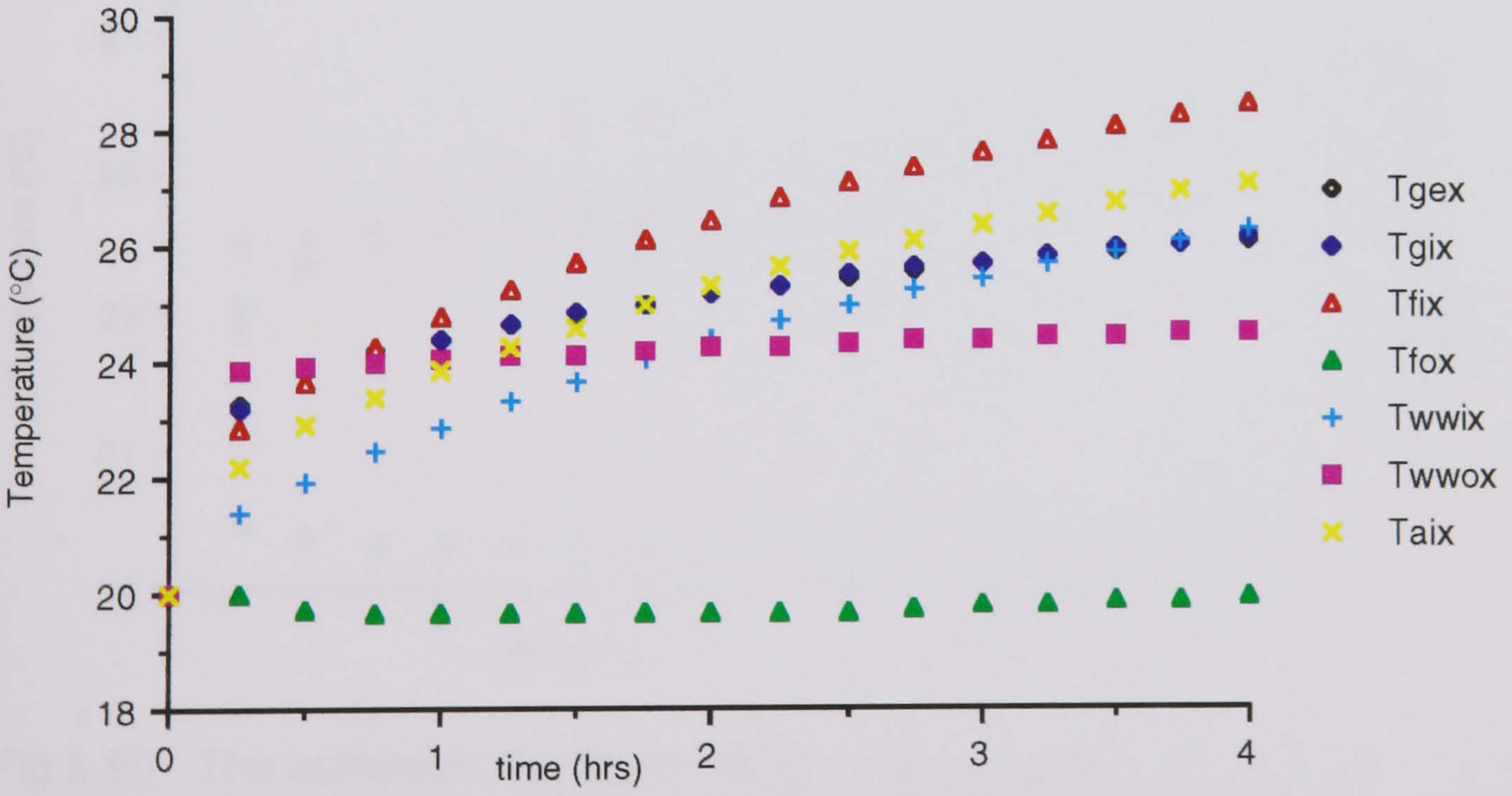

Fig 5.78 The computer model prediction of the temperature rise over 4 hours for a absorptive film with insolation at 0° angle of incidence where insolation is received by the outside also

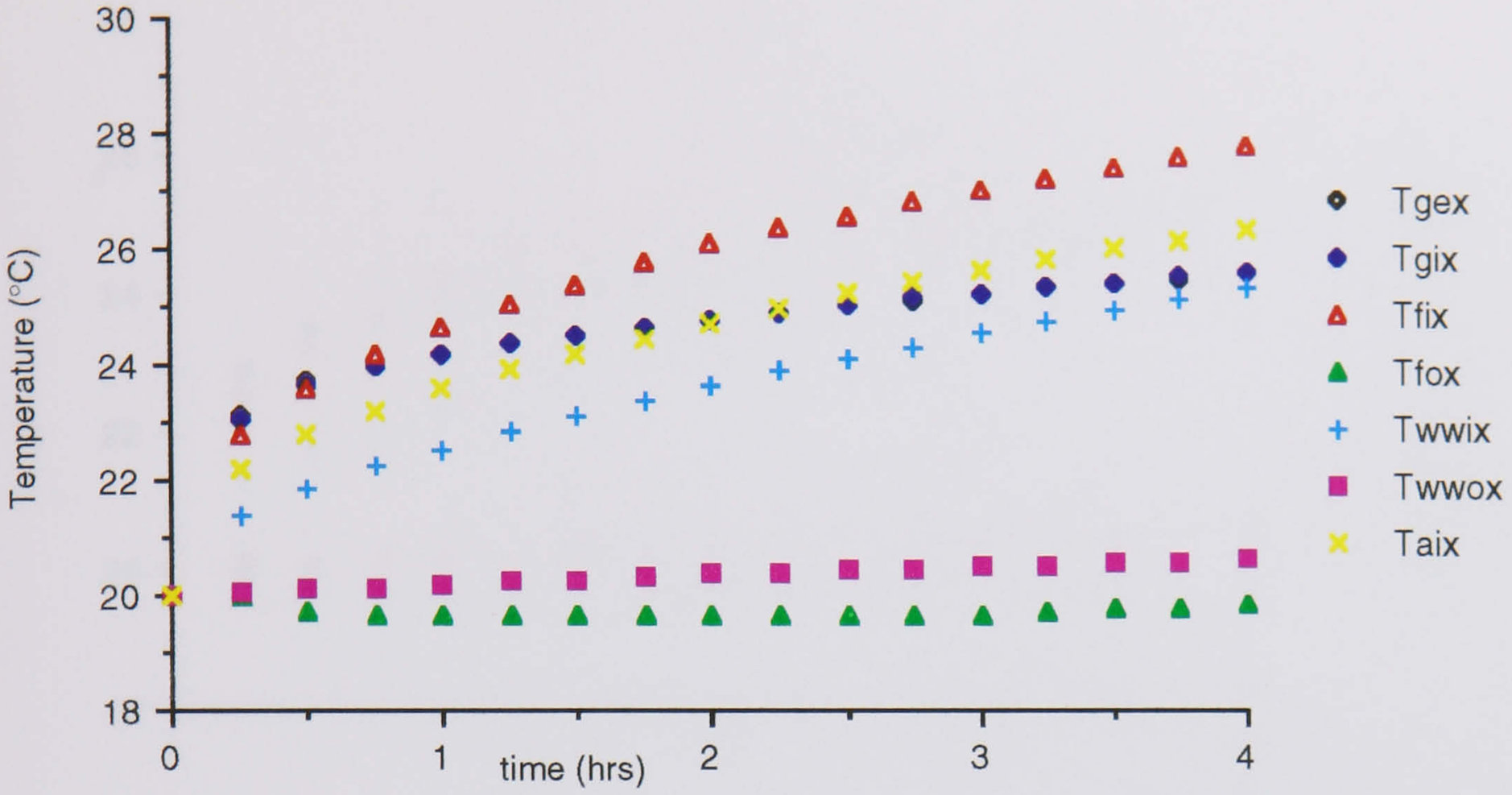

Fig 5.79 The computer model prediction of the temperature rise over 4 hours for a absorptive film with insolation at 10° angle of incidence

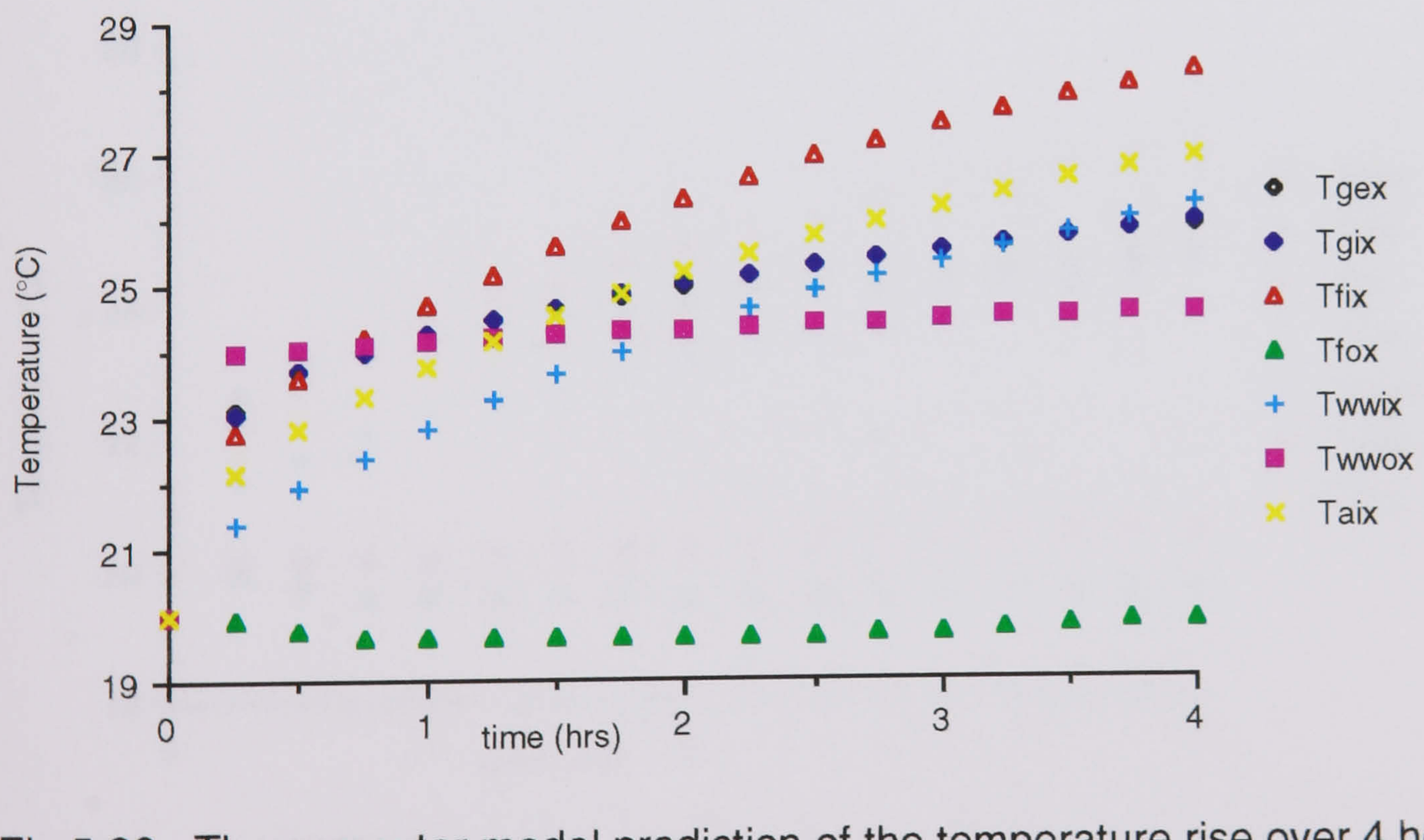

Fig 5.80 The computer model prediction of the temperature rise over 4 hours for a absorptive film with insolation at 10° angle of incidence where insolation is received by the outside also

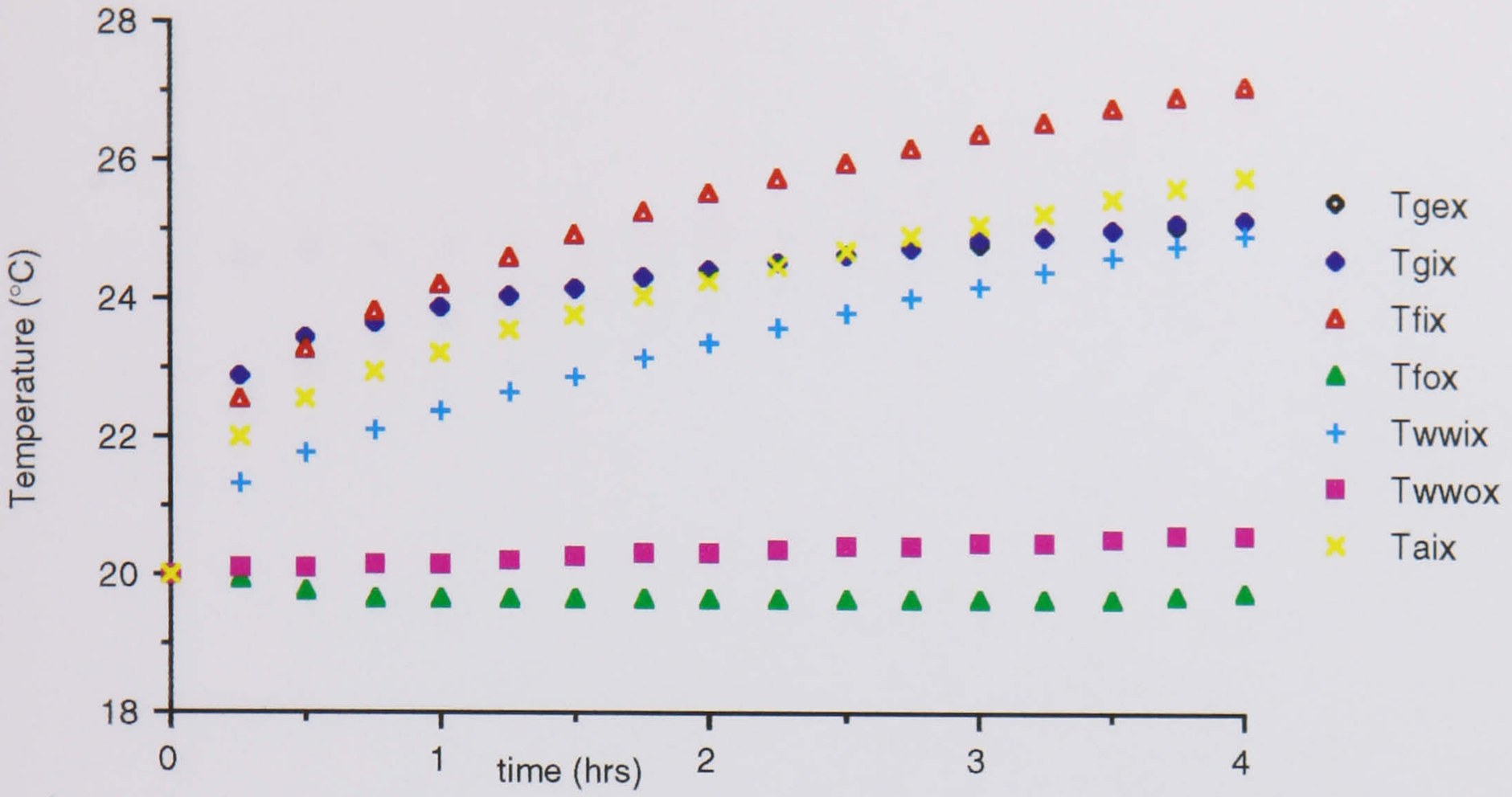

Fig 5.81 The computer model prediction of the temperature rise over 4 hours for a absorptive film with insolation at 20° angle of incidence

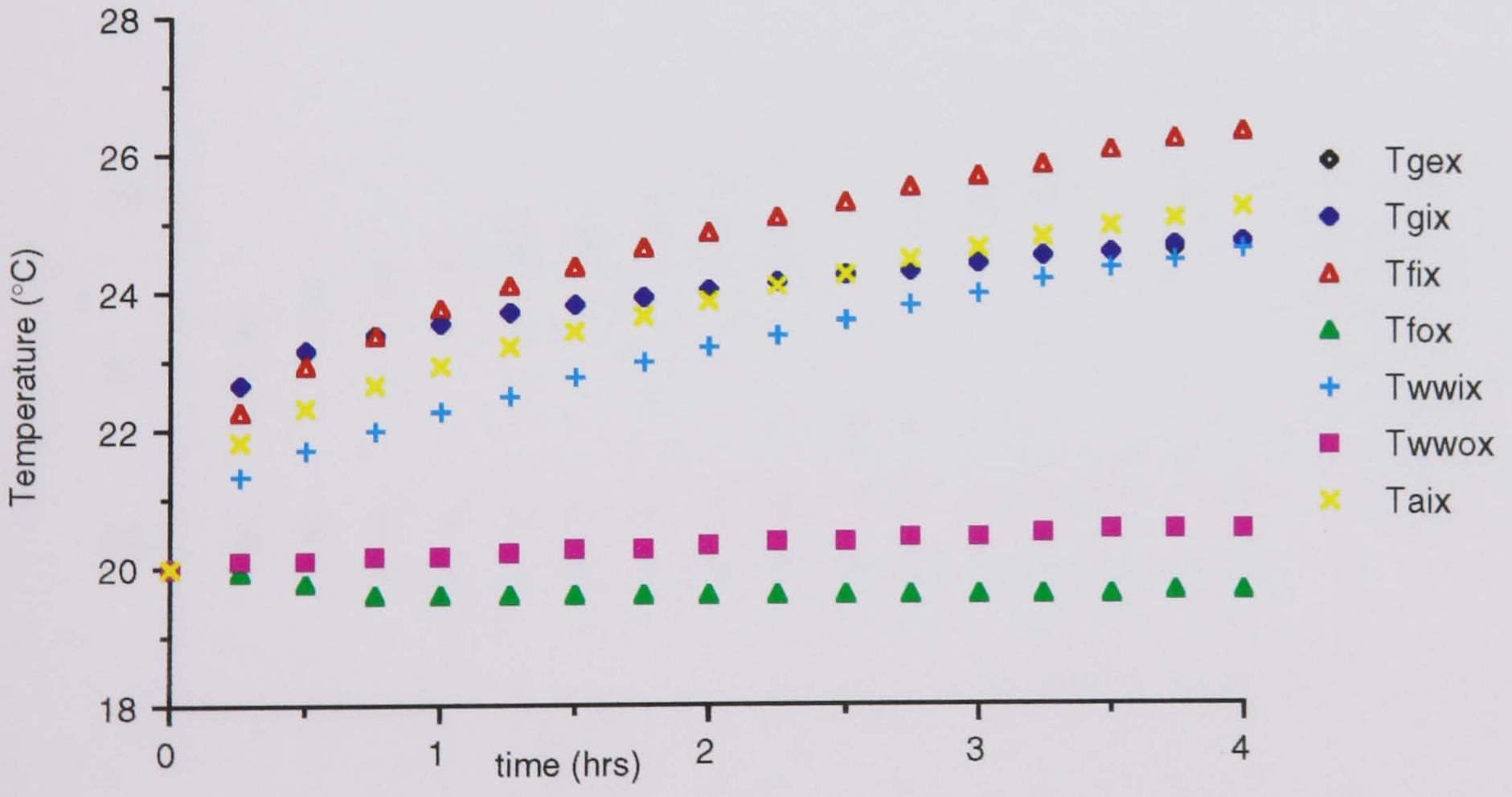

Fig 5.82 The computer model prediction of the temperature rise over 4 hours for a absorptive film with insolation at 30° angle of incidence

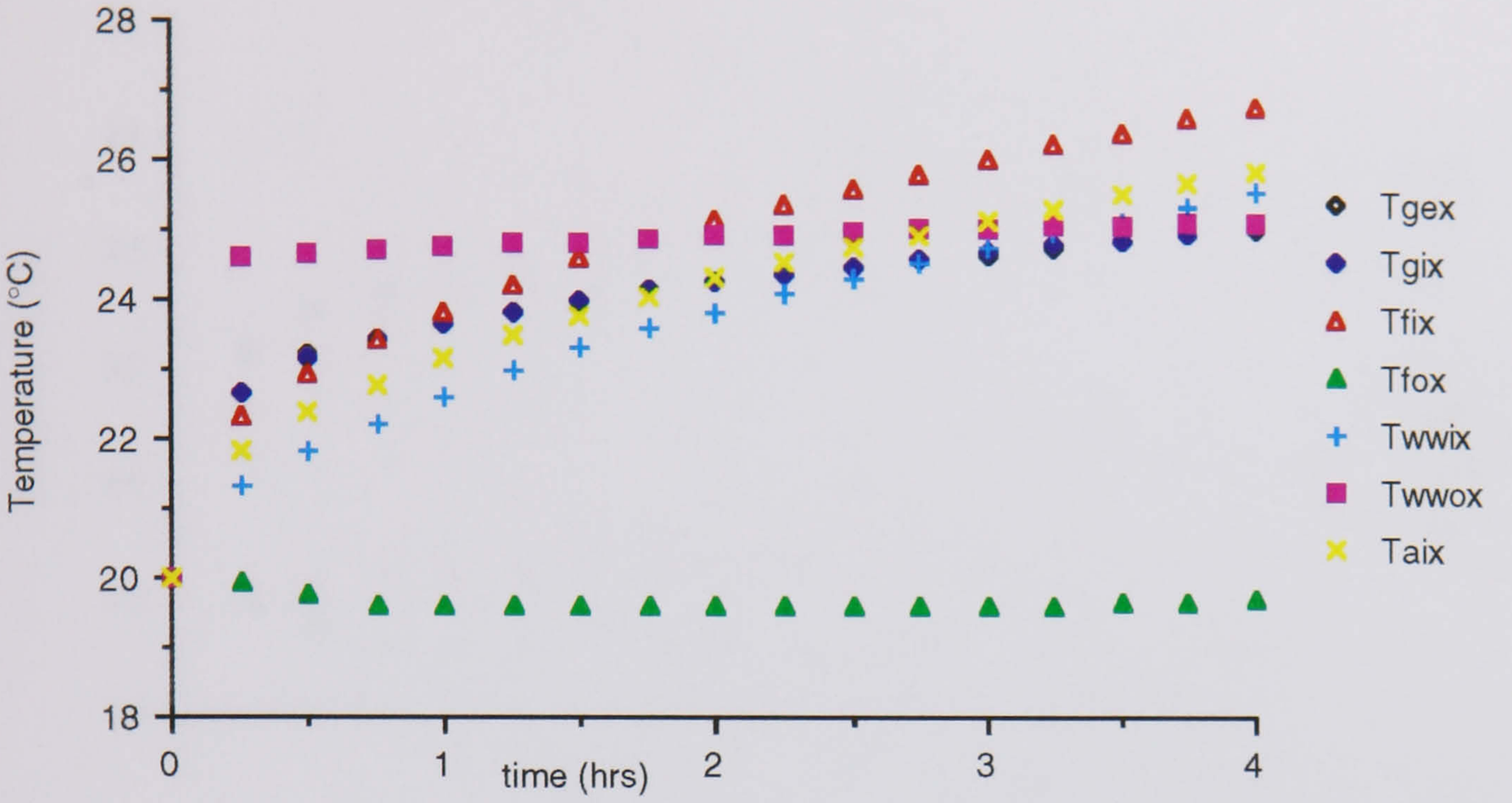

Fig 5.83 The computer model prediction of the temperature rise over 4 hours for a absorptive film with insolation at 30° angle of incidence where insolation is received by the outside also

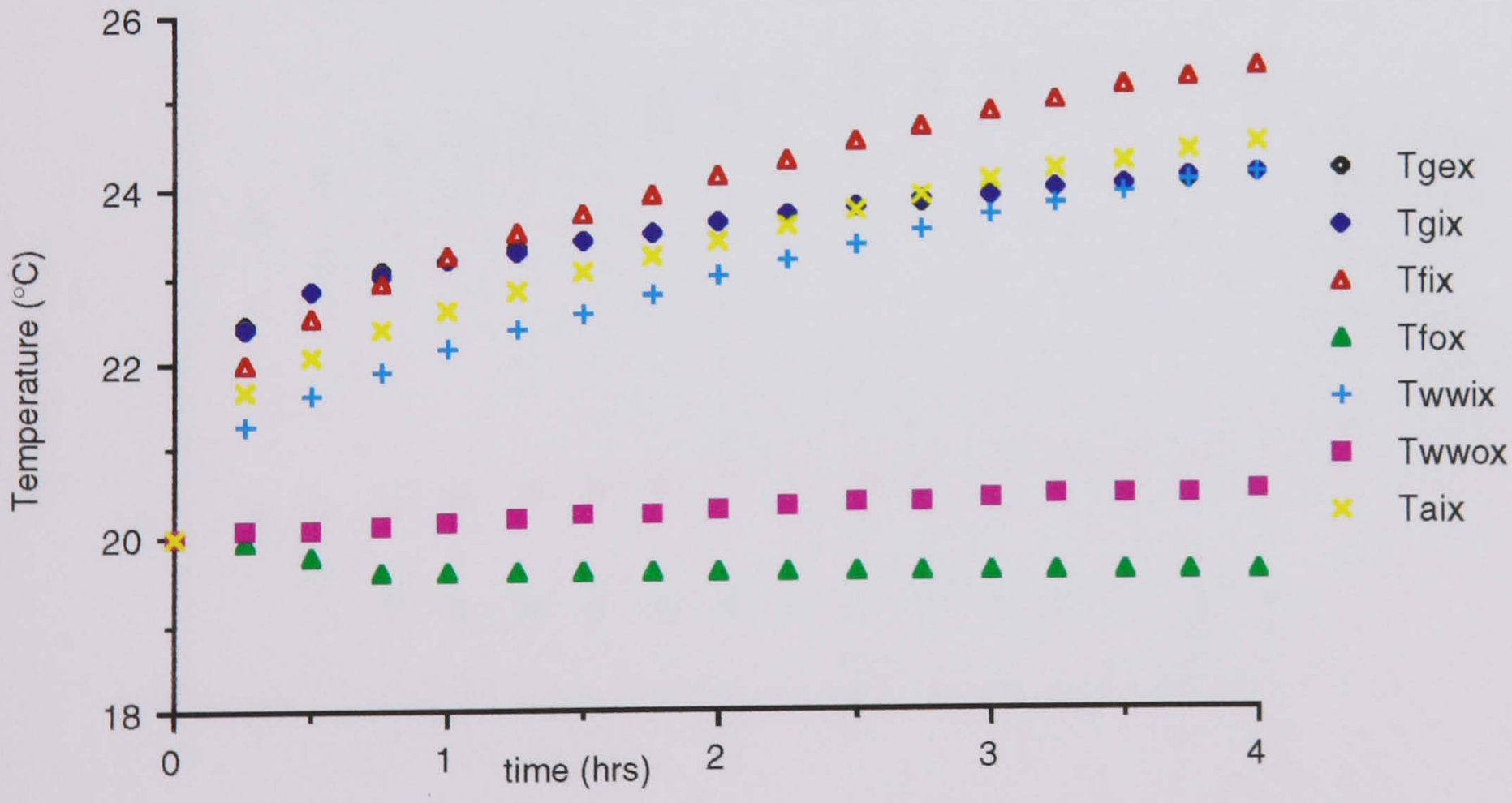

Fig 5.84 The computer model prediction of the temperature rise over 4 hours for a absorptive film with insolation at 40° angle of incidence

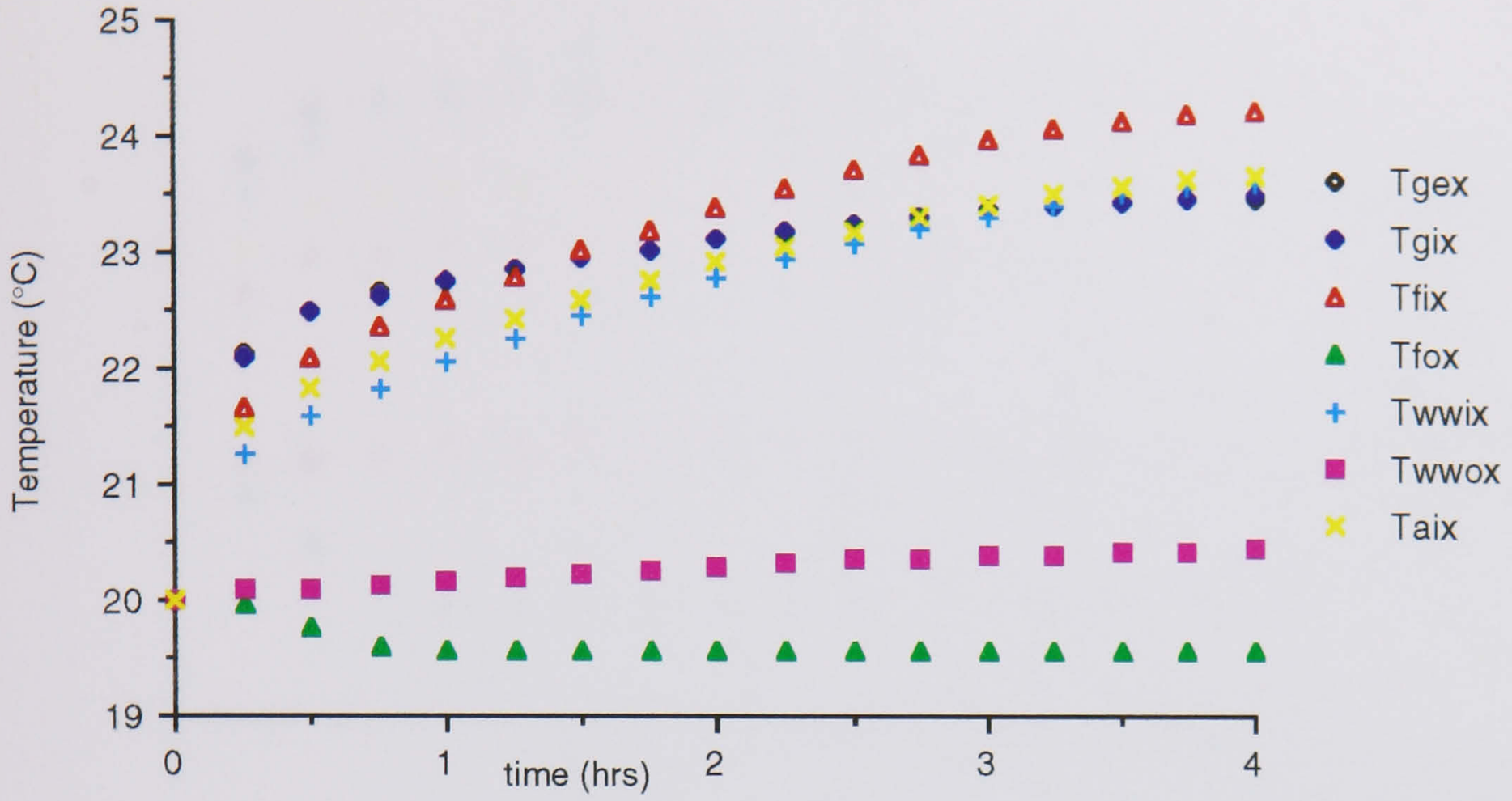

Fig 5.85 The computer model prediction of the temperature rise over 4 hours for a absorptive film with insolation at 50° angle of incidence

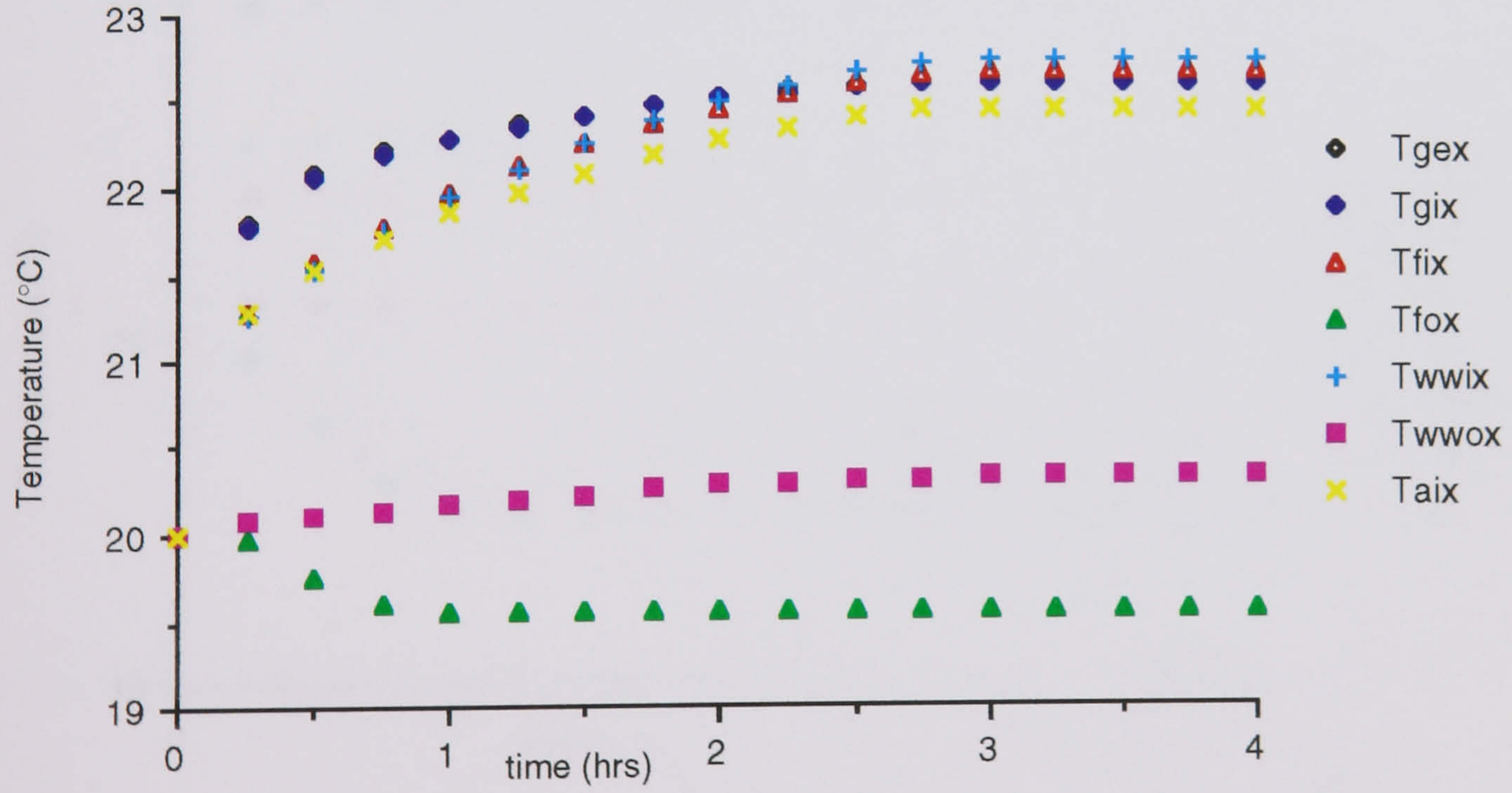

Fig 5.86 The computer model prediction of the temperature rise over 4 hours for a absorptive film with insolation at 60° angle of incidence

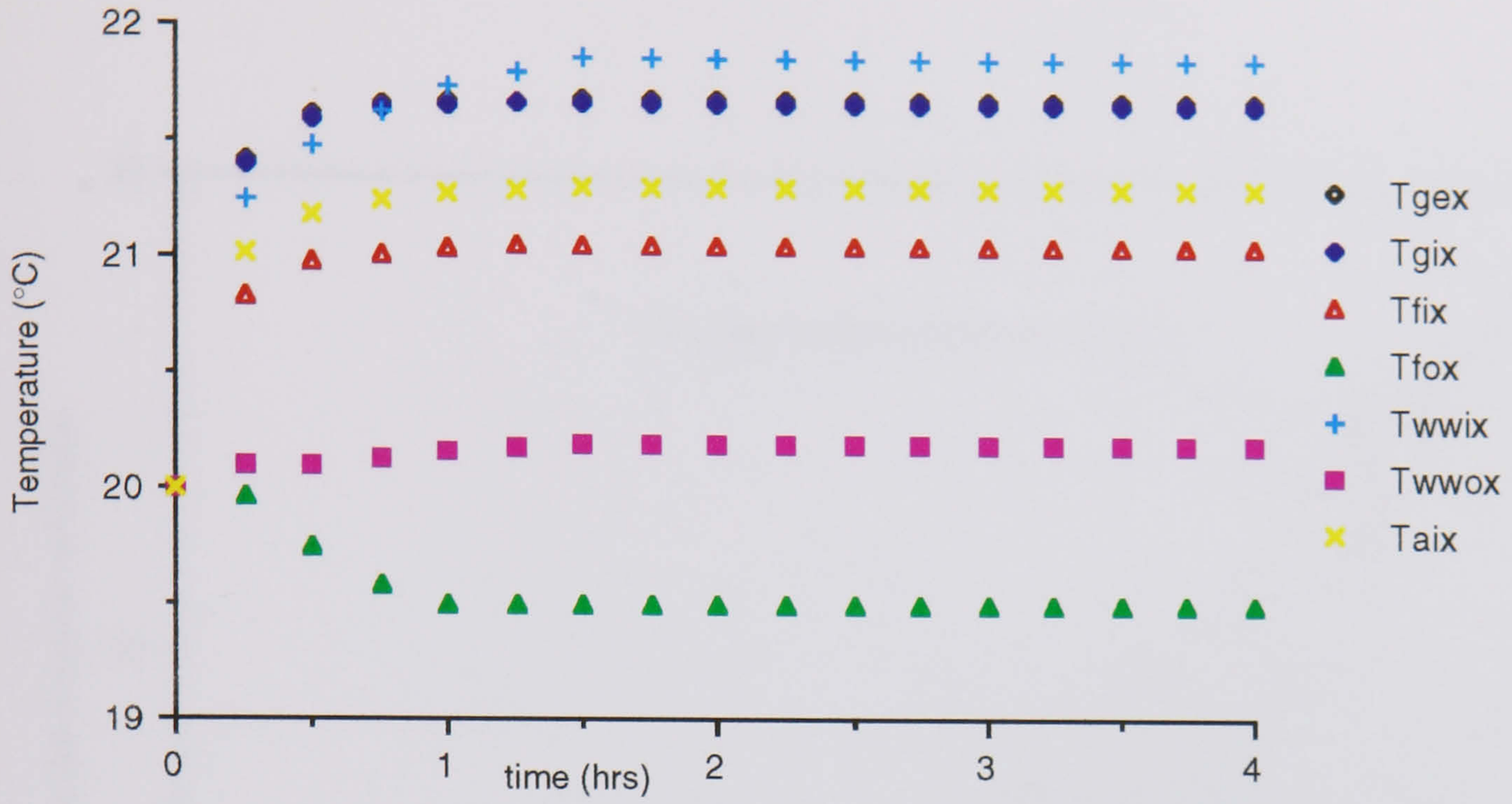

Fig 5.87 The computer model prediction of the temperature rise over 4 hours for a absorptive film with insolation at 70° angle of incidence

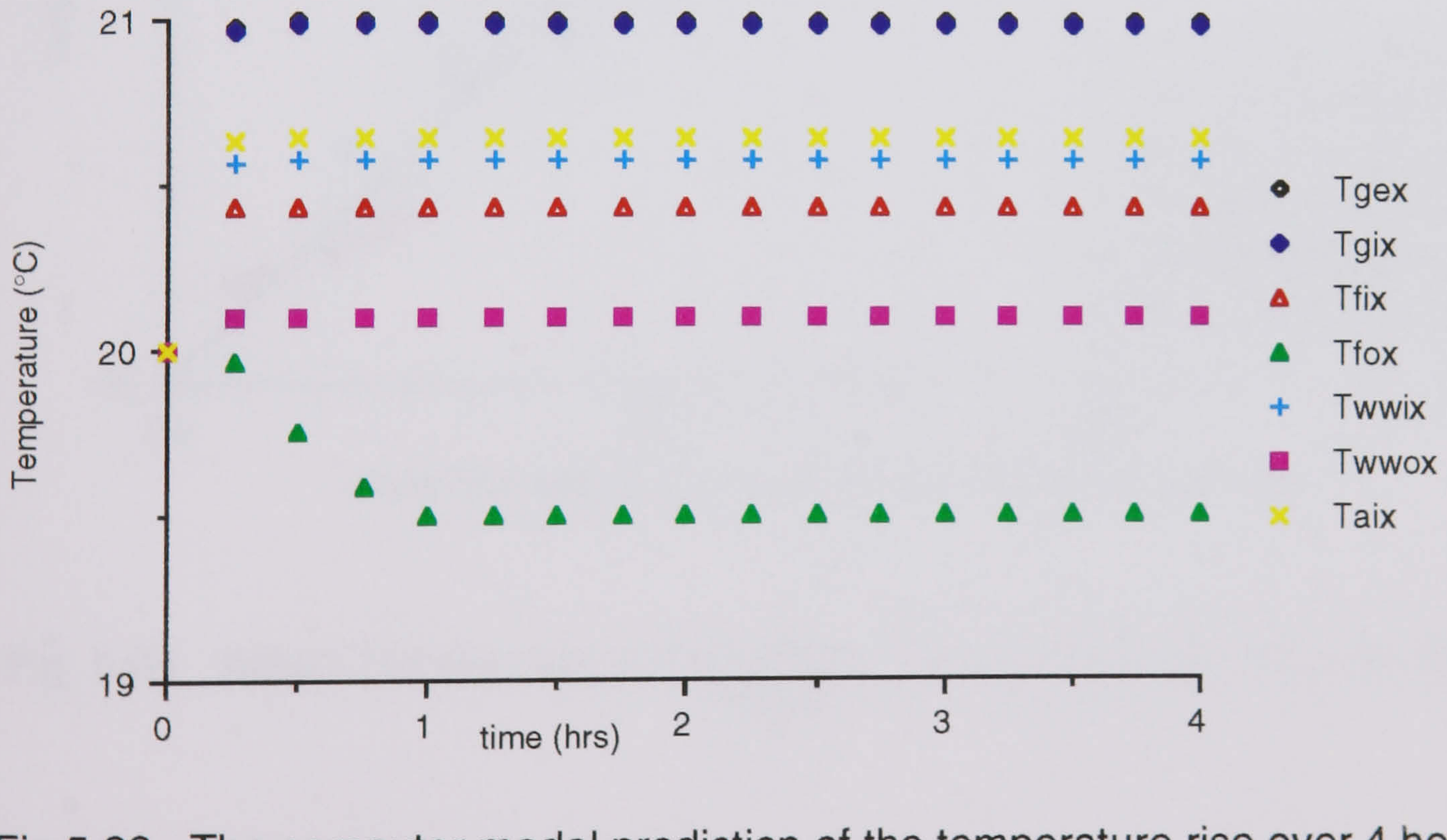

Fig 5.88 The computer model prediction of the temperature rise over 4 hours for a absorptive film with insolation at 80° angle of incidence

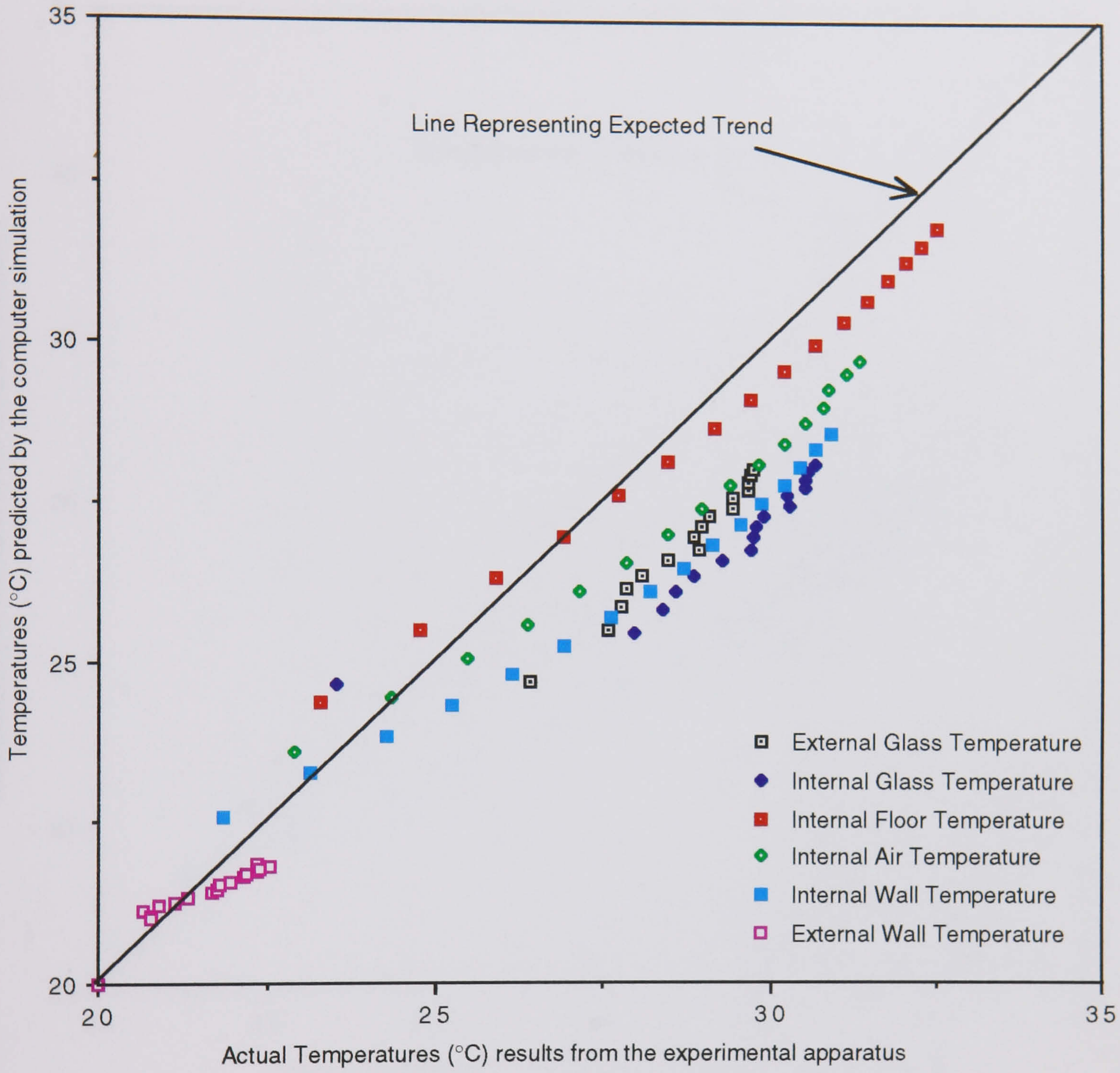

Fig 5.89 Actual Temperatures vs Predicted Temperatures for the clear float glass

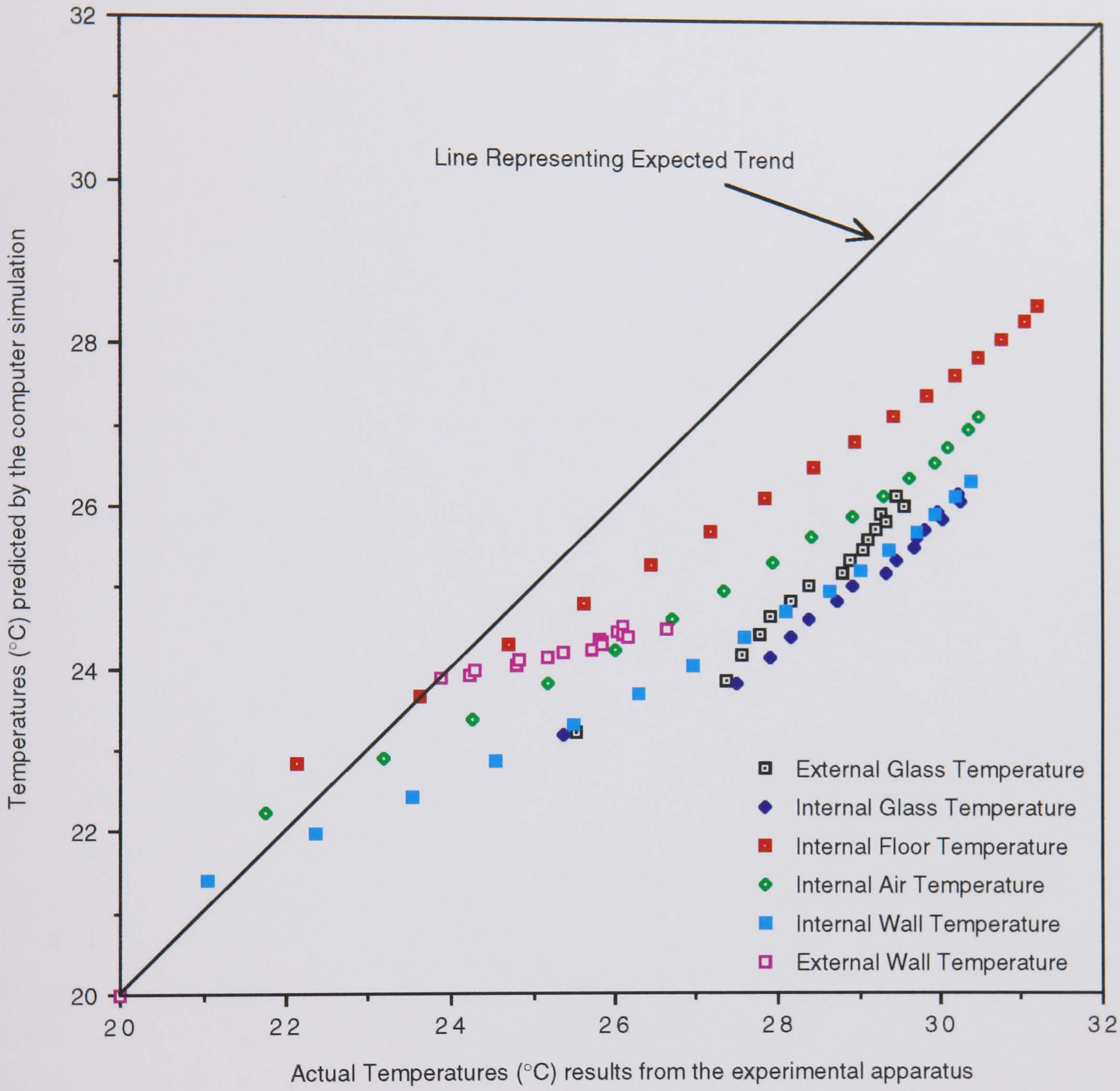

Fig 5.90 Actual Temperatures vs Predicted Temperatures for the absorptive film

BLANK IN ORIGINAL

Chapter 6

6.1 Discussion of Results

The design of the experimental apparatus gave rise to discrepancies due to its size once the angle of incidence was set above 10°. As the lamp was rotated away from a position, orthogonal to the glass, the amount of energy from the lamp which was incident upon the side of the box, increased. To avoid this, the exterior walls of the illuminated hot box were shielded. However, this then caused a packet of warm air to develop between the shielding and the hot box. This warm air caused anomalies in the data, where the outside surfaces of the box were hotter than the inside surfaces for a period after the experiments had started. It was decided that the shielding, which was added to the experimental hot box, should be included within the computer based model. As can be seen in the graphs for clearfloat, a good correlation occurred between the experimental results and those of the computer modelling, for the angles of incidence where shielding was present, see Figures (5.6 compare with 5.16, 5.8 compare with 5.19 & 5.9 compare with 5.21).

The results of the computer program did not correlate with the experimental data as well as had been hoped. This could be partly explained by the use of the manufacturers data of transmittance, reflectance and absorptance. This was due to a lack of knowledge at the time, concerning the absorptance index and refractive index of the films tested. Furthermore, several key assumptions were introduced so that the film system could be modelled. An attempt to model the actual film was not included within the computer program. Such a model would have required using a time increment of 1×10^{-6} seconds to secure stability. The limiting factor causing such a low time increment was the extreme thinness of the film itself. A time increment of 0.25 seconds was used within the program, prior to extending the model to examine samples of glass with films attached. A decision had to be taken to simplify the glass/film modelling. It was then decided to model the films thermal performance, that is, their thermal conductance, as part of the thermal conductance of the glass. This was done by using an effective thermal conductance of the glass and film. The emissivity of the internal glazing surface was then set to that of the film being tested. Although this simplified and reduced the conductive resistance to heat flow through the glass, it was considered to be a reasonable way of overcoming the problem, caused by the implied very small increment otherwise required. The time increment would have been less of a problem if an implicit transient model had been employed. However, this was not attempted as it

was desirable for the computer based simulation program to function on a personal computer.

6.2 Analysis of Results

The simulated solar energy transmittance and the thermal radiation, emitted by the window, to the interior space, were extracted from the experimental data obtained. From this data, the total solar energy transmittance could be calculated. Once the total solar energy gain was known, it was possible to calculate the degree of thermal comfort. The shading coefficient was introduced in the 1960s by ASHRAE as a simple and straightforward means of calculating solar gain, as reviewed by Vild (1964), and Smith and Pennington (1964). In 1991 McCluney, stated that the shading coefficient had become an inadequate method of determining the solar gain of a window, and that angle-dependent values of the solar heat gain coefficient were needed to characterise instantaneous or hourly performance.

The determination of the shading coefficient has been explained in depth elsewhere, (ASHRAE 1989). Briefly, it is the ratio of solar heat gain through a glazing system under a specific set of conditions, to the solar gain through a single light of reference glass under the same conditions. Within the ASHRAE guide, the measure of solar heat gain used to determine the shading coefficient, is determined by the sum of the directly transmitted solar energy, and that portion of the solar energy, which is absorbed and is then transmitted into the internal environment. The inward flowing fraction is determined by the thermal transmittance of the glazing system divided by the coefficient of heat transfer from the glass to the external environment. Therefore, the figure obtained is heavily dependent upon the velocity of the external air at the glass surface. Due to controlled conditions which were established within the laboratory, the heat loss from the external surface was driven by buoyancy convection and thermal radiation heat transfer only. Shading coefficients determined, from the experimental results, using the ASHRAE procedures, did not bear any resemblance to those stated by the manufacturer. This led to the development of a new procedure, to determine a coefficient of total solar energy gain which could be used to determine the shading coefficients of the films tested.

The heat admission through glass, q_{TOT}, can be calculated as shown in Equation 6.1.

$$q_{TOT} = I\tau + h_{rgi}\left(T_{gi} - T_{globe}\right) + h_{cgi}\left(T_{gi} - T_{ai}\right) \qquad (6.1)$$

where all the temperatures can be obtained from the experimental apparatus, and the coefficients of heat transfer can be determined using the equations below,

$$h_{rgi} = \sigma\varepsilon_{gi}A_g\left(T_{globe} + T_{gi}\right)\left(T_{globe}^2 + T_{gi}^2\right) \qquad (6.2)$$

$$h_c = \frac{Nuk_f}{L} \qquad (6.3)$$

where the Nusselt number, Nu, is determined by

$$Nu = 0.27Ra_L^{1/4} \qquad (10^5 \sim < Ra_L \sim < 10^{10}) \qquad (6.4)$$

and the Rayleigh number, Ra, is the product of the Grashof and Prandtl numbers, see Equation (6.5).

$$Ra_L = Gr.Pr = \frac{g\beta\left(T_{gi} - T_{ai}\right)L^3}{\nu\psi} \qquad (6.5)$$

These equations are the same as those used to determine the heat flux within the computer model, and so this allowed the computer model to be set up to determine the heat gain through glass.

The temperatures which were obtained from the illuminated hot box were used to determine figures for the total heat admission through glass. Due to the arrangement of the experimental apparatus, it can be assumed that the heat flow through the glass was a result of the internal environment being warmer than the external environment. Therefore the total heat admission was a result of solar gain alone. In using Equation (6.1), a figure of solar gain, q_{TOT}, for clearfloat glass and the films, could be obtained. The total solar gain for clearfloat glass and the films were determined from the experimental results. This having been done, a ratio of the total solar gain for the film, divided by that of clearfloat glass was obtained. These are shown in Table 6.1, along with the coefficient of total solar energy gain, which was calculated from the results of the computer based simulations, and the manufacturers given figure for the shading coefficient.

The total solar gain is critical in determining the size of the air-conditioning equipment. Therefore, by measuring the degree of total solar energy gain for angles of incidence between 0° and 80°, for a solar-control film, and comparing it to ordinary single glazing, a comparison can be made with other window films. Although the results for the insulating and reflective films did not match those given by the manufacturer (this being a result of the manufacturers unwillingness to disclose information concerning the refractive index and the absorptive index of the films) the result obtained for the absorptive film showed close agreement with the manufacturers stated shading coefficient. It was pleasing to see the similarities between the experimental results and those obtained from the computer modelling. The coefficient of total solar energy gain was calculated using the temperatures obtained from the computer based simulation. The physical properties of the films needed to obtain the coefficient, that is, the solar transmittance and internal surface emissivity, were the same as those used to obtain the coefficients from the experimental data. From this, it can be concluded that, even though the temperatures achieved during the computer based modelling were not as high as those measured during the experiments using the illuminated hot box, the predicted amount of energy being received by the internal environment from the lamp was proportionally the same. Therefore it can be concluded that the results obtained from the experiments using the illuminated hot box gave reasonable comparisons of the different types of solar-control films. However, the results obtained for the reflective and insulating films were consistently higher than those quoted by the manufacturer.

Film Type	Solar Gain of Film / Solar Gain of Glass from the experimental results	Solar Gain of Film / Solar Gain of Glass from the computer modelling results	Shading Coefficient as given by Manufacturer
Clearfloat	1	1	1
Reflective Film (RS220)	0.34	0.44	0.24
Absorptive Film (AT50)	0.79	0.74	0.8
Insulating Film (SB340)	0.56	0.56	0.39

Table 6.1 Comparison of measured solar gain with manufacturers figure of shading coefficient;

The coefficient determined for the total solar energy gain of the solar-control film can further be enhanced by adopting the 'coolness index'. The coolness index was developed at Lawrence Berkeley Laboratories, California (Arasteh, et.al. 1986), as a

means of measuring the overall thermal and lighting performance of a fenestration system. The shading coefficient and the coefficient of total solar energy gain both give a good indication of the thermal performance of a piece of glass. However, two different films may have the same total solar gain, but one will emit more daylight than the other. The coolness index describes the relationship between the thermal performance and the visible light transmittance for a given glazing. Figure 6.1 shows the calculated coefficients of total solar energy gain for the three films tested, along with the manufacturers given shading coefficients for a number of solar-control films, normalised against clear glass, vs light transmittance, at zero angle of incidence. The diagonal lines represent the coolness index.

It is interesting to note that the calculated coefficients of total solar energy gain which were plotted on the graph fell within their groupings, with the exception of the insulating film, SB340. It is also interesting to note that the absorbing films tend to have a low 'coolness index', that is, there is a greater reduction in light transmittance compared with the solar energy transmittance. The reflective films and the insulating films are seen to cluster together, demostrating the fact that they are similar films, as was discussed in Chapter 1. It can also be noted that the insulating films have a coolness index of about 1, which shows that light transmittance has not been sacrificed, where a reduction in the solar transmittance has been achieved.

The coolness index is calculated as the visible transmittance divided by the shading coefficient, or in the case shown in Figure 6.1, the coefficient of total solar energy gain. Where a glazing has a low coolness index, this is a result of a reduction in the solar gain achieved, with a penalty in the reduction of visible light. A high coolness index means that light is not sacrificed for solar control. However, this theory falls down because a high coolness index may be obtained by a film with a low shading coefficient and low visible transmittance.

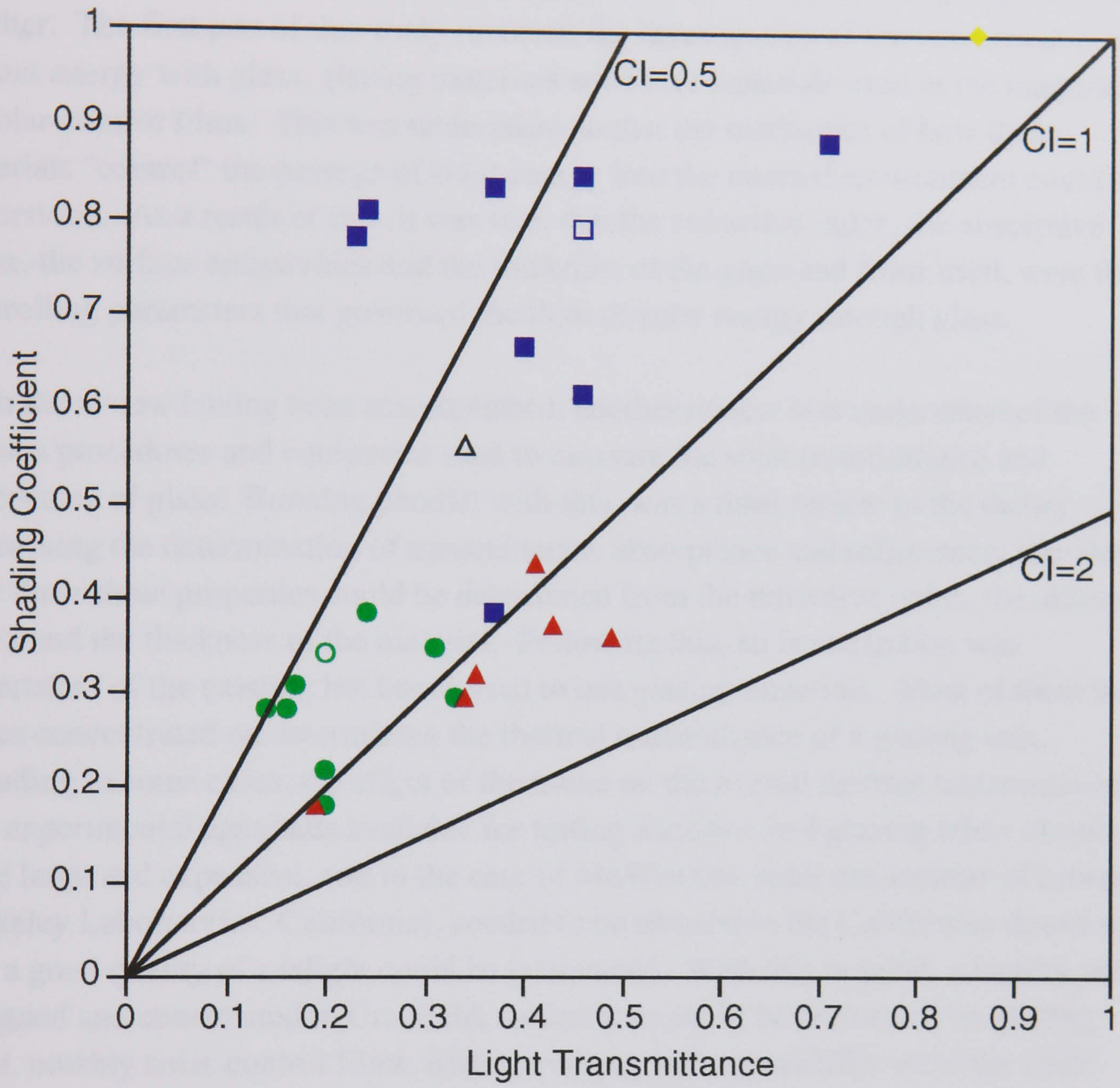

Figure 6.1 Shading Coefficient vs Light Transmittance for solar-control films at 0° angle of incidence;

6.3 Conclusion

The aim of this project was to design, build, test and verify a simple, laboratory based illuminated hot box so that solar-control films could be tested and compared with one another. The first part of this study involved the investigation of the interaction of solar radiant energy with glass, glazing materials and those materials used in the manufacture of solar-control films. This was undertaken so that the mechanics of how these materials "control" the passage of solar energy into the internal environment could be understood. As a result of this, it was seen that the refractive index, the absorptive index, the surface emissivities and the thickness of the glass and films used, were the controlling parameters that governed the flow of solar energy through glass.

With the review having been accomplished, another review was undertaken of the various procedures and equipment used to measure the solar transmittance and reflectance of glass. Running parallel with this, was a third review of the theory concerning the determination of transmittance, absorptance and reflectance, showing how these three properties could be determined from the refractive index, the absorptive index and the thickness of the material. Following this, an investigation was undertaken of the existing hot boxes used to test glazing materials. Most of these hot boxes concentrated on determining the thermal transmittance of a glazing unit, including in some cases, the effect of the frame on the overall thermal transmittance. The experimental apparatus available for testing windows and glazing when illuminated were large and expensive, and in the case of MoWitt (the solar calorimeter of Lawrence Berkeley Laboratories, California), needed to be situated in the Californian desert so that a good quality of sunlight could be guaranteed. With this in mind, a facility was designed and constructed in Cranfield, so that tests could be performed on glazing units, notably solar-control films, where accuracy and repeatability were the main criteria.

Once the illuminated hot box apparatus had been built and the power supply regulated, a number of tests were run using one sample of glass under the same conditions. The results obtained showed a high level of repeatability, and so a number of tests were carried out, these being documented in Chapters 3 and 5. To gain an understanding of the accuracy of the results, a computer program was written which modelled the experimental apparatus. The results which the computer model provided were used to calculate a coefficient of total solar energy gain, although there were some discrepancies between the predicted and the actual results. These results were compared with those achieved from the experimental data and showed that the experimental results could be taken as valid.

The discrepancies between the experimental results, the computer modelling results and the manufacturers data may be explained by the fact that information concerning the

absorptive index and the refractive index of the films was unknown, and that for the reflective and the insulating films, figures for the emissivities had to be assumed. The emissivities used were determined from information found in the text by Johnson, (1991). Further simplifications and assumptions which were established when developing the computer model, may have enhanced the errors caused by not knowing the emissivities of certain films, and the refractive and absorptive index of all the films tested. Although much emphasis has been placed on the problems arising from the experimental procedures which may have led to possible experimental errors, this does not imply that the computer predictions are perfect. However, it is felt that the results obtained were the best possible, from the methods used and the equipment available.

As well as the shortcomings of the experimental apparatus which were documented within the text, it should be noted that the size of the box was limited by a number of factors that may have led to the discrepancies within experimental results. These limiting factors include the length of the lamp available for this study (645mm long), and its control equipment which needed to be mounted on strong arms. This meant that the box had to fit between the arms. The depth of the illuminated hot box was kept as small as possible to hinder convection cells developing within the box, while at the same time being deep enough to accept a solarimeter. Finally, the size of the films supplied by the manufacturers limited the glazing test area to 600mm by 600mm. In retrospect, two different rigs could have been built; the first rig using the solarimeter to measure solar transmittance and the second rig then being a vertical hot box, which would have allowed the testing of glazing samples in a more realistic environmental situation, that is vertical, with the possibility of more accurate results.

The use of solar-control films in buildings is one of great debate. There is a need to reduce the global energy consumption, and although much effort has been put into energy use in new buildings, the main need is in reducing energy consumption within existing buildings. Horie (1980), stated that daylight is the most variable of all light sources; it varies in intensity, colour, direction, and diffusiveness. To employ such a simple device as a solar-control film involves considerable compromises. Whether or not solar-control films are an effective and economic means of achieving a reduction in energy consumption is not within the scope of this study. However unless a total replacement of the glazing of a building is considered, solar-control films offer only a partial solution in reducing the total solar energy gain of a building. A number of conclusions can be drawn from the results, and used to compare the thermal and visual performance of the films. From this comparison, uses for the different films have been highlighted.

The results showed that all the films reduce the internal temperatures of the illuminated hot box as compared with traditional float glass, see Figures 5.5, 5.26, 5.47 &5.68. The insulating and reflective films showed higher glass temperatures compared with the

absorbing glass, where the globe thermocouple (measuring the mean radiant temperature) and internal surface temperatures were higher. This was a result of a higher solar transmittance for the absorptive film, as compared with the solar transmittance for the reflective and insulating film, see Figures 5.2, 5.3 & 5.4. The higher glass temperatures for the reflective and insulating films highlights the fact that they absorb some of the solar energy incident upon the external glass surface, especially the near infra-red solar energy. The majority of the reflection from the reflective film occurs in the visible part of the electromagnetic spectrum, hence its name. The insulating films tested had a dark, matt finish. It's function is not primarily as a solar-control film, but for reducing the amount of radiant energy from the internal environment of the building which is transmitted to the exterior.

The reflective film tested would be of use on the exterior envelope of a building where a reduction in the cooling load on the air-conditioning plant is required, while at the same time reducing the transmittance of excess daylight, see Figure 6.1, which can cause discomfort for building occupants. The insulating film, while similar in nature to the reflective film, is specifically designed to reduce the flow of energy leaving a building. The matt finish of the insulating film tested would make it suitable for buildings where the reflection of glare and solar radiation to other parts of the urban environment would be hazardous. Examples of hazards include reflected glare, which may cause problems for vehicle drivers, and the reflection of solar energy into other buildings, in so doing causing glare and thermal discomfort for the occupants of the affected building.

The absorptive film tested would be of use in reducing the load upon an air-conditioning system, without a reduction in the quality of daylight transmittance, see Figure 6.1. However, the absorptive film would not be as effective in reducing the load on an air-conditioning system due to the higher mean radiant temperatures which will occur as compared with the use of a reflective film. Each of the films tested would provide a degree of security, in that the visual transmittance for each film is lower than that of clear float glass, and this may be the effect desired by the building manager when considering the use of a reflective film.

The usefulness of this project is that a computer program has been developed to determine the thermal performance of solar-control films. These results have been evaluated using experimental data. The correlations obtained from the computer based simulations can be used as input parameters for building thermal analysis simulation programs.

During the course of this study, a number of significant papers were published in the area of window testing using illuminated hot boxes; the majority during the last two years. These papers have deepened the understanding of how the thermal and

daylighting performance of glazing materials can be successfully undertaken. Two examples of experimental apparatus which have been built, are the illuminated hot box developed by Prasad (1993), and a window testing rig in Italy by Maccari (1994). Prasad's apparatus is illuminated using the sun and is housed in a trailer so it can be moved around Australia. Maccari's apparatus is laboratory based and measures the total energy flux through the glass by removing the energy, which is transmitted through the glass to the internal environment, by means of an absorber plate, measuring the temperature difference across the plate. This temperature difference represents the total energy transmitted through the glazing. A number of computer programs have also been written which can determine the transmittance and heat flux through a window. Two examples are, Window 4.1, which was developed at the Lawrence Berkeley Laboratory (Sullivan, 1994), and ENVSTD which was developed by Bean (1991). Both, use the theory set out in the ASHRAE Fundamentals Handbook.

During this study, a method of testing solar-control films for comparison has been expounded. It has been shown that the results which were achieved can be used to compare the solar thermal performance of solar-control films, and that this can be done quickly and accurately. The facility at Cranfield still needs some development before the apparatus can be said to be of use in determining standard coefficients for the total solar energy gain. This development can proceed, by noting the conclusions reached in this study. Further work will be needed on the experimental apparatus so that the results can be improved. This work should involve a new shield, so that the long wave thermal radiation transfer from the lamp to the glass is eliminated. This might be achieved by fixing a glass plate in front of the lamp, and using the fan which already cools the lamp, to also cool the plate. A new means of shielding the exterior sides of the illuminated hot box is also needed so that the energy from the lamp, incident upon the sides of the illuminated hot box is eliminated when testing at angles of incidence above 10°. An examination needs to be made of the difficulties encountered in modelling the thin films attached to the glass. The examination also needs to address the questions raised in Chapter 5, concerning the convection regime from the floor to the air, which might have restricted the accuracy of the results. More information needs to be sought concerning the physical properties of the films modelled. The simulation model could also be improved by using a more powerful computer and full computational fluid dynamic techniques.

Acknowledgements

I would like to thank all those within the School of Mechanical Engineering, at what used to be Cranfield Institute of Technology, especially Dr Bill Batty, who has been my long suffering tutor since I arrived to study initially for an MSc. He has been extremely helpful and thought provoking in his comments to me throughout my studies. I would also like to thank Mr Charlie Knight, whose work for me within the laboratories was invaluable. I would also like to thank members of staff and my fellow students who were supportive at all times, especially Prof. Doug Probert, Craig Scarisbrick and Stephen Welch. I wish to thank the Science and Engineering Research Council for the funding of this research work, and Madico Inc., 3M and Peter Spence at Courtaulds for supplying materials and information regarding their products.

I would also like to thanks those who became my friends outside the environs of Cranfield during my sojourn, especially, John Stevens, Karen and Michael Crilly and The Parkers. Thanks also are due to my colleagues at the centre for the Performance Research on the Built Environment, at the University of Ulster who have helped me and encouraged me to get this far.

Finally, I would like to thank Mam and Dad, Grandpa, Auntie Mair and Auntie Nesta and other members of my family for all the support they gave me during my studies. I would also like to thank my parents-in-law, James and Olive McCloy, for allowing me to take over their dining room during the summer of 1994 so that this work could be written up. Most importantly, I would like to thank my wife, Joanna, whom I married during my write-up year. Janny has been a great help to me. Being a primary teacher, she has been pressed into service as a proof reader, and without her support over the past two years, this thesis would not have been completed.

BLANK IN ORIGINAL

References

AGHEMO C, S BIAVA & M FILIPPI — The glazing: a challenge for thermal and visual comfort Proc. 2nd European Conference on Architecture, 4-8 Dec., Paris, France, 1989.

ALDERSON J H — Reflective solar control films for windows Heating and Vent Engr, v42, 501 pp 523-6, 1969

ARASTEH D, R JOHNSON AND S SELKOWITZ — Definition and use of a daylight "coolness" index Lawrence Berkeley Laboratory, LBL-20541 Berkeley, CA, 1986

ARASTEH D, SELKOWITZ S AND HARTMANN J — Detailed Thermal Performance Data on Conventional and Highly insulating window systems Proc. ASHRAE/DOE/BTECC Conference: Thermal Performance of the Exterior Envelopes of Buildings III, Dec. 2-5, 1985, Clearwater Beach, FL. pp 830-845

BEAN P — Using ENVSTD to compare glazing options ASHRAE Journal, November, pp22-28, 1991.

BEJAN A — Heat Transfer John Wiley & Son, New York, 1993

BORN M & E WOLK — Principles of Optics Pergamon Press, London, 1970

BOWEN RP, KP SOLVASON AND AG WILSON — Unique hot box cold room facility ASHRAE transactions, v67, pp 561-577, 1961

BOWEN RP & KP SOLVASON — A calorimeter for determining heat transmission characteristics of windows Proc. ASTM Conference on Thermal Insulation Materials Systems, p567-581, vol.stp922, 1984

BRUNELLO P AND R ZECCHIN — Characteristic parameters of windows Solar energy for refrigeration and air conditioning pp 325-338 International Institute of Refrigeration Commissions Jerusalem, 1982

BUREK SAM, B NORTON, & SD PROBERT — Transmission and Forward Scattering of Insolation through Plastic (Transparent and Semi-Transparent) Materials Solar Energy, v42, n6, pp 457-475, 1989

CLARKE JA — Energy simulation in building design Adam Hilger Ltd, Bristol, 1985

DE WAARD H & LAZARUS D — Modern Electronics Addison-Wesley, London, 1966

DUFFIE JA & WA BECKMAN — Solar energy thermal processes John Wiley & Son, New York, 1974

DUFFIE JA & WA BECKMAN — Solar engineering of thermal processes John Wiley & Son, New York, 1991

EAMES P — A unified numerical model for optics and heat transfer within line-axis concentrating solar energy collectors Cranfield PhD, 1990

ELMAHDY AH AND BOWEN RP — Laboratory determination of the thermal resistance of glazing units, ASHRAE transactions, v94, pp 1301-1316, 1988

EMC — Test Cell Studies Contractors Reports for ETSU Department of Energy, Harwell, 1990

GEORGE J — Preparation of Thin Films Marcel Dekker, New York, 1992

GEORGSON M, A ROOS AND C-G RIBBING — The influence of preparation conditions on the optical properties of titanium nitride based solar control films Journal of Vacuum Science and Technology v9 n4 pp 2191-2195, 1991

GOEBEL DG — Generalised integrating sphere theory Applied Optics v6, n1, pp 125-128, 1967

GOLDNER R B AND RD RAUH — Electrochromic Materials for Controlled Radiant Energy Transfer in Buildings Solar Energy Material v16, n5, pp 38-44 1987

GRACIN D AND U DESNICA — Windows with heat mirrors for energy conservation International Journal of Energy Research v8, pp 53-60, 1984

GRANQVIST C — Spectrally-Selective Surfaces for Heating and Cooling Applications TT1, SPIE Optical Engineering Press Bellingham 1989

GRIFFITHS P WJ BATTY, SD PROBERT & CA KNIGHT — Solar-Control Films Applied Energy v41, n4, pp 261-284, 1992

HARTIG K D MUNZ & M SCHERER — Industrial Realization of low-emittance oxide/metal/oxide films on glass Solar Energy Materials v16, n5, pp 9-13, 1987

HASSALL DNH — Transparent window insulation reduces air conditioning costs Australian Refrigeration and Air Conditioning v25, n4, pp 18-20, 1971

HEAVENS OS — Optical Properties of Thin Solid Films Dover Publications, New York, 1991

HEAVENS OS & RW DITCHBURN — Insight into Optics John Wiley & Sons Ltd, Chichester, 1991

HORIE CV — Solar Control Films for reducing light levels in building with daylight Congress Conservation within Historic Buildings pp 49-54, Vienna, 1980

HOWSON R P — Principles and properties of heat mirror coatings for domestic windows. In Solar Optical Materials, ed M Hutchins International Solar Energy Society, Pergamon, Oxford, 1988

HOWSON RP, MI RIDGE AND CA BISHOP — Production of transparent electrically conducting films by ion plating Thin Solid Films v80, pp 137-142, 1981

HOWSON RP, MI RIDGE, CA BISHOP & GP COTTMAN — The production of selective optical coatings on plastic sheet Proc. EEC seminar on energy saving in buildings Commission of the European Communities The Hague, 1984

HUTCHINS MG & P AGEORGES — Intercomparison of Measurement of Spectral Transmittance and Reflectance at Different Angles of Incidence, Final Report Project No.3413/1/0/177/1/91-BCR-UK(30), Community Bureau of Reference, Commission of the European Communities, Oxford, 1992

INCROPERA FP & DP DE WITT — Fundamentals of Heat and Mass Transfer Wiley, New York, 1981

JACQUE JA & HL KUPPENHEIM — Theory of the integrating sphere Journal, Optical Society of America v45, n6, pp 460-470, 1955

JENNINGS R — Some Reflections on coated glass The Steam and Heating Engineer v42, pp22-25, 1973

JOHNSON T E — Low-e glazing design guide Butterworth-Heinemann, Boston, MA, 1991

KARLSSON B — Construction of a 1m diameter integrating sphere for characterisation of transparent insulation materials Proceedings of the workshop on optical property measurement techniques Ispra, Italy October 1987 Ed. Aranovitch E, C Bassani, WB Gillett & JE Bates Commission of the European Communities, 1988 p61

KARLSSON T, C-G RIBBING, A ROOS & E VALKONEN — Window coatings for efficient energy control International Journal of Energy Resources v12, pp 23-29 1988

KLEMS JH — A Calibrated Hotbox for Testing Window Systems - Construction, Calibration, and measurements on Prototype High-Performance Windows Proceedings of the ASHRAE/DOE-ORNL Conference on the Thermal Performance of the Exterior Envelopes of Buildings, Orlando Florida, USA pp 338-346, 1979

KLEMS JH
U-values, solar heat gain and thermal performance - recent studies using the MoWitt ASHRAE transactions v95, Part 1 1989

KLEMS JK, S SELKOWITZ & S HOROWITZ
A mobile facility for measuring net energy performance of windows and skylights
Energy conservation in the Built Environment Proceedings of CIB W76 Third International Symposium), Vol III p3.1, Dublin, Ireland, 1982

LITTLER JG
Thermal balance at heat reflecting windows
Energy Resources v3, n2, pp 173-179, 1979

LYNES P
Principles of Natural Lighting
Elsevier, London, 1968

MACCARI A
private communication, June 1994.

MACLEOD HA
Thin-Film optical filters
Adam Higer Ltd, London, 1969

MAIN I G
Vibrations and waves in Physics
Cambridge University Press, Cambridge, 1978

MARKUS T A & E N MORRIS
Buildings, Climate and Energy
Pitman, London, 1980

MCCABE ME & HILL D
Field Measurement of Thermal And Solar/Opical Properties of insulating glass windows
ASHRAE Transcriptions v91, pp 1409-1424, 1987

MCCLUNEY R
The death of the Shading Coefficient
ASHRAE Journal, March, p36, 1991

MILBURN DI & KGT HOLLANDS
Solar transmittance measurements using an integrating sphere with broad area irradiation
Solar Energy, v52, n6, pp 497-507, 1994

MILLET J R
User requirements and performance assessment for window solar protection
Proc. CLIMA 2000 Conference, London, November 1993.

MINNE A
Glass coating: advanced technology for high performances
2nd European Conference on Architecture, ed. T Steemers & W Palz, Kluwer Academic Publishers, Dortrecht, The Netherlands, pp263-265,1990

MODEST M F
Radiative Heat Transfer
McGraw-Hill, New York, 1993

MORTIMER C E
Chemistry
Wadsworth Inc, Belmont, California, 1986

NORTON B
Solar Energy Thermal Technology
Springer-Verlag, London, 1992

PAPAMICHAEL K, J KLEMS & S SELKOWITZ
Determination and Application of Bi-directional Solar-Optical Properties of Fenestration Systems
Lawrence Berkeley Laboratory, University of California, Berkeley, Report LBL-25124, 1988

PATANKAR SV
Numerical heat transfer and fluid flow
Hemisphere Publishing, New York, 1980

PARSONS RA ed.
ASHRAE Handbook - Fundamentals
ASHRAE, Atlanta, 1989

PLATZER WJ
Directional-hemispherical solar transmittance data for plastic honey-comb-type structures
Solar Energy v49, n5, pp 359-370, 1992

PRASAD D
Solar-thermal performance of windows
PhD Thesis University of New South Wales, Sydney, 1993

PULKER H K
Coatings on Glass
Elsevier, Amsterdam, 1984

RANCOURT JD
Optical Thin Films
Macmillan, New York, 1987

RAYMENT R
Energy savings from sealed double and heat reflecting glazing units
Building Serv. Eng. Res. Technol. v10, n3, pp 123-127, London, 1989

REID E
Understanding Buildings
Longman, Harlow, 1984

RUBIN M
Solar Optical Properties of Windows
International Journal of Energy Research v6, pp 123-133, 1982a

RUBIN M
Calculating Heat Transfer Through Windows
International Journal of Energy Research v6, pp 341-349, 1982b

RUBIN M
Optical Properties of soda lime glasses
Solar Energy Materials, v12, pp 275-288, 1985

RUBIN M
R CRESWICK
& S SELKOWITZ
Transparent heat-mirrors for windows: thermal performance
Proc. 5th National Passive Solar Conference, ed Lampert C M
Pergamon Press, New York, pp 990-994, 1980

SHARPLES S,
JK PAGE
& CG SOUSTER
Incorporating body-tinted glazing into daylight computer models
Lighting Research and Technology v16, n3, pp 143-145, 1984

SHURCLIFF WA
Transmittance and reflection loss of multi-plate planar window of a solar-radiation collector: formula and tribulations of results for the case n=1.5
Solar Energy v16, pp 149-154, 1974

SIEGEL R — Net Radiation method for transmission through partially transparent plates
Solar energy v15, pp 273-276, 1973

SIEGEL R & JR HOWELL — Radiative Heat Transfer
McGraw Hill, New York, 1980

SMITH WA & PENNINGTON CW — Solar heat gain through double glass with between-glass shading
ASHRAE journal, October, pp 50-53, 1964.

SPENCE P — Courtaulds Performance Films, Private communication 1994

SPENCER AG, M GEORGSON, CA BISHOP, E STENBURG & RP HOWSON — Design and use of a vacuum system for high rate reactive sputtering of TiO2/TiN/TiO2 solar control films
Solar Energy Materials v18, pp87-95, 1988

SULLIVAN R — private communication, June 1994.

SWEITZER G, D ARASTEH & S SELKOWITZ — Effects of low-emissivity glazings on energy use patterns in non-residential buildings
Lawrence Berkeley Laboratories, LBL-21577, 1986

THIESSEN DR — Reflective solar-control film on windows gains acceptance
ASHRAE journal, v10, n10, pp 45-49, 1968

van STRAATEM JF — Thermal performance of buildings
Elsevier, Amsterdam, 1967

VILD DJ — Solar heat gain factors and shading coefficients
ASHRAE journal, October, pp 47-50, 1964

WIJEYSUNDERA NE — A net radiation method for the transmittance and absorptivity of a series of parallel regions
Solar Energy, v17, pp 75-77, 1975

YELLOT JI — Solar optical properties, heat transfer coefficients and shading coefficients for architectural glass
ASHRAE Journal, v13, n3, pp30-46, 1971

BLANK IN ORIGINAL

Appendix: The Transient Computer Program

Microsoft Quick BASIC Listing

Source File: Transient

Program Unit: MAIN

```
00001  'Program to determine temperatures of box under transient conditions
00002
00003  'define arrays
00004
00005
00006  DIM Tfixx (210)
00007  DIM Tfizxx (210)
00008  DIM Tfiaxx (210)
00009  DIM Tfiaaxx (210)
00010  DIM Tfibxx (210)
00011  DIM Tfibaxx (210)
00012  DIM Tficxx (210)
00013  DIM Tficaxx (210)
00014  DIM Tfidxx (210)
00015  DIM Tfidaxx (210)
00016  DIM Tfiexx (210)
00017  DIM Tfieaxx (210)
00018  DIM Tfifxx (210)
00019  DIM Tfifaxx (210)
00020  DIM Tfigxx (210)
00021  DIM Tfigaxx (210)
00022  DIM Tfihxx (210)
00023  DIM Tfiixx (210)
00024  DIM Tfijxx (210)
00025  DIM Tfikxx (210)
00026  DIM Tfoxx (210)
00027  DIM Tgixx (210)
00028  DIM Tgoxx (210)
00029  DIM Tgexx (210)
00030  DIM Twwixx (210)
00031  DIM Twwzxx (210)
00032  DIM Twwaxx (210)
00033  DIM Twwaaxx (210)
00034  DIM Twwbxx (210)
00035  DIM Twwbaxx (210)
00036  DIM Twwcxx (210)
00037  DIM Twwcaxx (210)
00038  DIM Twwdxx (210)
00039  DIM Twwdaxx (210)
00040  DIM Twwexx (210)
00041  DIM Twweaxx (210)
```

```
00042  DIM Twwfxx (210)
00043  DIM Twwfaxx (210)
00044  DIM Twwgxx (210)
00045  DIM Twwgaxx (210)
00046  DIM Twwoxx (210)
00047  DIM Twnixx (210)
00048  DIM Twnzxx (210)
00049  DIM Twnaxx (210)
00050  DIM Twnaaxx (210)
00051  DIM Twnbxx (210)
00052  DIM Twnbaxx (210)
00053  DIM Twncxx (210)
00054  DIM Twncaxx (210)
00055  DIM Twndxx (210)
00056  DIM Twndaxx (210)
00057  DIM Twnexx (210)
00058  DIM Twneaxx (210)
00059  DIM Twnfxx (210)
00060  DIM Twnfaxx (210)
00061  DIM Twngxx (210)
00062  DIM Twngaxx (210)
00063  DIM Twnoxx (210)
00064  DIM Twsixx (210)
00065  DIM Twszxx (210)
00066  DIM Twsaxx (210)
00067  DIM Twsaaxx (210)
00068  DIM Twsbxx (210)
00069  DIM Twsbaxx (210)
00070  DIM Twscxx (210)
00071  DIM Twscaxx (210)
00072  DIM Twsdxx (210)
00073  DIM Twsdaxx (210)
00074  DIM Twsexx (210)
00075  DIM Twseaxx (210)
00076  DIM Twsfxx (210)
00077  DIM Twsfaxx (210)
00078  DIM Twsgxx (210)
00079  DIM Twsgaxx (210)
00080  DIM Twsoxx (210)
00081  DIM Tweixx (210)
00082  DIM Twezxx (210)
00083  DIM Tweaxx (210)
00084  DIM Tweaaxx (210)
00085  DIM Twebxx (210)
00086  DIM Twebaxx (210)
00087  DIM Twecxx (210)
00088  DIM Twecaxx (210)
00089  DIM Twedxx (210)
00090  DIM Twedaxx (210)
00091  DIM Tweexx (210)
00092  DIM Tweeaxx (210)
```

```
00093  DIM Twefxx (210)
00094  DIM Twefaxx (210)
00095  DIM Twegxx (210)
00096  DIM Twegaxx (210)
00097  DIM Tweoxx (210)
00098  DIM Taixx (210)
00099
00100  'Physical constants
00101
00102  SB = 5.67E-08 'stefan boltzmann constant
00103  G  = 9.8  'gravity
00104
00105  filename$ = FILES$(0, "Enter a new file name")
00106
00107  DIM NLAY (4)
00108  DIM KLAY (4)
00109  DIM LL(2)
00110  DIM ELAY(2)
00111  DIM RAOR(4)
00112  DIM RAOI(4)
00113
00114  FOR z = 1 TO 4
00115  LET NLAY(z) = 1
00116  NEXT z
00117
00118  FOR z = 1 TO 2
00119  LET NKAY(z) = 0
00120  LET LL(z) = 0
00121  LET ELAY(z) = 0
00122  NEXT z
00123
00124  INPUT " How many layers in glazing ";X
00125  FOR Y = 1 TO X
00126  PRINT "Please input the values for layer ";Y
00127  INPUT "Refractive index",NLAY(Y)
00128  INPUT "Absorptive coefficient in (cm-1)",KLAY(Y)
00129  INPUT "Surface emissivity ",ELAY(Y)
00130  INPUT "Thickness, in mm",LL(Y)
00131  IF Y = 1 THEN
00132  LET EGE = ELAY(Y)
00133  LET EG = ELAY(Y)
00134  END IF
00135  IF Y = 2 THEN
00136  LET EG = ELAY(Y)
00137  END IF
00138  LET LL(Y) = LL(Y)*.001
00139  PRINT LL(Y)
00140  NEXT Y
00141
00142  LET NLAY(0) = 1
00143  LET NLAY(X+1) = 1
```

```
00144
00145  inputs:
00146
00147  INPUT "Angle of Incidence ", AOI
00148
00149  FLG = .21929-9.8609*10^(-4)*AOI-1.2678*10^(-5)*AOI^2
00150  FLF = .1725-1.2961*10^(-4)*AOI-1.9479*10^(-5)*AOI^2
00151  FLW = 2.8929*10^(-2)+3.1102*10^(-5)*AOI+5.5638*10^(-6)*AOI^2
00152
00153
00154  'Shape Factors - fixed
00155
00156  FGF = .52 'Shape factor glass - floor, floor - glass
00157  FFGW = .12 'Shape factor floor/glass - wall
00158  FWFG = .34 'shape factor wall - floor/glass
00159  FWW = .13 'Shape factor wall - wall
00160
00161  FLGT = FLG    '.052 'Shape factor lamp to glass taking into account thermal radiation
00162
00163  'FLF = FGF * FLG
00164
00165  'Physical characteristics of the box
00166
00167  AG = .59^2
00168  AF =.59^2
00169  AL = .655*.147
00170  ALA = .655 * .012
00171  AW = .59*.21
00172
00173
00174  I = 386 'lamp intensity  usually 386 or 425
00175
00176  'properties of materials D = density, C = specific heat capacity
00177
00178  'Glass
00179  DG = 2500 'was 2560 figures for glass taken from Kane and Laby
00180  CG = 670 'was 750 and 830
00181  KG = 1.05 'thermal conductivity glass
00182  EGE = .845 'emissivity of glass
00183  LG = .004 'thickness of glass
00184
00185  'Films
00186  KTF = .12 'thermal conductivity of Polypropylene
00187  DTF = 904 'density of polypropylene
00188  CTF = 1.92 'specfic heat capacity
00189  ETF = .25 'emissivity of polypropylene
00190
00191  'Plywood
00192  DW = 530 'was 560
00193  CW = 2760 'was 2500
00194  ETWF = .96 'emissivity thermal of walls and floor This is the value for black matt paint
```

```
00195  SAW = .9 'emissivity solar of walls and floor  This is the value for black matt paint
00196  LW = .024 'thickness wall
00197  LB = .012 'thickness floor
00198  KW = .14 'thermal conductivity plywood
00199  KF = KW
00200  KB = KW
00201
00202  'Polystyrene
00203  DP = 25
00204  CP = 1380 'was 1000
00205  KP = .03 'thermal conductivity polystyrene
00206  EP = .9 'emissivity of polystyrene
00207  LP = .02 'thickness polystyrene
00208
00209  'Characteristic lengths of the box
00210
00211  LBF = (.59^(2))/(.59*4)
00212  LBG = LBF
00213
00214
00215  DxG = LG/2
00216  DxF = LW/8
00217  DxW = LW/8
00218  DxB = LB/4
00219  DxP = LP/8
00220
00221  'Time differential
00222  DT = .25
00223
00224  'thermal diffusivity's
00225  TDG = KG/(DG*CG)
00226  TDW = KW/(DW*CW)
00227  TDF = KW/(DW*CW)
00228  TDB = KW/(DW*CW)
00229  TDP = KP/(DP*CP)
00230
00231  'Fourier Numbers
00232  FOG = TDG*DT/(DxG)^2
00233  FOF = TDF*DT/(DxF)^2
00234  FOW = TDW*DT/(DxW)^2
00235  FOB = TDB*DT/(DxB)^2
00236  FOP = TDP*DT/(DxP)^2
00237
00238  ' simplifications to allow quick programming
00239
00240  'Coefficient floor poly boundary
00241  CFPB = (DW*CW*DxF+DP*CP*DxP)/(2*DT)
00242
00243  'Coefficient wall poly boundary
00244  CWPB = (DW*CW*DxW+DP*CP*DxP)/(2*DT)
00245
```

```
00246  'Coefficient poly base boundary
00247  CPBB = (DP*CP*DxP+DW*CW*DxB)/(2*DT)
00248
00249
00250  'Determination of glass characteristics; transmittance, reflectance and absorption
00251
00252  ISf= .3482+.0009101*AOI-.0001083*AOI^2+5.367E-07*AOI^3+2.681E-08*AOI^4-3.718E-
10*AOI^5
00253  LET Sf = ISf/AF
00254  ISns=.1239+.000416*AOI-4.558E-05*AOI^2+1.012E-06*AOI^3-8.333E-09*AOI^4
00255  LET Sns = ISns/AW
00256  IF AOI < 20 THEN
00257     LET Se=1
00258     ELSE
00259        LET Se=0
00260     END IF
00261  IF AOI < 80 THEN
00262     LET Sw=1
00263     ELSE
00264     IF AOI = 80 THEN
00265        LET Sw=.81/AW
00266        ELSE
00267        IF AOI >80 THEN
00268           LET Sw=0
00269        END IF
00270     END IF
00271  END IF
00272
00274
00275  LET pi = 3.14159265#        'computer works in Radians so
00276  LET RAOI(1) = AOI*pi/180
00277  PRINT RAOI(1)
00278  IF AOI = 0 THEN
00279     FOR Y = 1 TO (X+1)
00280     RSUR(Y) = ((NLAY(Y)-NLAY(Y-1))/(NLAY(Y)+NLAY(Y-1)))^2     'reflection off surface
at 0 degrees
00281     NEXT Y
00282  ELSE
00283     IF AOI > 90 THEN
00284        GOSUB inputs
00285     ELSE
00286        IF AOI < 0 THEN
00287        GOSUB inputs
00288     ELSE
00289        RAOR(0) = RAOI(1)
00290        PRINT RAOR(0)
00291        FOR Y = 1 TO (X+1)
00292        LET RAOI(Y) = RAOR(Y-1)
00293        PRINT RAOI(Y);NLAY(Y-1);NLAY(Y)
00294        RAOR(Y) = ATN((-1+1/(1-(SIN(RAOI(Y))*(NLAY(Y-1)/NLAY(Y)))^2))^.5)    'angle
of refraction
```

```
00295          REVR(Y) = ( SIN(RAOR(Y)-RAOI(Y)))^2/( SIN(RAOR(Y)+RAOI(Y)))^2
00296          RMVR(Y) = ( TAN(RAOR(Y)-RAOI(Y)))^2/( TAN(RAOR(Y)+RAOI(Y)))^2
00297          RSUR(Y) = .5*(REVR(Y)+RMVR(Y))          'reflection at angle AOI
00298          NEXT Y
00299        END IF
00300      END IF
00301  END IF
00302
00303  nextstep:
00304
00305  FOR Y = 1 TO X
00306  ABSLAY(Y) = 1-EXP((-KLAY(Y)*(LL(Y)*100))/(COS(RAOR(Y))))
00307  NEXT Y
00308
00309  Ta = (1-RSUR(1))*(1-RSUR(2))*(1-RSUR(3))*(1-ABSLAY(1))*(1-ABSLAY(2))
00310  Tb = (1-RSUR(2)*RSUR(3)*(1-ABSLAY(2))^(2))*(1-RSUR(1)*RSUR(2)*(1-
ABSLAY(1))^(2))-(1-RSUR(2))^(2)*(1-ABSLAY(1))^(2)*(1-ABSLAY(2))^(2)*RSUR(1)*RSUR(3)
00311  T = Ta/Tb
00312  Ra = RSUR(2)*(1-RSUR(2)*RSUR(3)*(1-ABSLAY(2))^(2))+RSUR(3)*(1-RSUR(2))^(2)*(1-
ABSLAY(2))^(2)
00313  Rb = Tb
00314  R = RSUR(1)+(1-RSUR(2))^(2)*(1-ABSLAY(1))^(2)*(Ra/Rb)
00315  A = 1-T-R
00316
00317  PRINT "tra";T;"abs";A;"ref";R
00318
00319  Philip:
00320
00321  INPUT "U-value of glazing";U
00322
00323
00324  'That's the end of the coefficients, now the Temperatures, first known T
00325
00326  'Tae = 293
00327  INPUT "Base Temperature";Tae
00328  Tae = Tae + 273
00329  TL = 653
00330
00331  'at 0° start with the following temperatures
00332
00333  TX = Tae+.5
00334  Tfi=TX
00335  Tfiz=TX
00336  Tfia=TX
00337  Tfiaa=TX
00338  Tfib=TX
00339  Tfiba=TX
00340  Tfic=TX
00341  Tfica=TX
00342  Tfid=TX
00343  Tfida=TX
```

```
00344  Tfie=TX
00345  Tfiea=TX
00346  Tfif=TX
00347  Tfifa=TX
00348  Tfig=TX
00349  Tfiga=TX
00350  Tfih=TX
00351  Tfii=TX
00352  Tfij=TX
00353  Tfik=TX
00354  Tfo=TX
00355  Tgi=TX
00356  Tgo=TX
00357  Tge=TX
00358  Twwi=TX
00359  Twwz=TX
00360  Twwa=TX
00361  Twwaa=TX
00362  Twwb=TX
00363  Twwba=TX
00364  Twwc=TX
00365  Twwca=TX
00366  Twwd=TX
00367  Twwda=TX
00368  Twwe=TX
00369  Twwea=TX
00370  Twwf=TX
00371  Twwfa=TX
00372  Twwg=TX
00373  Twwga=TX
00374  Twwo=TX
00375  Twni=TX
00376  Twnz=TX
00377  Twna=TX
00378  Twnaa=TX
00379  Twnb=TX
00380  Twnba=TX
00381  Twnc=TX
00382  Twnca=TX
00383  Twnd=TX
00384  Twnda=TX
00385  Twne=TX
00386  Twnea=TX
00387  Twnf=TX
00388  Twnfa=TX
00389  Twng=TX
00390  Twnga=TX
00391  Twno=TX
00392  Twsi=TX
00393  Twsz=TX
00394  Twsa=TX
```

```
00395  Twsaa=TX
00396  Twsb=TX
00397  Twsba=TX
00398  Twsc=TX
00399  Twsca=TX
00400  Twsd=TX
00401  Twsda=TX
00402  Twse=TX
00403  Twsea=TX
00404  Twsf=TX
00405  Twsfa=TX
00406  Twsg=TX
00407  Twsga=TX
00408  Twso=TX
00409  Twei=TX
00410  Twez = TX
00411  Twea=TX
00412  Tweaa=TX
00413  Tweb=TX
00414  Tweba=TX
00415  Twec=TX
00416  Tweca=TX
00417  Twed=TX
00418  Tweda=TX
00419  Twee=TX
00420  Tweea=TX
00421  Twef=TX
00422  Twefa=TX
00423  Tweg=TX
00424  Twega=TX
00425  Tweo=TX
00426  Tai=Tae
00427  Tfe = 288
00428
00429  'now the equations
00430
00431  LET n = 1
00432  LET m =1
00433  LET q=1
00434
00435  Equations:
00436
00437  FOR m = 1 TO 3600
00438
00439      'Hc's as from rayleigh and nusselt no's
00440
00441      PRI = .85914-8.8947*10^(-4)*Tai+1.6806*10^(-6)*Tai^2-1.5496*10^(-
9)*Tai^3+6.9176*10^(-13)*Tai^4
00442      TDI = (-5.8362*10^(-2)-3.2022*10^(-3)*Tai+3.0389*10^(-4)*Tai^2-1.4132*10^(-
7)*Tai^3)*10^(-6)
00443      KAI = (-.166+9.7985*10^(-2)*Tai-3.2687*10^(-5)*Tai^2)*10^(-3)
```

```
00444     KVI = (-.16459+2.1022*10^(-3)*Tai+2.1027*10^(-4)*Tai^2-1.4692*10^(-
7)*Tai^3+5.8959*10^(-11)*Tai^4)*10^(-6)
00445
00446     PRA = .85914-8.8947*10^(-4)*Tae+1.6806*10^(-6)*Tae^2-1.5496*10^(-
9)*Tae^3+6.9176*10^(-13)*Tae^4
00447     TDA = (-5.8362*10^(-2)-3.2022*10^(-3)*Tae+3.0389*10^(-4)*Tae^2-1.4132*10^(-
7)*Tae^3)*10^(-6)
00448     KAA = (-.166+9.7985*10^(-2)*Tae-3.2687*10^(-5)*Tae^2)*10^(-3)
00449     KVA = (-.16459+2.1022*10^(-3)*Tae+2.1027*10^(-4)*Tae^2-1.4692*10^(-
7)*Tae^3+5.8959*10^(-11)*Tae^4)*10^(-6)
00450
00451     LET CVEA = 1/Tae
00452     LET CVEI = 1/Tai
00453
00454     Raglassex = (G*CVEA*(ABS(Tge-Tae))*LBG^3)/(KVA*TDA)
00455     Hcge = (.54*(Raglassex)^(1/4))*KAA/LBG
00456     Raglassin = (G*CVEI*(ABS(Tgi-Tai))*LBG^3)/(KVI*TDI)
00457     Hcgi = (.27*(Raglassin)^(1/4))*KAI/LBG
00458     Rafloorin = (G*CVEI*(ABS(Tfi-Tai))*LBF^3)/(KVI*TDI)
00459     Hcfi = (.54*(Rafloorin)^(1/4))*KAI/LBF
00460     Rafloorex = (G*CVEA*(ABS(Tfo-Tae))*LBF^3)/(KVA*TDA)
00461     Hcfe = (.27*(Rafloorex)^(1/4))*KAA/LBF
00462     Rawallwi = (G*CVEI*(ABS(Twwi-Tai))*.21^3)/(KVI*TDI)
00463     Hcwwi = (.68+((.67*(Rawallwi)^(1/4))/(1+(.492/PRI)^(9/16))^(4/9)))*KAI/.21
00464     Rawallwx = (G*CVEA*(ABS(Twwo-Tae))*.21^3)/(KVA*TDA)
00465     Hcwwo = (.68+((.67*(Rawallwx)^(1/4))/(1+(.492/PRA)^(9/16))^(4/9)))*KAA/.21
00466     Rawallei = (G*CVEI*(ABS(Twei-Tai))*.21^3)/(KVI*TDI)
00467     Hcwei = (.68+((.67*(Rawallei)^(1/4))/(1+(.492/PRI)^(9/16))^(4/9)))*KAI/.21
00468     Rawallex = (G*CVEA*(ABS(Tweo-Tae))*.21^3)/(KVA*TDA)
00469     Hcweo = (.68+((.67*(Rawallex)^(1/4))/(1+(.492/PRA)^(9/16))^(4/9)))*KAA/.21
00470     Rawallni = (G*CVEI*(ABS(Twni-Tai))*.21^3)/(KVI*TDI)
00471     Hcwni = (.68+((.67*(Rawallni)^(1/4))/(1+(.492/PRI)^(9/16))^(4/9)))*KAI/.21
00472     Rawallnx = (G*CVEA*(ABS(Twno-Tae))*.21^3)/(KVA*TDA)
00473     Hcwno = (.68+((.67*(Rawallnx)^(1/4))/(1+(.492/PRA)^(9/16))^(4/9)))*KAA/.21
00474     Rawallsi = (G*CVEI*(ABS(Twsi-Tai))*.21^3)/(KVI*TDI)
00475     Hcwsi = (.68+((.67*(Rawallsi)^(1/4))/(1+(.492/PRI)^(9/16))^(4/9)))*KAI/.21
00476     Rawallsx = (G*CVEA*(ABS(Twso-Tae))*.21^3)/(KVA*TDA)
00477     Hcwso = (.68+((.67*(Rawallsx)^(1/4))/(1+(.492/PRA)^(9/16))^(4/9)))*KAA/.21
00478
00479     'Biot Numbers
00480     BiG = Hcge*DxG/KG
00481
00482     IF m = 3600 THEN
00483        PRINT "Time = ";q;" store n=";n
00484     END IF
00485
00486     'Radiation heat transfer coefficients
00487
00488     Hrge = SB*EG*(Tge+Tae)*(Tge^(2)+Tae^(2))
00489     Hrgif = SB*(Tgi+Tfi)*(Tgi^(2)+Tfi^(2))/(((1-EG)/(AG*EG))+(1/(AG*FGF))+((1-
ETWF)/(AF*ETWF)))
```

```
00490     Hrfig = SB*(Tgi+Tfi)*(Tgi^(2)+Tfi^(2))/(((1-ETWF)/(AF*ETWF))+(1/(AF*FGF))+((1-
EG)/(AG*EG)))
00491     Hrfe = SB*ETWF*(Tfo+Tfe)*(Tfo^(2)+Tfe^(2))
00492     HrLg = SB*EG*(Tge+TL)*(Tge^(2)+TL^(2))
00493     Hrwf = SB*(Tfi+Twwi)*(Tfi^(2)+Twwi^(2))/(((1-
ETWF)/(AW*ETWF))+(1/(AW*FWFG))+((1-ETWF)/(AF*ETWF)))
00494     Hrfiw = SB*(Tfi+Twwi)*(Tfi^(2)+Twwi^(2))/(((1-
ETWF)/(AF*ETWF))+(1/(AF*FFGW))+((1-ETWF)/(AW*ETWF)))
00495     Href = SB*(Tfi+Twei)*(Tfi^(2)+Twei^(2))/(((1-
ETWF)/(AW*ETWF))+(1/(AW*FWFG))+((1-ETWF)/(AF*ETWF)))
00496     Hrfie = SB*(Tfi+Twei)*(Tfi^(2)+Twei^(2))/(((1-ETWF)/(AF*ETWF))+(1/(AF*FFGW))+((1-
ETWF)/(AW*ETWF)))
00497     Hrnf = SB*(Tfi+Twni)*(Tfi^(2)+Twni^(2))/(((1-
ETWF)/(AW*ETWF))+(1/(AW*FWFG))+((1-ETWF)/(AF*ETWF)))
00498     Hrfin = SB*(Tfi+Twni)*(Tfi^(2)+Twni^(2))/(((1-ETWF)/(AF*ETWF))+(1/(AF*FFGW))+((1-
ETWF)/(AW*ETWF)))
00499     Hrsf = SB*(Tfi+Twsi)*(Tfi^(2)+Twsi^(2))/(((1-ETWF)/(AW*ETWF))+(1/(AW*FWFG))+((1-
ETWF)/(AF*ETWF)))
00500     Hrfis = SB*(Tfi+Twsi)*(Tfi^(2)+Twsi^(2))/(((1-ETWF)/(AF*ETWF))+(1/(AF*FFGW))+((1-
ETWF)/(AW*ETWF)))
00501     Hrgiw = SB*(Tgi+Twwi)*(Tgi^(2)+Twwi^(2))/(((1-EG)/(AG*EG))+(1/(AG*FFGW))+((1-
ETWF)/(AW*ETWF)))
00502     Hrgin = SB*(Tgi+Twni)*(Tgi^(2)+Twni^(2))/(((1-EG)/(AG*EG))+(1/(AG*FFGW))+((1-
ETWF)/(AW*ETWF)))
00503     Hrgie = SB*(Tgi+Twei)*(Tgi^(2)+Twei^(2))/(((1-EG)/(AG*EG))+(1/(AG*FFGW))+((1-
ETWF)/(AW*ETWF)))
00504     Hrgis = SB*(Tgi+Twsi)*(Tgi^(2)+Twsi^(2))/(((1-EG)/(AG*EG))+(1/(AG*FFGW))+((1-
ETWF)/(AW*ETWF)))
00505     Hrwg = SB*(Tgi+Twwi)*(Tgi^(2)+Twwi^(2))/(((1-
ETWF)/(AW*ETWF))+(1/(AW*FWFG))+((1-EG)/(AG*EG)))
00506     Hreg = SB*(Tgi+Twei)*(Tgi^(2)+Twei^(2))/(((1-
ETWF)/(AW*ETWF))+(1/(AW*FWFG))+((1-EG)/(AG*EG)))
00507     Hrng = SB*(Tgi+Twni)*(Tgi^(2)+Twni^(2))/(((1-
ETWF)/(AW*ETWF))+(1/(AW*FWFG))+((1-EG)/(AG*EG)))
00508     Hrsg = SB*(Tgi+Twsi)*(Tgi^(2)+Twsi^(2))/(((1-
ETWF)/(AW*ETWF))+(1/(AW*FWFG))+((1-EG)/(AG*EG)))
00509     Hrwwe = SB*EP*(Tae+Twwo)*(Tae^(2)+Twwo^(2))
00510     Hrwee = SB*EP*(Tae+Tweo)*(Tae^(2)+Tweo^(2))
00511     Hrwne = SB*EP*(Tae+Twno)*(Tae^(2)+Twno^(2))
00512     Hrwse = SB*EP*(Tae+Twso)*(Tae^(2)+Twso^(2))
00513     Hreww = SB*ETWF*(Twei+Twwi)*(Twei^(2)+Twwi^(2))/(((1-
ETWF)/(AW*ETWF))+(1/(AW*FWW))+((1-ETWF)/(AW*ETWF)))
00514     Hrwew = Hreww
00515     Hrnww = SB*ETWF*(Twni+Twwi)*(Twni^(2)+Twwi^(2))/(((1-
ETWF)/(AW*ETWF))+(1/(AW*FWW))+((1-ETWF)/(AW*ETWF)))
00516     Hrwnw = Hrnww
00517     Hrsww = SB*ETWF*(Twsi+Twwi)*(Twsi^(2)+Twwi^(2))/(((1-
ETWF)/(AW*ETWF))+(1/(AW*FWW))+((1-ETWF)/(AW*ETWF)))
00518     Hrwsw = Hrsww
00519     Hrnew = SB*ETWF*(Twei+Twni)*(Twei^(2)+Twni^(2))/(((1-
ETWF)/(AW*ETWF))+(1/(AW*FWW))+((1-ETWF)/(AW*ETWF)))
```

```
00520     Hrenw = Hrnew
00521     Hrsew = SB*ETWF*(Twei+Twsi)*(Twei^(2)+Twsi^(2))/(((1-
ETWF)/(AW*ETWF))+(1/(AW*FWW))+((1-ETWF)/(AW*ETWF)))
00522     Hresw = Hrsew
00523     Hrsnw = SB*ETWF*(Twni+Twsi)*(Twni^(2)+Twsi^(2))/(((1-
ETWF)/(AW*ETWF))+(1/(AW*FWW))+((1-ETWF)/(AW*ETWF)))
00524     Hrnsw = Hrsnw
00525
00526
00527     Tgea =
2*FOG*((BiG+Hrge*(DxG/KG))*Tae+Tgo+ALA*FLGT*HrLg*TL*(DxG/(AG*KG))+I*A*(FLG+(1-
SAW)*T*(FLF*Sf*AF*FGF+FLW*AW*FWFG*(Sw+Se+2*Sns)))*(((DxG)^2)/(2*KG)))
00528     Tgeb = (1-2*FOG*(1+BiG+ALA*FLGT*HrLg*(DxG/(AG*KG))+Hrge*(DxG/KG)))*Tge
00529     Tgex = Tgea + Tgeb
00530     Tgoa = FOG*(Tge+Tgi+I*A*(FLG+(1-
SAW)*T*(FLF*Sf*AF*FGF+FLW*AW*FWFG*(Sw+Se+2*Sns)))*(((DxG)^2)/KG))
00531     Tgob = (1-2*FOG)*Tgo
00532     Tgox = Tgoa + Tgob
00533     Tgij =
2*FOG*(Tgo+(DxG/KG)*(Hcgi*Tai+(1/AG)*(Hrfig*Tfi+Hrwg*Twwi+Hrng*Twni+Hreg*Twei+Hrsg*T
wsi)+I*A*(DxG/2)*(FLG+T*(1-SAW)*(AF*FGF*FLF*Sf+FLW*AW*FWFG*(Sw+Se+2*Sns)))))
00534     Tgii = Tgi*(1-2*FOG*(1+(DxG/KG)*(Hcgi+(1/AG)*(Hrfig+Hrwg+Hrng+Hreg+Hrsg))))
00535     Tgix = Tgij + Tgii
00536     Tqfi = 2*FOF*(Tfiz+(DxF/KW)*(Hcfi*Tai+I*T*(FLF*Sf*SAW+(1-
SAW)*FLW*AW*FWFG*(Sw+Se+2*Sns))+(1/AF)*(Hrgif*Tgi+Href*Twei+Hrsf*Twsi+Hrnf*Twni+Hr
wf*Twwi)))
00537     Tpfi = (1-2*FOF*(1+(DxF/KW)*(Hcfi+(1/AF)*(Hrgif+Hrwf+Href+Hrsf+Hrnf))))*Tfi
00538     Tfix = Tqfi + Tpfi
00539     Tfizx = FOF*(Tfi+Tfia)+(1-2*FOF)*Tfiz
00540     Tfiax = FOF*(Tfiz+Tfiaa)+(1-2*FOF)*Tfia
00541     Tfiaax = FOF*(Tfia+Tfib)+(1-2*FOF)*Tfiaa
00542     Tfibx = FOF*(Tfiaa+Tfiba)+(1-2*FOF)*Tfib
00543     Tfibax = FOF*(Tfib+Tfic)+(1-2*FOF)*Tfiba
00544     Tficx = FOF*(Tfiba+Tfica)+(1-2*FOF)*Tfic
00545     Tficax = FOF*(Tfic+Tfid)+(1-2*FOF)*Tfica
00546     Tfidx = (((KW/DxF)*Tfica+(KP/DxP)*Tfida)/CFPB)+(1-
((KW/DxF)+(KP/DxP))/CFPB)*Tfid
00547     Tfidax = FOP*(Tfid+Tfie)+(1-2*FOP)*Tfida
00548     Tfiex = FOP*(Tfida+Tfiea)+(1-2*FOP)*Tfie
00549     Tfieax = FOP*(Tfie+Tfif)+(1-2*FOP)*Tfiea
00550     Tfifx = FOP*(Tfiea+Tfifa)+(1-2*FOP)*Tfif
00551     Tfifax = FOP*(Tfif+Tfig)+(1-2*FOP)*Tfifa
00552     Tfigx = FOP*(Tfifa+Tfiga)+(1-2*FOP)*Tfig
00553     Tfigax = FOP*(Tfig+Tfih)+(1-2*FOP)*Tfiga
00554     Tfihx = (((KP/DxP)*Tfiga+(KW/DxB)*Tfii)/CPBB)+(1-((KP/DxP)+(KW/DxB))/CPBB)*Tfih
00555     Tfiix = FOB*(Tfih+Tfij)+(1-2*FOB)*Tfii
00556     Tfijx = FOB*(Tfii+Tfik)+(1-2*FOB)*Tfij
00557     Tfikx = FOB*(Tfij+Tfo)+(1-2*FOB)*Tfik
00558     Tfox = 2*FOB*(Tfik+(DxB/KB)*(Hcfe*Tae+Hrfe*Tfe))+(1-
2*FOB*(1+(DxB/KB)*(Hcfe+Hrfe)))*Tfo
```

```
00559     Twwix = (2*FOW*(Twwz+(DxW/KW)*(Hcwwi*Tai+I*T*(FLW*Sw*SAW+(1-
SAW)*(FLF*Sf*AF*FWFG+FLW*AW*FWW*(Se+2*Sns)))+(1/AW)*(Hreww*Twei+Hrsww*Twsi+Hr
nww*Twni+Hrgiw*Tgi+Hrfiw*Tfi)))+(1-
2*FOW*(1+(DxW/KW)*(Hcwwi+(1/AW)*(Hreww+Hrsww+Hrnww+Hrgiw+Hrfiw))))*Twwi)
00560     Twwzx = FOW*(Twwi+Twwa)+(1-2*FOW)*Twwz
00561     Twwax = FOW*(Twwz+Twwaa)+(1-2*FOW)*Twwa
00562     Twwaax = FOW*(Twwa+Twwb)+(1-2*FOW)*Twwaa
00563     Twwbx = FOW*(Twwaa+Twwba)+(1-2*FOW)*Twwb
00564     Twwbax = FOW*(Twwb+Twwc)+(1-2*FOW)*Twwba
00565     Twwcx = FOW*(Twwba+Twwca)+(1-2*FOW)*Twwc
00566     Twwcax = FOW*(Twwc+Twwd)+(1-2*FOW)*Twwca
00567     Twwdx = (((KW/DxW)*Twwca+(KP/DxP)*Twwda)/CWPB)+(1-
((KW/DxW)+(KP/DxP))/CWPB)*Twwd
00568     Twwdax = FOP*(Twwd+Twwe)+(1-2*FOP)*Twwda
00569     Twwex = FOP*(Twwda+Twwea)+(1-2*FOP)*Twwe
00570     Twweax = FOP*(Twwe+Twwf)+(1-2*FOP)*Twwea
00571     Twwfx = FOP*(Twwea+Twwfa)+(1-2*FOP)*Twwf
00572     Twwfax = FOP*(Twwf+Twwg)+(1-2*FOP)*Twwfa
00573     Twwgx = FOP*(Twwfa+Twwga)+(1-2*FOP)*Twwg
00574     Twwgax = FOP*(Twwg+Twwo)+(1-2*FOP)*Twwga
00575     Twwox = 2*FOP*(Twwga+(DxP/KP)*Tae*(Hcwwo+Hrwwe))+(1-
2*FOP*(1+(DxP/KP)*(Hcwwo+Hrwwe)))*Twwo
00576     Tweix = (2*FOW*(Twez+(DxW/KW)*(Hcwei*Tai+T*I*(FLW*Se*SAW+(1-
SAW)*(FLF*Sf*AF*FWFG+FLW*AW*FWW*(Sw+2*Sns)))+(1/AW)*(Hrwew*Twwi+Hrsew*Twsi+Hr
new*Twni+Hrgie*Tgi+Hrfie*Tfi)))+(1-
2*FOW*(1+(DxW/KW)*(Hcwei+(1/AW)*(Hrwew+Hrnew+Hrsew+Hrgie+Hrfie))))*Twei)
00577     Twezx = FOW*(Twei+Twea)+(1-2*FOW)*Twez
00578     Tweax = FOW*(Twez+Tweaa)+(1-2*FOW)*Twea
00579     Tweaax = FOW*(Twea+Tweb)+(1-2*FOW)*Tweaa
00580     Twebx = FOW*(Tweaa+Tweba)+(1-2*FOW)*Tweb
00581     Twebax = FOW*(Tweb+Twec)+(1-2*FOW)*Tweba
00582     Twecx = FOW*(Tweba+Tweca)+(1-2*FOW)*Twec
00583     Twecax = FOW*(Twec+Twed)+(1-2*FOW)*Tweca
00584     Twedx = (((KW/DxW)*Tweca+(KP/DxP)*Tweda)/CWPB)+(1-
((KW/DxW)+(KP/DxP))/CWPB)*Twed
00585     Twedax = FOP*(Twed+Twee)+(1-2*FOP)*Tweda
00586     Tweex = FOP*(Tweda+Tweea)+(1-2*FOP)*Twee
00587     Tweeax = FOP*(Twee+Twef)+(1-2*FOP)*Tweea
00588     Twefx = FOP*(Tweea+Twefa)+(1-2*FOP)*Twef
00589     Twefax = FOP*(Twef+Tweg)+(1-2*FOP)*Twefa
00590     Twegx = FOP*(Twefa+Twega)+(1-2*FOP)*Tweg
00591     Twegax = FOP*(Tweg+Tweo)+(1-2*FOP)*Twega
00592     Tweox = 2*FOP*(Twega+(DxP/KP)*Tae*(Hcweo+Hrwee))+(1-
2*FOP*(1+(DxP/KP)*(Hcweo+Hrwee)))*Tweo
00593     Twnix = (2*FOW*(Twnz+(DxW/KW)*(Hcwni*Tai+T*I*(FLW*Sns*SAW+(1-
SAW)*(FLF*Sf*AF*FWFG+FLW*AW*FWW*(Se+Sw+Sns)))+(1/AW)*(Hrenw*Twei+Hrsnw*Twsi+
Hrwnw*Twwi+Hrgin*Tgi+Hrfin*Tfi)))+(1-
2*FOW*(1+(DxW/KW)*(Hcwni+(1/AW)*(Hrwnw+Hrsnw+Hrenw+Hrgin+Hrfin))))*Twni)
00594     Twnzx = FOW*(Twni+Twna)+(1-2*FOW)*Twnz
00595     Twnax = FOW*(Twnz+Twnaa)+(1-2*FOW)*Twna
00596     Twnaax = FOW*(Twna+Twnb)+(1-2*FOW)*Twnaa
```

```
00597     Twnbx = FOW*(Twnaa+Twnba)+(1-2*FOW)*Twnb
00598     Twnbax = FOW*(Twnb+Twnc)+(1-2*FOW)*Twnba
00599     Twncx = FOW*(Twnba+Twnca)+(1-2*FOW)*Twnc
00600     Twncax = FOW*(Twnc+Twnd)+(1-2*FOW)*Twnca
00601     Twndx = (((KW/DxW)*Twnca+(KP/DxP)*Twnda)/CWPB)+(1-
((KW/DxW)+(KP/DxP))/CWPB)*Twnd
00602     Twndax = FOP*(Twnd+Twne)+(1-2*FOP)*Twnda
00603     Twnex = FOP*(Twnda+Twnea)+(1-2*FOP)*Twne
00604     Twneax = FOP*(Twne+Twnf)+(1-2*FOP)*Twnea
00605     Twnfx = FOP*(Twnea+Twnfa)+(1-2*FOP)*Twnf
00606     Twnfax = FOP*(Twnf+Twng)+(1-2*FOP)*Twnfa
00607     Twngx = FOP*(Twnfa+Twnga)+(1-2*FOP)*Twng
00608     Twngax = FOP*(Twng+Twno)+(1-2*FOP)*Twnga
00609     Twnox = 2*FOP*(Twnga+(DxP/KP)*Tae*(Hcwno+Hrwne))+(1-
2*FOP*(1+(DxP/KP)*(Hcwno+Hrwne)))*Twno
00610     Twsix = (2*FOW*(Twsz+(DxW/KW)*(Hcwsi*Tai+T*I*(FLW*Sns*SAW+(1-
SAW)*(FLF*Sf*AF*FWFG+FLW*AW*FWW*(Se+Sw+Sns)))+(1/AW)*(Hresw*Twei+Hrwsw*Twwi+
Hrnsw*Twni+Hrgis*Tgi+Hrfis*Tfi)))+(1-
2*FOW*(1+(DxW/KW)*(Hcwsi+(1/AW)*(Hrwsw+Hresw+Hrnsw+Hrgis+Hrfis))))*Twsi)
00611     Twszx = FOW*(Twsi+Twsa)+(1-2*FOW)*Twsz
00612     Twsax = FOW*(Twsz+Twsaa)+(1-2*FOW)*Twsa
00613     Twsaax = FOW*(Twsa+Twsb)+(1-2*FOW)*Twsaa
00614     Twsbx = FOW*(Twsaa+Twsba)+(1-2*FOW)*Twsb
00615     Twsbax = FOW*(Twsb+Twsc)+(1-2*FOW)*Twsba
00616     Twscx = FOW*(Twsba+Twsca)+(1-2*FOW)*Twsc
00617     Twscax = FOW*(Twsc+Twsd)+(1-2*FOW)*Twsca
00618     Twsdx = (((KW/DxW)*Twsca+(KP/DxP)*Twsda)/CWPB)+(1-
((KW/DxW)+(KP/DxP))/CWPB)*Twsd
00619     Twsdax = FOP*(Twsd+Twse)+(1-2*FOP)*Twsda
00620     Twsex = FOP*(Twsda+Twsea)+(1-2*FOP)*Twse
00621     Twseax = FOP*(Twse+Twsf)+(1-2*FOP)*Twsea
00622     Twsfx = FOP*(Twsea+Twsfa)+(1-2*FOP)*Twsf
00623     Twsfax = FOP*(Twsf+Twsg)+(1-2*FOP)*Twsfa
00624     Twsgx = FOP*(Twsfa+Twsga)+(1-2*FOP)*Twsg
00625     Twsgax = FOP*(Twsg+Twso)+(1-2*FOP)*Twsga
00626     Twsox = 2*FOP*(Twsga+(DxP/KP)*Tae*(Hcwso+Hrwse))+(1-
2*FOP*(1+(DxP/KP)*(Hcwso+Hrwwe)))*Twso
00627     Taix =
(AG*(Tfi*Hcfi+Tgi*Hcgi)+AW*(Hcwwi*Twwi+Hcwei*Twei+Hcwsi*Twsi+Hcwni*Twni))/(AG*(Hcfi+H
cgi)+(Hcwwi+Hcwei+Hcwni+Hcwsi)*AW)
00628
00629     ChangeTemps:
00630
00631     LET Tfi = Tfix
00632     Tfia = Tfiax
00633     Tfib = Tfibx
00634     Tfic = Tficx
00635     Tfid = Tfidx
00636     Tfie = Tfiex
00637     Tfif = Tfifx
00638     Tfig = Tfigx
```

```
00639     Tfih = Tfihx
00640     Tfii = Tfiix
00641     Tfij = Tfijx
00642     Tfik = Tfikx
00643     Tfiaa = Tfiaax
00644     Tfiba = Tfibax
00645     Tfica = Tficax
00646     Tfida = Tfidax
00647     Tfiea = Tfieax
00648     Tfifa = Tfifax
00649     Tfiga = Tfigax
00650     Tfiz = Tfizx
00651     Tfo=Tfox
00652     Tgi=Tgix
00653     Tgo=Tgox
00654     Tge=Tgex
00655     Twwi=Twwix
00656     Twwz=Twwzx
00657     Twwa=Twwax
00658     Twwb=Twwbx
00659     Twwc=Twwcx
00660     Twwd=Twwdx
00661     Twwe=Twwex
00662     Twwf=Twwfx
00663     Twwg=Twwgx
00664     Twwaa=Twwaax
00665     Twwba=Twwbax
00666     Twwca=Twwcax
00667     Twwda=Twwdax
00668     Twwea=Twweax
00669     Twwfa=Twwfax
00670     Twwga=Twwgax
00671     Twwo=Twwox
00672     Twni=Twnix
00673     Twnz=Twnzx
00674     Twna=Twnax
00675     Twnb=Twnbx
00676     Twnc=Twncx
00677     Twnd=Twndx
00678     Twne=Twnex
00679     Twnf=Twnfx
00680     Twng=Twngx
00681     Twnaa=Twnaax
00682     Twnba=Twnbax
00683     Twnca=Twncax
00684     Twnda=Twndax
00685     Twnea=Twneax
00686     Twnfa=Twnfax
00687     Twnga=Twngax
00688     Twno=Twnox
00689     Twsi=Twsix
```

```
00690     Twsz=Twszx
00691     Twsa=Twsax
00692     Twsb=Twsbx
00693     Twsc=Twscx
00694     Twsd=Twsdx
00695     Twse=Twsex
00696     Twsf=Twsfx
00697     Twsg=Twsgx
00698     Twsaa=Twsaax
00699     Twsba=Twsbax
00700     Twsca=Twscax
00701     Twsda=Twsdax
00702     Twsea=Twseax
00703     Twsfa=Twsfax
00704     Twsga=Twsgax
00705     Twso=Twsox
00706     Twei=Tweix
00707     Twez=Twezx
00708     Twea=Tweax
00709     Tweb=Twebx
00710     Twec=Twecx
00711     Twed=Twedx
00712     Twee=Tweex
00713     Twef=Twefx
00714     Tweg=Twegx
00715     Tweaa=Tweaax
00716     Tweba=Twebax
00717     Tweca=Twecax
00718     Tweda=Twedax
00719     Tweea=Tweeax
00720     Twefa=Twefax
00721     Twega=Twegax
00722     Tweo=Tweox
00723     Tai=Taix
00724
00725     LET q = q + 1
00726
00727  NEXT m
00728
00729  Store:
00730
00731   LET Tfixx(n) = Tfix - 273
00732  Tfiaxx(n) = Tfiax - 273
00733  Tfibxx(n) = Tfibx - 273
00734  Tficxx(n) = Tficx - 273
00735  Tfidxx(n) = Tfidx - 273
00736  Tfiexx(n) = Tfiex - 273
00737  Tfifxx(n) = Tfifx - 273
00738  Tfigxx(n) = Tfigx - 273
00739  Tfihxx(n) = Tfihx - 273
00740  Tfiixx(n) = Tfiix - 273
```

```
00741  Tfijxx(n) = Tfijx - 273
00742  Tfikxx(n) = Tfikx - 273
00743  Tfoxx(n)=Tfox - 273
00744  Tgixx(n)=Tgix - 273
00745  Tgoxx(n)=Tgox - 273
00746  Tgexx(n)=Tgex - 273
00747  Twwixx(n)=Twwix - 273
00748  Twwaxx(n)=Twwax - 273
00749  Twwbxx(n)=Twwbx - 273
00750  Twwcxx(n)=Twwcx - 273
00751  Twwdxx(n)=Twwdx - 273
00752  Twwexx(n)=Twwex - 273
00753  Twwfxx(n)=Twwfx - 273
00754  Twwgxx(n)=Twwgx - 273
00755  Twwoxx(n)=Twwox - 273
00756  Twnixx(n)=Twnix - 273
00757  Twnoxx(n)=Twnox - 273
00758  Taixx(n)=Taix - 273
00759
00760  LET m = 1
00761  LET n = 1 + n
00762  PRINT n,q
00763
00764  IF q < 57600&  THEN GOSUB Equations      '288000 for 24hrs
00765
00766  Final:
00767
00768  LET w = n-1
00769
00770  'filename$ = FILES$(0, "Enter a new file name")
00771
00772  OPEN filename$ FOR OUTPUT AS #1    'open file
00773
00774  'PRINT "This sub routine  stores the results on disk"
00775  'PRINT
00776  PRINT #1,"The Temperatures are "
00777  PRINT #1,"Tgex,Tgox,Tgix,Tfix,Tfox,Twwix,Twwox,Taix"
00778
00779  FOR n = 1 TO w
00780
00781  PRINT
#1,Tgexx(n);",";Tgoxx(n);",";Tgixx(n);",";Tfixx(n);",";Tfoxx(n);",";Twwixx(n);",";Twwoxx(n);",";Taixx(
n)
00782
00783  NEXT n
00784
00785  CLOSE #1                          ' close file
00786
00787
00788
00789  AlterTemperaturestoCentigrade:
```

```
00790   LET Tge = Tge -273
00791     Tgo = Tgo -273
00792     Tgi = Tgi -273
00793     Tfi = Tfi-273
00794     Tfia = Tfia-273
00795     Tfib = Tfib-273
00796     Tfic = Tfic-273
00797     Tfid = Tfid-273
00798     Tfie = Tfie-273
00799      Tfo = Tfo-273
00800     Twwi = Twwi-273
00801     Twni = Twni-273
00802     Twsi = Twsi-273
00803     Twei = Twei-273
00804     Twwo = Twwo-273
00805     Twno = Twno-273
00806     Twso = Twso-273
00807     Tweo = Tweo-273
00808     Tai = Tai-273
00809
00810
00811  filename1$ = FILES$(0, "Enter a new file name")
00812
00813  OPEN filename1$ FOR OUTPUT AS #2    'open file
00814
00815  PRINT "This sub routine  stores the results on disk"
00816  PRINT
00817  PRINT #2,"The Temperatures are "
00818  PRINT #2,"Tge - ";Tge;"                Tgo - ";Tgo
00819  PRINT #2,"Tgi - ";Tgi
00820  PRINT #2,"Tfi - ";Tfi;"               Tfo - ";Tfo
00821  PRINT #2,"Twwi - ";Twwi;"              Twwo - ";Twwo
00822  PRINT #2,"Twei - ";Twei;"              Tweo - ";Tweo
00823  PRINT #2,"Twni - ";Twni;"              Twno - ";Twno
00824  PRINT #2,"Twsi - ";Twsi;"              Twso - ";Twso
00825  PRINT #2,"Tai - ";Tai
00826  CLOSE #2                              ' close file
00827
00828  PRINT "The Temperatures are "
00829  PRINT "Tge - ";Tge;"                Tgo - ";Tgo
00830  PRINT "Tgi - ";Tgi
00831  PRINT "Tfi - ";Tfi;"                Tfo - ";Tfo
00832  PRINT "Twwi - ";Twwi;"               Twwo - ";Twwo
00833  PRINT "Twei - ";Twei;"              Tweo - ";Tweo
00834  PRINT "Twni - ";Twni;"              Twno - ";Twno
00835  PRINT "Twsi - ";Twsi;"              Twso - ";Twso
00836  PRINT "Tai - ";Tai
00837  PRINT
00838  INPUT "Press return to continue";FINISH
00839
00840  END
```

Appendix II: Schematic diagrams and plots not included in main text

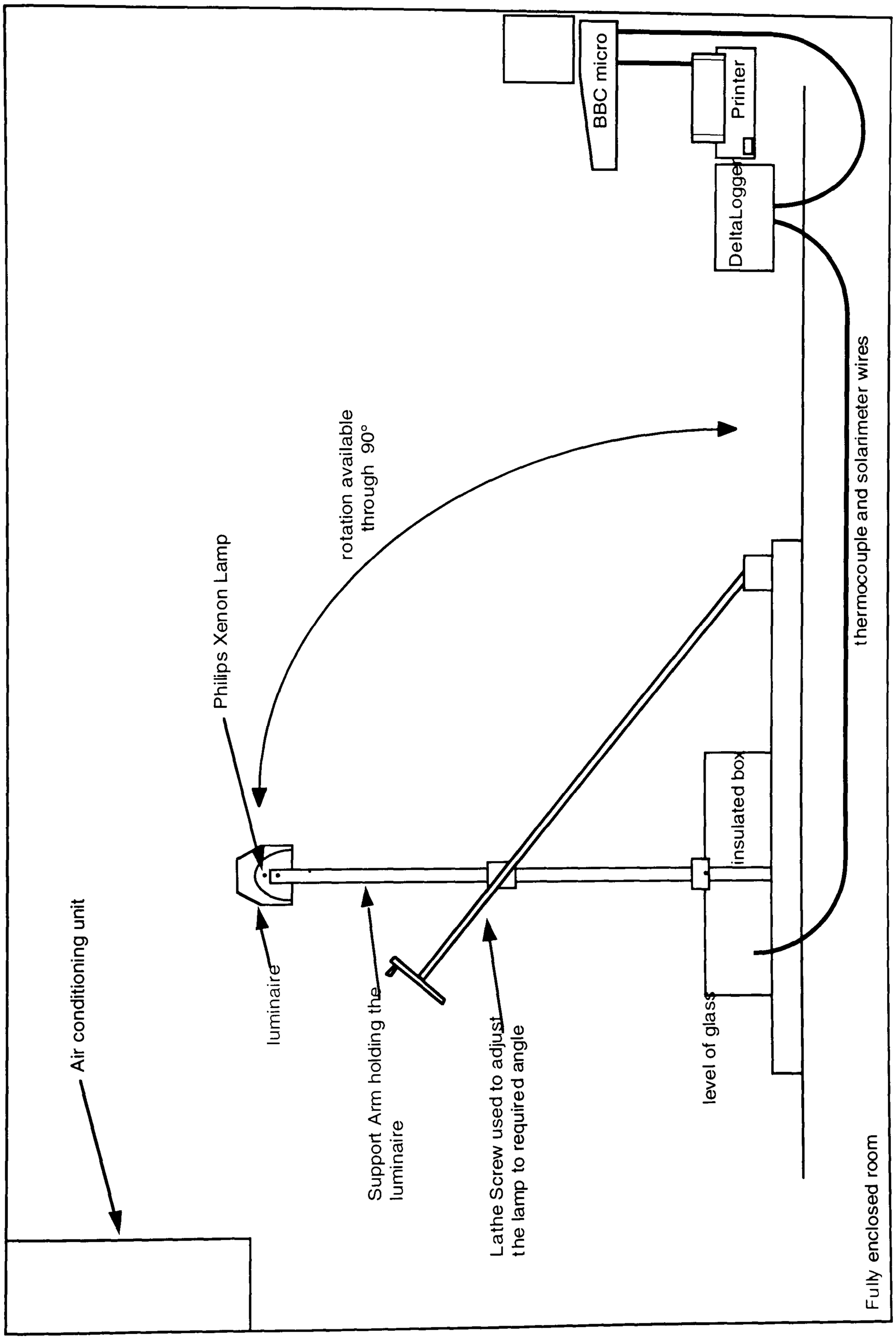

Figure AII.1: A Schematic diagram of the experimental apparatus and the environmental room.

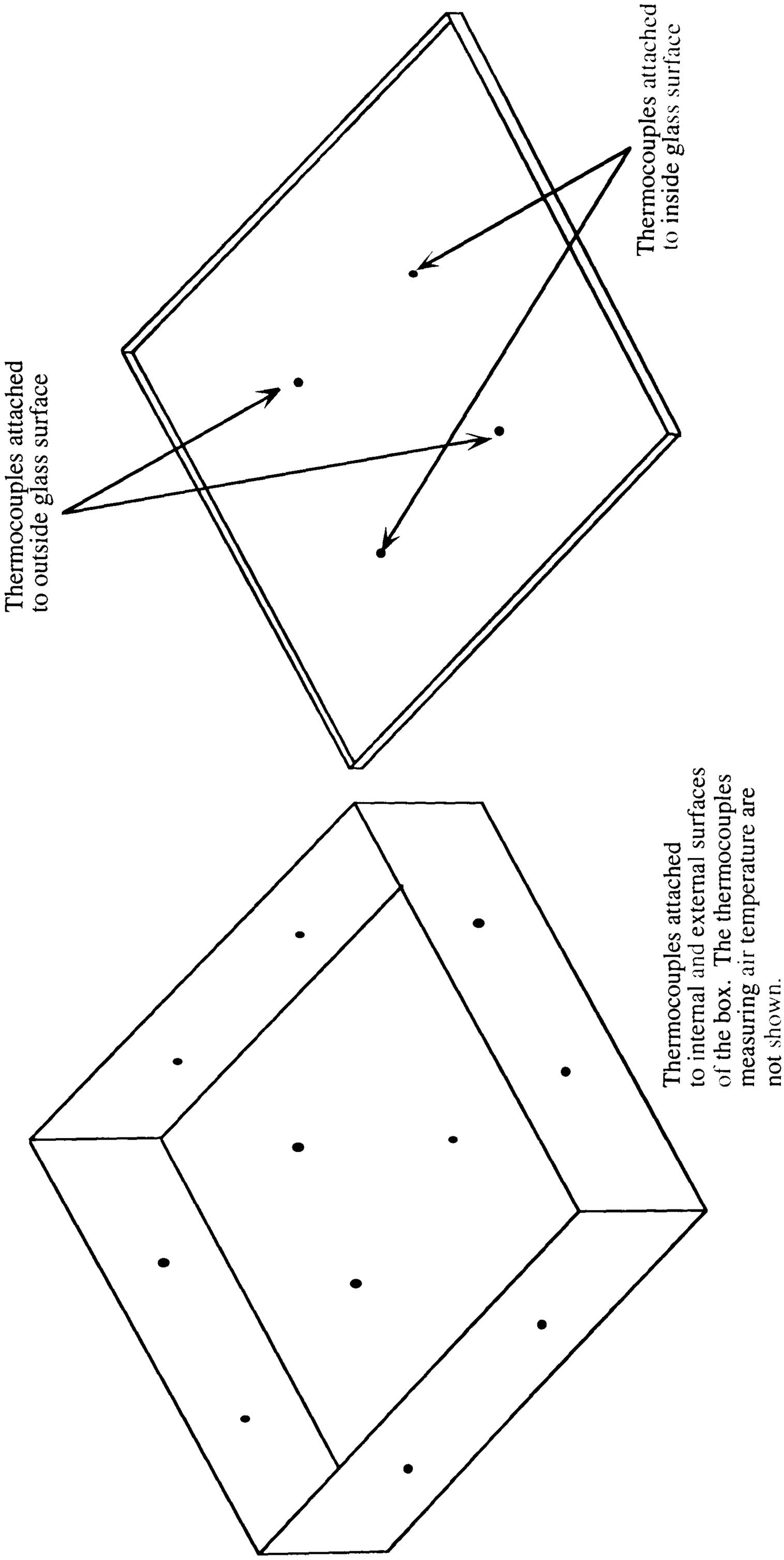

Figure AII.2: A Schematic diagram showing the positions of the thermocouples used to measure the temperatures of the illuminated hot box

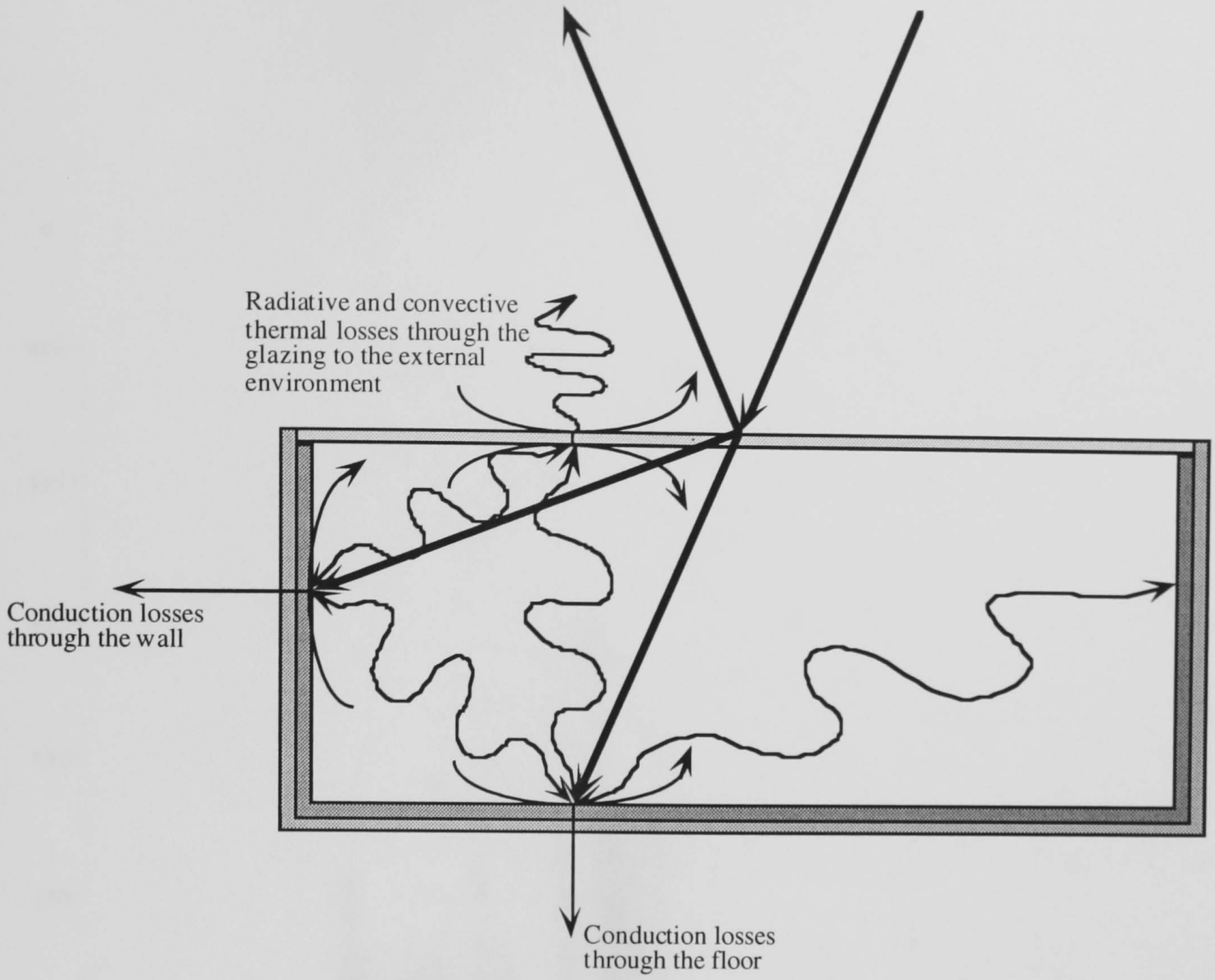

Radiative exchange between surfaces and radiative losses from glazing surface

Conduction losses through the walls and floor to the external environment

Convection losses from the walls and floor to the internal air

Short wave radiation heat transfer from the lamp to the box

Figure AII.3: Schematic diagram showing the thermal processes within the experimental illuminated hot box. This is a two-dimensional representation and a number of the heat paths have been removed for clarity.

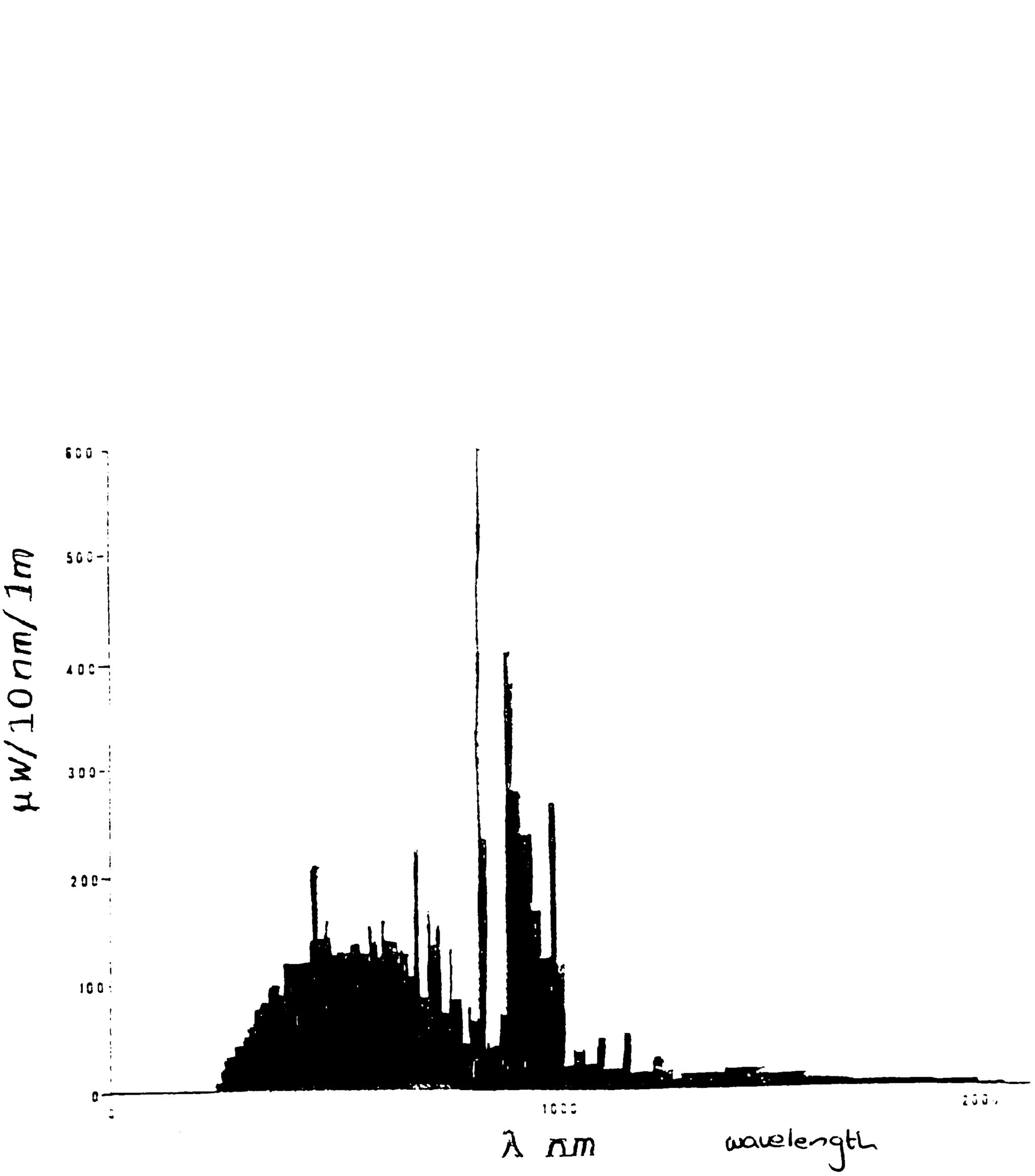

Figure AII.4: Spectral composition of light from a pulsed xenon lamp (Eames, 1990)